UAB
Universitat Autònoma de Barcelona

Ecology and processes of mercury detoxifying marine bacteria

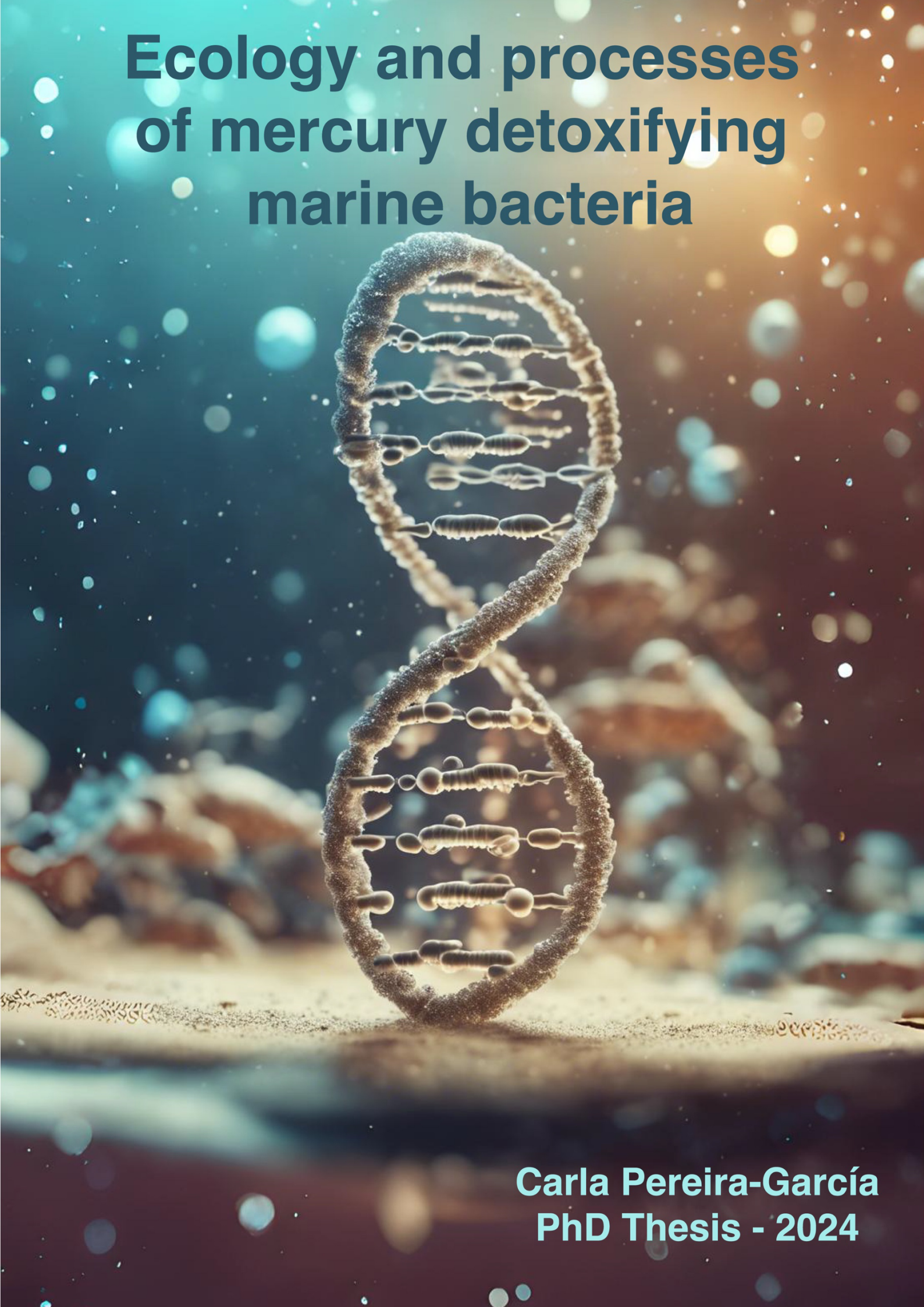
Carla Pereira-García

ADVERTIMENT. L'accés als continguts d'aquesta tesi queda condicionat a l'acceptació de les condicions d'ús establertes per la següent llicència Creative Commons:  https://creativecommons.org/licenses/?lang=ca

ADVERTENCIA. El acceso a los contenidos de esta tesis queda condicionado a la aceptación de las condiciones de uso establecidas por la siguiente licencia Creative Commons:  https://creativecommons.org/licenses/?lang=es

WARNING. The access to the contents of this doctoral thesis it is limited to the acceptance of the use conditions set by the following Creative Commons license:  https://creativecommons.org/licenses/?lang=en

Ecology and processes of mercury detoxifying marine bacteria



Carla Pereira-García

PhD Thesis - 2024

Doctoral thesis

Doctoral Program in Microbiology



Department of Genetics and Microbiology

2024

Ecology and processes of mercury detoxifying marine bacteria

Ecología y procesos de bacterias marinas detoxificadoras de mercurio

Ecologia i processos de bacteris marins detoxificadors de mercuri

Carla Pereira-García

Department of Marine Biology and Oceanography

Institute of Marine Sciences (ICM-CSIC)

Directors:

Dra. Silvia G. Acinas

Department of Marine Biology and Oceanography
Institute of Marine Sciences (ICM-CSIC)

Dra. Andrea G. Bravo

Department of Marine Biology and Oceanography
Institute of Marine Sciences (ICM-CSIC)

Director and academic tutor:

Dra. Olga Sánchez

Department of Genetics and Microbiology
Autonomous University of Barcelona

A todas las mujeres que lucharon para que yo pueda
dedicarme a lo que quiera y amar a quien quiera.
A todas las mujeres que siguen luchando
para que esto no cambie.
Gracias.

"*Somos distintas das que comezaron*
Na nosa pel gardámolo legado
Alén das bombas soubemos pararnos
Sin sexo, nin carne, nin putos coidados

Non asumímolo voso pecado
Facédela guerra cos ollos pechados
Non recoñecedes nin o propio bandoA acrópole canta

[…]

E que unha e outra e outra vez
Escoitando a vosa merda sen saber por que
Somos as fillas de todas as que se plantaron e dixeron
Que, que, que!"

–Fillas de Cassandra

"*Los viejos tenemos el conocimiento.*
Los adultos tienen la seguridad.
Los niños tienen la ilusión.
Pero sois los jóvenes los que tenéis el poder para cambiar el mundo"

- Laura Gallego, Las hijas de Tara.

"No estoy aceptando las cosas que no puedo cambiar,
estoy cambiando las cosas que no puedo aceptar."

- Angela Davis

Table of contents

Agradecimientos i

Preface v

Abbreviations vii

Summary 3

Resumen 5

Resum 7

Introduction 13

From element to contaminant 13

Marine mercury cycle 15

Sources of Hg into the oceans 15

Hg transformations in the ocean 16

The biological mercury cycle 18

Mercury methylation: *hgcAB* genes 18

The *mer* operon 19

Approaches to study microorganisms involved in the mercury cycle 23

Mercury and the global change 25

Hypothesis and Objectives 31

Chapter 1: Potential impact of tide-regulation barriers on the formation of methylmercury 37

Abstract 37

Introduction 38

Methods 39

Site of Study 39

Sampling sites 40

Sampling, core processing and incubations 40

Benthic Chambers 41

Laboratory Analyses 42

Results 45

Characteristics of the two contrasted sampling sites 45

Experiments with oxygen limitation: changes in THg, MMHg, k_m and sediment properties. 47
Changes in THg and MMHg in benthic chambers 51
Discussion 52
Contrasting SG and OS study sites 52
Increase in methylmercury formation and concentration in a simulated MOSE closing-event 53
Negative consequences of oxygen depletion events on coastal Hg cycling 54
Conclusions 55
Chapter 2: Novelty and metabolic versatility of uncultured bacteria with capacity to detoxify inorganic mercury and methylmercury from marine sediments 61
Abstract 61
Introduction 62
Material and Methods 63
Sample collection, DNA/RNA extraction and library preparation 63
The MERCLUB Microbial Gene Catalogue 63
Generation of MERCLUB Hg-detoxification Reference Gene Catalogue (Hg-RGC). 64
MERCLUB Metagenome Assembled Genomes (MAGs) construction 65
Fragment recruitment analysis 65
Phylogenetic analysis 66
Functional and metabolic analysis of MAGs. 66
Data visualizations. 66
Results and Discussion 68
A deep look into the microbial taxa involved in Hg^{II} reduction and MMHg demethylation in Hg-impacted marine sediments 68
Diversity and novelty of microbial MAGs containing *merAB* genes 72
Metabolic and functional diversity of the *merA and merB* MAGs genomes 74
Prevalence and transcriptional activity of the *merA* and/or *merB* MAGs 79
Conclusion 82
Chapter 3: Unmasking the physiology of mercury detoxifying bacteria from polluted sediments 87
Abstract 87

Introduction 88
Methods 89
Study areas and isolation 89
Physiological tests 90
Growth curves 91
Continuous culture experiments 91
Measurement of Hg concentration and Hg detoxification rates 93
DNA and RNA extraction 93
Measurement of *merA* gene transcription 93
Genome assembly and annotation of the selected candidate 93
Results 95
Preliminary selection of candidates and physiological assays 95
Growth curves and specific growth rates of selected candidates 97
Mercury removal from selected candidates 97
Growth in continuous culture and measurement of Hg detoxification rates 100
merA gene transcription 102
Genomic analysis of *Pseudomonas putida* MERCC_1942 103
Discussion 103
Conclusion 105
Chapter 4: Genomic and transcriptomic characterization of methylmercury detoxification in a deep ocean *Alteromonas mediterranea* ISS312 109
Abstract 109
Introduction 110
Materials and methods 111
Strain selection. 111
Growth curves. 112
DNA and RNA extraction. 112
Genome sequencing and assembly. 112
RNA sequencing and transcriptomic analysis. 113
Recruitment of Mer enzymes in metatranscriptomics of *Tara* Oceans. 113
Data availability 114

Results and Discussion 114
Genetic characterization of *mer* operons in *Alteromonas* sp. ISS312. 114
Physiological responses of *Alteromonas mediterranea* ISS312 to MMHg 116
Prevalence of *merAB* genes related to *Alteromonas mediterranea* ISS312 across oceans layers. 123
Conclusion 126
General discussion 131
Will global change enhance MMHg formation? The case study of the Venice Lagoon (Chapter 1) 131
Prokaryotes involved in MMHg demethylation and Hg^{II} reduction in sediments (Chapters 2 and 3) 135
Is Hg bioremediation possible based on isolated cultured bacteria from Hg contaminant environments? (Chapters 3 and 4) 138
Alteromonas mediterranea ISS312: a case study 139
Future research 140
Conclusions 145
Bibliography 151
List of figures 185
List of tables 190
Supplementary material 195
Supplementary figures 195
Supplementary Tables 203

Agradecimientos

Llegue al ICM por casualidad, completa y maravillosa casualidad. ¿Quién me iba a decir a mí que algo tan simple como escoger unas prácticas iba a marcar tanto mi vida? Gracias a toda la gente que me ha acompañado en estos años, a todas las que me han ayudado y guiado o me han recordado que tenía que comer cuando estaba en un *hyperfocus* o me han hecho reír a carcajadas en los pasillos. Sin vosotras nada de esto hubiera sido posible.

Gracias a mis directoras por creer en mí y darme esta oportunidad. Aun me sorprende la suerte que he tenido al teneros de jefas. Silvia, gracias por acogerme y enseñarme y gracias por siempre compartir tu entusiasmo por la ciencia marina conmigo. Olga, siempre tan amable y dispuesta a apoyarme en todo lo que he querido hacer. Y finalmente gracias a Andrea, me introdujiste al maravillo mundo del mercurio y a su gente, pero me has enseñado mucho más que ciencia! Me has mostrado el tipo de jefa y de científica que aspiro a ser, gracias no solo por ser mi supervisora si no también mi amiga!

Quiero agradecer a toda la gente que ha contribuido a este trabajo, tanto del ICM como de la UAB:

Gracias Pablo por ser enseñarme prácticamente todo lo que se de informática, todo un mundo nuevo gracias a ti. Felipe, siempre con tu adorable sonrisa, gracias por siempre tener una palabra amable. Marta, me enseñaste a hacer ilustraciones informativas y bonitas, pero además compartiste conmigo cafés, risas, quejas y birras. Espero que aun queden más por compartir. Isa, me dejaste ser tu sombra y aprender de ti tanto como quise, fuiste amable y te convertiste en una de las primeras amigas que hice en Barcelona, gracias por todo, por los días eternos que se pasaban en nada, por escucharme y apoyarme, por todo lo que me has enseñado, que es mucho y sobre todo gracias por tu sincera amistad!

Nuria, gracias por siempre darme chachara en el despacho y por *talk science* siempre que quería. Verónica y Mireia por todo su ayuda de lab y por esos cafés a media mañana que me salvaban el día. Y sobre todo a Elena, por pensar y por remar conmigo para que todo saliera adelante! Siempre estabas dispuesta a ayudar y

¡Ay mis mercurias! María, Julia, Ester, Arne, Céline y Gemma. Sois el mejor grupo que nadie podría pedir! Gracias por las reuniones de una hora que duran 2 y media, por todas las comidas compartidas, por tantas risas y por existir. Gracias por siempre tener tiempo para mirar mis figuras o para discutir mierdas varias conmigo. Y gracias por todo el apoyo moral estos últimos meses, espero poder siempre tener el privilegio de llamaros amigas!

Gracias a todo el despacho de máquinas por amenizar los largos días de trabajo. Especialmente a Dani, primera persona que me dio la bienvenida al ICM, a Sergio fiel compañero, siempre espalda con espalda y a Carlota gracias por tantos cafés y chacharas, gracias por ser mi editora en esta tesis, espero que allí donde vayamos sigamos contestándonos los Whatsapps tres semanas después de recibirlos! Gracias a mis Xab/vis, por siempre estar dispuestos a criticar el cistema conmigo, por compartir no solo el trabajo conmigo si no también la vida! Os quiero y nos vemos en el orgullo, maricones!!!

Hay mucha más gente a la que agradecer del ICM, por organizar seminarios, TEMAs, micromix, Young Researchers y todas las demás actividades que tanto he disfrutado a lo largo de los años pero sería imposible mencionar a todo el mundo. Si que hay una persona a la que querría dar las gracias, Sara gracias por ser mi mentora estos años y guiarme por la locura que es hacer una tesis! Hablar contigo siempre me reconforta y espero poder seguir haciendo aunque ya no sea estudiante.

An especial mention to Dr. David Amouroux, Dr. Emmanuel Tessier and Dr. Bastien Duval! Thank you for welcoming me into your lab, for teaching me and for always answering all my questions, no matter how stupid or crazy they were! My stay in Pau could have been very stressful and instead you made it so wonderful and fun, I feel very lucky that I had the chance to meet you all and I hope we get the chance to meet again soon!

Por supuesto nada de esto habría sido posible sin mis amigos y mi familia, que me han hecho la persona que soy ahora y me han acompañado a lo largo no solo de estos años si no de todos los anteriores.

Mi familia salmantina, Cristina, Valle, Marta y Carmen. Da igual donde nos lleve la vida, siempre vais a estar conmigo. Hicisteis que una ciudad que jamás había pisado fuera mi casa, me aceptasteis como era y me ayudasteis a valorarme a mí misma. Gracias por estéis donde estéis siempre coger el teléfono cuando llamo, prometo siempre coger cuando llaméis vosotras. Os quiero.

¡Biociosos, queridos, qué fantasía es teneros en mi vida! Espero que siempre siga sintiendo que no pasa el tiempo cuando os veo y que me hagáis reír siempre más que la vez anterior. Candela, Nerea, David, Jorge y especialmente Víctor, compañero de cachimbas y de largas discusiones en los días malos. Ángel y Carlos, espero poder seguir en vuestra vida otros 25 años, aunque ya no vaya a ser en la misma ciudad, siempre os llevo en mis recuerdos! Os echo de menos!

Belén, que pena no habernos hecho amigas antes, habría podido disfrutar 4 años extras de tu maravillosa presencia! Elena y Sandra, mis supervivientes (ya solo Sandra sobrevive), gracias por dejarme desahogarme, por sacarme por ahí y enseñarme el monte, por compartir tantas cosas bonitas conmigo. Menos mal que os tenía junto mi durante estos años!

Luis, a ti no se ni como empezar a darte las gracias; eres de lo mejor que tengo en mi vida! Gracias por aguantar mi desorden y por siempre escucharme los dramas, gracias por tantas horas de compañía que no las puedo ni contar, gracias por los juegos, las risas, las birras a las 2 de la mañana filosofando sobre la vida, gracias por apoyarme contra Dolors, gracias por tener un humor tan negro como el mío, gracias por acceder a co-oficiar mi boda, gracias por existir. Te adoro!

Iria and Kieran, thanks for moving to Barcelona and making my life that much better! Thank you for being there to make everything funnier and happier! Thank you for sharing days and nights, trips, beaches, garages, and so many more things with me. You came into my life and

became so important to me, I can not imagine my life without you anymore, I love you guys so much!

Andrea, mi *soulmate*. La gente tiene esta absurda noción de que tu alma gemela tiene que ser tu pareja pero a veces la encuentras y se vuelve tu mejor amiga. Tuve la suerte de encontrarte muy joven y espero no perderte nunca! Vamos ya por los que, 16 años de risas, llantos, vivencias, roturas de costillas y corazones, lasañas, series favos, libros favos, novios ficticios (ajam Jax) y cientos de cosas más que hemos compartido en todos estos años. Espero seguir compartiendo contigo mi vida porque es mejor gracias a que tu estas en ella.

Por último gracias a mi familia, somos ruidosos y estamos todos un poco zumbados pero me alegro de ser parte de esta inmensa jauría Pereiras y Matos! Gracias especialmente a mis abuelas y abuelos, que tanto me cuidaron y que ahora ya no están con nosotros. Os echo de menos cada día! Gracias a mis padres por todo lo que habéis hecho por mi. Papa, me enseñaste que todo el mundo tiene miedo pero que lo realmente importante es no dejar que el miedo te paralice. Gracias a mi madre por siempre luchar para que saliera adelante, por contar palabras cada noche conmigo hasta que aprendí a leer como los otros niños, por no dejarme pensar que no era suficiente solo por tener dificultades, si no fuera por ti esta tesis no existiría. Gracias por ser la mejor madre del mundo! Gracias a mi hermana Lara, eres mi luz en el camino, eres el ángel que me cicatrizo todas mis heridas, tu sí que eres lo más inspirador! Y gracias también por casarte con Eli y traerla a ella y a Bruno a mi vida! Elisa, no podría tener una cuñada mejor, eres tan graciosa, tan generosa, tan inteligente y tan buena que cada día me sorprendes. Bruno, es un bebe así que no se entera de nada pero le quiero tanto!

Por último gracias a mi mujer. Águeda, cariño, eres todos mis ojalas! Gracias por estar a mi lado en todos los momentos, duros, raros, estresantes, maravillosos o en los mejores de mi vida, gracias por quererme tal y como soy, gracias por ilusionarte cuando te cuento cosas del trabajo aunque no entiendas nada, gracias por ser la mejor humana de Gala, gracias por traer siempre luz y cariño a mi vida. Gracias por la vida que estamos compartiendo y gracias por todo lo que vamos a compartir en el futuro. Te quiero nena!

Preface

This thesis contains a general introduction, four chapters considered the body of the thesis and a general discussion. The scientific chapters are written in paper format. Described below are the publication details and the contributions of the co-authors for each scientific chapter.

Chapter 1 will be submitted to Journal of Hazardous Materials before this thesis is defended.

Potential impact of tide-regulation barriers on the formation of methylmercury

Carla Pereira-García, Andrea G. Bravo, Claudia Cosio, Andrea Gallorini, Simone Leoni, Daniele Cassin, Stéphane Guédron, Thierry Adatte, Miguel Cabrera, Olga Sanchez, Silvia G. Acinas, David Amouroux, Roberto Zonta, Janusz Dominik, Jean-Luc Loizeau

Authors contributions:

CPG: Software, formal analysis, investigation, data curation, visualization, and writing – original draft, review and editing. AGB: Conceptualization, methodology, investigation, data curation, writing – original draft and review and editing, supervision, project administration and funding acquisition. CC: investigation, writing – review and editing. AG: Investigation, formal analysis, data curation, and writing – review and editing. SL: Investigation, formal analysis, data curation, and writing – review and editing. DC: Investigation, formal analysis and writing – review and editing. SG: Investigation, formal analysis, and writing – review and editing. TA: Investigation, formal analysis, data curation, and writing – review and editing. MC: Investigation, formal analysis, data curation, and writing – review and editing. OS: Supervision, writing – review and editing. SGA: Supervision, writing – review and editing. DA: Resources, laboratory analyses, writing – review and editing. RZ: Conceptualization, methodology, investigation, formal analysis, writing – review and editing, resources, project administration and funding acquisition. JD: Conceptualization, investigation, methodology, formal analysis, writing – review and editing. JLL: Conceptualization, methodology, investigation, formal analysis, resources, writing – review and editing, project administration and funding acquisition.

Chapter 2 is still being prepared for publication.

Chapter 3 is adapted from a publication:

Pereira-García, C., Del Amo, E. H., Vigués, N., Rey-Velasco, X., Rincón-Tomás, B., Pérez-Cruz, C., Sanz-Sáez, I., Hu, H., Bertilsson, S., Pannier, A., Soltmann, U., Sánchez, P., Acinas, S. G., Bravo, A. G., Alonso-Sáez, L., & Sánchez, O. (2024). Unmasking the physiology of mercury detoxifying bacteria from polluted sediments. Journal of Hazardous Materials, 133685. https://doi.org/10.1016/j.jhazmat.2024.133685

Authors contributions:

CPG: Conceptualization, methodology, software, formal analysis, investigation, visualization, and writing – original draft as well as review and editing. EHdA: Conceptualization, methodology, software, formal analysis, investigation, and writing – original draft as well as

review and editing. NV: Investigation, formal analysis and writing – review and editing. XRV Investigation and writing – review and editing. BRT: Investigation. CPC Investigation and writing – review and editing. ISS: Investigation and writing – review and editing. HH: Investigation and formal analysis. SB: Conceptualization and supervision. AP: Methodology, investigation, formal analysis and writing – original draft as well as review and editing. US: Methodology, investigation, formal analysis, resources and writing – review and editing. PS: Software and data curation. SGA: Conceptualization, supervision, funding acquisition and writing – review and editing. AGB: Conceptualization, methodology, and supervision. LAS: Conceptualization, funding acquisition, resources, project administration and writing – review and editing. OS: Conceptualization, methodology, investigation, formal analysis, resources, funding acquisition, project administration and writing – original draft as well as review and editing.

Chapter 4 is adapted from a publication:

Pereira-Garcia, C., Sanz-Sáez, I., Sánchez, P., Coutinho, F. H., Bravo, A. G., Sánchez, O., & Acinas, S. G. (2024). Genomic and transcriptomic characterization of methylmercury detoxification in a deep ocean Alteromonas mediterranea ISS312. Environmental Pollution, 347, 123725. https://doi.org/10.1016/j.envpol.2024.123725

Authors contributions:

CPG: Conceptualization, Formal analysis, Investigation, Methodology, Software, Visualization, Writing – original draft, Writing – review & editing. ISS: Conceptualization, Investigation, Methodology, Writing – review & editing. PS: Resources, Software. FHC: Formal analysis, Writing – review & editing. AGB: Funding acquisition, Supervision, Writing – review & editing. OS: Funding acquisition, Writing – review & editing. SGA: Conceptualization, Formal analysis, Funding acquisition, Project administration, Resources, Supervision, Writing – review & editing.

Abbreviations

AAS	Atomic Absorption Spectrophotometry
AFS	Atomic Fluorescence Spectroscopy
ANI	Average Nucleotide Identity
BCN	Barcelona
BIX	Biological Index
CDOM	Coloured dissolved organic matter
CDS	Coding DNA sequences
Clh-a	Chlorophyll A
COG	Cluster of Orthologous Groups
CS	Suances estuary
CV	Cold vapor
D	Dilution rate
DAPI	4´, 6´-diamino-2-phenylindole
DCM	Deep Chlorophyll Maximum
DE	Differentially expressed
DNRA	Dissimilatory nitrate reduction to ammonium
DMHg	Di-methylmercury
DOC	Dissolved organic carbon
DOM	Dissolved organic matter
DO	Dissolved oxygen
dPCR	Digital PCR
EC	Enzyme Commission numbers
EN	Nervión estuary
ENA	European Nucleotide Archive
EPS	Exopolysaccharides
ESL	Extreme Sea Level
F	Pump flux
FC	Fold-Change
FDOM	Fluorescent dissolved organic matter
FeRB	Iron Reducing Bacteria

FI	Fluorescence Index
FRA	Fragment Recruitment Analysis
GC	Gas chromatography
GI	Genomic Island
GTDB	Genome Taxonomy Database
Hg	Mercury
Hg^0	Elemental mercury
Hg^{II}	Divalent mercury
Hg-RGC	Hg Reference Gene Catalog
HI	Hydrogen Index
HIX	Humification Index
HPLC	High pressure liquid chromatography
HMM	Hidden Markov models
ICP-MS	Inductively Coupled Plasma Mass Spectrometry
IHg	Inorganic mercury
k_m	Methylation rate constant
KPH	Köpmanholmen
LOD	Limit of Detection
LOQ	Limit of Quantification
MAG	Metagenomic assembled genome
MeHg	Methylmercury
MERCC	MERCLUB Culture Collection
MES	Mesopelagic
MetaG	Metagenomic
MetaT	Metatranscriptomic
MGE	Mobile Genetic Elements
MIC	Minimum inhibitory concentration
MINC	Mineral Carbon
MMHg	Mono-methylmercury
MOSE	Modulo Sperimentale Elettromeccanico
OD	Optical density

OI	Oxygen Index
OM	Organic matter
OS	Osellino
PBS	Phosphate Buffered Saline
PCA	Principal Component Analysis
PCoA	Principal Coordinates Analysis
PMA	Phenylmercuric acetate
PVDF	Hydrophobic polyvinylidene fluoride
RPKG	Reads recruited Per Kilobase of the genome per Gigabase of the metagenome
RT	Room temperature
SG	San Giuliano
SGD	Submarine groundwater discharge
SOD	Sediment oxygen demand
SRB	Sulphate Reducing Bacteria
SRF	Surface
SS	Steady State
SSMS	Soil Substrate Membrane System
TC	Total Carbon
THg	Total mercury
TMM	Trimmed Mean of M-values
TN	Total Nitrogen
TOC	Total Organic Carbon
TPM	Transcript per Million
μ	Growth rate


Summary
Resumen
Resum

Summary

Mercury (Hg) is a toxic and widespread metal. Monomethylmercury (MMHg) is a potent neurotoxic and especially worrisome due to its bioaccumulation and biomagnification through the aquatic food webs. In aquatic systems, MMHg is form mainly in sediments by prokaryotes carrying the *hgcAB* genes. MMHg demethylation and Hg^{II} reduction can also take place in sediments, performed by prokaryotes containing the *mer* genes. Operon *mer* has two enzymes, *merA* (mercuric reductase) which converts Hg^{II} to Hg^{0}, and *merB* (organomercurial lyase) which is responsible for the degradation of MMHg to Hg^{II}. Methylation has been extensively studied since the discovery of the *hgcAB* gene cluster in 2013. However, studying MMHg demethylation in the environment has been very difficult, thus the main players involved in this process and the main factors controlling their activity remain largely unknown.

In the first chapter, I incubated sediments from the Venice Lagoon to simulate a MOSE (barrier system) closing event in two seasons, summer and autumn, and to determine the impact of tide-regulating barriers in the formation of MMHg. In summer, I found an increase in the concentration of DOC and an enrichment of proteinaceous substances and reactive humic acids, a higher MMHg concentration in the water column and higher methylation rates in incubated sediment cores after 48h. Both higher methylation rates and increased MMHg concentrations could potentially enhance bioaccumulation in the lagoon's biota. These results are especially worrisome in the context of global change in which the lagoon will closed more frequently for longer times due to the increasing number of flooding events. Moreover, the expected raise in temperature might increase MMHg formation rates and/or prolong the warmer season during which MMHg is formed in sediments.

In Chapter 2, by combining metagenomic and metatranscriptomic data from sediments, my results shed light on the ecology and functional traits of the *merA* and/or *merB* containing prokaryotes. The MERCLUB-MAG Collection was reconstructed (with 803 MAGs) and the *merAB* containing MAGs were extracted (45 MAGs) to study their abundance, activity and metabolic capacities. The main findings are i) *merB* was more frequent and active than *merA*, ii) *merAB* containing MAGs had a high level of taxonomic novelty, although Gammaproteobacteria was the most predominant taxa and iii) the *merAB* containing MAGs had very diverse metabolisms.

Parallelly, the MERCLUB Culture Collection was obtained with the intention of finding the best candidate to be used in bioremediation strategies. Initially, 46 isolates were chosen for general physiological assessment, and after a selection process, the growth rates and the Hg removal capacities of three final candidates – *Aeromonas* sp. MERCC_1069, *Pseudomonas putida* MERCC_1942 and *Bacillus* sp. MERCC_2852 were determined. *Aeromonas* sp. was highly efficient in batch cultures, although *Pseudomonas putida* MERCC_1942 was finally selected to be optimized using the continuous culture technique to achieve maximum Hg removal in the bioremediation process. Strain MERCC_1942 grown at

high growth rates presented the highest removal efficiency and thus was the proposed candidate for bioremediation.

Lastly, I used *Alteromonas mediterranea* ISS312, which is globally and vertically distributed throughout oceans, to study the effects of MMHg in its growth and in its gene's expression. I sequence the genome and characterized the *mer* genes, showing that it has 4 different operons. Secondly, I performed a transcriptomic experiment in which I compared control (not amended) and samples amended with 5 μM of MMHg. In the amended cultures, I observed a longer lag phase in the growth curve, and differential expression of some but not all of the *mer* genes. Additionally, the *mer* genes presented very diverse co-expression patterns among them. These results indicate that this bacterial strain can be used as a model microorganism for MMHg demethylation and Hg^{II} reduction.

Resumen

El mercurio (Hg) es un metal tóxico y extendido. El monometilmercurio (MMHg) es un potente neurotóxico especialmente preocupante debido a su bioacumulación a través de las redes alimentarias acuáticas. En los sistemas acuáticos, el MMHg se forma principalmente en los sedimentos por procariotas que portan los genes *hgcAB*. La desmetilación de MMHg y la reducción de Hg^{II} también ocurren en sedimentos, realizadas por procariotas con los genes *mer*. El operón *mer* tiene dos enzimas, *merA* (Hg^{II} reductasa), que convierte Hg^{II} en Hg^{0}, y *merB* (alquilmercurio liasa), que es responsable de la degradación de MMHg a Hg^{II}. La metilación se ha estudiado ampliamente desde el descubrimiento de los genes *hgcAB* en 2013. Sin embargo, estudiar la desmetilación ambiental del MMHg ha sido muy difícil, y los principales actores involucrados y los principales factores que controlan su actividad siguen siendo en gran medida desconocidos.

En el primer capítulo, incubé sedimentos de la laguna de Venecia para simular un evento de cierre de MOSE (sistema de barreras) en verano y otoño, y así determinar el impacto de las barreras en la formación de MMHg. En verano, encontré un aumento en la concentración de DOC y un enriquecimiento de sustancias proteicas y ácidos húmicos reactivos, una mayor concentración de MMHg en el agua y mayores tasas de metilación en los sedimentos incubados después de 48 h. Tanto las altas tasas de metilación como el aumento de las concentraciones de MMHg podrían incrementar la bioacumulación en la laguna. Estos resultados son particularmente preocupantes en el contexto de cambio global en el que la laguna se cerrará con mayor frecuencia durante períodos más prolongados debido al creciente número de inundaciones. Además, el aumento esperado de la temperatura podría aumentar las tasas de formación de MMHg y/o prolongar la estación cálida durante la cual se forma MMHg.

En el capítulo 2, combinando datos metagenómicos y metatranscriptómicos de sedimentos, se caracteriza la ecología y los rasgos funcionales de los procariotas que contienen *merA* y/o *merB*. Se reconstruyó la colección MERCLUB-MAG (con 803 MAG) y se extrajeron los MAG que contenían *merAB* (45 MAG) para estudiar su abundancia, actividad y capacidades metabólicas. Los principales hallazgos son que i)*merB* fue más frecuente y activo que *merA*, ii)las Gammaproteobacteria fueron el taxon más predominante pero hay una alta novedad taxonómica y iii)los MAG que contenían *merAB* tienen metabolismos muy diversos.

Paralelamente se obtuvo la colección de cultivos MERCLUB con la intención de encontrar el mejor candidato para utilizar en biorremediación. Inicialmente, se eligieron 46 aislados para una evaluación fisiológica general y, tras un proceso de selección, evalué las tasas de crecimiento y de eliminación de Hg de tres candidatos finales: *Aeromonas* sp. MERCC_1069, *Pseudomonas putida* MERCC_1942 y *Bacillus* sp. MERCC_2852. *Aeromonas* sp. fue eficiente en cultivos discontinuos, aunque finalmente se seleccionó *Pseudomonas putida* MERCC_1942 para optimizar la eliminación de Hg en cultivo continuo. La cepa MERCC_1942 cultivada a altas tasas de crecimiento presentó la mayor eficiencia de eliminación y es propuesta para la biorremediación.

Por último, utilicé *Alteromonas mediterranea* ISS312, que se distribuye globalmente en las distintas profundidades del océano, para estudiar los efectos del MMHg en su crecimiento y en la expresión de sus genes. Secuencié el genoma y caractericé los genes *mer*, mostrando que tiene 4 operones diferentes. En segundo lugar, comparando muestras suplementadas con 5 μM de MMHg con muestras control, observé una fase de latencia más larga y una expresión diferencial de algunos, pero no de todos, los genes *mer*. Además, los genes *mer* presentaron patrones de coexpresión muy diversos. Estos resultados indican que esta cepa bacteriana se puede utilizar como modelo para estudiar desmetilación y la reducción de Hg.

Resum

El mercuri (Hg) és un metall tòxic i estès a l'ambient. El monometilmercuri (MMHg) és un potent neurotòxic especialment preocupant a causa de la seva bioacumulació a les xarxes tròfiques aquàtiques. En els sistemes aquàtics, el MMHg es forma principalment als sediments per procariotes portadors dels gens *hgcAB*. La desmetilació de MMHg i la reducció de Hg^{II} també ocorren en sediments, realitzades per procariotes amb els gens *mer*. L'operó *mer* té dos enzims, MerA (Hg^{II} reductasa), que converteix Hg^{II} en Hg^{0}, i MerB (organomercuri liasa), que és responsable de la degradació de MMHg a Hg^{II}. La metilació ha estat àmpliament estudiada des del descobriment dels gens *hgcAB* el 2013. En canvi, estudiar la desmetilació ambiental del MMHg ha estat molt difícil, per això els principals actors i els factors involucrats en la seva activitat segueixen sent bastant desconeguts.

Al primer capítol de la tesi, vaig incubar sediments de la llacuna de Venècia per simular un esdeveniment de tancament de les barreres MOSE a l'estiu i la tardor, per determinar l'impacte de les barreres en la formació de MMHg. A l'estiu, vaig trobar un augment en la concentració de DOC (Carboni Orgànic Dissolt) i un enriquiment de substàncies protèiques i àcids húmics reactius, una concentració més gran de MMHg a l'aigua i majors taxes de metilació en els sediments incubats després de 48 h. Tant les altes taxes de metilació com l'augment de les concentracions de MMHg podrien incrementar la bioacumulació a la llacuna. Aquests resultats són particularment preocupants en el context de canvi global en el qual la llacuna es tancarà més sovint durant períodes més prolongats degut a l'augment d'inundacions. A més, l'increment esperat de la temperatura podria augmentar les taxes de formació de MMHg i/o perllongar l'estació càlida durant la qual es forma MMHg.

Al capítol 2, combinant dades metagenòmiques i metatranscriptòmiques de sediments, es dóna llum sobre l'ecologia i els trets funcionals dels procariotes que contenen *merA* i/o *merB*. Es va reconstruir la col·lecció MERCLUB-MAG (amb 803 MAG) i es van seleccionar els MAG que contenien *merAB* (45 MAG) per estudiar-ne l'abundància, l'activitat i les capacitats metabòliques. Les principals troballes són que i)*merB* era més freqüent i actiu que *merA*, ii)les Gammaproteobacteria eren el tàxon més predominant però hi havia una alta novetat taxonòmica i iii)els MAG que contenien *merAB* tenien metabolismes molt diversos.

Paral·lelament es va obtenir la col·lecció de cultius MERCLUB amb la intenció de trobar el millor candidat per utilitzar en bioremediació. Inicialment, vaig triar 46 aïllats per a una avaluació fisiològica general i, després d'un procés de selecció, vaig determinar les taxes de creixement i eliminació de Hg de tres candidats finals: *Aeromonas* sp. MERCC_1069, *Pseudomonas putida* MERCC_1942 i *Bacillus* sp. MERCC_2852. *Aeromonas* sp. va ser eficient en cultius en batch, però finalment es va seleccionar *Pseudomonas putida* MERCC_1942 per optimitzar l'eliminació de Hg en cultiu continu. La soca MERCC_1942 cultivada a altes taxes de creixement presentava una major eficiència d'eliminació de mercuri i ha estat proposada per a finalitats de bioremediació.

Finalment, vaig utilitzar Alteromonas mediterranea ISS312, que es distribueix global i verticalment als oceans, per estudiar els efectes del MMHg en el seu creixement i en

l'expressió dels seus gens. Vaig seqüenciar el genoma i vaig caracteritzar els gens mer, mostrant que té 4 operons diferents. En segon lloc, comparant mostres suplementades amb 5 μM de MMHg amb mostres control, vaig observar una fase de latència més llarga i una expressió diferencial d'alguns gens *mer*. A més, els gens *mer* presentaven patrons de coexpressió molt diversos. Aquests resultats indiquen que aquesta soca bacteriana es pot utilitzar com a model per estudiar la desmetilació i la reducció de Hg.

Introduction



Introduction

From element to contaminant

Mercury is considered among the most toxic heavy metal and it is in the top 10 chemicals of public health concern (World Health Organization, 2020). The chemical symbol for mercury, Hg, comes from the Latin name for liquid mercury (silvery water), hydrargyrum; it is the only metal that is liquid at room temperature, constituting a bad conductor of temperature but a good conductor of electricity. It has a high density and antifungal/antibacterial properties. Hg has been largely used throughout history for different purposes (Figure 1). For example, between 5000 and 2000 b.C., Chinese utilized cinnabar (HgS) to prepare red ink to use as art decoration and in bureaucracy (Clarkson & Magos, 2006; The Met Museum, 2009). Also, liquid Hg has been found in Egyptian tombs (1500 b.C.) and in Maya sepulchers built 1000 years later. Between the 1500s-1900s it was used as treatment for different medical conditions, like skin infections or syphilis among others. The Swiss physician and alchemist Paracelsus, the 'father of toxicology', noted that a little amount of Hg could heal, although too much was fatal. Until mid-19th century, monomethylmercury (MMHg) could not be synthesized in the laboratory, but since then MMHg and other organomercurials have been used as antiseptic and antibacterial agents, or antifungals for agricultural purposes, and it was even added to vaccines. Indeed, the use of Hg for commercial purposes dramatically increased in the last century (Horowitz et al., 2014) and, as a consequence, Hg concentrations rised in all earth compartments, i.e. atmosphere, soils, rivers, lakes, reservoirs, ocean, biota, etc (Obrist et al., 2018; UNEP, 2018).

Over the years, cases of Hg poisoning have been reported worldwide (Elhassani, 1982; Gochfeld, 2003). MMHg poisoning in Minamata Bay was first described in Japan between 1953 and 1960 (Harada, 1995). The Chisso Coorporation's industrial chemical plant was responsible for Hg emissions and the contamination of the Minamata Bay, leading to a catastrophic environmental disaster. The contamination started as early as 1918, the pollution continued, and from 1950 the effects were devastating – fish floating face up, birds falling from the sky and mammals, like pigs or cats, falling into madness and dying (Harada, 1978). There were 2,271 officially diagnosed patients with the Minamata disease (i.e. Hg poisoning), but tens of thousands showed neurological damage concurring with MMHg poisoning (Yorifuji & Tsuda, 2014), in addition to the significant damage caused to the environment (Akito et al., 2014). Other outbreaks occurred worldwide during the 50's and 60's but the next major outbreak happened in Iraq during the early 70's (Bakir et al., 1973). Unlike in Minamata, where the exposure lasted for decades, in Iraq there was an acute exposure in a short period of time, 1.5 years. The outbreak was due to the treatment of wheat seeds with an alkyl-Hg fungicide that were only supposed to be used to grow new plants, but instead were used for human and animal consumption. There were more than 7000 reported cases and 460 hospital deaths attributed to Hg poisoning in rural Iraq during this short period (Bakir et al., 1973). During the 90's, new cases of Hg poisoning were described: 37 people had to be evacuated from their homes because of high Hg concentrations in the air (Fiedler et al.,

1999), and in the Brazilian Amazon MMHg exposure was correlated with reduced psychomotor performance and neurobehavioral changes (Dolbec et al., 2000). Very recently, a multigenerational study was conducted among the Grassy Narrows First Nation, a Canadian indigenous community, linking generational exposure to Hg with suicide attempt among their children and young adults (Mergler et al., 2023).

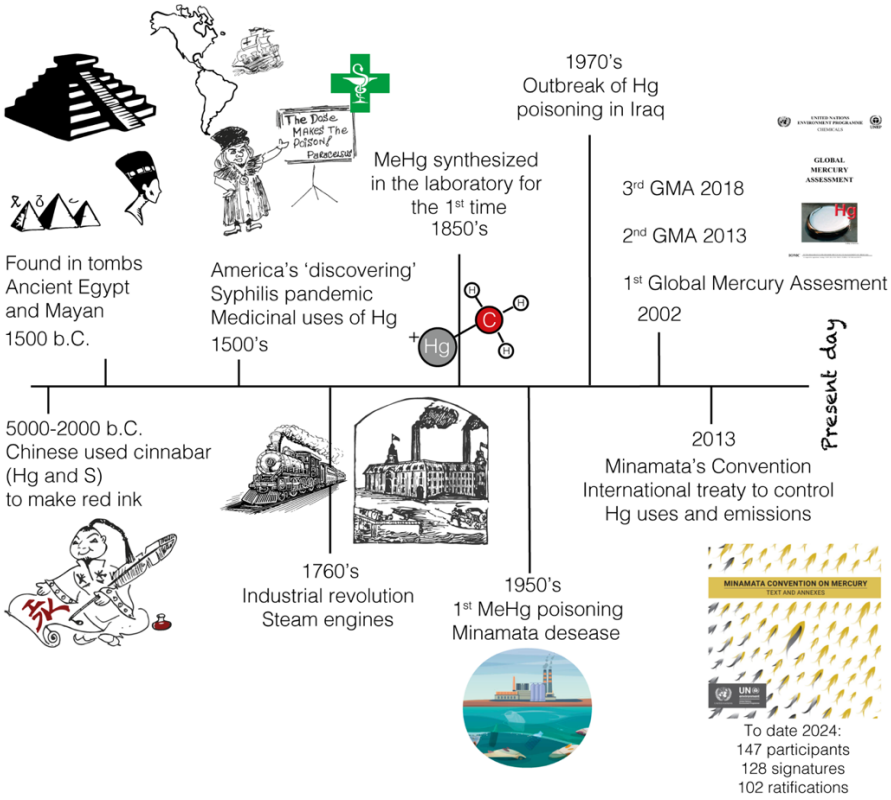


Figure 1: Timeline of Hg uses, poisonings and legislation throughout history.

There are three types of Hg sources that can be emitted into the environment: natural, anthropogenic and re-emissions of Hg already emitted to the environment (Figure 2). Natural sources come from volcanoes and rock weathering and represent only 10 % of the total emissions, whereas anthropogenic sources currently account for 30 % of the total emissions (UNEP, 2013). Re-emissions of Hg to the atmosphere represent 60 % of the emissions (UNEP, 2018), but it is nearly impossible to determine if its origin is natural or anthropogenic, so they has been considered as legacy Hg. In this context, it has been estimated that humans have released about 1,540 Gg of Hg (1.54 x 1012 grams) of which 73 % was released after the 1850's (Streets et al., 2017). Over the past 150 years, an increase of 450 % has been found in the environment, with higher percentages of legacy Hg, which in turn increases re-emissions (Amos et al., 2013; UNEP, 2013).

In particular, there are three main species of Hg in the environment: i) elemental mercury (Hg^0), a volatile form with a long residence time in the atmosphere, allowing it to travel long distances; ii) mercuric or divalent mercury (Hg^{II}), more soluble and with strong affinity for many ligands, especially those containing sulfur; and iii) methylmercury (MeHg), either monomethylmercury (MMHg) or dimethylmercury (DMHg). MMHg can be accumulated in

biota (Mason et al., 1995), and DMHg is a volatile form of organic Hg. The increase of Hg in the environment is of major concern as all chemical forms of Hg are toxic and in severely exposed humans may cause irreversible effects (UNEP & IOMC, 2002).The main symptoms of Hg poisoning, regardless of the species, are neurological: ataxia, loss of sight or hearing, tremors, or in severe cases madness, coma, or death (Clarkson & Magos, 2006; Elhassani, 1982). Moreover, MMHg effects are more severe in developing brains, thus children or fetuses are the most sensitive to its effects (Choi et al., 1978). Hg^0 as a volatile form can be inhaled and produce lung damage, whereas Hg^{II} mostly consumed as salts can be nephrotoxic (Clarkson & Magos, 2006; UNEP & IOMC, 2002). Most human exposure to Hg^0 and Hg^{II} is occupational or through Hg-containing products like dental amalgam (UNEP, 2018). However, the most important MMHg exposure route is through diet– fish, shellfish and marine mammals- (Mason et al., 2012), because MMHg can be bioaccumulated and biomagnified, especially in aquatic food webs. However, MMHg bioaccumulation has also been recently studied in rice grain and it was found that rice consumption in some areas might pose a greater health risk than fish (Zhang et al., 2010).

Due to the rise of Hg levels and the increased awareness of Hg poisoning, over the course of 20 years, all through the 1990's and early 2000's, local regulations were imposed (UNEP & IOMC, 2002) but in 2013 a global treaty was signed, the Minamata Convention on Mercury. The Minamata Convention, ratified in 2017 (minamataconvention.org), is a legal instrument of regulation on Hg emissions worldwide and has the final aim to reduce Hg in the environment and protect human and environmental health (Eriksen & Perrez, 2014; UN, 2013).

In this global context, the ocean plays a key role in the cycling of Hg, as it is the largest reservoir of Hg apart from the deep mineral reservoir (Amos et al., 2013) and the primary source of seafood largely consumed worldwide. As seafood consumption is the main source of Hg for human population, the fate of Hg in the ocean is directly related to human health.

Marine mercury cycle

Sources of Hg into the oceans

Hg can enter the ocean by atmospheric deposition, rivers or estuaries, submarine groundwater discharge (SGD), or submarine geogenic activity (i.e. hydrothermal vents) (Mason et al., 2012). The largest source of Hg into the ocean is atmospheric deposition – 80 % of the total Hg^{II} in the atmosphere is deposited in the oceans (Horowitz et al., 2017). Both Hg^0 and Hg^{II} can be found in the atmosphere and be deposited in the ocean (Jiskra et al., 2021) but also in other water bodies, soils and vegetation as well, by either wet or dry deposition (Horowitz et al., 2017). Hg found in soils or plants will eventually be transported into rivers or lakes through surface runoff or through leaking from the soil to groundwater and eventually reach the ocean through those rivers (Liu et al., 2021) or through SGD (Wang et al., 2018). Some of the most important industries that release Hg into the aquatic systems are: non-ferrous metal production, including gold, zinc, lead, copper, and aluminum (>240 Mg/year), municipal domestic wastewater (>150 Mg/year) and coal-fired power plants and

coal washing (> 90 Mg/year), which contribute large amounts to the total budget of Hg entering rivers, lakes and oceans (Obrist et al., 2018; UNEP, 2018). In the 2018 Global Mercury Assessment, artisanal and small-scale gold mining was excluded from the general budgets due to the large uncertainties found in the numbers, but it is estimated the major source of Hg and it releases (to both land and water) can reach 1220 Mg/year.

The percentage of MMHg as total-Hg (THg) and the vertical distribution and speciation of Hg in the ocean do not follow a clear pattern across ocean basins (Bowman, et al., 2020). The concentration of Hg in coastal areas, in either sediments or waters, is dependent of the above-mentioned inputs and is very variable among sites (Bloom et al., 2004; Chakraborty et al., 2014; Ruelas-Inzunza et al., 2013; Sharif et al., 2014). However, the concentration in the open ocean seems to be driven mainly by atmospheric deposition (Bowman, et al., 2020; DiMento et al., 2019; Mason et al., 2017; Soerensen et al., 2014). The Hg speciation and vertical distribution is the result of a balance between Hg transport and Hg transformations that take place in the environment.

Hg transformations in the ocean

Once Hg reaches surface ocean, Hg^{II} and Hg^{0} can be reduced or oxidized respectively and/or re-emitted to the atmosphere (Gworek et al., 2016; Figure 2). Hg^{II} in the ocean might: i) bound to organic matter or inorganic particles and eventually sink into deeper layers of the ocean or into the sediment or ii) be methylated to form MMHg along the water column or in the sediments. The methylation of Hg^{II} has been recently studied as a biological transformation mediated by prokaryotes containing the *hgcAB* gene cluster (Parks et al., 2013). Besides the presence of these microorganisms, there are physico-chemical conditions that may influence the bioavailability of Hg^{II} such as the composition of the organic matter (Chiasson-Gould et al., 2014; Moreau et al., 2015; Schartup et al., 2015) as well as the activity of the whole microbial community, including those containing the *hgcAB* gene cluster such as temperature (Guimarães et al., 2006), oxygen concentrations or salinity (Compeau & Bartha, 1984). Subsequently, the formed MMHg, can be bioaccumulated and biomagnified through the aquatic food webs (Mason et al., 2012; UNEP, 2018). MMHg can also be demethylated back to Hg^{II}, either photochemically (Seller et al., 1996) or biotically through the *merB* gene (Spangler, et al., 1973) or methylated again to form the gaseous dimethylmercury (DMHg) (Baldi et al., 1993). While photochemical demethylation might be a significant contributor to the total demethylation in freshwaters and in surface waters (Black et al., 2012; Seller et al., 1996), biological demethylation is likely to dominate in the aphotic areas, such as the deep ocean and sediments.

The concentrations of both THg and MeHg in open ocean waters are at picomolar concentrations (Bowman et al., 2016; Cossa et al., 2009, 2011; Dastoor et al., 2022; Gionfriddo et al., 2016), which makes very difficult to obtain accurate Hg measurements in the water column. Additional analytical challenges arise when we try to measure the volatile forms of Hg (Hg^{0} and DMHg) (Bowman, et al., 2020). Some studies report MeHg concentrations, which include both MMHg and DMHg (e.g. Bratkič et al., 2017), others state

both separately (e.g. Bowman et al., 2015; Munson et al., 2015) and others only describe dissolved gaseous Hg (Hg^0 and DMHg, e.g. Kotnik et al., 2007; Monperrus et al., 2007), which makes difficult to have an overview of the Hg speciation along the water column (Kleindienst et al., 2023). In order to measure Hg concentrations in environmental samples, there are three general steps: i) extraction of all Hg species from the sample, ii) separation of Hg species and iii) detection. In the separation step, three common techniques can be used: gas chromatography (GC), high pressure liquid chromatography (HPLC) and cold vapor (CV), which can be coupled with one or multiple detectors to obtain the desired measurements, such as ICP-MS (Inductively Coupled Plasma Mass Spectrometry) which has the lowest limit of detection among the methods available for Hg measurement, or AFS (Atomic Fluorescence Spectroscopy) which is the most popular (Huang, 2024; Leermakers et al., 2005). Using ICP-MS allows to quantify individual isotopes of Hg and to apply the isotopic dilution methodology (Hintelmann & Evans, 1997). Besides, this last method can be used to determine not only THg and MeHg concentrations, but also Hg transformations (methylation and demethylation) (Monperrus et al., 2007, 2008; Rodríguez-Castrillón et al., 2008).

Considering that concentrations of THg and MeHg in the ocean water column are in the picomolar range and that measuring the changes in such small concentrations is methodologically very difficult, Hg transformation rates have been rarely detected (Despins et al., 2023; Lehnherr et al., 2011; Monperrus et al., 2007; Munson et al., 2018). As most of the ocean is aphotic, it is expected that biological processes dominate the Hg cycle, so it is of great importance to study the microorganisms responsible for the reactions in order to understand the global Hg cycle.

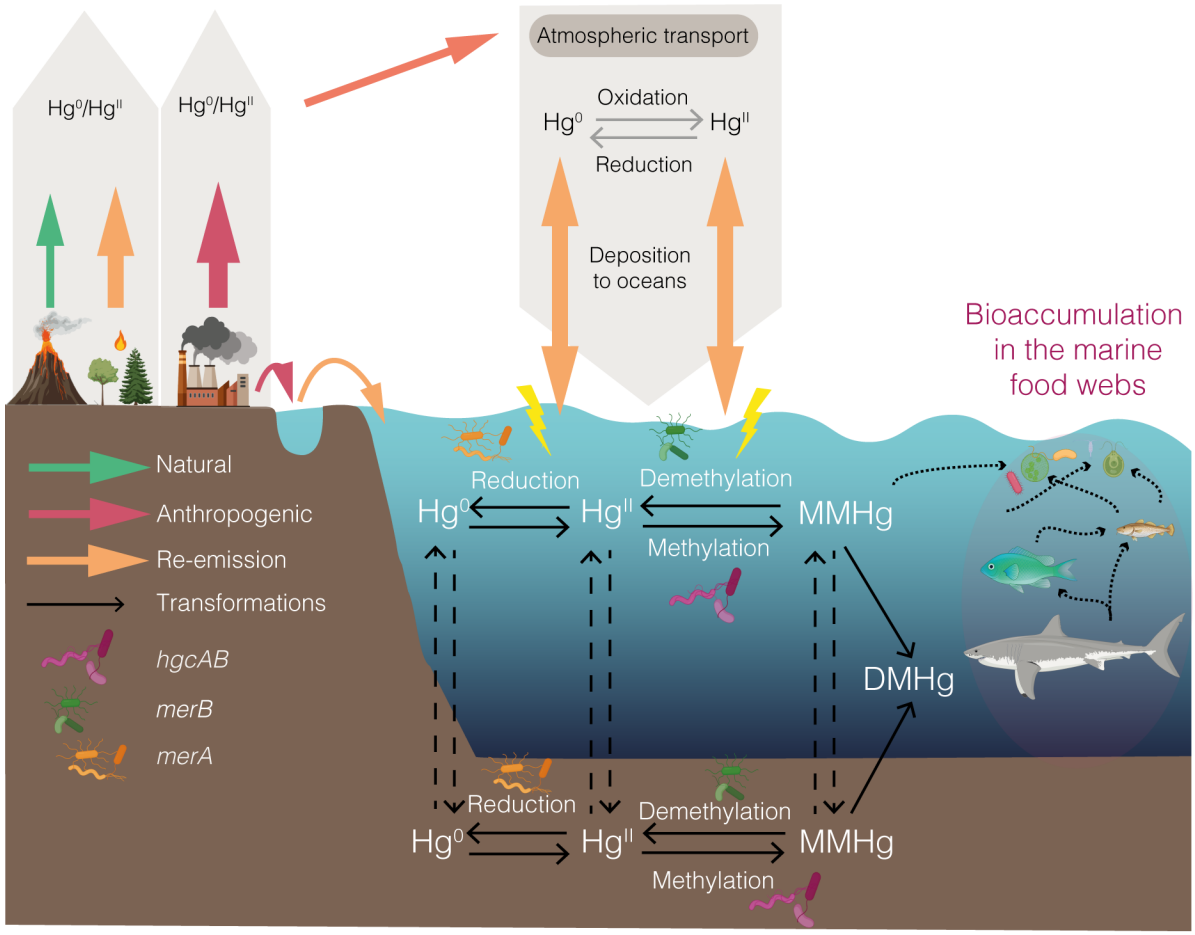


Figure 2: The marine Hg cycle. The shown transformations focus on the processes, occurring either in sediments or in the seawater column. Hg^0: elemental mercury. Hg^{II}: divalent mercury. MMHg: Monomethylmercury. DMHg: Dimethylmercury. Figure modified from Sanz-Saez, 2020.

The biological mercury cycle

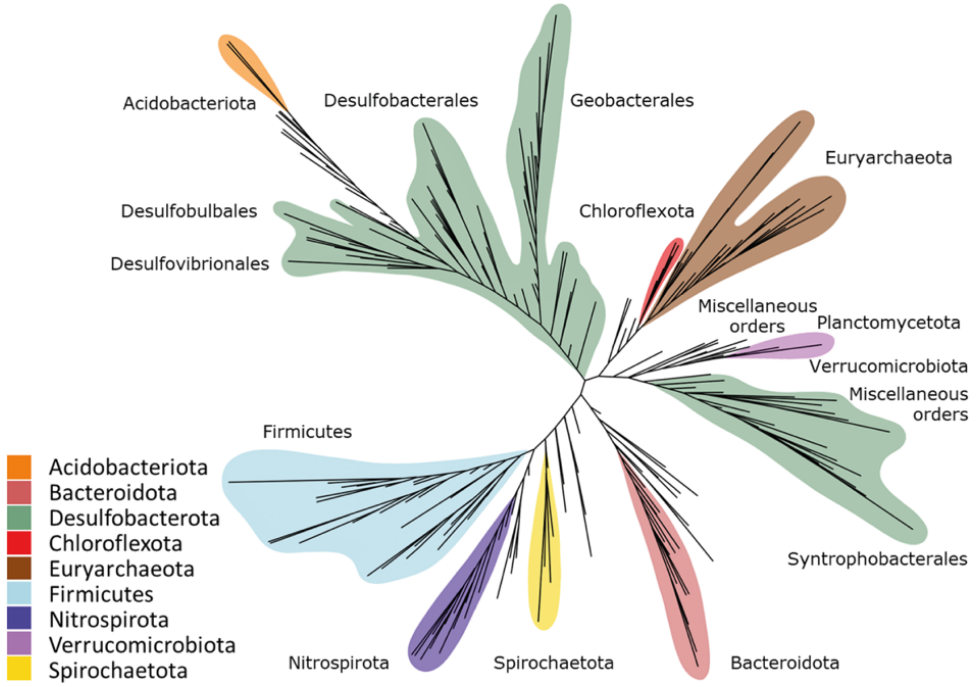
There are several transformations in the Hg cycle that can be carried out by microorganisms. Thus, methylation, demethylation and reduction can be mediated through different prokaryotic genes and have a prevailing role in the marine Hg cycle.

Mercury methylation: *hgcAB* genes

Biotic Hg methylation is carried out by the gene cluster *hgcAB* (Parks et al., 2013) which codes for protein HgcA, a cobalamin-dependent methyltransferase, and HgcB, which works as an electron transfer in the reaction (Smith et al., 2015). Historically, Hg methylation has been associated to the activity of sulphate-reducing (SRB) (Compeau & Bartha, 1985) and iron-reducing bacteria (FeRB) (Fleming et al., 2006), but later, several studies revealed that this metabolic capacity was more diverse than previously thought including Desulfobacterota (SRB), Acidobacteriota, Verrucomicrobiota, Marinimicrobia, Spirochaetota or Euryarchaeota (methanogenic archaea) among others (Figure 3) (Capo, et al., 2023; Gilmour et al., 2013; Gionfriddo et al., 2016; Lin et al., 2021, 2023). Methylation is primarily found in anoxic and oxygen deficient environments, like sediments, wetland or ponds, or anoxic water columns

(Bravo et al., 2015; Drott et al., 2008; Herrero Ortega et al., 2018; Lehnherr et al., 2011; Malcolm et al., 2010; Tjerngren et al., 2012); but recently it has been shown that methylation might also occur in oxic water columns (Capo, et al., 2023; Gascón Díez et al., 2016; Rodríguez et al., 2022). Capo et al. (2023) and Gascón Díez et al. (2016) highlighted the role of suspended particles in methylation as they might provide a micro-anoxic environment to the Hg methylation prokaryotes (typically anaerobic) within a normoxic ecosystem.

Figure 3: Simplified unrooted phylogenetic tree of *hgcA* sequences from the Hg-MATE database



(Gionfriddo et al., 2021). Taxonomy is based on the GTDB classification. Microbial groups with the highest diversity of *hgc*+ microorganisms are denoted by colours. Illustration from Capo et al. (2023).

The *mer* operon

As mentioned above, MMHg demethylation can be biotically mediated by the action of a diverse group of prokaryotic organisms, harboring the *mer* operon, and could be the main way of MMHg demethylation in the aphotic layers of the ocean. Biological demethylation is usually followed by the reduction of Hg^{II}, so the final products would be a methyl group (CH_3^+) and Hg^0. This chain reaction is mediated by two enzymes coded in the *mer* operon: *merA* and *merB* (Barkay et al., 2003). Gene *merA* encodes for a mercuric reductase (MerA) and is a cytosolic flavin-dependent disulfide oxidoreductase (Furukawa & Tonomura, 1972). MerA is responsible for transforming Hg^{II} into Hg^0 and confers narrow-spectrum resistance (resistance only to inorganic mercury) (Figure 4) (Furukawa & Tonomura, 1972; Izaki et al., 1974; Summers & Lewis, 1973). Gene *merB* encodes for an organomercurial or alkylmercury lyase and is responsible for breaking the bond between the carbon and Hg (Figure 4)

(Schottel, 1978; Tezuka & Tonomura, 1976). There are different variants of these enzymes, with more affinity to certain substrates , e.g. in *Pseudomonas* sp. K62, variant S-1 can use

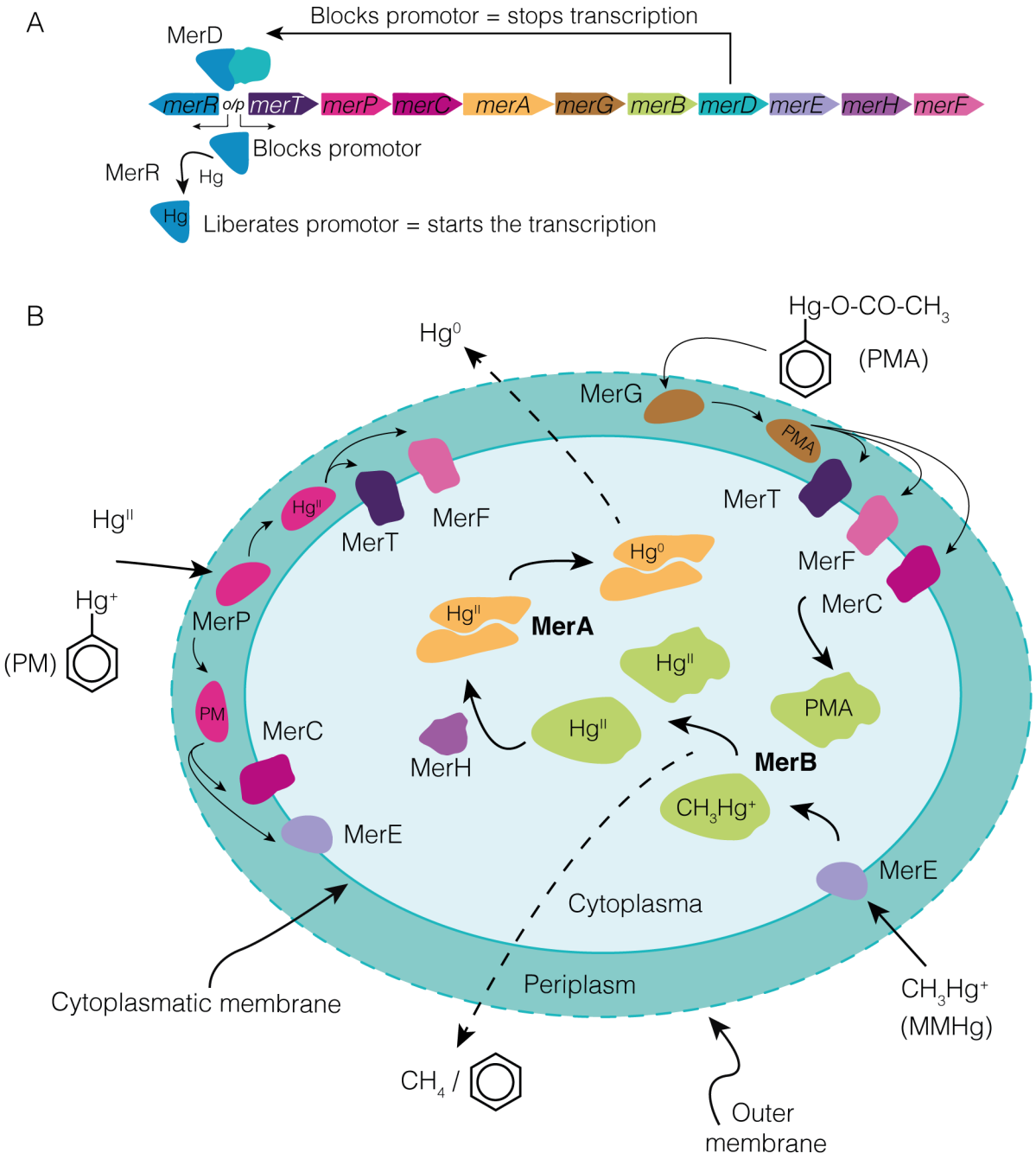


Figure 4: A. Generic *mer* operon with all possible genes. Note that not all genes need to be present in the operon to be functional and confer Hg resistance. B. Cellular *mer* -encoded Hg resistance mechanisms. The outer membrane is dashed, illustrating that is not present in all prokaryotes. The colors of various Mer proteins correspond with the colors of the genes that encode for these proteins in panel A. PMA: phenylmercuric acetate. MMHg: Monomethylmercury. PM: phenylmercury. Modified from Lin et al., (2011).

phenylmercuric acetate (PMA), p-chloromercuric benzoate (PCMB) and MMHg as substrates, while S-2 variant utilizes PMA and PCMB as well, but no activity was reported with MMHg (Tezuka & Tonomura, 1976, 1978). MerB confers broad-spectrum resistance and historically it was assumed that *merB* could only appear as part of the *merA* containing operon; nonetheless, a large number of *merB* genes have been recently found in microbial genomes without the *merA* (Christakis et al., 2021).

The regulating components of the *mer* operon are MerR (coded in *merR*), a transcriptional activator-repressor (O'Halloran et al., 1989; O'Halloran & Walsh, 1987), MerD (encoded in *merD*) which is antagonist of MerR (Mukhopadhyay et al., 1991; Nucifora et al., 1989) and MerO, an operator laying between the promotor and the structural genes. In 'normal conditions' with no Hg^{II} present, MerR forms a non-transcriptional complex with RNA polymerase and binds to MerO, blocking the promotor of the *mer* operon. On the other hand, in the presence of Hg^{II}, it binds to MerR, changing its conformation and liberating the promotor, thus allowing for the transcription to begin (Figure 4) (Brown et al., 2003). MerD is transcribed alongside the rest of the *mer* operon components but in small amounts and binds to MerO and to MerR, blocking again the promotor and stopping the transcription (Champier et al., 2004).

The *mer* operon can have one or multiple transporters, either membranal, cytosolic or periplasmic. The membrane located proteins can have a different number of transmembrane helices: MerT (with a variant number of transmembrane helices), MerC (with four) and MerF and MerE (with two) are inner membrane transporters of mercuric compounds (Figure 4) (Barkay et al., 2003; Lin et al., 2011; Sone et al., 2013). MerP, a periplasmatic protein, enhances the uptake of Hg, promoting the entrance of Hg^{II} when coupled with membrane transporter MerF or MerT, and the uptake of phenylmercury ($C_6H_5Hg^+$) when coupled with MerE or MerC (Sone et al., 2013). MerG, as well as MerP, is a periplasmatic protein and it targets the specific compound phenylmercuric acetate (PMA) (Lin et al., 2011). Additionally, a new transporter, MerH, has been described as a cytoplasmic metallochaperone, that may play two roles in mercury resistance: facilitate the transport of Hg^{II} to MerA and coregulate the transcription with MerR (Figure 4) (Schelert et al., 2013).

A wide diversity of bacteria are able to resist and transform Hg due to the presence of plasmids (Clark et al., 1977; Foster, 1987; Miki et al., 1978; Novick & Roth, 1968; Olson et al., 1979; Schottel, 1978; Smith, 1967; Weiss et al., 1977) which makes prokaryotes containing the operon *mer* very diverse taxonomically. Additionally, *mer* genes as well as other resistance genes (to other metals or to antibiotics) have been associated with the presence of genomic islands (Ivars-Martinez et al., 2008; Pathak et al., 2020), mobile genomic elements that can be horizontally transferred to make bacteria more versatile. Christakis et al. (2021) compiled a database with 7544 *merA* genes distributed among 49 phyla (12 archaeal and 37 bacterial, Figure 5) and 1936 *merB* genes assigned to 17 phyla (2 archaeal and 15 bacterial). Most of the studied *merA* genes belong to Pseudomonadota (53 %), and specially to Gammaproteobacteria, while most of the studied *merB* genes belong to Bacillota (41 %). Some of the genomes reported in Christakis et al. (2021) contained up to eight copies of

merA or *merB* gene, a phenomenon most likely to occur when the microorganism lives in a contaminated site.

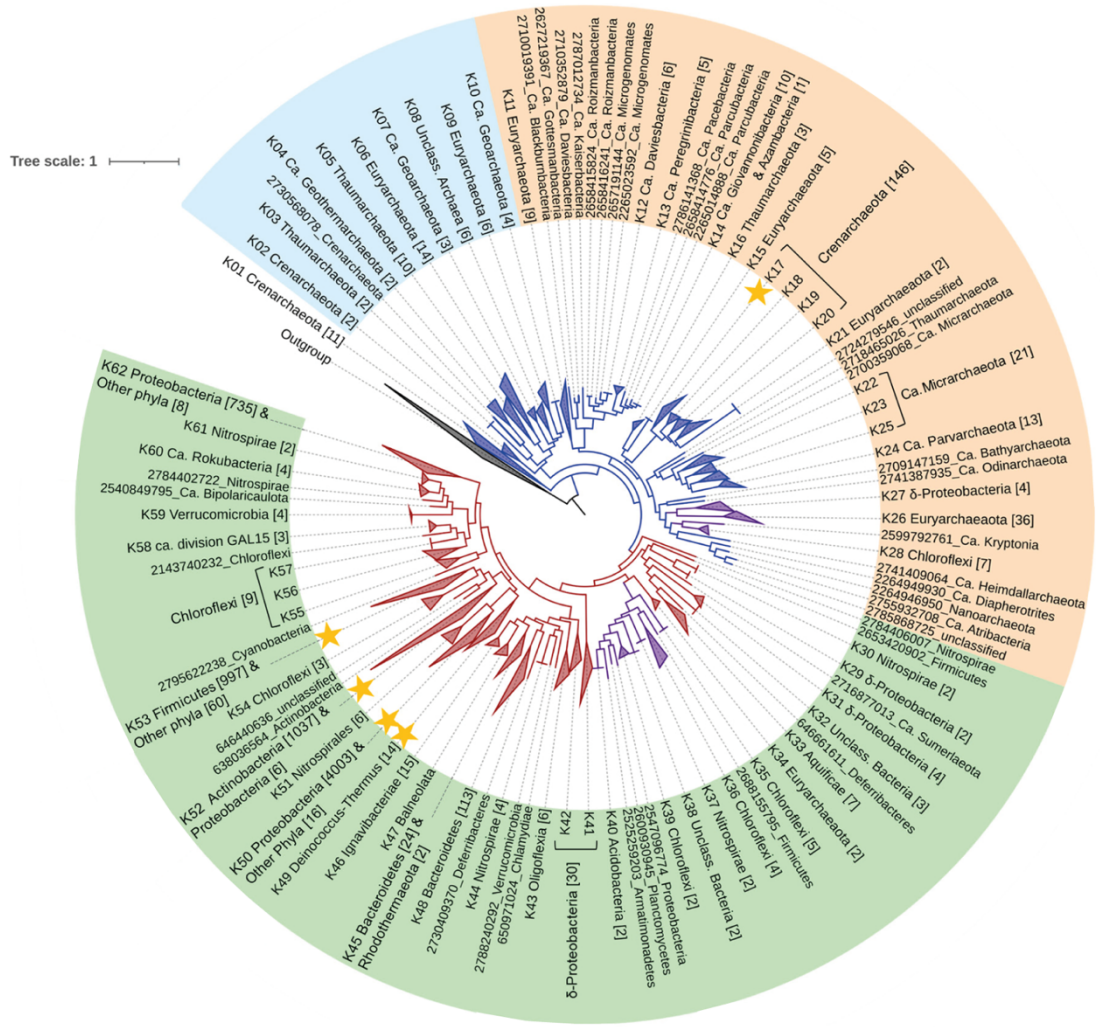


Figure 5: Phylogenetic tree of MerA protein homologs (plasmid MerA not included). Archaeal clade are colored in blue and bacterial clades in red, while purple-colored clades denote mixed lineages. The colors covering the labels denote the three main groups of MerA: group A in light blue, group B in orange and group C in green. The outgroup consists of 6 bacterial and archaeal dihydrolipoamide dehydrogenase sequences. Tree scale is in amino acid substitutions per site. Yellow stars mark lineages in which MerA activity has been confirmed. Illustration from Christakis et al. (2021).

Approaches to study microorganisms involved in the mercury cycle

Traditionally, many of the first microbial-related discoveries were possible thanks to cultures (microorganisms that can grow under laboratory conditions). Culture-dependent techniques include traditional methods such as enrichment cultures and more innovative methods like microencapsulation. Classical enrichment cultures assume a defined group of conditions (temperature, nutrients, oxygen, etc) to enrich or select for certain microorganisms (Overmann et al., 2017). The first Hg-resistant bacteria, a clinical isolate of *Staphylococcus aureus*, was discovered in 1960 (Moore, 1960). Green (1962) and Smith (1962) started to study Hg resistance in pathogens causing epidemics in hospitals and concluded that the mercury resistant strains were more common in the "epidemic" strains. In 1964, Magos et al. demonstrated for the first time that bacteria can volatilize Hg, and in 1967, Smith used 55 isolates to describe the R factors (later called plasmids), which were responsible for Hg as well as other metals resistance. During the 1970's and 1980's many studies were done to characterize the Hg resistance and the *mer* genes. Thus, the mechanism of MerA was unveiled by using protein extracted and purified from *Escherichia coli* (Izaki et al., 1974; Komura et al., 1971; Komura & Izaki, 1971). The functioning of MerB was discovered in *Pseudomonas* (Furukawa & Tonomura, 1971) and further characterized as a group of proteins (Tezuka & Tonomura, 1976, 1978), while *mer* containing plasmids were studied with the purpose of understanding diversity and ecology of Hg resistant microorganisms (Clark et al., 1977; Miki et al., 1978; Schottel, 1978; Summers & Lewis, 1973; Summers & Silver, 1972; Weiss et al., 1977). While most people focused on the molecular biology aspect, some researchers started to investigate the ecology of the Hg resistant bacteria in aquatic systems, (Nelson & Colwell, 1975; Spangler, Spigarelli, Rose, & Miller, 1973) or the effects of Hg in the physiology and growth of the cells (Vaituzis et al., 1975). Later molecular studies centered on the transporters and regulation, like for example the role of MerT and MerP in the Hg resistance (Hamlett et al., 1992; Lund & Brown, 1987) or the discovery and characterization of the regulators MerR (I. W. Lee et al., 1993; O'Halloran et al., 1989; O'Halloran & Walsh, 1987) and MerD (Champier et al., 2004; Mukhopadhyay et al., 1991; Nucifora et al., 1989).

Simultaneously, the biological formation of MMHg was also studied (Jensen & Jernelöv, 1969; Wood et al., 1968). In the mid 80's, Compeau and Bartha associated Hg methylation in sediments to sulfate reducing bacteria (Compeau & Bartha, 1985). Other studies further proved the connection between sulfate reduction and Hg^{II} methylation (Gilmour et al., 1992; King et al., 2001) but during the early 2000's other two groups of prokaryotes proved to be methylators, i.e., FeRB (Fleming et al., 2006) and methanogens (Hamelin et al., 2011; Yu et al., 2013). While the genetic bases of Hg resistance (*mer* operon) were heavily studied last century, the genes responsible for methylation (*hgcAB* genes) were not discovered until 2013 by Parks et al. in which they used *Desulfovibrio desulfuricans* ND132 and *Geobacter sulfurreducens* to demonstrate that the knockout's of the *hgcAB* genes (same bacteria without the genes) did not methylate. After the *hgcAB* genes were found, Gilmour et al. (2013) preselected cultures with *hgcAB* genes, as well as genomes closely related to them and

tested their methylation capacities, increasing the number (from 6 to 20) and the diversity (from only Deltaproteobacteria to Firmicutes and Archaea) of Hg^{II} methylators.

Culture-dependent techniques are necessary in many fields of both research and industry, and they might provide an incredible and invaluable source of information about the morphology, physiology, and metabolic characteristics of prokaryotes. Cultures allow to answer fundamental questions of how Hg can affect prokaryotes at a cellular level. Additionally, isolates can be used in different industrial processes, including bioremediation, which is defined as the use of either naturally occurring or deliberately introduced microorganisms to consume and break down environmental pollutants, in order to clean a polluted site. As series of studies have proposed the use of microorganisms like *Pseudomonas* sp. (Chang & Law, 1998; Horn et al., 1994; Okino et al., 2000; von Canstein et al., 1999) or *Bacillus* sp. (Dash et al., 2014; Huang et al., 1999; Kaur et al., 2022) as Hg bioremediators for different contaminated environments or wastes.

On the other hand, the so-called culture-independent methodologies revolutionized in the 80's the study of microbial diversity, previously constrained by our inability to grow the majority of microorganisms, and allowed their identification circumventing cultivation. Thus, culture-independent methods allow a more complete picture of the diversity of microbial assemblages. In the 80's, Barkay and colleagues designed and used in environmental samples the first DNA probe to detect *mer* genes by DNA-DNA hybridization without prior isolation (Barkay et al., 1985, 1989). Environmental studies continued with the development of PCR (Polymerase Chain Reaction), which was first used to find *merRTP* genes in soils (Bruce et al., 1992, 1995) and later used to measure the expression of *merA* and *merB* by real time PCR (RT-PCR) (Jeffrey et al., 1994, 1996; Nazaret et al., 1994; Schaefer et al., 2004). The use of PCR for studying *hgcAB* genes was delayed because the gene was not discovered until 2013 (Parks et al., 2013). Some of the first studies analyzed the diversity of *hgcA* in wetlands (Schaefer, Kronberg, et al., 2014) and the relationship among methylation rates and *hgcA* transcripts (through RT-qPCR) (Bravo et al., 2016). The primers were improved to obtain as much diversity as possible (Christensen et al., 2016; Gilmour et al., 2018; Gionfriddo et al., 2020). Recent advances (early 2000's) in technology, such as high-throughput sequencing and the development of bioinformatic tools, allowed to analyze massive amounts of microbial genes (DNA) or transcripts (RNA) (i.e. metagenomics or metatranscriptomics) to study all genes present in a microbial community. Thus, molecular techniques allowed to study not only the *mer* but also the *hgcAB* genes in unexplored environments like the Antarctic sea ice (Gionfriddo et al., 2016), or open ocean (Bowman, et al., 2020), obtaining incredibly large datasets from around the world for both *merAB* (Christakis et al., 2021) and *hgcAB* (Podar et al., 2015; Villar et al., 2020). Moreover, metagenomic reads can be assembled into contigs and later binned into genomes, the so-called Metagenomic Assembled Genomes (MAGs). MAGs are composite genomes of populations from natural communities that provide insights into the ecology, function and evolution of marine microbial taxa. Using this approach, Lin et al. (2021) found in the Saanich inlet (Canada) a previously overlooked phylum (Marinimicrobia) that might be an important

methylator. Furthermore, Capo et al. (2022) was able to reconstructed 10 MAGs with *hgcA* from the Baltic sea water column and was able to conclude that the methylating community is more metabolically versatile than previously thought, presenting different metabolisms among the different redox conditions.

More recently, studies have combined cultures with a multi-omics approach to better understand Hg methylation and Hg detoxification processes inside the cell. LaVoie & Summers (2018) used *E. coli* to characterize the transcriptomics changes in the presence of PMA and $HgCl_2$. Some have used culturable methylators to found the biological function of *hgcAB* (Gionfriddo et al., 2023; Qian et al., 2016). Others have evaluated different aspects of the physiology of Hg resistance (An et al., 2019; Zheng et al., 2018). However, none of them assessed the demethylation of MMHg and the transcriptomic changes that might occur in this process.

Mercury and the global change

Our world is enduring extreme situations, like over-population or immense exploitation of the change. There are chemical, physical and anthropogenic drivers that affect and will continue to affect the Hg cycle and MMHg formation in the environment (Krabbenhoft & Sunderland, 2013). Many of the global change effects are irreversible, especially in the ocean and sea ice (IPCC, 2021). Global change effects are becoming more intense in the recent years, and they affect directly and indirectly the Hg cycle. Direct effects like higher temperatures or droughts will mobilize Hg due to wildfires (Kumar et al., 2018) or loss of permafrost and sea ice (Dastoor et al., 2022; Lim et al., 2020; Schuster et al., 2018) which accounts for an incredible large reservoir – 49,000 Mg compared with the 4000 Mg of Hg found in the atmosphere (Sonke et al., 2023). It is unknown what percentage will be re-mobilized and end in the ocean, but it may very well be a factor of global importance in the upcoming decades.

Increasing sea temperature (Cheng et al., 2019) decreases oxygen solubility in the oceans (Breitburg et al., 2018; Schmidtko et al., 2017), disrupts the distribution of nutrients, which can cause the stratification of the water (Hutchins & Fu, 2017; Sonke et al., 2023), and change the microbial community which further contributes to the two prior consequences (Sonke et al., 2023). Both the expansion of oxygen minimum zones and the eutrophication might enhance hypoxic conditions in the ocean and specially in coastal areas (Breitburg et al., 2018) which will favor anaerobic metabolisms prone to Hg^{II} methylation (Sonke et al., 2023).

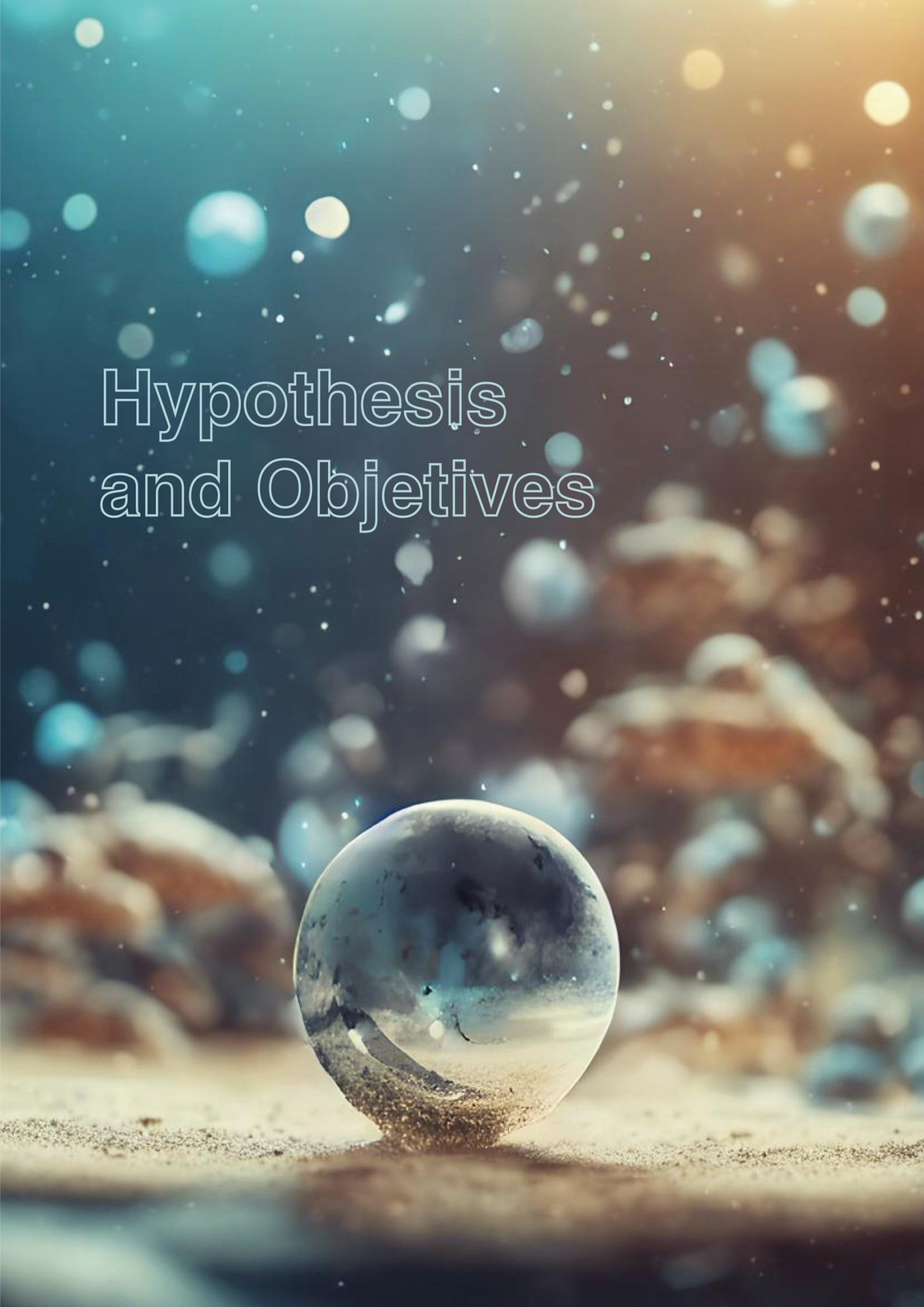
Although Hg emissions have been regulated under the Minamata convention, a directive which is supposed to decrease Hg levels in the environment, it has been modeled that the MMHg concentrations in fish (Atlantic bluefin tuna) tissues would increase with the temperature rise, even taking into consideration the expected decrease in MMHg concentrations in waters (Schartup et al., 2019). Additionally to modeling the scenarios of higher temperature and lower MMHg concentrations, Schartup et al. (2019) analysed the impact of chanes in the food web structure in MMHg concentration of two commercially interesting species (Atlantic cod and Spiny dogfish). Due to overharvesting clupeids, both species had to change their diet, but cod changed it to larger fish or lobster (with less MMHg

than clupeids) and dogfish changed it to squid and other cephalopods (with more MMHg than clupeids). The changes in diet resulted in changes in the bioaccumulation pattern, having a cod population with less MMHg in their tissues and a dogfish with a heavier load of MMHg. This study showed that the consequences of current human actions (e.g. overfishing) can determine human exposure to MMHg.

Lastly, sea level rise is expected to increase the risk of flooding in coastal areas (Vousdoukas et al., 2018) which is known to release Hg as well as nutrients (Singer et al., 2016). The risk and cost of flooding can be managed by hard protection structures, like barriers or dikes, and soft or ecosystem-based protection systems such as beach nourishment. Another adaptative measures that can be taken are accommodation of the areas at risk (e.g. elevating buildings or land reclamation) and retreat (e.g. temporal or permanent relocations) which are highly unlikely due to their economic cost (Dedekorkut-Howes et al., 2020). These adaptations, especially the protective ones either hard or soft, may affect the environmental conditions and Hg cycling in the area.

All in all, the monitoring of MMHg concentrations in biota and environmental samples, the measurement of Hg^{II} methylation potentials and the study of methylating and MMHg demethylating bacterial communities is of great importance in the context of global change.

Hypothesis and Objetives



Hypothesis and Objectives

The general aim of this thesis is to improve the current understanding of the ecology and physiology of marine bacteria involved in the Hg cycle and evaluate their potential role in biological transformations (methylation, demethylation, and reduction) from both an environmental and a cellular perspective.

To achieve this major goal, this thesis addresses specific objectives summarized in Figure 6 and is structured into four chapters aimed to:

- Measure the Hg methylation of sediments in the Venice Lagoon and assess the risk of increased MMHg concentrations in coastal areas due to global change (Chapter 1).
- Explore the ecology and functional capacity of Hg-resistant prokaryotes, especially for demethylating and reducing microbial taxa (Chapter 2).
- Isolate and characterize the candidate with the best performance for bioremediation of Hg polluted environments (Chapter 3).
- Establish the transcriptional patterns during the demethylation of MMHg to improve our understanding of this process at a cellular level (Chapter 4).

In a current scenario of an increase of Hg environmental levels produced during the last century, combined with the urban development in coastal areas and the expected increase in water temperature and decrease in oxygen caused by the global change, I hypothesize that MMHg levels might raise in the ocean at a global change. To test this hypothesis, Chapter 1 focuses on the Venice Lagoon (Italy), a unique study site extremely affected by human-induced alterations and global change. To prevent flooding during high tides or 'Aqua altas' in Venice, the government built a system of barriers (MOSE) that can close the lagoon and reduce its communication to the Adriatic Sea. The number of high tides has dramatically increased in the last century and thus the risk of flooding and the number of times that the lagoon needs to be closed. While the lagoon is isolated, the water exchange diminishes and oxygen concentration in the water column may decrease. Additionally, higher sea temperatures and enhanced bacterial activity can contribute to further deoxygenate the waters of the Venice Lagoon. These conditions could potentially boost the growth of anaerobic methylating bacteria and thus increase MMHg concentrations. In this chapter, by combining a field study with laboratory experiments, I showed enhanced MMHg formation in sediments and MMHg concentrations in water during a simulated MOSE-closing event in the Venice Lagoon.

It has been established that methylation occurs mainly in the sediment, and the advances in microbial communities sequencing approaches have provided the opportunity to study the ecology and function of prokaryotes involved in this process in great detail. However, information on the performance of the demethylating community in marine sediments is still lacking. Chapter 2 describes the composition, abundance, and activity of the demethylating and reducing prokaryotes in contaminated sediments from three areas of the coast of Europe (Cantabrian Sea, Mediterranean Sea and Baltic Sea) involved in the Hg cycle through 'omics'

approaches. Using metagenomics, I was able to reconstruct Metagenome-Assembled Genomes (MAGs) and characterize them at a taxonomic, functional, and metabolic level. Furthermore, using metatranscriptomics, I investigated how these microbial genomes (MAGs) were actively transcribed as whole genomes and at the level of the *mer* genes. A total of 45 MAGs with Hg related genes (*merAB*) associated to phylogenetic diverse taxa and with different transcriptional patterns, were found in the studied sediments. This study thus showed that demethylating and reducing communities were conducted by diverse taxa and potentially active in sediments.

In a global scenario of increased MMHg concentrations and in the context of the legally binding Minamata Convention, it is necessary to develop management strategies that decrease Hg levels in the environment. I hypothesized that bacteria isolated from different Hg-impacted marine compartments (seawater and sediments) could potentially be used to decrease MMHg and Hg in controlled conditions and be applied for bioremediation. The objective of Chapter 3 was to find the best candidate for marine sediment Hg bioremediation. Using the same Hg-contaminated sediments from chapter 2, a large culture collection was obtained. The Hg detoxification capacity was tested and characterized in a total of 46 Hg resistant bacteria from the MERCLUB Culture Collection (MERCC). For one of this strains, the conditions for Hg detoxification were optimized using the continuous culture technique, a highly efficient methodology utilized to study bacterial physiology under controlled environmental parameters. This chapter pointed that the strain *Pseudomonas putida* MERCC_1942 was the best candidate for Hg bioremediation under continuous culture conditions when grown at high growth rates.

The physiology and expression patterns of a *mer* operon might help to better predict the occurrence and relevance of this process in the ocean at a global scale. In Chapter 4, taking advantage of the large bacterial heterotrophic culture collection (MARINHET), I performed a genomic characterization of the strain *Alteromonas mediterranea* ISS312, a bacterium with multiple *mer* operons that is globally and vertically distributed in the ocean. In this chapter, the transcriptional changes in expression patterns during different growth phases were described for the four different *mer* operons.

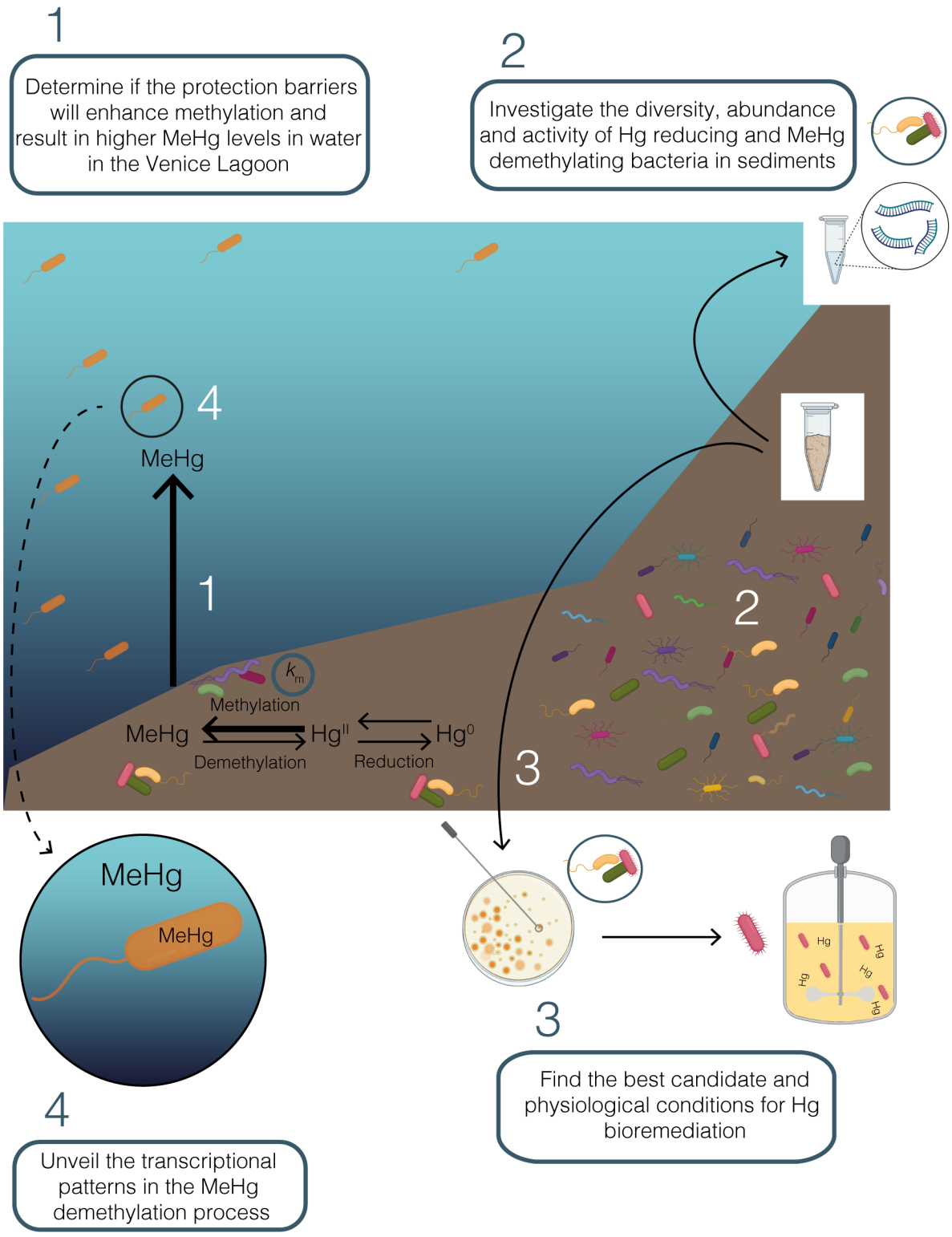
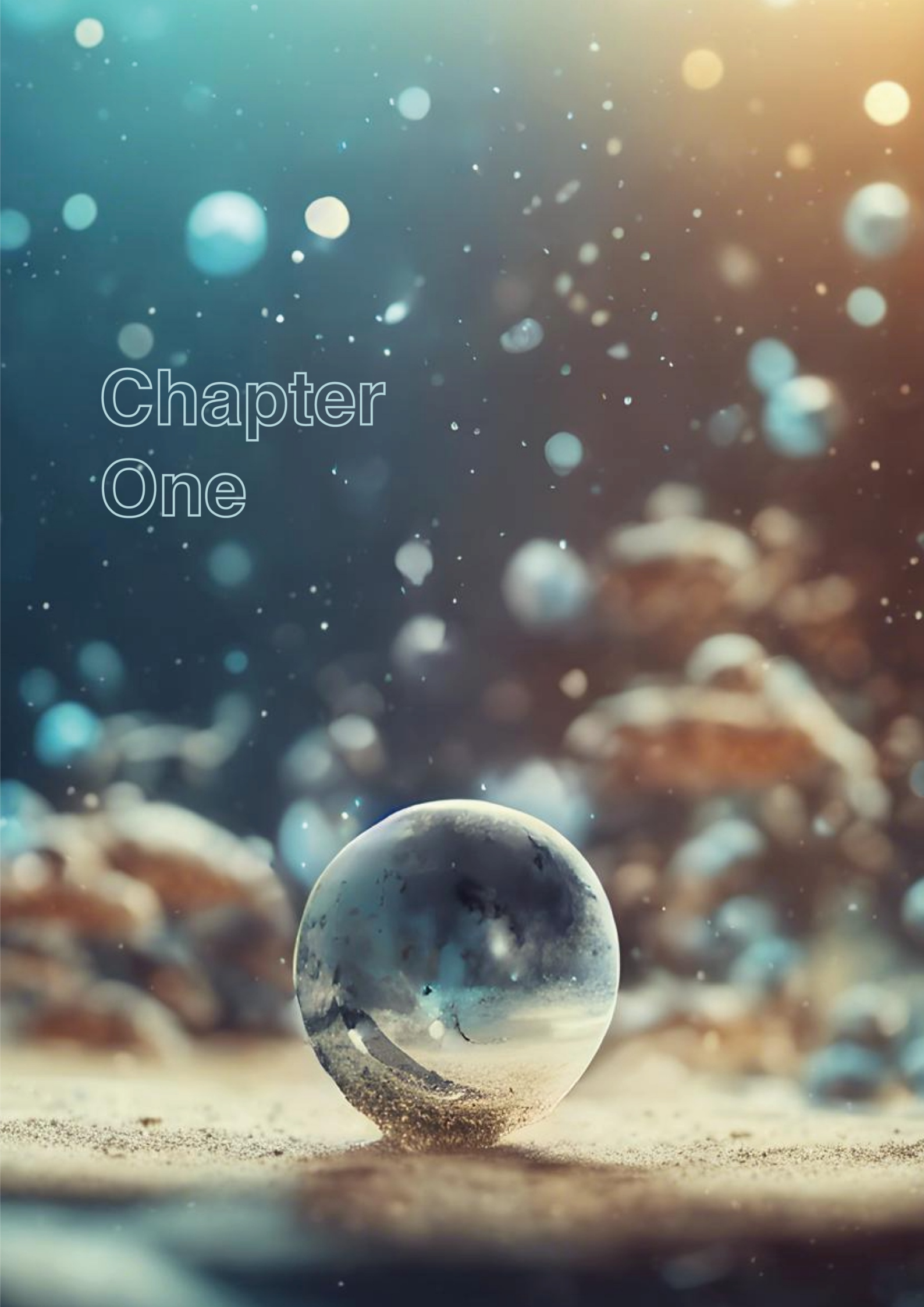


Figure 6: Graphic representation of the main research question or objective of each chapter of this thesis.


Chapter
One

Chapter 1: Potential impact of tide-regulation barriers on the formation of methylmercury

Abstract

Monomethylmercury (MMHg), one of the most toxic pollutants, is formed mainly under anaerobic conditions. The "Modulo Sperimentale Elettromeccanico" (MOSE), built to temporarily close the Venice Lagoon and to protect the city from high tide events, induces changes in the hydrological regime, reducing water circulation with the subsequent decrease in the dissolved oxygen concentrations of the lagoon. In this study, we assessed the potential changes in sediment and overlying water physico-chemistry in a simulated MOSE closing-event by incubating intact sediment cores for 48h in the laboratory and installing in situ benthic chambers. A significant increase in total dissolved Hg and MMHg concentrations in the water column was observed, associated with an increase in MMHg formation rates in incubated cores. In particular, MMHg formation rates doubled during the simulated MOSE closing-event. A release of dissolved organic carbon and an enrichment of proteinaceous substances and reactive humic acids in the overlying waters was also observed during incubation, which could explain the increase in MMHg accumulation in the overlying waters. Our study highlights that hydrological changes caused by the MOSE closure may increase MMHg concentrations within the Venice Lagoon and thus favor the accumulation of Hg in aquatic food webs.

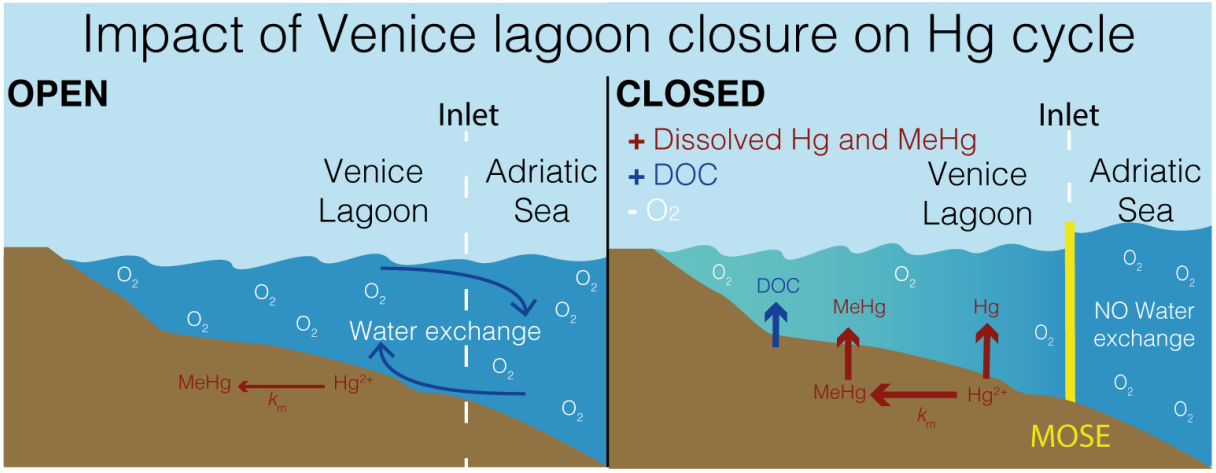


Figure 7: Graphical abstract of Chapter 1; left half represents the normal conditions of the lagoon with the MOSE open, and right half represents the changes in conditions when the MOSE is closed. k_m: Hg^{II} methylation rate constant. DOC: Dissolved organic carbon.

Introduction

Mercury (Hg) is one of the top ten chemicals of public health concern (World Health Organization, 2020), and particularly its methylated form (monomethylmercury – MMHg) which has the greatest potential for environmental and human health detriment. MMHg can be bioaccumulated and biomagnified through the aquatic food webs, making fish consumption the major source of human exposure to Hg. The methylation of inorganic Hg to MMHg occurs mainly under anoxic conditions (Eckley & Hintelmann, 2006; Pak & Bartha, 1998) and it is mediated by the activity of anaerobic microorganisms carrying specific genes (*hcgAB*) (Parks et al., 2013). Sediments, prone to anoxic conditions, stand out as a favored environment for Hg methylation. Other factors such as organic matter (OM) concentration and composition also influence Hg methylation in sediments. For example, fresh or autochthonous OM rich in proteins or low molecular mass molecules favor Hg methylation (Bouchet et al., 2018; Bravo et al., 2017; Chiasson-Gould et al., 2014; Schaefer et al., 2014). Meanwhile, recalcitrant OM enriched in high molecular mass or aromatic molecules strongly binds Hg, making it less bioavailable and thus reducing Hg methylation rates (Bravo et al., 2017; Chiasson-Gould et al., 2014; Graham et al., 2013; Herrero et al., 2018; Soerensen et al., 2017).

Coastal areas and coastal lagoons are under increasing human pressure from activities such as port operations and industrial development. Additionally, they are vulnerable to the effects of climate change, including rising sea levels and increased temperature. An increase of only 1 to 10 cm in sea level could double flooding events in areas with a narrow water levels range in only 5 years (Taherkhani et al., 2020), dramatically affecting coastal areas. These coastal environments have significant economic importance due to fisheries and mariculture activities, and thus is imperative to install or strengthen flood protection to safeguard the coastline and prevent massive population displacement (Vousdoukas et al., 2018). Current trends show that sea temperature is rising at an accelerated rate due to climate change (Cheng et al., 2019). Increasing temperature leads to higher consumption of dissolved oxygen (DO) due to the higher bacterial respiration activity (Nydahl et al., 2013) and reduced DO solubility in the surface ocean (Schmidtko et al., 2017), both causing a decline in the DO concentration in the oceans (Breitburg et al., 2018), especially in coastal areas (Amos et al., 2017; Pitcher et al., 2021).

An exemplary illustration of the multifaceted challenges these areas confront can be found in the Venice Lagoon, where all these diverse concerns converge with the installation of the high tides protection system, “Modulo Sperimentale Elettromeccanico” (MOSE, *Experimental Electromechanical Module*). The Venice Lagoon has long been recognized as a Hg contaminated area (Bloom et al., 2004; Pavoni et al., 1992; Rosati et al., 2020) with an important MMHg biomagnification (Dominik et al. 2014). The high tides that submerge Venice are becoming more aggressive and more frequent due to sea level rise and local geodynamics (Lionello, 2012; Lionello et al., 2021; Scarascia & Lionello, 2013). As protection against flooding, the construction of the MOSE began in 2003. These mobile barriers isolate for hours or days the lagoon from the sea, stopping water exchange between them. Under

these new hydrological conditions of the lagoon, the water renewal time is expected to increase as a whole (Ferrarin et al., 2013) with a potential risk of nutrients and contaminants accumulation in the water column (National Research Council, 2000). Increased frequency of high tides and thus longer duration of lagoon closure is expected to result in water stagnation, stratification, and eventually the occurrence of hypoxic or anoxic events in the lagoon (Leoni et al., 2022), favorable for enhanced Hg methylation.

To test the potential consequences of mobile flood protection barriers (MOSE), we combined field sampling (sediment coring, benthic chambers) with laboratory experiments and studied the impact of hydrodynamic and biogeochemical changes in the production and release of MMHg from the sediments to the water column. We simulated a MOSE closing-event by collecting sediment cores at two contrasted sites of the Venice lagoon, Osellino (OS) and San Giuliano (SG), which were incubated for 48h to assess the changes in sediment and porewater chemistry including the concentration of MMHg, Hg^{II} methylation rate constants, and the organic matter concentration and composition. Our study provides new insights into the risks of increasing MMHg concentrations in a context of MOSE where DO depletion events in the lagoon are expected to occur more frequently.

Methods

Site of Study

The Venice Lagoon (Figure 8) is the largest wetland system in Italy, and it has been widely described in the literature in terms of functioning and ecosystem characteristics (e.g., Zonta et al., 2018 - and references therein). The surface area is 550 km^2, including mudflats, tidal marshes, islands and a complex network of channels and tidal creeks. The average depth is 1.2 m and shallow water areas account for 75 % of the total surface area, but the depth increases to over 10 m in the main channels. The lagoon has three inlets that connect it to the Adriatic Sea with water residence times ranging from 24 h close to the inlets to 20 days in the more confined areas of the lagoon (Ferrarin et al., 2013). Releases from a chlor-alkali plant operating in the industrial area of Porto Marghera emitted Hg into the Venice Lagoon (Figure 8) during the second half of the 20^{th} century (Zonta et al., 2007). Tides have a strong influence in the complex distribution of Hg and other contaminants along the lagoon and also between the sediment and the water column (Guédron et al., 2012). The average surface water temperature of the lagoon is 17.6 °C with a large seasonal variation; the lowest temperatures are in January (7.8 °C) and the highest in July (26.3 °C) (Amos et al., 2017 - and references therein).

The MOSE system (Trincardi et al., 2016) was operated for the first time in October 2020 (Mel et al., 2021) and with it, the Venice Lagoon has become the first large lagoon in the world with a regulated flow. Up to December 2023, MOSE has been activated 66 times, and barrier closures have lasted from a few hours to 2 days, with a typical closure time of 4 to 5 hours (Alberti et al., 2023) mainly in autumn, when flood conditions occur more frequently due to weather-marine forcing factors (Camuffo, 1993).

Sampling sites

Two shallow sites with different continental influences were selected (Figure 8): i) Osellino (OS), located very close to the mainland and at about 300 m from the mouth of a freshwater tributary of the lagoon, the Canale Osellino, although not directly affected by the outflow of this watercourse; ii) San Giuliano (SG), located at about 1.3 km south of the mouth of Canale Osellino, in a sector with greater water exchange and a water depth of 56 cm, compared to 24 cm at OS, as referred to the zero level of the tide gauge for the lagoon. OS is more confined than SG, presenting a higher water renewal time, lower hydrodynamics, and finer sediment grain size with higher organic carbon content (Leoni et al., 2022). Both sites belong to areas characterized by a high Hg accumulation in surface sediments (Zonta et al., 2018).

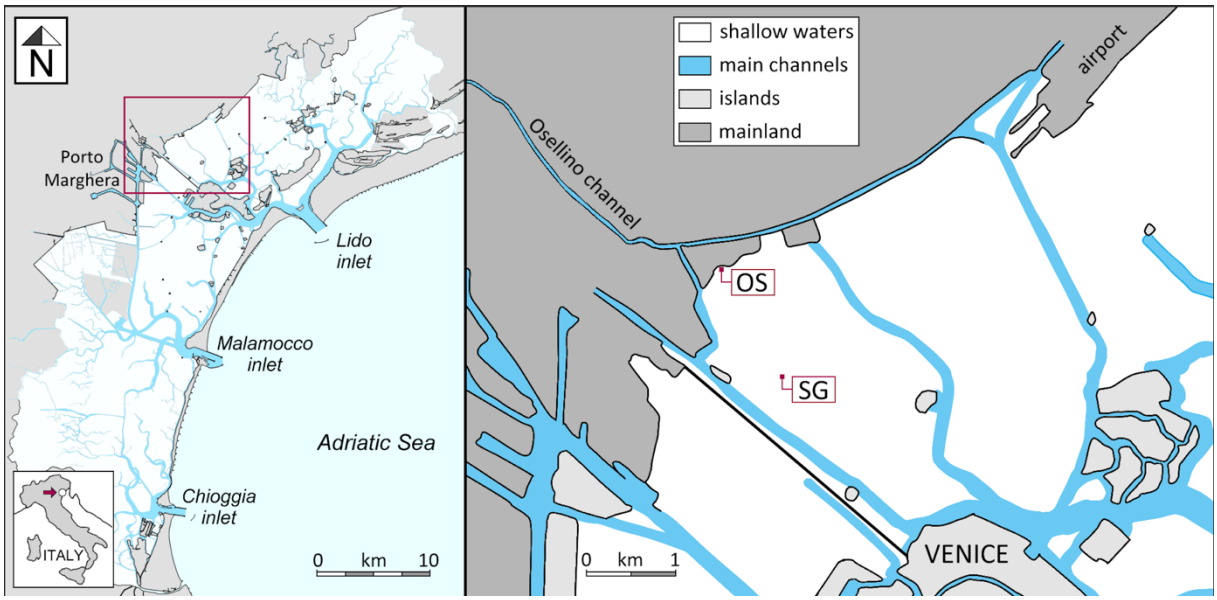


Figure 8: Location of the two studied sites Osellino (OS, 45.4750°, 12.2859°) and San Giuliano (SG, 45.4638°, 12.2949°) in the Venice Lagoon (in the insert).

Sampling, core processing and incubations

Sampling campaigns were performed in November 2019 and in September 2021. In both periods, seven sediment cores (core number: 6-11 in Nov 2019 and 13-18 Sep 2021) were collected at each site by a diver driving manually Plexiglas tubes (13.4 cm internal diameter) into the sediment. Cores were collected with 28 cm of overlying water, immediately sealed to avoid contact with atmospheric O_2 and carefully transported to the laboratory avoiding resuspension. Three cores from each sampling site were directly processed under an inert atmosphere (N_2- filled glove box) to avoid oxidation of sediment and pore water; these cores represent the initial, pre-closing conditions of the lagoon ("fresh cores"). Prior to core sectioning, 750 mL of overlying water was collected with a peristaltic pump and filtered (Sterivex filter 0.45 µm) for dissolved organic matter characterization and trace element analysis, including total mercury (THg) and MMHg. Then sediment was vertically extruded, and two sediment layers were subsampled, corresponding to 0-2 and 2-4 cm depths. Aliquots of sediment were used for direct determination of water content and grain size. The

remaining sediment was centrifuged in metal-free tubes (4000 rpm, for 60 min at 4 °C) to extract porewater. Supernatant was filtered (Sterivex filter 0.45 µm) in the N_2-filled glove box and directly fixed with HCl (Ultrex, 0.4 %). The pellets were freeze-dried for organic matter characterization (C and N content, hydrogen (HI) and oxygen (OI) indices), and determination of THg, MMHg, and trace element content. Four sediment cores from each site were incubated in a dark room at the lagoon water temperature at the time of collection, i.e., 14°C in Nov 2019 and 24°C in Sep 2021, to simulate stagnation of the water column. After approximately 48h of incubation in a N_2 atmosphere, other three cores (incubated cores) were processed in the glove box as described for fresh cores (Figure 9). The fourth core from each site was used for in-situ core profiling (see below).

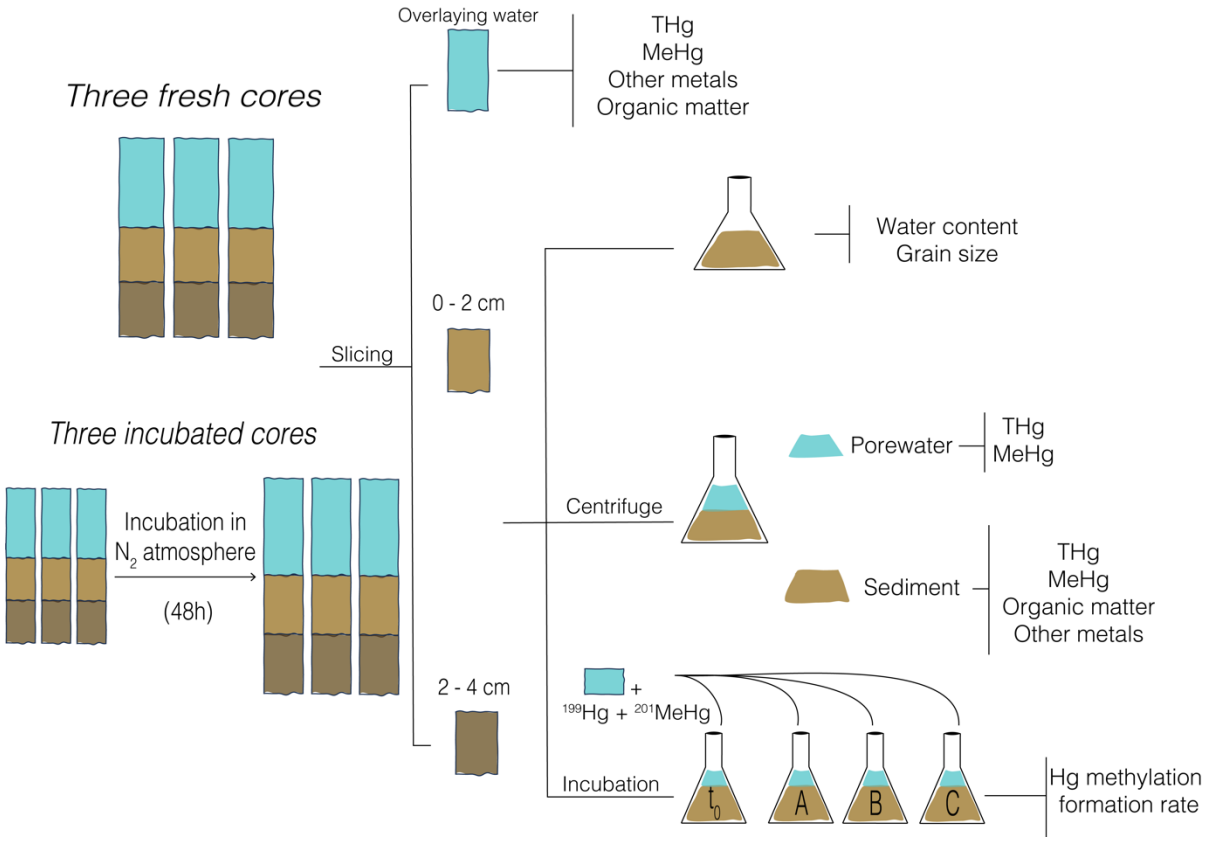


Figure 9: Scheme of the methodology pipeline for incubations and core processing.

Benthic Chambers

Concurrent with coring, a PVC cylindrical benthic chamber (described in Leoni et al., 2022) was deployed at both sites for about 48h in Sep 2021. The chamber was 30 cm in diameter and 27 cm high, with 6 cm of the chamber driven into the sediment (Figure 10). A multi-parameter water probe (Aquaprobe AP 2000; Aquaread Ltd, England) was placed in the center of the chamber to determine the DO concentration in the isolated water over time. At the end of the exposure period, water samples were collected from each benthic chamber.

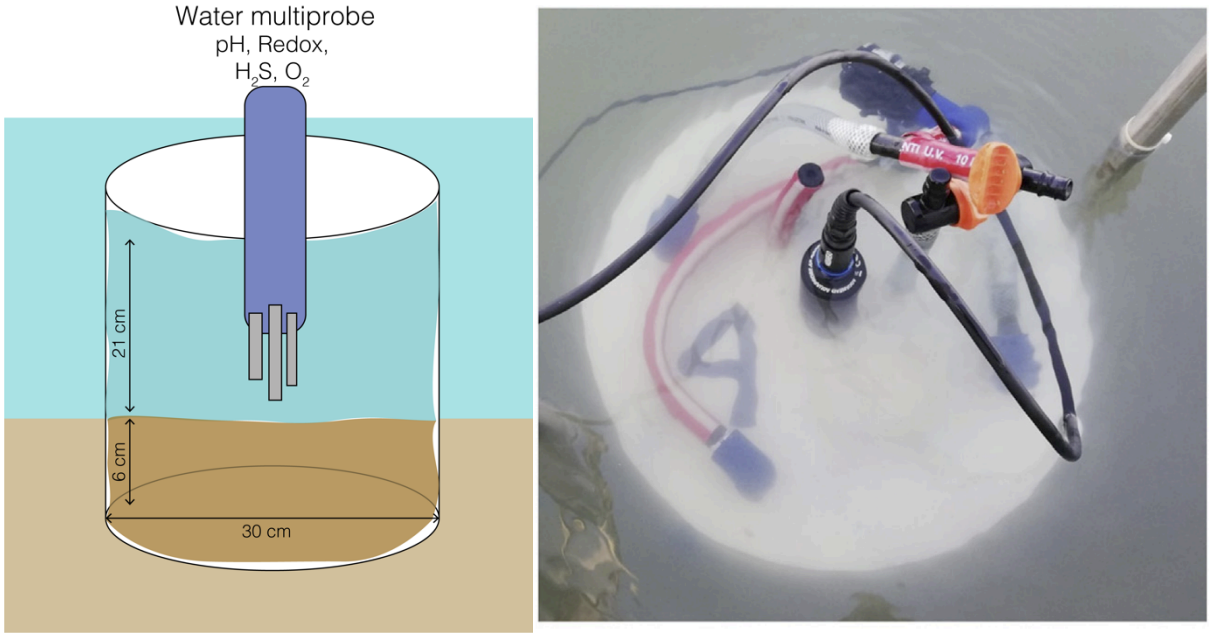


Figure 10: Drawing (left) and photo (right) of the benthic chamber.

Laboratory Analyses

In situ core profiling in September 2021

The fourth incubated core (for each site) was used to measure DO and H_2S concentrations and redox potential (E_H) along a water-sediment vertical profile, by means of a 500-µm microelectrodes (Unisense®, Denmark). The vertical profiles were measured with a resolution of 500 µm, with double measurement for each point and a conditioning time of 25 seconds. The profile analysis started from a position such as to intercept both the well-mixed water phase and the diffusive boundary layer (about 5 mm above the surface of the sediment). For each subsequent profile (at 24 and 48 hours of incubation), the sensors were moved a few millimeters to avoid insertion into the borehole resulting from the previous analysis.

Sedimentological and geochemical analyses

Water content was determined by weighing samples before and after oven drying at 60 °C. Particle grain size distribution was determined on wet sediments using a laser diffraction Coulter LS-100 analyzer following the procedure described by Loizeau et al. (1994). Characterization and quantification of the organic matter (OM) were performed on dry, powdered bulk sediment using Rock-Eval 6 following the method described by Behar et al. (2001) and Espitalié et al. (1985, 1986). The standard used was IFP 160000 Rock-Eval, and the analyses were carried out on 50-100 mg of powdered dry sediment under standard conditions. Analytical precision was higher than 0.05 wt % for Total Organic Carbon (TOC) and Mineral Carbon (MINC),10 mg HC g^{-1} TOC for the hydrogen index (HI), and 10 mg CO_2 g^{-1} TOC for the oxygen index (OI). Total nitrogen (TN) concentrations were analyzed in a CHN Elemental Analyzer (Carlo Erba Flash EA 1112 HNS/MAS200) using approximately 10 mg of

dry powdered sediment. The precision was better than 1 % based on an internal standard and replicate samples.

Hg, MMHg and trace element analyses

THg in sediments was analyzed by Cold Vapor Atomic Absorption Spectrophotometry (CVAAS) using a Direct Mercury Analyzer (DMA-80 II, MWS GmbH, Switzerland). All analyses were run in triplicate. The limit of detection (LOD) and working range were 0.01 ng and 0.05-600 ng, respectively. The relative error was usually ±5 % and always less than 10 %. The concentrations obtained for repeated analyses of the certified reference material never exceeded the specified range of concentrations given for SRM 2702 (NIST). THg on water samples was analyzed by Cold Vapor Atomic Fluorescence Spectrometry (CVAFS) (Merx Model III, Brooks Rand, USA) following the EPA Method, revision E 1631 (US-EPA, 2002), with a calculated LOD of 0.06 ng/L and a calculated limit of quantification (LOQ) of 0.2 ng/L. To control the quality of the analysis, two different reference materials were used: ORMS-5 (National Council Research Canada), 26.2 ng/L, which gave a recovery percentage of 88.8 % ± 1.2 %, and a standard solution purchased from Brooks Rand (USA), diluted at 4 ng/L. The percentage of recovery of repeated analyses was between 94.1 % ± 2.5 % and 96.3 % ± 1.3 %. Field and filtration blanks were measured to evaluate the possible contamination during sampling; they reached 0.17 ± 0.04 ng/L in Nov 2019 and 1.0 ± 0.1 ng/L in Sep 2021.

MMHg analysis on sediment were carried out using a HNO_3 leaching/CH_2Cl_2 extraction method (Bloom 1989). The solution was analyzed by CVAFS following the EPA Method 1631 (US-EPA, 2002). The certified reference material used in the MMHg analysis (ERM-CC580, European Commission) showed between 91.8 % ± 5.2 % and 98.7 % ± 1.6 % recovery. MMHg analysis on water samples collected in Nov 2019 (overlying water, porewater and water from benthic chambers) was carried out by CVAFS (Merx Model III, Brooks Rand, USA) after distillation following the EPA Method 1630 analysis procedure (US-EPA, 2001), with a calculated LOQ of 0.09 ng/L. To check the accuracy of the analysis we used a spiked sample of a known concentration that showed a recovery efficiency between 89.5 % ± 8.2 % and 96.6 % ± 1.0 %. As this LOQ was close to or higher than the MMHg concentrations observed in some samples, MMHg analyses in pore and overlying waters of samples collected in Sep 2021 were performed at the University of Grenoble. Filtered MMHg concentrations were analyzed using an ethylation purge and trap-gas chromatograph-AFS analyzer (Tekran® 2700 Methyl Mercury Auto-Analysis System) following published protocols (Bowman & Hammerschmidt, 2011; Guédron et al., 2014). All samples were run in duplicate and quantified using the standard addition technique. The calculated LOQ was 0.02 ng/L.

Trace elements in water (filtered and acidified with 1 % suprapure HNO_3) and in sediments were analyzed using quadrupole-based inductively coupled plasma mass spectrometry (ICP-MS, model 7700 series, Agilent). Sediment digestion was performed in Teflon bombs heated to 150 °C in analytical grade 2 M HNO_3 according to the Swiss Soil Protection Ordinance (OSol, OFEV, 1998). The total variation coefficients for triplicate sample measurements were better than 10 %.

Potential Hg methylation rate constants

A slurry (sediment and overlaying water) of each core, fresh and incubated, were amended with ^{199}Hg (ISC Science, Spain) in a glove box and were either directly frozen (1 aliquot, t_0) or incubated in a dark room for 24h before to be frozen (3 replicates). Determination of Hg transformation rate constants were carried out according to Rodriguez-Gonzalez et al., (2013). These determined rate constants are potential methylation rate constants (k_m). Briefly, inorganic Hg and MMHg were extracted from 50 mg of freeze-dried sediments with 5 mL HNO_3 (6 N) under focused microwave treatment and analyzed by species specific isotope dilution gas chromatography (GC, Trace GC Thermofisher) hyphenated to an inductively coupled plasma mass spectrometer (ICP-MS, X Series Thermofisher). Methodological detection limits for Hg species were 0.03 ng/g. The extraction and quantification were validated with a CRM (IAEA-405) and recoveries were 102 ± 7 and 97 ± 4 % for MMHg and inorganic Hg, respectively. The concentration of the formed MMHg deriving from the enriched isotope ^{199}Hg was calculated by isotopic pattern deconvolution methodology (Rodriguez-Gonzalez et al., 2013).

Fluorescent and Colored Dissolved Organic Matter

The filtered overlaying water samples were used for the characterization of optical properties of dissolved organic matter (DOM). Fluorescent and Colored Dissolved Organic Matter (FDOM and CDOM) were measured simultaneously using a Horiba Aqualog spectrofluorometer. Duplicate fluorescence excitation emission matrices (EEMs) were collected for each sample in a 1-cm pathlength quartz cuvette using freshly produced MilliQ water as blank. Fluorescence was recorded from 240 to 600 nm of excitation at 3 nm increments, emission was recorded in the same range (240-600 nm) every 8 pixels (~3 nm) using the instrument CCD detector, and the signal integration time was set to 2 seconds using the medium gain setting. Absorbance spectra were collected simultaneously to EEMs using the same wavelength range and increments used for EEM excitation.

Data processing was performed in R using the *staRdom* and *pavo* packages (Maia et al., 2013; Pucher et al., 2019). Briefly, CDOM spectra were inspected, and noise was manually removed before interpolation of the deleted wavelengths, the spectra were then base-corrected by subtracting the average absorbance between 580-600 nm. Spectral slopes were calculated in the ranges 275-295 nm (S275:295) and 350-400 nm (S350:400) and the slope ratio (SR) between them (Helms et al., 2008). Absorbance values at selected wavelengths were extracted from the spectra (abs254, abs300) and the absorbance ratio E2:E3 (abs250/abs365) was calculated (P. Li & Hur, 2017). For FDOM processing, MilliQ blank fluorescence was first subtracted and the regions of the EEMs affected by Raman and Rayleigh scatter excluded and values interpolated (Lawaetz & Stedmon, 2009). Inner filter effects were corrected using the absorbance of each sample (Kothawala et al., 2013). Several FDOM parameters were calculated (Table S1): fluorescence index (FI), humification index (HIX) and biological index (BIX), as well as the common fluorescence peaks A, C, M, T, and B, which were normalized by total fluorescence and are presented as relative abundances (Coble, 1996; Huguet et al., 2009; McKnight et al., 2001; Ohno, 2002).

Statistical analysis and data visualization

The statistical analyses (PCA and ANOVA analysis) were performed with package stats 4.3.2 and visualization was generated with ggplot2 3.4.4. (Wickham, 2016) and multi-panels with gridExtra 2.3 (Auguie, 2015) of R (R Core Team, 2013). The figures were combined and post-processed using Illustrator 24.0.1. The map of the study sites was drawn with CorelDraw.

Results

Characteristics of the two contrasted sampling sites

Geochemical sites description

A Principal Component Analysis (PCA, Figure 11) was performed to explore the differences and similarities between sediments at the two sites (OS and SG), between sampling campaigns (Nov 2019 and Sep 2021) and conditions (fresh and incubated). This analysis resulted in two main components explaining ~66 % of the variability and showing a greater difference between years in SG compared to OS. The variables used to characterize sediment showed no significant differences between depths (0-2 and 2-4 cm) or conditions and thus the data were combined using means and standard deviation (n=12) (Table S2). No significant differences were found at OS site between sediments sampled at the two periods (Figure 11; Table S2). In contrast, at site SG, all variables except mean particle diameter showed significantly different values between the two periods: lower water content, TOC, N, HI, OI and higher for C/N ratio, MinC in 2021 than in 2019 (Table S2, Figure 11). The comparison between sites for 2019 and 2021 is shown in table S2 using OS/SG ratio of the respective values. In 2019 only TOC was significantly higher, but the differences between sites were considerable in 2021 (Figure 11, Table S2). The dissolved organic carbon (DOC) measured in the overlying water was 2.31±0.13 and 2.37±0.22 mg/L in OS and SG respectively in 2019. In 2021, the DOC was higher at both sites, 4.17 in OS and 4.07 mg/L in SG (Table S3).

THg and MMHg concentrations in sediments, and overlying and pore waters in fresh cores

Concentrations of THg in sediments were similar between years and depths but differed across sites, being 0.86 ± 0.06 (n=12) and 0.93 ± 0.05 (n=12) mg/kg in OS and SG respectively. Between Nov 2019 and Sep 2021, MMHg levels experienced a notable decline at both sites. In Sep 2021, the values, with a maximum of 0.25 µg/kg, were at least 50 % lower than those recorded in Nov 2019, where the maximum value was 0.56 µg/kg. Moreover, concentrations of MMHg decreased with depth (Table S4).

THg concentrations in porewaters and overlying waters were significantly lower in Nov 2019 compared with Sep 2021 (Table S5) in both sites. In porewaters from Nov 2019, we found THg concentrations ranged from 1.9 to 6.2 ng/L, with the exception of OS 2-4 cm sample that reached 17.1 ng/L. In Sep 2021, THg concentrations in porewaters varied across depths and sites (Figure 12A and 12B), ranging from 7.7 to 20.4 ng/L and from 8.9 to 23.4 ng/L in OS and SG, respectively. THg concentrations peaked in the 2-4 cm layer, reaching 14.0 ± 5.6 ng/L (n=3, Sep 2021 in fresh cores) in OS, while in SG they peaked at 0-2 cm, reaching 14.8

± 7.6 ng/L (n=3, Sep 2021 in fresh cores). In filtered overlying waters, THg concentrations measured during the 2019 sampling campaign were close or below the detection limits (LOD = 0.06 ng/L), but during the 2021 campaign they increased up to 3.2 ± 0.1 ng/L in OS and 4.4 ± 0.4.

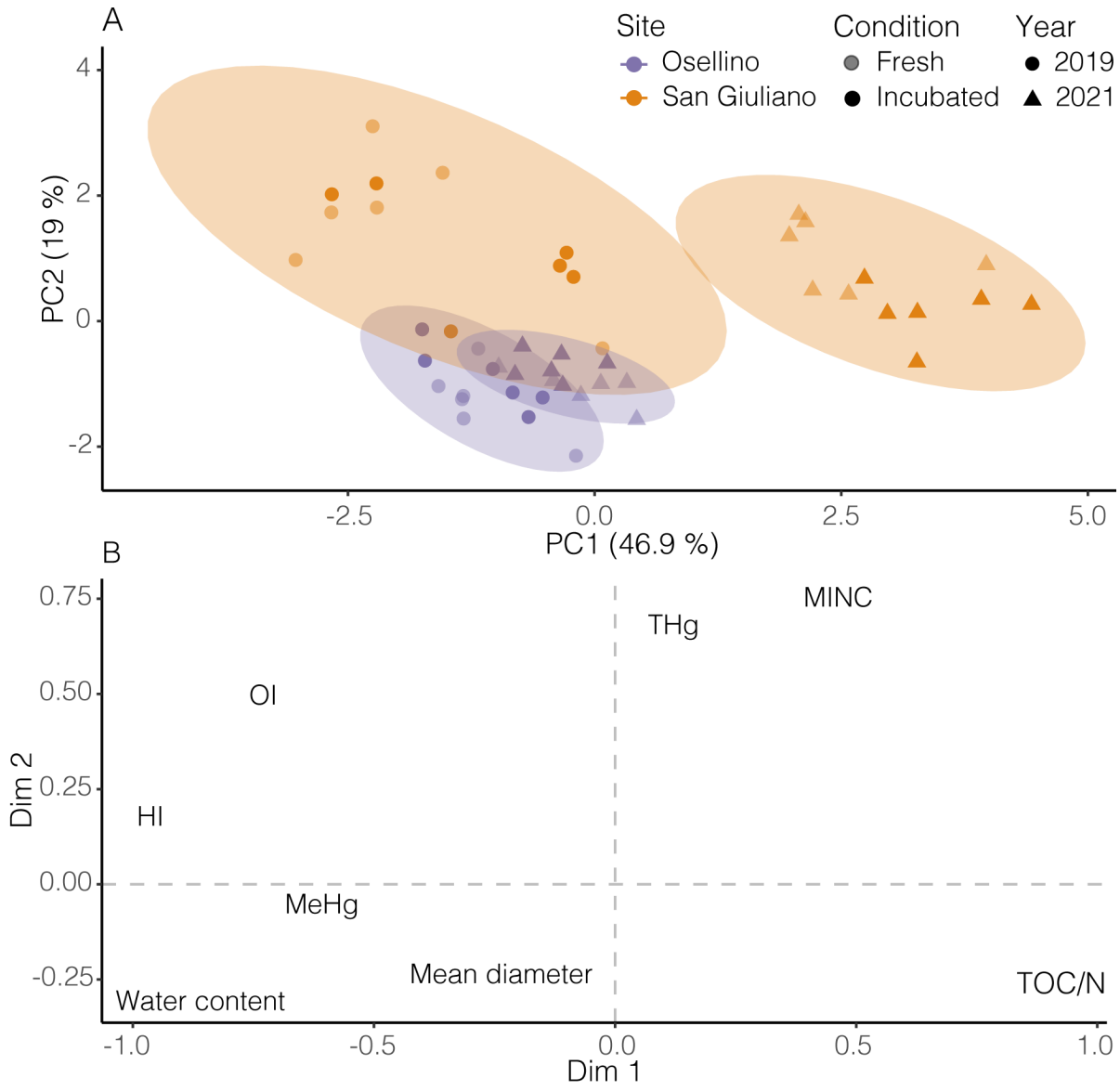


Figure 11: Principal Component Analysis (PCA) of fresh sediments (n = 24) showing the explained variability arising from principal components 1 (PC1) and 2 (PC2) based on general sediment attributes, mercury concentrations (THg and MMHg) and organic matter traits, as presented in (A) the scores plot displaying the 24 samples and (B) the loadings plot displaying the characteristics used.

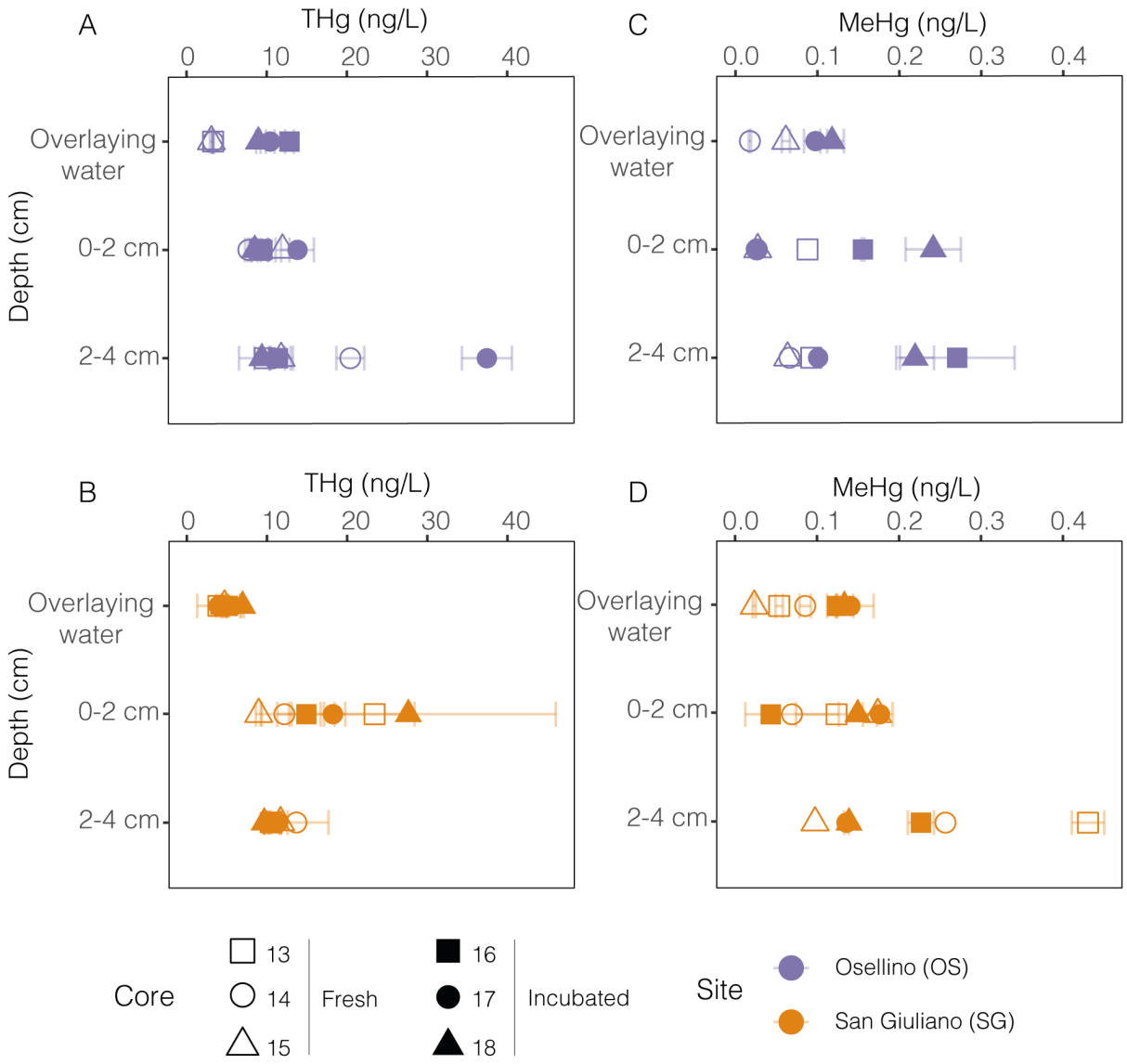


Figure 12: Vertical profiles of THg (A and B) and MMHg (C and D) concentrations in overlying water and porewater of six sediment cores from OS site (A and C, purple) and SG site (B and D, orange) collected in Sep 2021. Open symbols represent the measurements performed in fresh cores (cores number 13, 14 and 15) and closed symbols refer to the incubated cores (cores number 16, 17 and 18). Error bars correspond to the standard deviation of analytical triplicates.

Experiments with oxygen limitation: changes in THg, MMHg, k_m and sediment properties.

Oxygen, redox and hydrogen sulfide

Sediment cores were incubated to simulate a MOSE-closing event in two different periods (Nov 2019 and Sep 2021). In 2019, at the end of incubation, DO levels at the sediment-water interface dropped to 0.07 and 0.3 mg/L in OS and SG cores, respectively. Concentrations of Mn in the overlying waters did not vary indicating no significant changes in the redox conditions during the 2019 incubations. THg and MMHg concentrations did not vary after 48h incubation. In contrast, in 2021, relevant changes in DO, redox potential (E_H) and H_2S

(only in OS) profiles were observed after 24h and 48h of incubation (Figure S1). Although both sites had similar DO concentrations (5.12 mg/L) at 5 mm above the sediments, in OS the DO concentrations decreased progressively to a value of 0.4 mg/L at the sediment-water interface, while in SG, DO concentrations were fairly constant but dropped drastically to a value of 1.9 mg/L at the sediment-water interface. In both sites, the DO decreased in overlying waters and sediments after 24h. The E_H profiles agreed with O_2 profiles. In OS, the core reached negative E_H values at ~5 mm depth and decreased progressively with depth to a minimum value at 2 cm depth (Figure S1). In SG, negative E_H values started at 10 mm depth below the sediment-water interface after 24h incubation time (-164 mV) and continued decreasing with depth. Concomitant to the decrease in O_2 and E_H, we observed an important increase of dissolved Mn in the overlying water of OS and SG (Table S6). Lastly, H_2S profiles also concurred with the E_H, accordingly, higher H_2S concentrations were observed in OS compared with SG. In OS, H_2S appeared at 5 mm depth and continued increasing with depth and over time (24h and 48h, Figure S1).

THg and MMHg concentrations and Hg methylation rate constants

In Nov 2019, THg and MMHg concentrations did not significantly changed in porewater after 48h of incubation (Table S5), but this observation should be tempered by the relatively large LOQ on the MMHg analyses. In contrast, in Sep 2021, THg concentrations increased significantly from 3.2 to 10.8 ng/L in the OS overlying waters after 48h of incubation while they remained similar in SG (4.4 and 5.3 ng/L); however, the high variability of replicates makes comparisons difficult. MMHg concentrations rose in both overlying water and porewater of OS after incubation (Figure 12 and Table S5). In SG, the rise in MMHg concentrations occurred in the overlying waters – reaching approximately the same value as in OS (around 0.1 ng/L, Figure 13) but remained within the same range in porewater before and after incubation (Figure 12 and Table S5).

In Nov 2019, differences in potential methylation rate constants (k_m; i.e. MMHg formation rate constants) between fresh and incubated cores were not prominent (Figure 13A and 13C). In contrast, in Sep 2021, k_m almost doubled at both sites after 48 h. Surface sediments (0-2 cm) presented an increase from 0.017 to 0.029 d^{-1} in OS and from 0.009 to 0.017 d^{-1} in SG (Figure 13B and 13D). In the 2 - 4 cm sediment layer, a similar trend was observed, with a smaller increase compared to surface sediments.

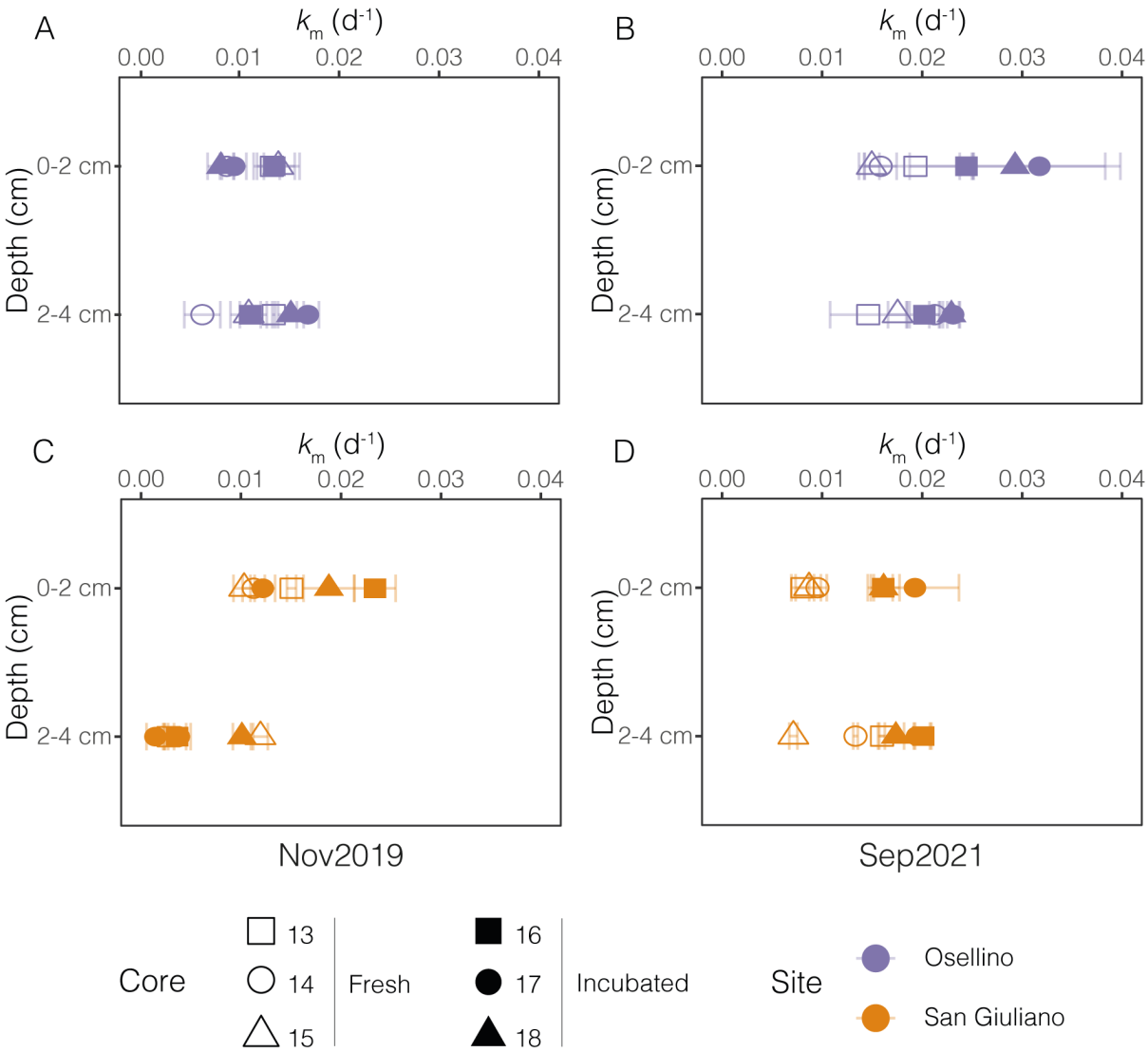


Figure 13: Potential Hg methylation rate constants (k_m, d-1) determined in both sites (OS in purple and SG in orange) during the 2019 (A and C) and 2021 (B and D) incubations. Open and close symbols refer to fresh and incubated cores respectively. Error bars correspond to the standard deviation of the three replicates per core.

DOC content and DOM properties in overlying water

In Nov 2019, no significant changes in the concentration of dissolved organic carbon (DOC) or the composition of the dissolved organic matter (DOM) were found after incubation of the sediment cores (Table S3). By contrast, in Sep 2021, DOC in the overlying waters of OS increased significantly from 4.2 mg/L to 10.6 mg/L during the incubation (Figure 14 and Table S3). A smaller increase in DOC from 4.1 to 6.0 mg/L was also observed in SG (Figure 14 and Table S3).

Regarding the optical properties of DOM in the overlying water, the fluorescence index (FI) was ~1.40 with no differences between years or sites, and a slight increase after incubation for the 2021 sampling reaching ~1.48 (Table S3). The humification index (HIX) was similar between sites and condition but showed differences between years, being ~0.85 in 2019

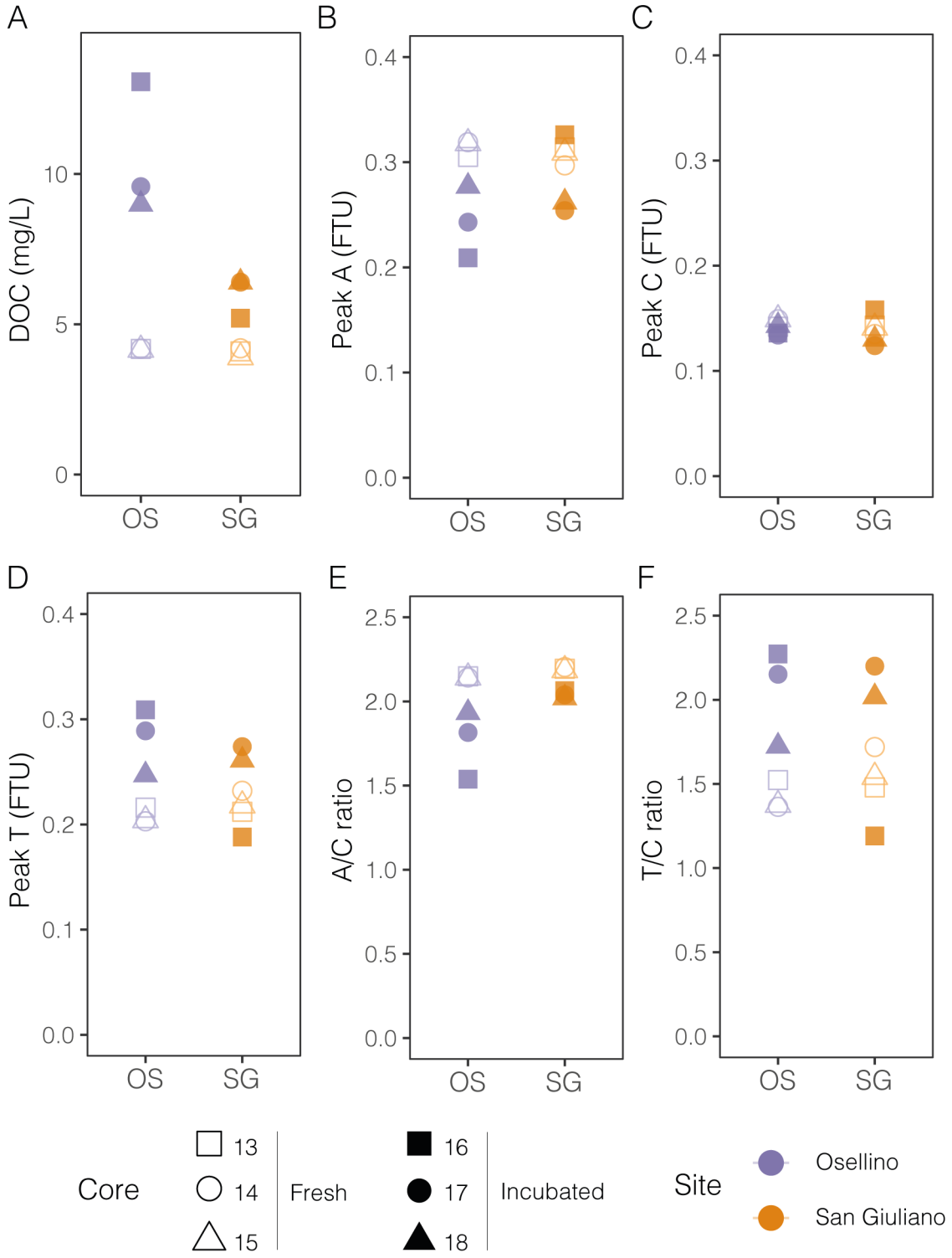


Figure 14: DOC and fluorescent dissolved organic matter (FDOM) characterization of the overlying water collected in the Sep 2021 sampling campaign. Values of fresh (open symbols) and incubated cores (close symbols) from both sites (OS in purple and SG in orange). Peaks A, C and T are normalized by total fluorescence.

and ~0.71 in 2021 (Table S3). Different DOM fluorescent peaks showed changes during the 2021 incubations (Figure 14). Humic peak A and marine peak M decreased significantly after incubation in OS overlying water. Humic peak C, remained unchanged after incubation. In contrast, a different trend was observed in SG, as peaks A, C and M were not affected by the incubation (Figure 14 and Table S3). Both sites, and especially OS, presented a smaller A/C peak ratio after incubation (Figure 14). An increase in the C/M ratio was also observed (Table S3). Peaks T and B, associated to tryptophane and tyrosine respectively, increased in overlying waters during the incubation in both sites (Figure 14 and Table S3). The T/C ratio, used as a proxy of the proportion of proteinaceous substances (often more available for bacteria) over the humic substances also increased during the incubation, with a greater increase in OS than in SG (Figure 14).

Taken together DOC and optical properties of DOM, our results hint towards a release of organic matter from the sediments to the overlying waters, with an associated enrichment in labile/available substances (more proteinaceous), and a higher proportion of reactive humic substances (decrease in A/C ratio), all likely promoting MMHg formation in surface sediments and overlying waters.

Changes in THg and MMHg in benthic chambers

In Sep 2021, benthic chambers were deployed at OS and SG to measure *in situ* DO consumption and to complement the incubations performed in laboratory conditions. The confined overlying water reached total anoxia after 11 and 18 h in OS and SG, respectively (Figure 15). After 48h, concentrations of THg, MMHg and DOC and organic matter composition were measured in the overlying water. THg concentrations were 13.5 ng/L in OS and 10.4 ng/L in SG (Table S7). The increment in OS is comparable to the one observed in the overlying water of the sediment cores during the incubation (THg concentrations increased from 3.2 to 10.7 ng/L, Figure 12). In the SG benthic chamber, however, THg concentrations were higher compared to those in the cores (4.4 ng/L in fresh cores and 5.3 ng/L in incubated cores, Figure 12). In benthic chambers, MMHg concentrations after 48h were 0.07 ng/L in OS and 0.13 ng/L in SG (Table S7). These MMHg concentrations are similar to those measured in incubated cores (0.11 and 0.13 ng/L in OS and SG respectively, Figure 12), although a lower MMHg concentration was observed in the OS benthic chambers than in the incubated cores. Both DOC content and DOM composition of the benthic chambers were similar to the values found in the fresh cores of the experiments (Table S3 and Table S7). Additionally, Mn, that is released from the sediment to the overlying water when E_H decreases, increased during benthic camber deployment from 28.5 to 216 µg/L and from 7.4 to 115 µg/L in OS and SG respectively, as observed in incubated sediment cores.

Discussion

Contrasting SG and OS study sites

The PCA analysis shows that sediments from OS in both sampling years and from SG in Nov 2019 are very similar with respect to the analyzed sedimentological characteristics (grain size and organic matter content and composition). Surface sediments from SG in Sep 2021 are different, with lower water content, OM and HI (indicating more degraded OM). Additional observations of sediment cores (CT image, trace element profiles – not shown) strongly suggests more dynamic sedimentary conditions at site SG, which, furthermore, is located in an area with a greater probability of sediment disturbance by anthropogenic activities.

THg concentrations in sediments are slightly lower than those measured by Zonta et al., (2018) in the vicinity of Osellino canal, being 1.66 mg/kg in Zonta et al. and ranging between 0.8 to 0.98 mg/kg in this study. In the overlying and pore waters, the differences between sampling campaigns could be a result of the tides. In Nov 2019, the samples were taken during an ebb tide, while in Sep 2021, they were collected during a flood tide. This interpretation agrees with the results of Guédron et al. (2012), who observed higher concentrations of THg in both locations during the flood tide. Guédron et al. (2012) reported the same trend with MMHg concentrations, but we do not observe a higher MMHg concentration in flood tide than in ebb.

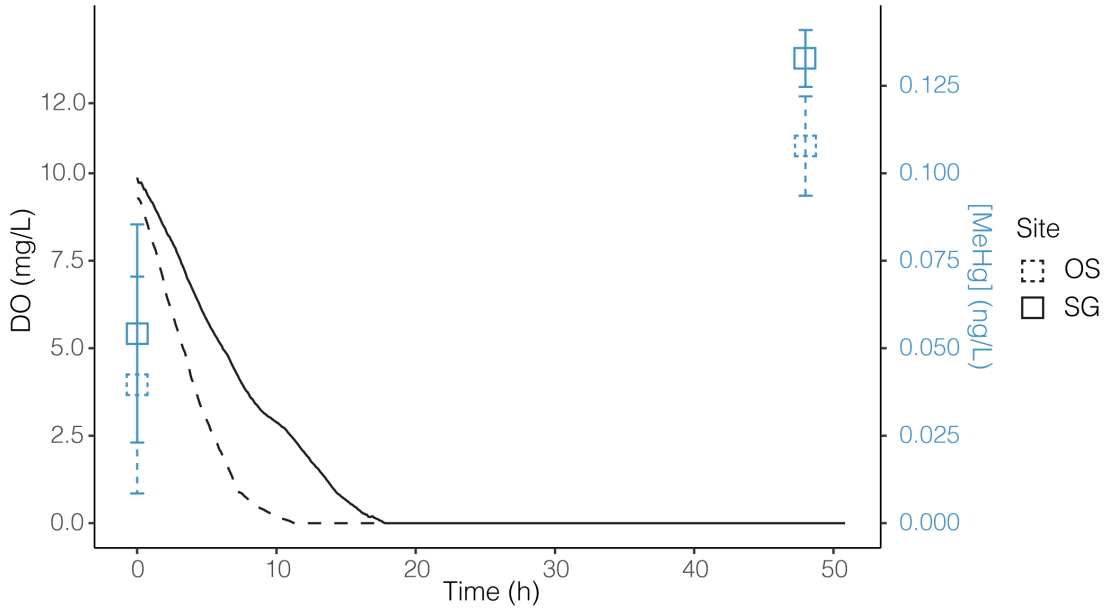


Figure 15: Conceptual figure coupling the consumption of dissolved oxygen (DO, lines) in benthic chambers in Sep 2021 with the simultaneous increase in methylmercury concentration (MMHg, squares) in the overlying waters of fresh (t0) and incubated cores (48h).

Increase in methylmercury formation and concentration in a simulated MOSE closing-event

Our study consistently showed an increase in MMHg concentrations in overlying waters after both simulations of the MOSE closing-event: benthic chambers (Table S7) and incubation of sediment cores (Figure 12C and 12D). This increase in MMHg concentrations was associated with oxygen depletion and a decrease in E_H (Figure 15, Table S2), as observed in 2021. Decreases in E_H have been associated with a release of DOC and an enrichment of humic substances in porewaters, especially under sulfate-reducing conditions (Gan et al., 2020). Indeed, Hg is strongly bound to sulfur sites of organic matter, in particular humic acids (Skyllberg et al., 2006) and, as a consequence, positive correlations between THg and DOC concentrations have often been reported in aquatic systems (Bravo et al., 2017, 2018; Herrero Ortega et al., 2018; Schartup et al., 2015; Taylor et al., 2019) and in our experiments (Figure 16, r = 0.96, p-value < 0.001). In our incubations, DOC concentrations in overlying waters doubled and reached up to ~ 6 and 10 mg/L in SG and OS, respectively. A previous study conducted under laboratory conditions, showed that an increase in DOC led to a raise in Hg-availability until ~ 11 mg/L and then to a decline at higher DOC concentrations (Chiasson-Gould et al., 2014). The increase of DOC could have thus similarly increased Hg availability during the simulated MOSE-closing event. Moreover, we observed in the present

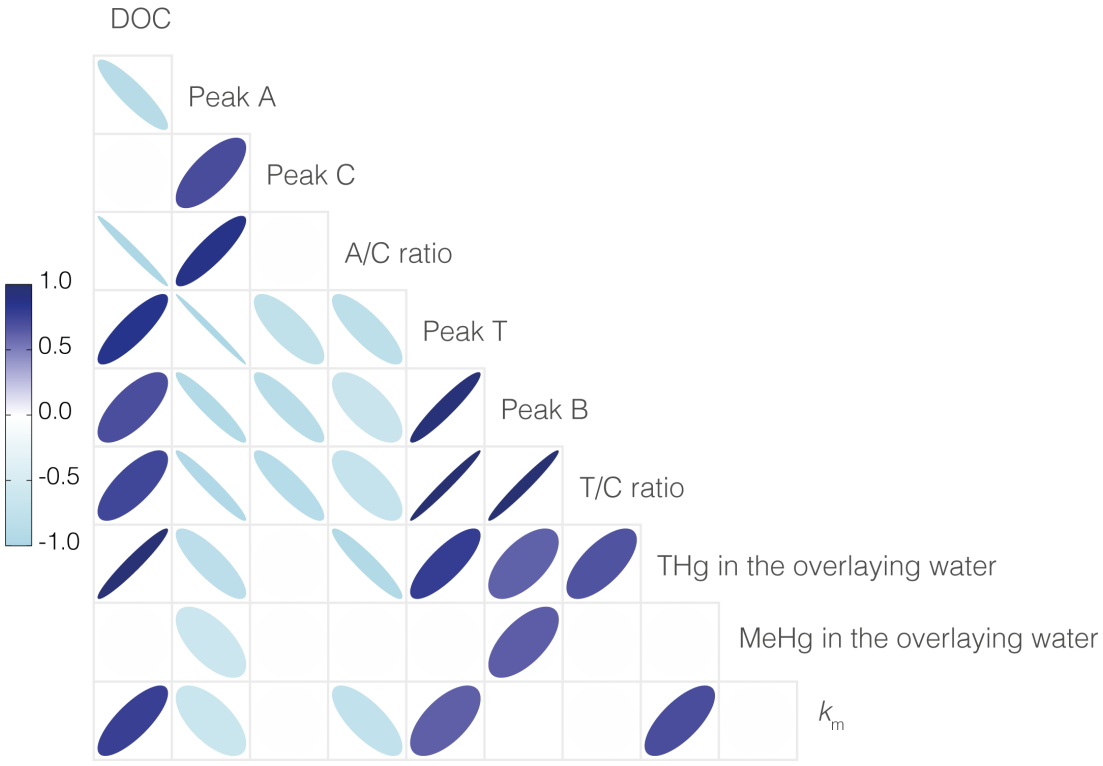


Figure 16: Pearson correlation matrix between k_m, Hg and MMHg concentrations and organic matter composition. Data from both fresh and incubated cores from Sep 2021 sampling were used to construct the Pearson correlation matrix. Only significant (p<0.05) correlations are shown.

study a decrease of humic peak A but also of the A/C peak ratio (Figure 14 and Table S3), indicating an enrichment in degraded humic compounds of porewater which could result from an intense sulfate reduction (Gan et al., 2020). Indeed, the A/C ratio correlated negatively with the k_m (r = -0.75 and p-value = 0.0054, Figure 16). After 48h, we also observed an enrichment in labile protein-like substances (peak T, Figure 14), generally produced by the activity of bacteria and phytoplankton (Coble, 1996b; Lønborg et al., 2010; Romera-Castillo et al., 2011) and was positively correlated to the k_m measured in surface sediments (Figure 16, r = 0.63). Taking all this into consideration, it is plausible that the increase in MMHg concentrations in overlying waters observed in this study resulted from an enhanced *in situ* Hg^{II} methylation (Figure 13), fostered by the release of available Hg, associated to the increase in DOC (Bravo et al., 2017; Chiasson-Gould et al., 2014; Soerensen et al., 2017), and labile dissolved organic matter (peak T) (Figure 14) (Herrero Ortega et al., 2018).

Noteworthy to mention that Hg^{II} methylation and MMHg demethylation after 48h incubation have likely reached a steady state (Bouchet et al., 2013; Rodriguez-Gonzalez et al., 2013) and we can assume that measured potential methylation reflect the net MMHg formation in sediment. Hg methylation rate constants measured in this study were higher than pristine coastal sediments such as those of the Gulf of Trieste (Bratkič et al., 2017), but ranged within the known limits for the Venice Lagoon described in previous studies (Guédron et al., 2012; Han et al., 2007) and other urban coastal areas (Bouchet et al., 2013; Cesário et al., 2017). Bouchet et al. (2013) also measured higher values of k_m during the warmer season in the Arcachon Bay (France).

The observed increase in MMHg concentrations in the overlying water in our experiments of Sep 2021 could impact MMHg biomagnification because filter-feeding benthic bivalves have been identified as key organisms in the transfer of MMHg from sediments to higher levels of the food chain in the Venice Lagoon (Bloom et al., 2004; Dominik et al., 2014) and in other Mediterranean lagoons, like Grado and Marano (Giani et al., 2012). Furthermore, the bioavailability of Hg might have increased at the measured DOC concentrations and thus could lead to enhanced Hg accumulation in food webs (French et al., 2014).

Negative consequences of oxygen depletion events on coastal Hg cycling

Temperature is one of the key factors to consider in the current situation of the Venice Lagoon. To study the potential impact of MOSE closing-events in different times of the year, we performed the same experiment in different seasons. In 2019, we collected the sediments in November, and incubated them at the water temperature (14°C) simulating the autumn conditions. In 2021, we collected the cores in September and incubated them at 24 °C, simulating the end of summer conditions. These differences in setup helped us to understand what could potentially happen if the MOSE closes when temperatures are higher, either because closure occurs earlier in the year with respect to the present situation or because temperatures increase during the fall due to climate change. During the Nov 2019 campaign, we did not observe any significant changes in the concentration or composition of organic matter or in k_m after incubation. In contrast, the results of the Sep 2021 campaign showed a

different outcome. In Nov 2019, there was still some DO in the water after 45h, whereas in Sep 2021 there was no DO after only 11 or 18h (OS and SG respectively; Figure 15). Although we measured similar DO concentrations at both sites at the beginning of the experiment in 2021, we detected a faster reduction of DO in OS than in SG. A considerably lower sediment oxygen demand (SOD) throughout the year was measured at sites close to SG than near OS (Leoni et al., 2022). This may explain a lower k_m at SG compared to OS not only in September, but during all warm months. Moreover the increase in protein-like substances suggest a higher bacterial activity. This effect was more pronounced in OS and helps to explain the faster decrease in DO. Higher bacterial activity, less DO and an enrichment of proteinaceous OM, potentially caused by MOSE-closing events, are important drivers for Hg methylation (Bravo et al., 2017). However, the differences observed between SG and OS highlights that the impact of MOSE-closing events may not be homogeneous across the lagoon, and that further studies are required to better constrain and predict the effects of MOSE in the increase in MMHg concentration in the entire lagoon.

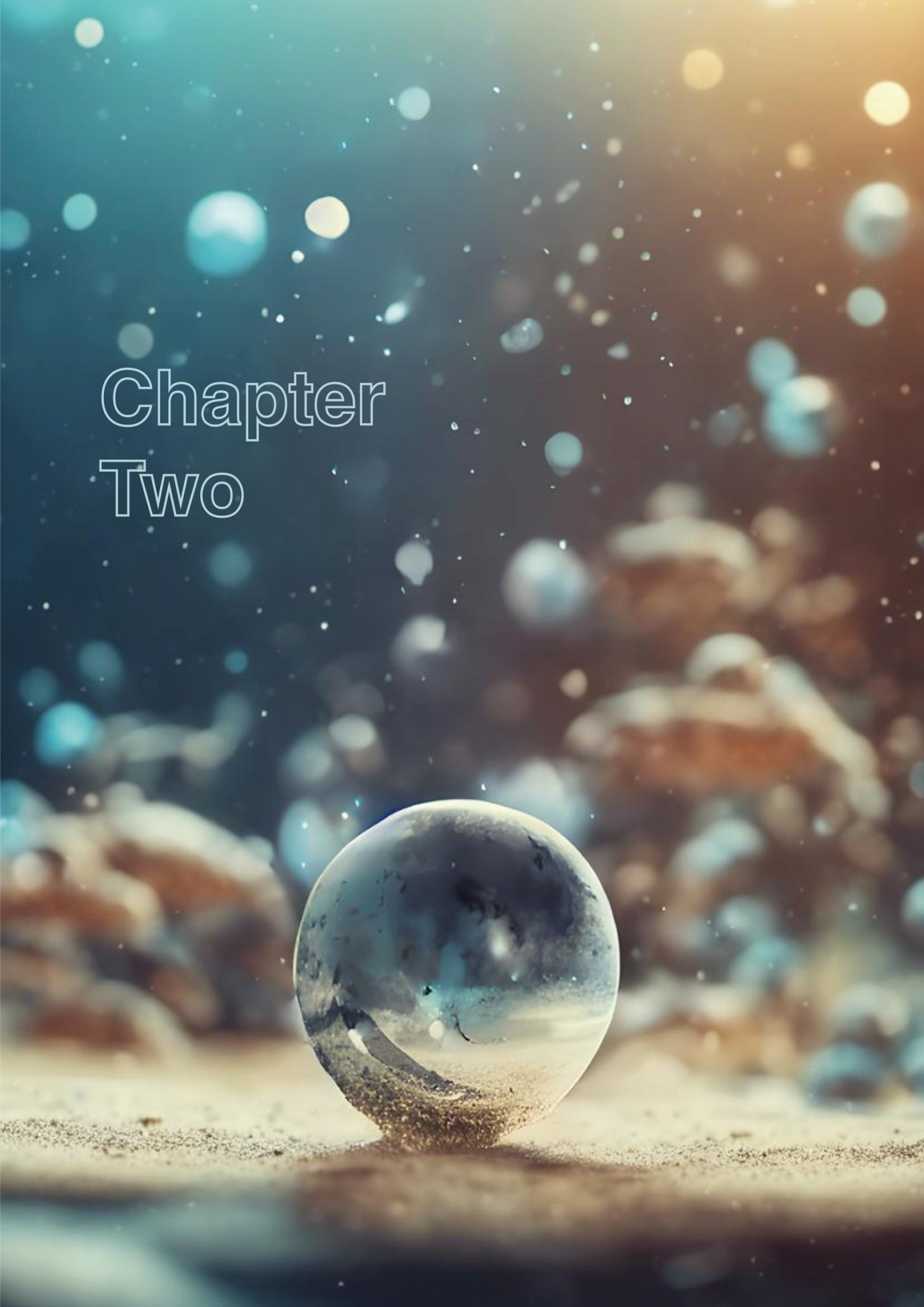
As a consequence of rising temperatures, the sea level increases (Lionello et al., 2021; Trincardi et al., 2016), a fact that has been observed in the Venice Lagoon, where the number of flooding events have doubled in the last decade (2010s) (Lionello et al., 2021). Currently, the MOSE closes for short periods of time and during cold months of the year, minimizing the impact of the MOSE on the sediment oxygen demand (Leoni et al., 2022) but the ongoing global change could modify the situation. As sea temperature rises (Amos et al., 2017; Cheng et al., 2019), the SOD will start to increase, more rapidly in confined areas (such as OS) where unusually high values of SOD were already found (Leoni et al., 2022). At the same time, higher temperature might lead to a decline in oxygen solubility (Schmidtko et al., 2017) and enhanced bacterial activity (Nydahl et al., 2013), also favoring MMHg formation in the lagoon.

Overall, our study shows that the difference in MMHg formation and MMHg concentrations found after incubation between the two assessed seasons would be intensified by the rising temperature and this may result in periods of MMHg formation as the MOSE closes more often and for longer periods. As well, a larger increase of MMHg formation in marginal sites such as OS during a MOSE closing event, may act as a hot spot for MMHg formation to then be redistributed across the lagoon during the tidal cycling (Guédron et al., 2012) and potentially enter the food web.

Conclusions

The MOSE was built to isolate temporarily the Venice Lagoon from the Adriatic Sea during high tide events and protect the city of Venice and its cultural heritage from flooding. In this study, we simulated the potential effect of a prolonged MOSE-closing event and showed that MMHg concentrations increased in porewaters and overlying waters as a result of an enhanced MMHg formation caused by a release of labile DOC. This increase might have a relevant impact on MMHg accumulation in the Venice Lagoon biota. In the context of global change, with rising temperatures and declining oxygen concentrations in coastal areas prone to MMHg methylation, our study highlights the need to monitor the MMHg concentrations

after activation of the MOSE system, especially during warm months. Low water temperatures do not foster a relevant DO consumption and therefore do not enhance MMHg formation but long-lasting MOSE closure at higher temperatures in the future may lead to an increase in MMHg concentrations in water and food webs of the Venice Lagoon.


Chapter
Two

Chapter 2: Novelty and metabolic versatility of uncultured bacteria with capacity to detoxify inorganic mercury and methylmercury from marine sediments

Abstract

Monomethylmercury (MMHg) is one of the most worrisome contaminants nowadays; it is neurotoxic for humans, and it can bioaccumulate and biomagnify through aquatic food webs. Despite the global relevance of marine sediments as repositories of Hg pollution, there is limited information available on ecologically relevant taxa involved in Hg^{II} reduction and MMHg demethylation in these ecosystems. One of the microbial strategies for the detoxification of MMHg is through the *mer* operon that contains two enzymes, the *merB,* organomercurial lyase, and the *merA,* mercuric reductase, which enable MMHg demethylation and Hg^{II} reduction, sequentially transforming this toxic into the volatile form Hg^{0}. In this study, we sequenced 30 microbial metagenomes and 24 metatranscriptomes from marine sediments collected from 10 different Hg-impacted sites of three marine regions: Bay of Biscay (Nervión and Suances), the Mediterranean (Barcelona) and Baltic Sea (Köpmalhlmen) to unveil the ecologically relevant microbial taxa responsible for MMHg detoxification. Here, we built the Hg-detoxification Reference Gene Catalogue (Hg_RGC) with 74 and 188 *merA/merB* genes respectively derived from our MERCLUB Reference gene Catalogue and applied genome-resolved metagenomics to assemble 803 Metagenome-Assembled Genomes (MAGs) of medium and high quality named as MERCLUB Microbial MAGs. From those, we detected 45 bacterial MAGs containing the *merA* and/or *merB* genes to evaluate the ecology, biogeography, metabolic and potential activity of MMHg detoxifying bacteria and archaea from contaminated sediments. Two MAGs with almost complete genomes contained both *merA* and *merB* genes and were related to Actinomycetales (*Microbacterium* sp.) and Rhodobacterales. We also recovered MAGs containing *merA* or *merB* genes from previously overlooked phyla such as Krumholzibacteriota or Abyssubacteria. A comprehensive phylogenetic analysis for *merA* and *merB* was performed integrating *merAB* genes from our Hg_RGC catalogue and MERCLUB MAGs from the same sites, allowed us to infer their phylogenetic diversity and highlighted the need of both approaches (catalog and MAGs) to have a more complete view of the abundant and rare microbial taxa involved in Hg detoxification. Finally, we identified which taxa actively transcribed *merA/merB* in the sediments studied, pointing to Gammaproteobacteria as relevant active taxa. Our results emphasize the complexity and metabolic versatility of bacteria involved in Hg^{II} reduction and MMHg demethylation within marine sediments, influencing the overall Hg bioavailability and ecological impacts, which is key for exploring Hg removal strategies.

Introduction

Bacterial and archaeal taxa involved in mercury (Hg) detoxification in aquatic sediments have garnered significant attention due to their pivotal role in mitigating Hg toxicity in these ecosystems. Hg in aquatic environments binds to fine sediment particles through different mechanisms (Scanu et al., 2016), establishing coastal sediments as both a sink (Chakraborty et al., 2014) and a source of Hg to offshore pelagic food webs (Fitzgerald et al., 2007). Microorganisms play a key role not only in the formation of monomethylmercury (MMHg), but also in detoxification and MMHg degradation in the environment (Grégoire & Poulain, 2018). These microorganisms possess specific genetic mechanisms, such as the *mer* genes, that enable them to demethylate MMHg and reduce Hg^{II}, transforming it into the volatile form Hg^{0} (Boyd & Barkay, 2012). In particular, the *merB* gene, coding for organomercurial lyase, is responsible for the transformation of MMHg into Hg^{II}, followed by the reduction of Hg^{II} to Hg^{0} by the action of the mercuric reductase enzyme, encoded by the *merA* gene (Barkay & Gu, 2022; Boyd & Barkay, 2012). One or both enzymes can be found in the *mer* operon, which is considered a key mechanism for microbial mercury resistance (Boyd & Barkay, 2012; Naguib et al., 2018; Nascimento & Chartone-Souza, 2003; Norambuena et al., 2020) and has also a great value in bioremediation approaches (Dash et al., 2014; Joshi et al., 2021; Priyadarshanee et al., 2022; Saranya et al., 2017).

The *mer* genes are distributed globally and present in multiple environments: researchers found *merA* in Antarctic sea-ice (Gionfriddo et al., 2016), *merB* and *merR* (Bowman et al., 2020) and *merA* in the Arctic(Møller et al., 2014), *merAB* in European lagoons (Vigneron, et al., 2021), *merA* in American thermal springs (Wang et al., 2011), *merAB* across all oceans (Sanz-Sáez, et al., 2021) and *merAB* in marine sediments from around the globe (Narita et al., 1999; Ní Chadhain et al., 2006; Pepi et al., 2011; Rincón-Tomás et al., 2023). Additionally, the microorganisms carrying *mer* genes are widely distributed across the prokaryotic tree of life (Christakis et al., 2021).

Despite the global relevance of marine sediments as repositories of Hg, the information available on Hg^{II} reduction and MMHg demethylation in these systems is limited because the reactions catalyzed by *merAB* have been originally associated with oxygenated environments and therefore the exploration of the *merAB* genes in more anoxic marine sediments ecosystems has been overlooked. Spangler et al. (1973) found facultative anaerobes with the capacity to demethylate MMHg and Schaefer et al. (2002) demonstrated that *mer* genes could be expressed anaerobically, still most of the studies have been conducted in aerobic environments like the seawater column (e.g. Bowman et al., 2020; Sanz-Sáez et al., 2022) or freshwaters (e.g. Møller et al., 2014; Sadhukhan et al., 1997). Traditionally, MMHg demethylators and Hg^{II} reducers have been studied in culture either aerobic (Narita et al., 2003; Pepi et al., 2011, 2013; Spangler et al., 1973) or anaerobic (Spangler et al., 1973) however, the role and importance of these cultures in the Hg cycle remains unknown. The few published studies reporting *merA* genes in culturable bacteria from marine sediments have identified Bacillota (formerly Firmicutes), Gammaproteobacteria, and some Archaea (Binish et al., 2021; Narita et al., 1999; Pepi et al., 2011, 2013).

Within the omics era, the use of metagenomics and metatranscriptomics analyses have allowed the identification of ecologically relevant uncultured bacteria containing *mer* genes (Rincón-Tomás et al., 2023; Vigneron et al., 2021). A recent metagenomic study in three estuaries located in the Bay of Biscay, highly impacted by Hg pollution due to industrial activities, pointed out the role of Desulfobacterota, a phylum previously associated only with Hg^{II} methylation, as Hg^{II} reducers, since *merA* genes were identified in some Desulfobacterota genomes (Rincón-Tomás et al., 2023).

Bacterial MMHg degradation was previously found in sediments (Oremland et al., 1991) and more recently, Rincón-Tomás et al. (2023) found ten *merB* genes in estuarine sediment samples but the number of studies researching the *merB* mediated demethylation are very limited. It is still unknown how prevalent prokaryotes involved in Hg detoxification, both Hg^{II} reduction and MMHg demethylation, are in different marine sediments. Thus, our study focused on i) the identification of specific microbial groups with the genetic capability to demethylate MMHg and reduce Hg^{II} and ii) the study of their potential transcriptional activity in sediments with contrasting Hg concentrations and different geographical locations to provide a better understanding of Hg cycling.

Material and Methods

Sample collection, DNA/RNA extraction and library preparation

Surface sediment samples (n = 30, including 10 samples with triplicates) were collected in 2019-2020 at four coastal sites in three locations (Figure S2 and Table S8): Bay of Biscay (Nervión and Saja river estuaries in Spain; stations CS14, CS3, CS4, CS7, EN15, EN17, ENAsua, ENAxpe), Mediterranean (BCN4 station, Barcelona, Spain) and Baltic Sea (KPH station, Köpmanholmen, Sweden). Samples were kept at -80 ^{o}C until further processing for DNA/RNA extraction. Total environmental RNA and DNA was extracted using the RNEasy PowerSoil Total RNA kit followed by the PowerSoil DNA Elution kit (Qiagen), following the manufacturer's protocol.

The libraries for the metagenomes were prepared with TruSeq DNA PCR-free preparation kit and the libraries for the metatranscriptomics were prepared with TruSeq stranded mRNA library preparation kit without polyA selection (Illumina). Both sets of samples, metagenomic and metatranscriptomics, were sequenced paired-ended in one NovaSeq 6000 S4 lane (Figure 17).

The MERCLUB Microbial Gene Catalogue

Metagenome processing

A total of 30 metagenomes from 10 locations were processed to obtain a redundant gene set to build the gene catalog. Raw reads were cleaned and trimmed with fastp v0.21 (Chen et al., 2018) (options --length_required 50 --adapter_sequence= CTGTCTCTTATACACATCTCCGAGCCCACGAGACATGTGTATAAGAGACA --adapter_sequence_r2= CTGTCTCTTATACACATCTCGCAGGGGATAGTCAGATGACGCTGCCGACGAATGTGTATA

AGAGACA --cut_tail --cut_window_size 1 --cut_mean_quality 25 --trim_front1 4 --trim_tail1 1 --correction --overrepresentation_analysis --trim_poly_g). Clean reads were assembled in megahit v1.2.8 (Li et al., 2016) with options --presets meta-large --min-contig-len 500.

Assembled contigs were processed with prokka v1.14.6 (Seemann, 2014) with options --metagenome --gcode 11. Prokka provides the gene prediction as well as a basal annotation, that comprises identification of coding DNA sequences (CDS), annotated as clusters of orthologous groups (COGs) and Enzyme Comission numbers (EC). Prokka also identifies and annotates transfer RNAs (tRNAs and tmRNAs), ribosomal RNAs (rRNAs) and CRISPR arrays. Amino acid sequences from all predicted CDS were further annotated against the KEGG orthology database (KO, release 98.0, Kanehisa & Goto, 2000) with kofamscan v1.3.0 (Aramaki et al., 2019) and against the Pfam database (El-Gebali et al., 2019; release 34.0) with HMMR v3.3 (Eddy, 2011) with options --domtblout -E 0.1 and then filtered accordingly, so that the best hit for each model aligned with no overlaps to the target CDS.

MERCLUB Microbial Gene Catalog generation

The MER-CLUB Microbial Gene Catalogue was obtained by clustering all DNA coding sequences larger than 100 bp predicted in each metagenome (n = 28,676,531) at 95 % of similarity in mmseqs2 (Steinegger & Söding, 2017; commit 13-45111) with options -c 0.9 --min-seq-id 0.95 --cluster-mode 2 --cov-mode 1. The MERCLUB Microbial Gene Catalogue currently counts with over 16 million non-redundant genes (16,102,394). The annotation of each gene cluster was inherited from the annotation of the seed of the gene cluster obtained previously. Our catalogue displayed high novelty with many genes eluding annotation: 46 % of genes were annotated with PFAM, and 17.4 % were annotated with KEGG Kos.

Generation of MERCLUB Hg-detoxification Reference Gene Catalogue (Hg-RGC).

Extracting merA and merB genes from MERCLUB Microbial Gene Catalogue.

Custom Hidden Markov Models (HMM) for *merA* and *merB* genes in the amino acid space were built querying UniProtKB for the KEGG orthologs (KO) identifier K00520 and K00221, respectively (BioStudies accession number S-BSST1154; Rincón-Tomás et al., 2023). We examined our MER-CLUB Microbial Gene Catalog for *merA* and *merB* gene candidates by selecting sequences annotated with the custom HMMs (HMMR v3.3; Eddy, 2011), plus all sequences annotated as either *merA* (K00520) or *merB* (PF03243, K00221). Annotation as *merA* or *merB* genes was confirmed by checking the presence of conserved amino acids (a cysteine pair at positions 207 and 212, numbered based on the MerA from *Bacillus* sp. RC607, and a cysteine pair at positions 96 and 159 based on the MerB on plasmid R831b; (Gionfriddo et al., 2016).

Taxonomy of merA and merB genes

The *merA* and *merB* genes taxonomy was estimated by comparing the amino acid sequences to UniRef90 (mmseqs2) selecting the taxonomic assignation of the best hit.

MERCLUB Metagenome Assembled Genomes (MAGs) construction

Clean reads from each site were assembled on megahit v 1.2.8 (Li et al., 2016 ; options --min-contig-len 2000 --meta-large) and then all individual metagenomes were back-mapped to each of the 10 site co-assemblies in bowtie v2.3.2 (Langmead & Salzberg, 2012) allowing all matches. The 30 mapping files for each site were used to calculate an abundance profile of each contig across all metagenomes metabat v2.12.2 (Kang et al., 2019) and this information, together with the tetranucleotide frequencies, was used to group the contigs into a total of 2885 genomic bins. These 2885 genomic bins were assessed for genome completeness and contamination using single copy gene sets in checkM v 1.1.3 (Parks et al., 2015). All bins which were more than 50 % complete and had less than 10 % of contamination were estimated to be medium quality MAGs (Bowers et al., 2017) and used for downstream processing. A total of 803 medium quality MAGs were annotated using prokka v 1.14.6 (Seemann, 2014), supplemented with protein families (PFAM v34.0, HMMER v3.3) (Wheeler et al., 2012) and KEGG orthologs (KO; kofamscan v1.3.0, KEGG release 98) (Aramaki et al., 2019).

We identified *merA* and *merB* genes within the MER-CLUB MAGs dataset (Figure 17) using the same procedure used for the MERCLUB Hg-detoxification Reference Gene Catalogue (Hg-RGC).

Fragment recruitment analysis

MAG abundance and their cumulative transcriptional activity were estimated by fragment recruitment analysis (FRA). First, we made a blastn v2.13.0 (Altschul, 1997) database with the concatenated sequences of the assembled contigs of each of the 803 MAGs. Then, the reads of the 30 metagenomes and 24 metatranscriptomes were randomly subsampled to the smallest sequencing depth value (61,809,851 fragments reads for metagenomes and 3,719,416 for metatranscriptomes) with bbtools v38.08 (reformat.sh; https://sourceforge.net/projects/bbmap/). Only reads with alignment coverage larger than 90 % and sequence identity larger than 95 % were kept for downstream analyses. In addition, we discarded reads mapping any region annotated as rRNA to avoid spurious hits to highly conserved regions. Only MAGs with at least 20 % of horizontal genomic coverage (meaning that at least 20 % of their assembled contigs were covered by recruited reads) were assumed to be present in the samples (Royo-Llonch et al., 2021). MAGs with less than 20 % horizontal genome coverage were thus considered spurious mappings and absent from the samples. Consequently, metatranscriptomics reads mapping to the latter MAGs were as well discarded from further analysis. The abundance and the total transcriptional activity of each MAG were expressed as the number of mapped reads per genomic (MAG size) kilobase (RPKG), as the normalization per metagenome size was previously done by subsampling the metagenomes.

Phylogenetic analysis

The MerA and MerB protein sequences extracted for both the gene catalog and MAGs catalog were used to construct a phylogenetic tree (Figure 17). The phylogenetic analysis was performed with MEGAX (Kumar et al., 2018). The alignment was created with the default options of MUSCLE within MEGAX. Maximum-likelihood phylogenetic reconstruction (bootstrap: 1000) was done using the Jones–Taylor–Thornton model by MEGAX (Kumar et al., 2018). In the same manner, the phylogenetic analysis was done for the genes of the MAGs. Phylogenetic tree editing was done in R (R Core Team, 2013) using the following packages, ggtree v.3.10 (G. Yu et al., 2017), ggtreeExtra v.1.12 (Xu et al., 2021) and ggplot2 v.3.4.4 (Wickham, 2016). Post-processing was done in Illustrator CC 2020 (Adobe).

Functional and metabolic analysis of MAGs.

The KEGG orthologs of the MAGs were obtained (KO; kofamscan v1.3.0, KEGG release 98; Aramaki et al., 2019). To explore the metabolic capabilities of the MAGs, we used KEGG-Decoder (Graham et al., 2018) to study their metabolic capacities (carbon fixation, hydrogen oxidation, sulfur, nitrogen and methane metabolisms) as well as other functional genes related to mobility, biofilm formation and other metal resistances genes.

Data visualizations.

All data visualizations included in this manuscript have been generated with the R package ggplot2 v.3.4.4 (R Core Team, 2013; Wickham, 2016). Multi-panels and post-processing were done in Illustrator CC 2020 (Adobe).

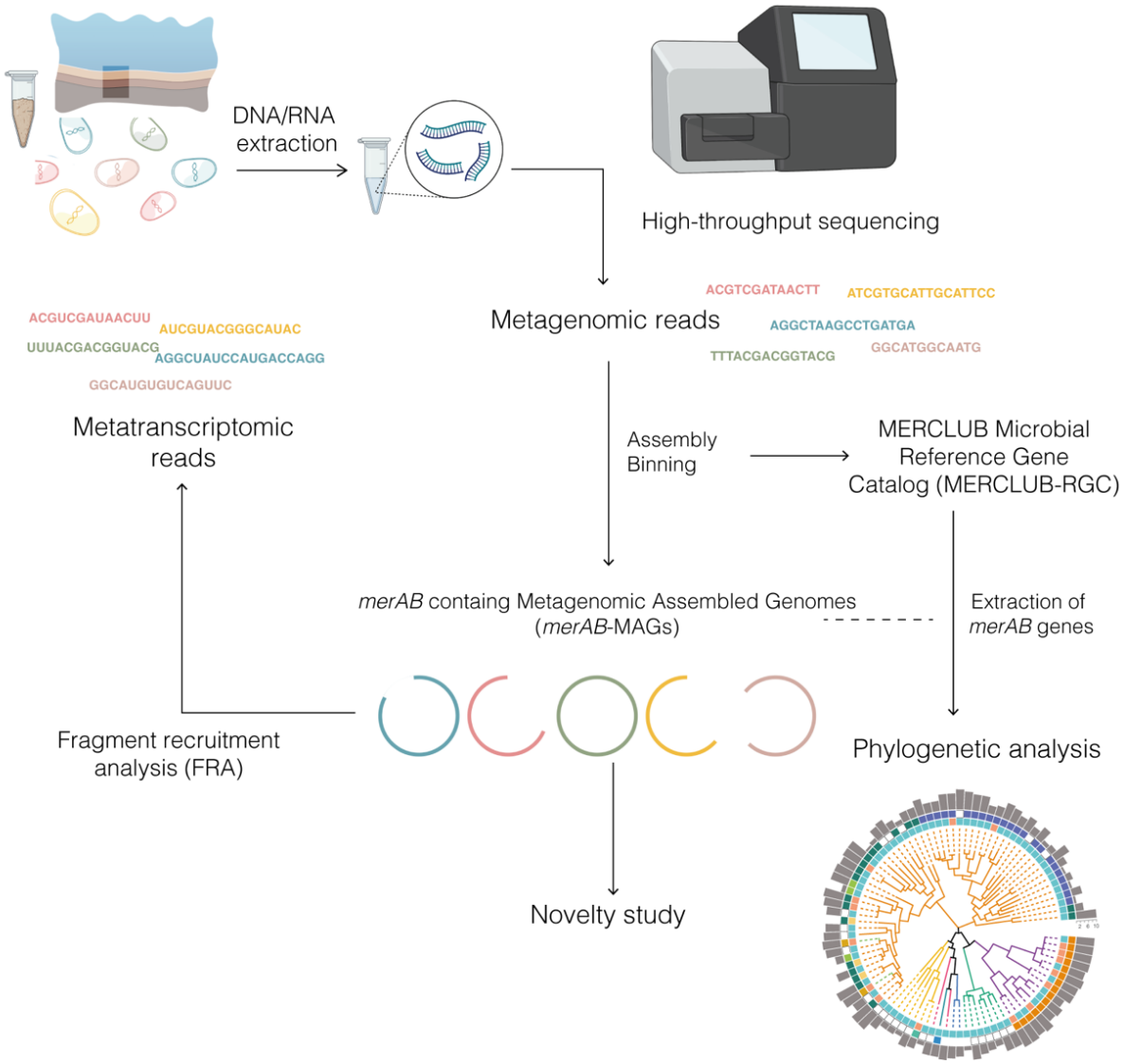


Figure 17: Diagram of the methodology used in Chapter 2, from sample collection to assembling and post analyses.

Results and Discussion

A deep look into the microbial taxa involved in Hg^{II} reduction and MMHg demethylation in Hg-impacted marine sediments

We sequenced 30 microbial metagenomes from marine sediments collected from 10 different Hg-impacted sites of three marine regions: Bay of Biscay (Nervión and Suances), the Mediterranean Sea (Barcelona) and Baltic Sea (Köpmanholmen). Our analysis showed that the three replicates of each of the 10 sampling points were very similar in terms of both taxonomic (mTag analysis) and k-mer composition. Due to the high complexity of sediment metagenomes, we decided to co-assemble the replicates of each site to increase the sequencing space. These metagenomes were co-assembled to generate the MERCLUB Microbial Gene Catalog with a total of 16,102,394 non-redundant genes. Using a custom Hidden Markov Models (HMM) for *merA* and *merB* genes (see details in M&M), we identified 74 *merA* and 188 *merB* genes conforming the Hg-Reference Gene catalogue (Hg-RGC). Using the same HMM models for *merA* and *merB* genes we identified a total of 45 bacterial MAGs (Figure 18) having *merAB* genes from our MER-CLUB MAGs database with a total of 803 MAGs. Of those, 16 MAGs contained the *merA* gene and 35 had the *merB* gene. Phylogenetic analyses were performed integrating a total of 90 *merA* (Figure 19) and 223 *merB* (Figure 20) genes derived from both approaches (Hg-RGC and MERCLUB MAGs dataset). Only 20 % and 18.6 % of the *merA* and *merB* genes of the Hg-RGC catalog were later found in the MAGs respectively, while only one *merA* (EN17.27_02336) was recovered in the MAGs dataset but was not present in the catalog (its highest identity was 83.33 % with MERCLUB-RGC-v1.1_003126404).

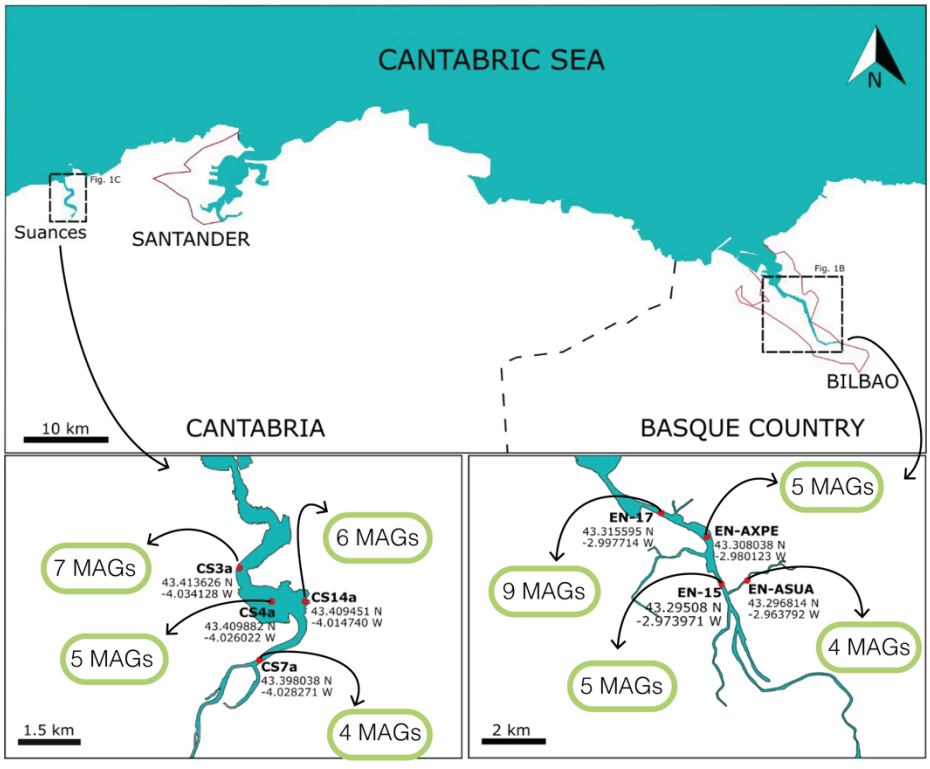


Figure 18: Location of the 45 MAGs containing *merA* and/or *merB* genes out of the 803 MERCLUB MAGs dataset generated from 3 principal sites (Figure S2). The 45 MAGs analyzed in detail were derived from the sites located in the Basque Country and Cantabria.

Out of the 90 *merA* genes, 88 of them belonged to 8 different phyla: Actinomycetota, Armatimonadota, Bacillota_A, Chloroflexota, Gemmatimonadota, Krumholzibacteriota, Pseudomonadota and Verrucomicrobiota (Figure 19), while two of them were not assigned to any phylum. Krumholzibacteriota was not previously found as a *merA* containing phyla (Christakis et al., 2021). Out of the 90 *merA*, 58.8 % of them (53) were assigned to the phylum Pseudomonadota, in the same range as the 53.7 % (4050 out of 7544) found in the study from Christakis et al. (2021). Among one of the Pseudomonadota clusters, we found two *merA* genes belonging to the same MAG (CS7.241) assigned to Krumholzibacteriota (Figure 19). The homologs of these two genes in the Hg-RGC were assigned as Pseudomonadota with no further assignation. The taxonomy in the catalog is based only on *mer* gene sequences, and *mer* genes can be horizontally transferred, so it is plausible that the assignation in the catalog was misleading. No other genes belonging to Krumholzibacteriota were found in the Hg-RGC, this phylum was only found in the MAGs dataset. However, four of the phyla were only found in the Hg-RGC catalog, Armatimonadota, Bacillota_A, Gemmatimonadota, and Verrucomicrobiota, and the last two have not been described in the previous database from Christakis et al. (2021). However, Vigneron et al. (2021) found Verrucomicrobiota in their MAGs. Overall, Pseudomonadota was the most prevalent phylum, present in the ten stations, with four sequences belonging to the catalog and two belonging to the MAGs. Besides, other Pseudomonadota (Alphaproteobacteria and Gammaproteobacteria), Krumholzibacteriota, and 12 out of the 15 Actinomycetota were present in most (eight or nine) stations (Figure 19).

On the other hand, most *merB* genes (198) belonged to 12 phyla: Abyssobacteria, Acidobacteriota, Actinomycetota, Candidatus Dadabacteria, Chloroflexota, Desulfobacterota, Desulfobacterota_F, Euryarchaeota (Archaea), Gemmatimonadota, Nitrospirota, Pseudomonadota, Zixibacteria (Figure 20); other 25 *merB* genes were not assigned to any phylum. Three of them (Abyssobacteria, Acidobacteriota and Candidatus Dadabacteria) were not present in the previous database from Christakis et al. (2021) and two of them, Desulfobacterota and Desulfobacterota_F, were previously categorized as Deltaproteobacteria (phylum Pseudomonadota). Almost three thirds (73.37 %) of *merB* genes were assigned to the phylum Pseudomonadota compared to the 26.62 % found in Christakis et al. (2021). Such differences may be linked to the fact that the dataset built in Christakis et al. (2021) integrated a wide variety of habitats while our study is mainly focused on marine sediments. Among the Pseudomonadota clusters, we found three genes taxonomically assigned to Archaea instead of Bacteria (Figure 20). Although *merB* genes were identified in archaea in the Hg-RGC, we did not find them among the archaeal MAGs. As well, we found in the catalog Chloroflexota (adding 7 genes to the 7 already described in Christakis dataset) and Gemmatimonadota (adding two new genes to the single gene present in Christakis dataset) which were not present in the *merA* and/or *merB* containing MAGs. Only 6 genes, all belonging to MAGs, were present in the ten stations. They all belong to the same genus UBA9214 from the order Thiohalobacterales (Gammaproteobacteria). Actinomycetota, Desulfobacterota, Desulfobacterota_F and Psedomonadota are the other taxa corresponding to the most prevalent genes (present in eight/nine stations) (Figure 20).

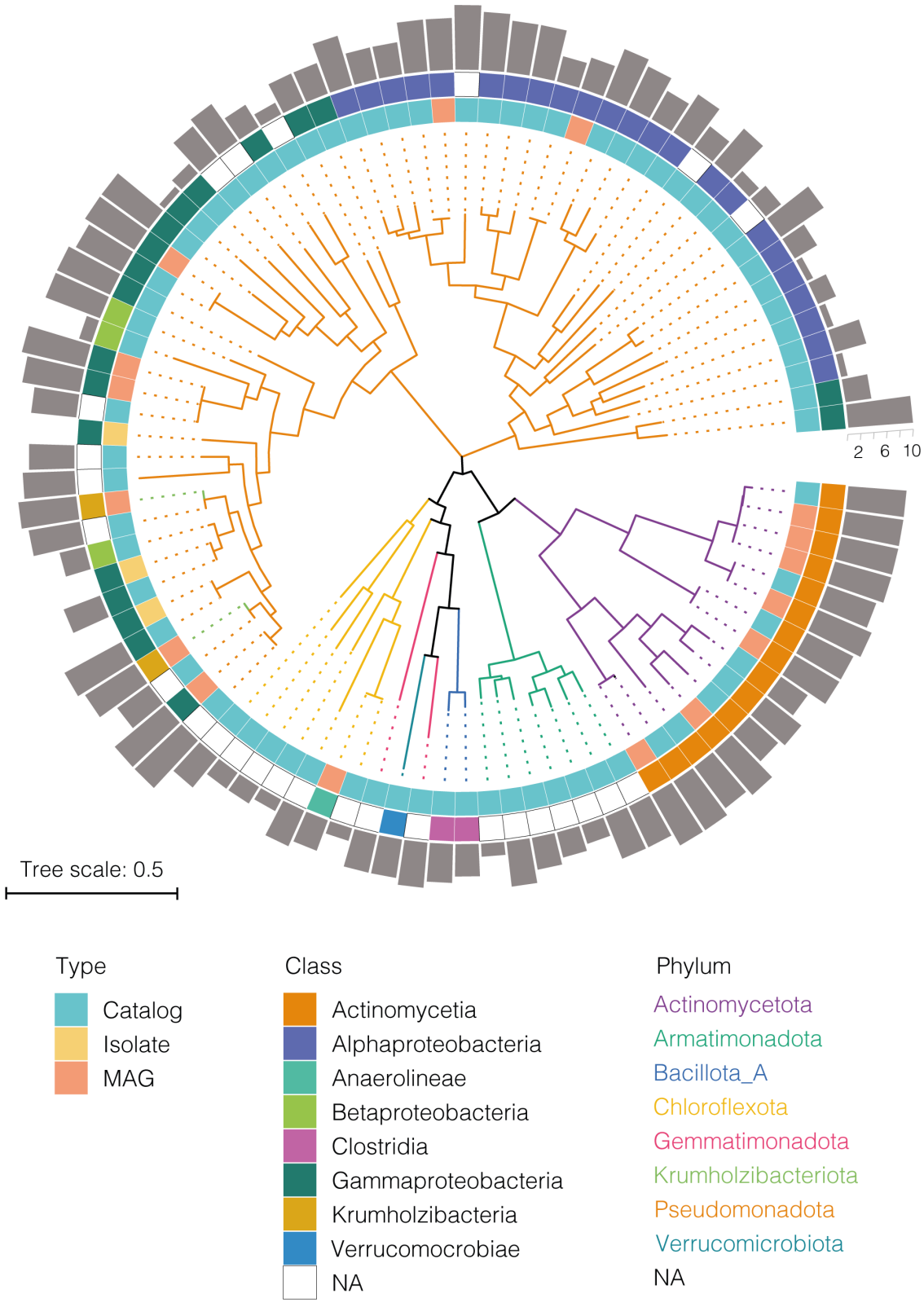


Figure 19: Phylogenetic analysis integrating 90 MerA amino acid sequences retrieved from both Hg-RGC and MERCLUB MAGs datasets. The analysis includes 3 extra sequences from isolates of the MERCLUB Culture Collection. The histogram (in grey) represents the number of sites in which the sequence was found. The colors of the lines in the phylogenetic tree correspond to the phylum.

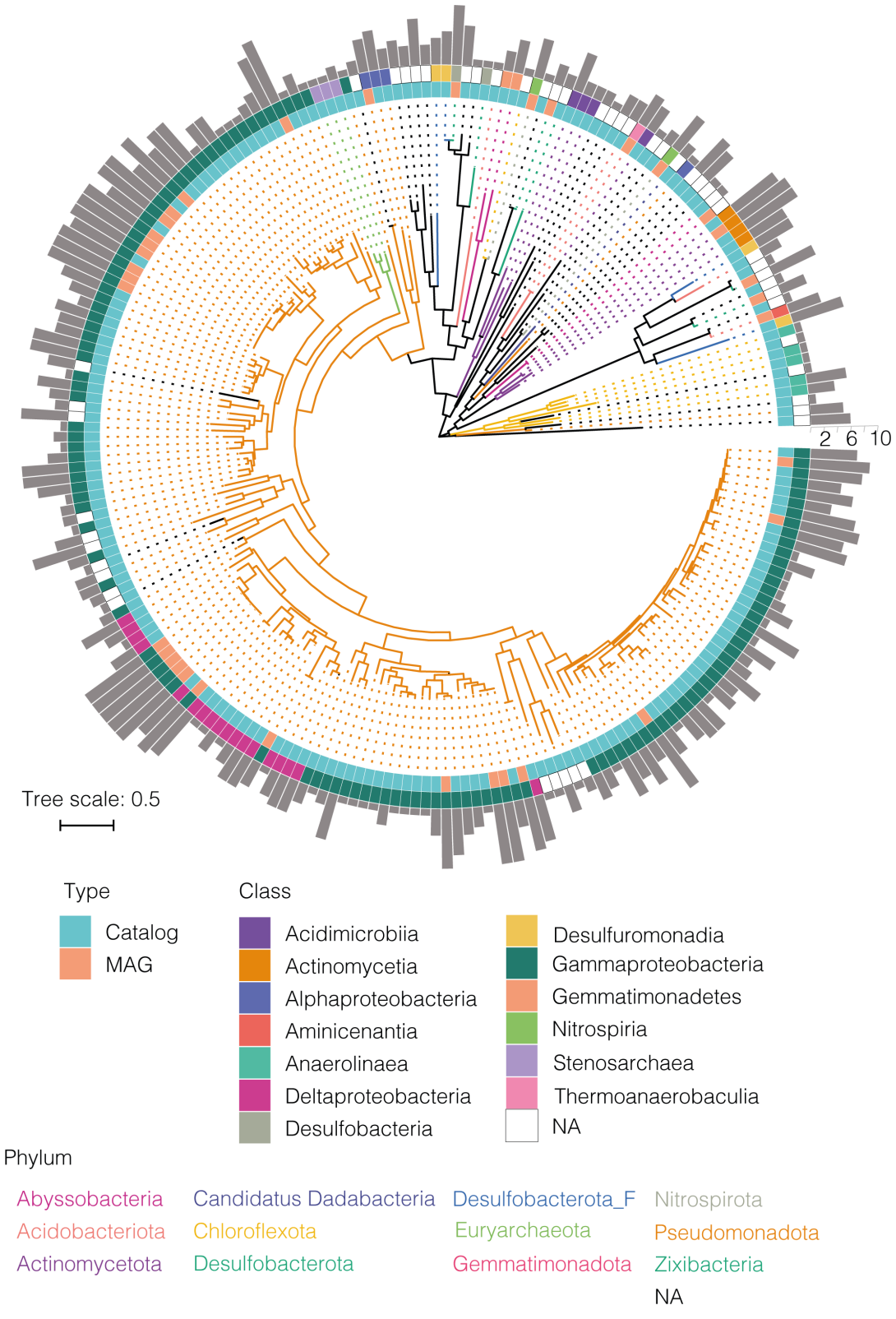


Figure 20: Phylogenetic analyses integrating 223 MerB amino acid sequences retrieved from both Hg-RGC and MERCLUB MAGs datasets. The histogram (in grey) represents the number of sites in which the sequence was found. The colors of the lines in the phylogenetic tree correspond to the phylum.

The Hg-RGC catalog provided a greater diversity of *merAB* genes, with the identification of a higher number of classes, which is relevant to get a deeper view of the microbial taxa involved in the reduction and demethylation of mercury. However, it lacked the genomic context of those taxa. For that reason, the reconstructed metagenomic assembled genomes (MAGs) provided essential genomic information to infer a deeper understanding of the metabolic and functional traits of these ecologically relevant taxa.

Diversity and novelty of microbial MAGs containing *merAB* genes

From the MERCLUB MAGs database, 45 bacterial MAGs were identified as having *merA* and/or *merB* genes, and in six of them an entire operon was reconstructed (Figure S3). No *merA* and/or *merB* genes were retrieved from the 27 archaeal MAGs, suggesting that Hg detoxifying archaea were rare or absent. Two MAGs contained both *merA* and *merB* genes (EN17-bin.27 and EN17-bin.60), 13 had only *merA* (1 had two merA genes) and the other 30, had only *merB* (three had two *merB* genes). They belonged to 9 phyla: Abyssubacteria, Acidobacteriota, Actinobacteriota, Chloroflexota, Desulfobacterota, Krumholzibacteriota, Nitrospirota, Proteobacteria and Zixibacteria (Figure 21). As summary, 62.2 % of the identified MER-CLUB MAGs with *merA* and/or *merB* genes belonged to Proteobacteria, 28 out of the 45, with most of them (26) associated to Gammaproteobacteria and affiliated to 6 different orders, such as Arenicellales, Burkholderiales, Chromatiales Pseudomonadales, Thiohalobacterales, and SZUA-229 (Figure 21). The phylogenetic analysis of the *merA* of the MAGs allows us to identify three clusters, one with the enzymes belonging to Actinobacteriota, one with the Gammaproteobacteria and the Krumholzibacteriota, which we already mention as a possible horizontal gene transfer, and one the Alphaproteobacteria and one Aerolineae (Figure S4A). For *merB*, we also found three clusters: one with all the Gammaproteobacteria and three more sequences (Zixibacteria, Nitrospirota and Alphaproteobacteria), one with a few different taxa and one with just one sequence belonging to Desulfobacteriota (Figure S4B).

Only two of the MAGs were classified at the species level (Figure 21), while 95.5 % of the *merA* and/or *merB* containing MAGs remained unclassified at this level, suggesting that the novelty within the MERCLUB MAGs containing *merA* and/or *merB* genes from Hg-impacted sediments was higher than other studies, which showed lower percentages of unclassified MAGs within the archaea and bacteria, ranging between 80-85 % (Alneberg et al., 2020; Royo-Llonch et al., 2021) or 58-68 % (Acinas et al., 2021).

As we mentioned before, *merA* nor *merB* genes from Krumholzibacteriota were included in the latest database made by Christakis et al. (2021), although in a very recent study, Ma et al. (2023) reconstructed three Krumholzibacteriota MAGs with the *merA* gene in soil samples (GenBank assembly ID: GCA_035649275.1, GCA_035649435.1 and GCA_036398135.1). The MAG belonging to Krumholzibacteriota from our work (CS7-bin.241) was recovered from station CS7 (Bay of Biscay), with a Hg concentration of 1315 ± 214 ng of Hg/g total. Even though CS7-bin.241 was recreated from a station in the Suances area, it is present in 9 out of 10 sampling sites, only missing in Sweden (KPH0to2cm). This MAG is 78.62 % complete

and 3.35 % contaminated. It has two *merA* genes; for one of the genes, we were able to reconstruct the entire operon (Figure S3). This phylum's first representative, *Krumholzibacterium zodletonense*, was recovered from an anoxic sulfide and sulfur-rich spring (Zodletone spring) in southwestern Oklahoma (Youssef et al., 2019) and the phylum has no culture representative.

The Abyssubacteria MAG (EN17-bin.217) is 98.9 % complete and only 3.48 % contaminated. Even though it is almost 100 % complete, it has <71 % ANI with the three available genomes from this phylum (GenBank assembly ID: GCA_016215705.1, GCA_003598085.1 and GCA_003598055.1) (He et al., 2021; Momper et al., 2018) pointing out to represent a different species and even genera (Sangal et al., 2016). Even though this taxon was neither included in Christakis et al. (2021) study, all three public genomes have the *merA* gene, and only one has *merB* as well (GCA_003598055.1). On the other hand, the representatives for Zixibacteria among our MAGs did not have *merA*, but only *merB,* as previously reported (Christakis et al., 2021). Curiously, one of the three sequences from Zixibacteria is in one cluster and two in the other (Figure S4B). We also detected one MAG identified as Desulfosudaceae (EN17-bin.295), a family with a single genus (*Desulfosudis*) that belongs to the Desulbacterota phylum. This MAG displayed a genome completeness of 79.25 % and displayed the *merB* gene but no *merA,* as recently observed in some Desulbacterota MAGs related to Desulfuromonadia in similar sediments (Rincón-Tomás et al., 2023).

Lastly, the two MAGs containing both *merA* an *merB* genes were reconstructed from station EN17 (the station with the second highest Hg concentration, 6601 ± 179 ng Hg/g total): one (EN17-bin.27) is a 2.5 Mbp MAG (100 % complete, 0.69 % contamination) from order Actinomycetales (*Microbacterium* sp.) and the other (EN17-bin.60) is a 3.8 Mpb MAG (90.6 % complete, 3.3 % contamination) from order Rhodobacterales. We reconstructed an entire operon in EN17-bin.60 which has both enzymes (Figure S3). It was in the EN17 station where the highest number of MAGs was recovered and also where the highest taxonomic diversity of MAGs with *merA* and/or *merB* genes was found, from 5 different phyla including Abyssubacteria, Actinobacteriota, Desulfobacterota, Proteobacteria and Zixibacteria.

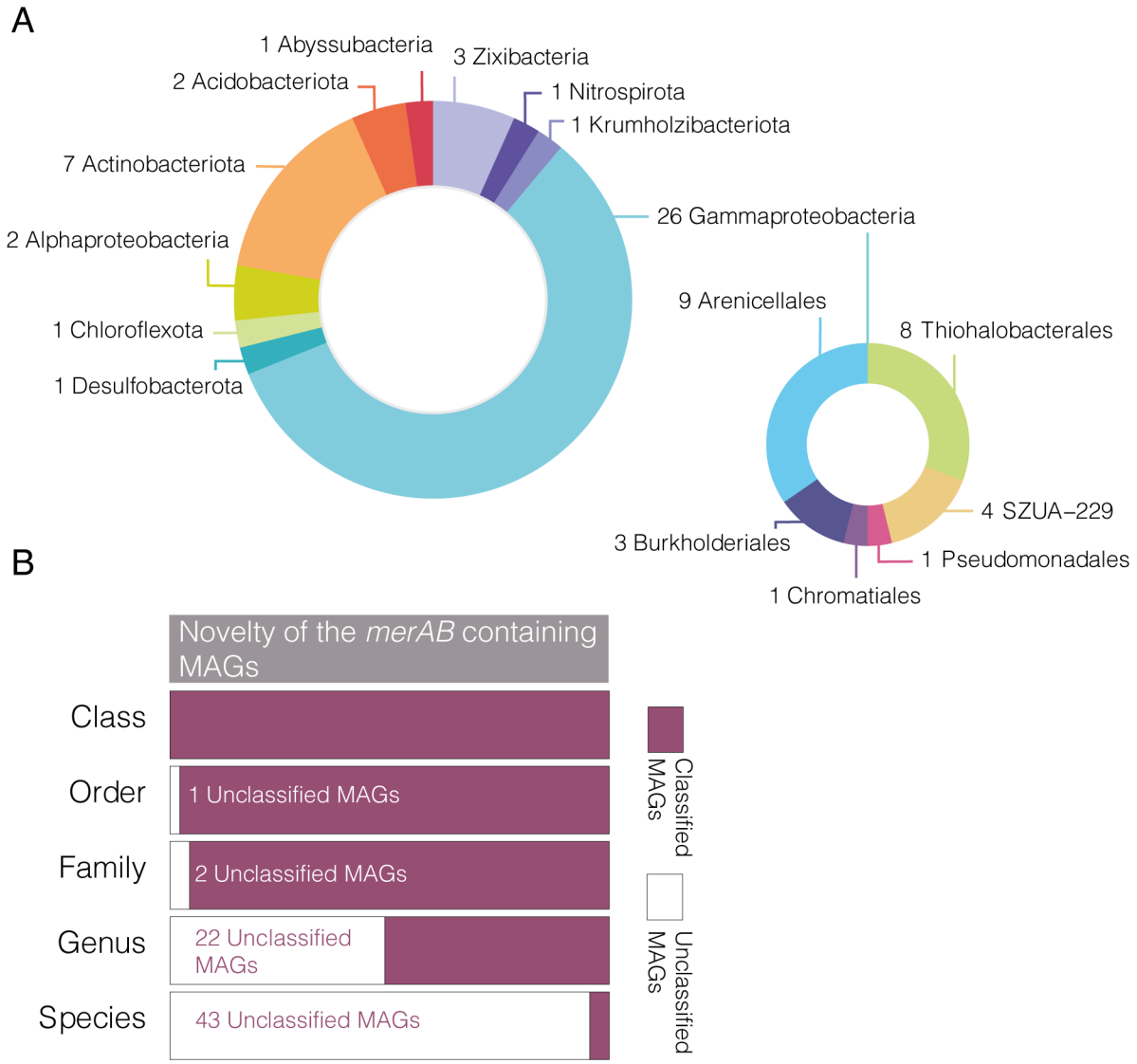


Figure 21: Taxonomic annotation and novelty of the MERCLUB MAGs containing *merA* and/or *B* genes. A) Phylogenomic-based taxonomy of the 45 MERCLUB MAGs dataset at the phylum level (except for Proteobacteria that were split at the class level). Gammaproteobacteria were further visualized at the order level as well. The figures indicate the number of MAGs for each taxonomic level. B) Stacked bar plot for novelty quantification of the *merAB* containing MERCLUB MAGs (x-axis) at different taxonomic ranks (y-axis). The taxonomically unclassified portion is depicted in white; the taxonomically classified portion is shown in dark magenta.

Metabolic and functional diversity of the *merA and merB* MAGs genomes

The metabolic diversity of the MAGs harboring *merA and/or merB* genes was investigated to determine what metabolisms were more prevalent among the bacterial genomes with the genetic potential for Hg^{II} reduction and MMHg demethylation in coastal marine sediments (Figures 22 and 23). We observed that chemolithoautotrophic metabolisms were associated with most of the MAGs related to Gammaproteobateria, and present in Arenicellales, Burkholderiales, Chromatiales, and Thiohalobacterales. These MAGs represented 62.2 % (26 out 45) of the MAGs containing either *merA* or *merB* genes (Figure 23) and only 4 of them showed *merA*, while 22 harbored *merB* and none of them had both genes. These results

highlight the importance of studying *merB* genes not only as a complement of *merA* (Christakis et al., 2021). The Calvin Cycle pathway was present (with the essential RubisCo genes) in 11 MAGs (24.4 %) mostly associated to Arenicellales, although two MAG were assigned to Burkholderiales and Thiohalobacterales. These bacteria are potentially capable of fixing CO_2 and produce new organic biomass using as energy source either the thiosulfate oxidation by the SOX complex or the H_2 oxidation by NiFe and NAD-reducing hydrogenases. Both sources of energy were present in almost all the Gammaproteobacterial MAGs (Figure 23). Interestingly, many of the above-mentioned MAGs also displayed the key marker genes for multiple steps of denitrification, dissimilatory nitrate reduction or dissimilatory sulfate reduction, pointing out their metabolic versatility. Some of them showed the capacity for chemotaxis or flagellar development but none of them showed the potential for biofilm formation (Figure 24).

The metabolic reconstruction of the three *merB* containing MAGs, assigned to the phylum Zixibacteria (previously known as RGB-1 lineage), included *mttB* gene for methanogenesis via trimethylamine, *hao* gene for nitrification and dissimilatory sulfur reduction, reflecting a mixotrophic lifestyle (Figure 23). The phylum Zixibacteria has been also found in sediments from aquifers and contains pathways and complexes involved in aerobic growth, oxidation or reduction of ferric/ferrous iron, arsenate/arenite and nitrate/nitrite, hydrogen metabolism, and anaerobic respiration via nitrite reduction, as well as fermentation to propionate, acetate, ethanol, and butyrate (Castelle et al., 2013). Thus, overall, their versatile metabolism enables Zixibacteria to thrive in changing redox environments. Additionally, all three genomes of Zixibacteria have the necessary genes for flagellar development and for chemotaxis, as well as the arsenic resistance operon (*arsCBRA*) and cobalt and ferrous iron transporters (*corA* and *feoB*) (Figure 24).

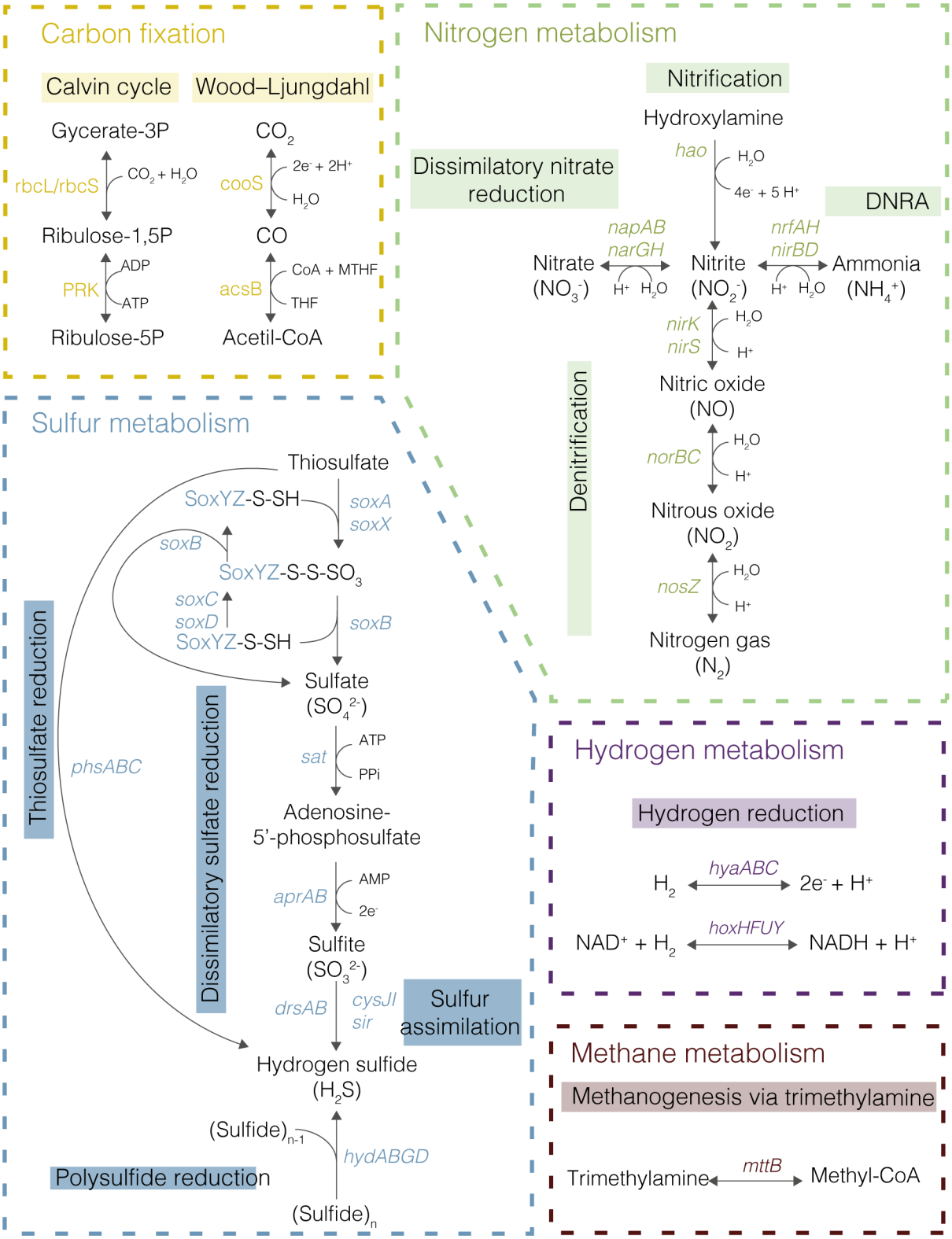


Figure 22: Metabolic pathways of the 45 MAGs harboring *merA* and/or *merB* genes involved in inorganic carbon fixation (yellow), nitrogen (green), sulfur (blue), hydrogen (purple) and methane (red), shown with the names of the genes. A complete list of the KO involved in all represented pathways is indicated in Table S9 as well as in github.com/bjtully/BioData/tree/master/KEGGDecoder (Graham et al., 2018)

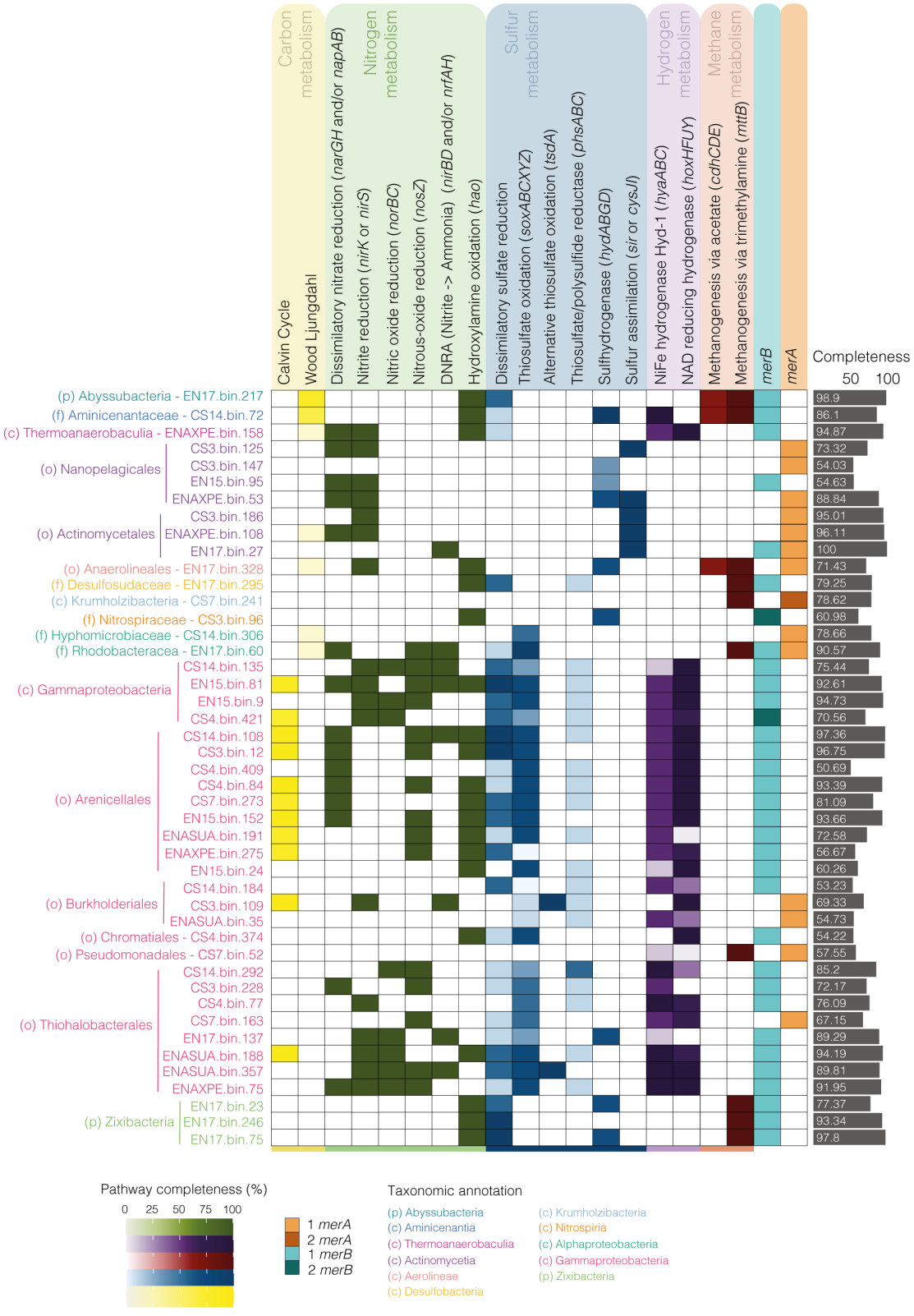


Figure 23: Metabolic potential of the 45 MAGs containing *merA* and/or *merB* genes. Each MAG is colored based on its taxonomic affiliation at the highest possible resolution. Different pathways associated with Sulfur, Nitrogen, Methene, Hydrogen, and Carbon metabolism are shown in different colors.

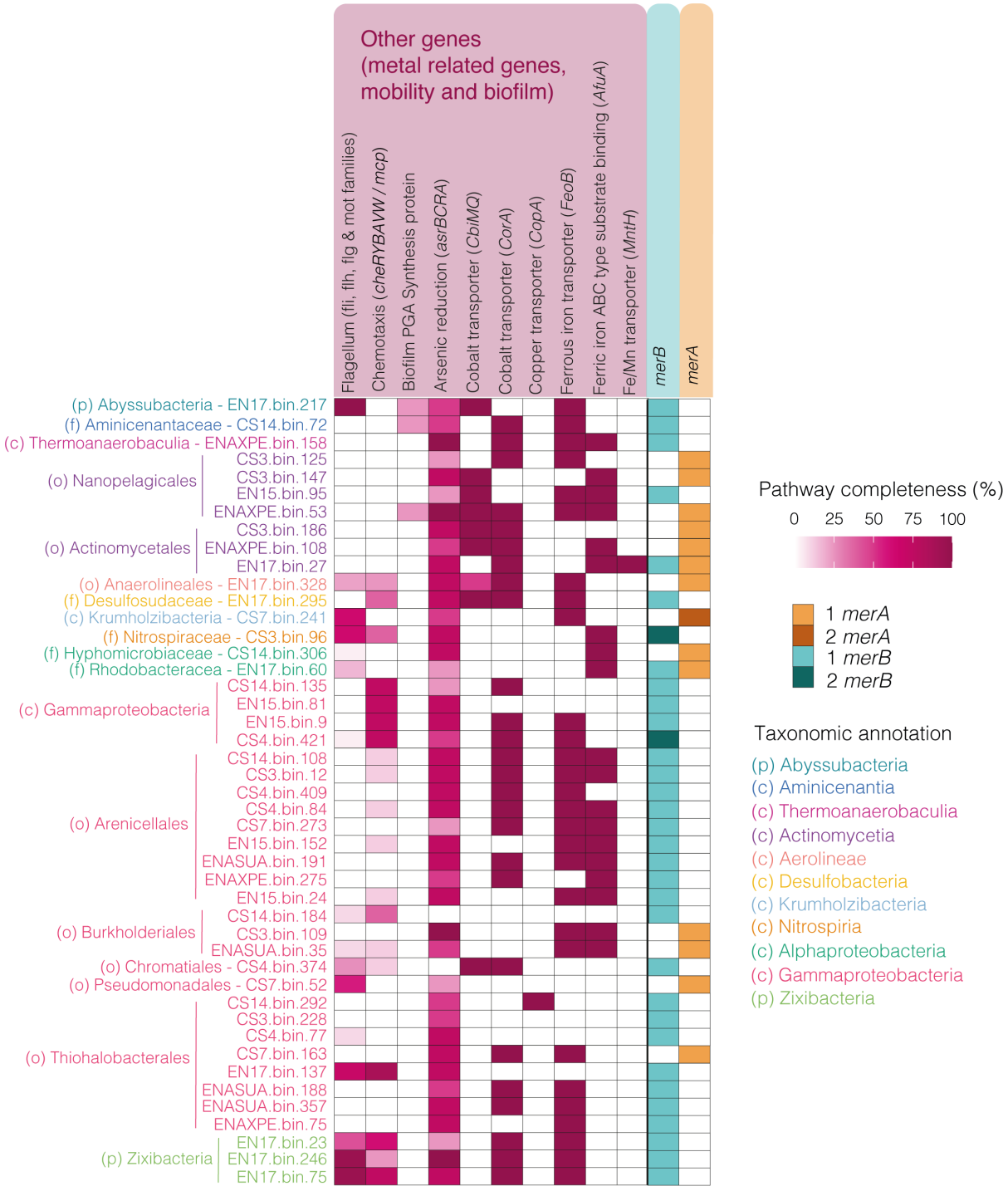


Figure 24: Functional traits associated to metal metabolism, motility, and biofilm formation of the 45 *merAB* MAGs. Each MAG is colored based on its taxonomic affiliation at the highest possible resolution.

The phylum Krumholzibacteriota (MAG CS7.bin.241) has never been described to contain *merB* but as mentioned earlier, three genomes with *merA* have been recently reconstructed (Ma et al., 2023). Even though CS7.bin.241 has a 78 % completeness, it has a quite incomplete metabolism (Figure 23). The only complete route is part of the methane metabolism (methanogenesis via trimethylamine; *mttB* gene) which hints at a restrictive lifestyle. It displayed a quite complete flagellum but no chemotaxis and no biofilm formation, as well as arsenic reduction (~50 % completeness) and a ferrous iron transporter (*FeoB*).

The only two MAGs that contained both *merAB* genes in their genomes, associated with Actinomycetales (EN17.bin27) and Rhodobacteracea (EN17.bin60), presented the enzymes required for dissimilatory nitrate reduction to ammonium (DNRA). The different Actinomycetales (except EN17.bin.27), displayed the responsible genes for dissimilatory nitrate and nitrite reduction and additional sulfur pathways (sulfhydrogenase and sulfur assimilation) (Figure 23) but they had no genes for biofilm or flagellum formation nor chemotaxis (Figure 24). On the other hand, EN17.bin60 displayed a higher metabolic versatility with multiple routes involved in nitrate, sulfur and methane metabolisms (Figure 23).

Our results indicate that chemolithoautotrophic metabolism may significantly contribute to the primary production of organic matter in the marine sediments studied as previously suggested by other studies (Boschker et al., 2014; Lipsewers et al., 2017). It has even been reported that chemolithoautotrophic bacterial production may even equal or exceed organoheterotroph bacterial production in sediments (Howarth, 1984). Thus, chemolithoautotrophic bacteria may be involved in key geochemical processes, including sulfur, nitrogen, and carbon cycling, while they are adapted to survive in the dark, often in anoxic marine sediments.

Prevalence and transcriptional activity of the *merA* and/or *merB* MAGs

We evaluated the abundance and transcriptional activity of those 45 MAGs with *merA* and/or *merB* genes exploring their biogeography and prevalence in different Hg-impacted sediments. Our results indicated that all recovered MAGs exhibited transcriptional activity (Figure 25), with the exception of stations EN17 and CS14, where metatranscriptomic data could not be obtained. Among the most abundant MAGs we found EN17.bin.217 (Abyssubacteria), EN17.bin.27 (Actinomycetales), EN17.bin.75 (Zixibacteria), CS14.bin.72 (Aminicenantaceae), and CS3.bin.125 (Nanopelagicales), all of them in the station in which they were recovered. In contrast, the highest transcriptional abundance was found in BCN4, from which no *merA* containing MAGs were recovered; EN17.bin.137 (Thiohalobacterales), CS14.bin.135 and EN15.bin.81 (Gammaproteobacteria) had the highest transcriptional activity.

Most of the Gammaproteobacteria were present in all samples, both in the metagenomes and the metatranscriptomes, except for Sweden (KPH0to2cm) that only had 9 Gammaproteobacteria MAGs present (Figure 25). In Sweden, we only found one additional MAG, Desulfosudaceae, which was present in all samples from Biscay (Nervión and Suances) but not in Barcelona. Two MAGs, ENAXPE.bin.158 (Thermoanaerobaculia) and

EN17.bin.60 (Rhodobacteraceae), were present in all Nervión samples (EN15, EN17, ENAXPE and ENASUA) and in the Barcelona sample (BCN4) but not in Suances or Köpmanholmen. Additionally, there was one MAG, CS14.bin.72 (Aminicenantaceae) that was present only in Suances samples (CS14, CS3, CS4 and CS7), and one in the Nervión samples (EN17) (Figure 25). The seven Actinomycetia were present in all samples from Biscay, and all but one (CS3.bin.125) were present in Barcelona (Figure 25). The three representatives of Zixibacteria had different patterns of presence and abundance (Figure 25).

A further detailed analysis revealed that the *merB* was transcribed at higher levels than *merA* (Figure 26), which could explain why no MMHg could be detected in the samples (Pereira-García et al., 2024). The highest transcription of *merA* was related to the Thiohalobacterales present in two stations, followed by *Azonexus* and Krumholzibacteria. Interestingly, the two *merA* gene copies of the MAG affiliated to Krumholzibacteria displayed different expression levels in different stations (Figure 26A). On the other hand, the highest expression of *merB* gene was assigned to Arenicellales, present in 4 stations, followed by one Gammaproteobacteria and one Chromatiales. The MAG with two *merB* gene copies associated with a gammaproteobacterial MAG (CS4-bin.421) displayed a transcriptional signal only in one of the gene copies (CS4.421_00314) at the time of sampling. Additionally, a low expression of other 8 Gammaproteobacteria was detected (Figure 26B). Environmental MMHg demethylation rates are rarely measured due to the experimental and analytical challenges involved, but due to the high transcripts per million (TPM) values found in the metatranscriptomes, we strongly believe that MMHg demethylation is taking place in our sediments. Curiously, we did not find any expression of *merA and merB* either in Barcelona nor Sweden.

Interestingly, the number of *merA* (90) and *merB* (223) genes (Hg-RGC and MERCLUB MAGs Collection) recovered from our sediments differs from previous studies in which the number of *merA* genes was always higher than the number of *merB* genes (Christakis et al., 2021; Rincón-Tomás et al., 2023; Vigneron et al., 2021). In general, *merA* tends to be more prevalent likely because the percentage of MMHg in total Hg tends to be low (Bowman et al., 2020). Furthermore, until recently, studies have focused only in *merA* and the *merB* gene is only mentioned as part of the same operon (Jeffrey et al., 1996; Nakamura et al., 2001; Ní Chadhain et al., 2006), but we recovered 30 MAGs (12 high-quality and 18 medium-quality) in which there is only *merB*. The enzymatic activity of only *merB* containing MAGs is further supported by the transcriptional activity of such MAGs and especially by the TPM of the *merB* genes (Figure 26B). The functional transcription of a only *merB* operon has already been demonstrated in a culturable *Altermononas mediterranea* ISS312 (Pereira-Garcia et al., 2024) and *Escherichia coli* (Krout et al., 2022). Lin et al. (2023) proposed that *merB* appeared as a defense mechanism to *hgcAB* activity of Hg^{II} methylation and therefore, we would expect a higher abundance and activity of *merB* in environments with a high production of MMHg such as in marine sediments.

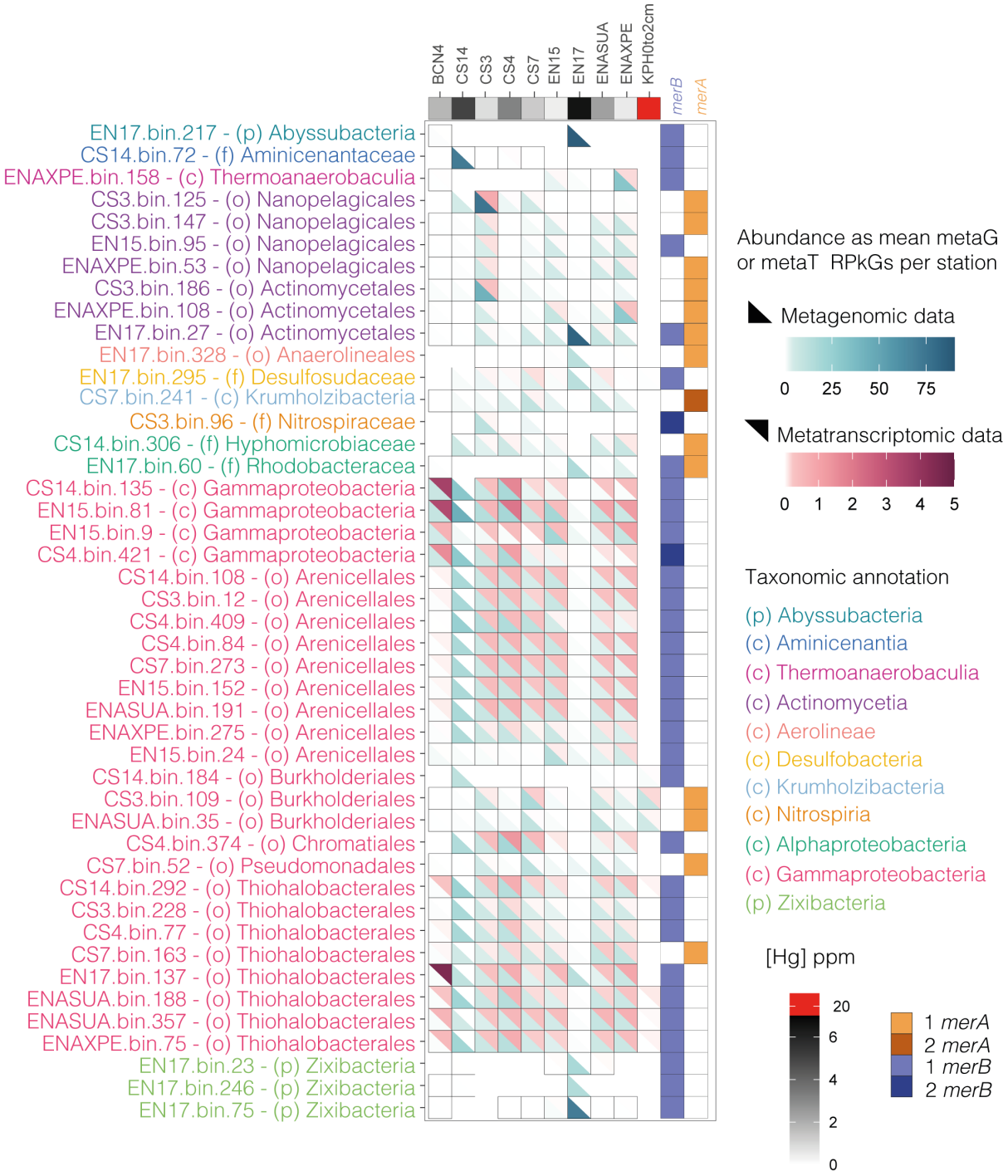


Figure 25: Abundance and transcriptional activity measured by RPKG for each MAG and across the different Hg-impacted sediments. The metatranscriptomes of stations CS14 and EN17 were absent due to their low quality.

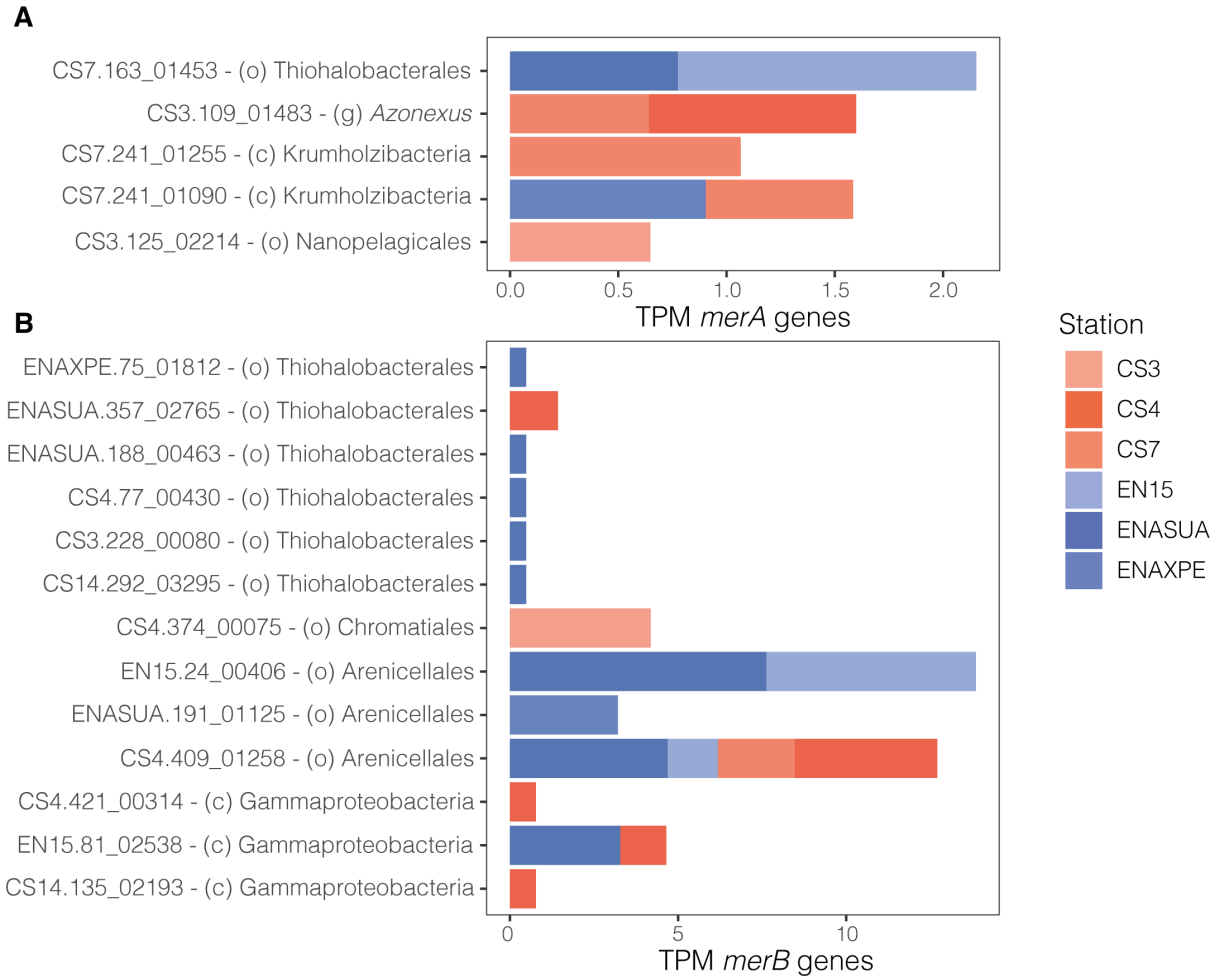
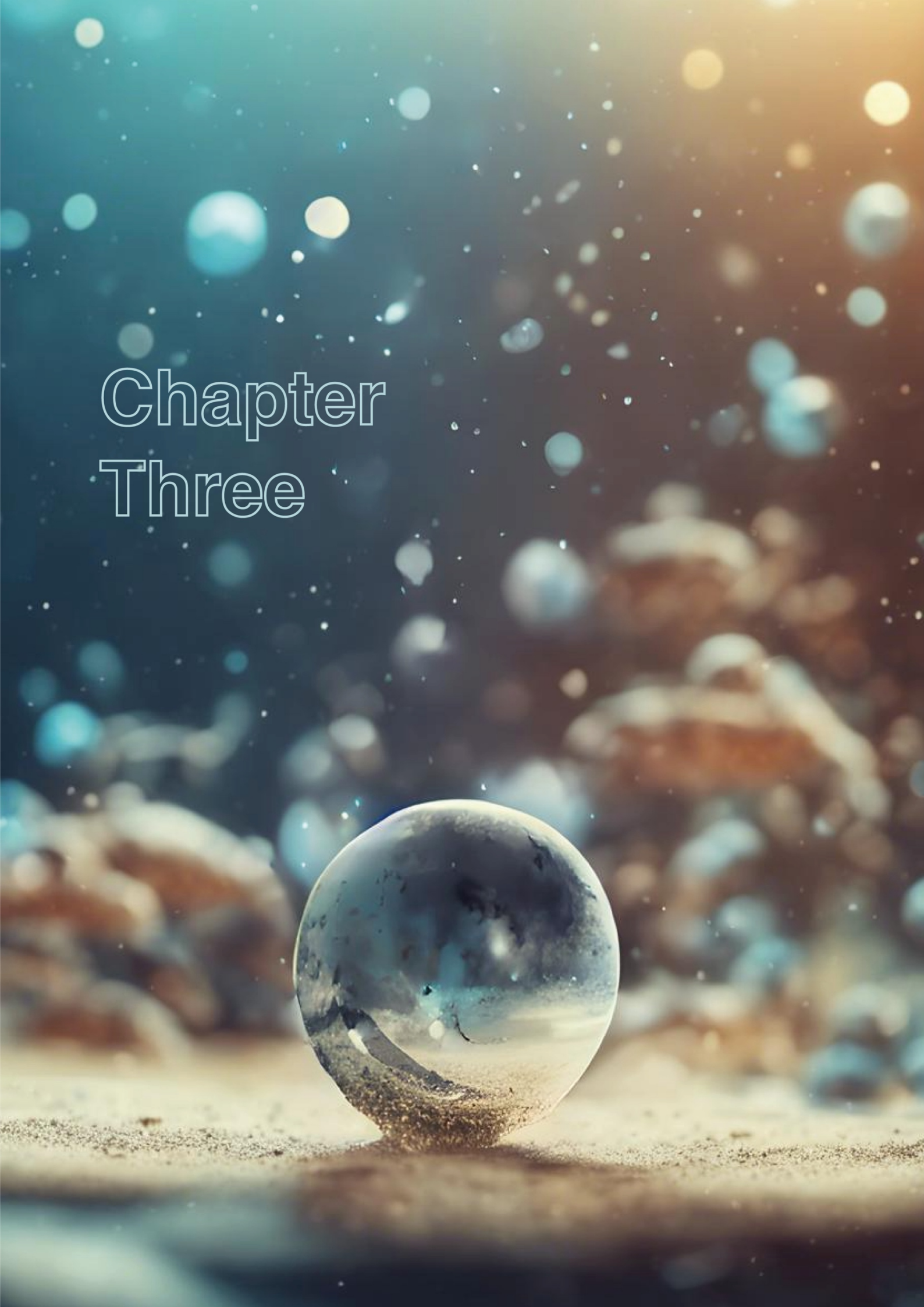


Figure 26: Transcriptional level of *merA* (A) and *merB* (B) genes expressed by Transcript Per Million (TPM).

Conclusion

Our findings highlight the crucial role of the transcription of the *merB* gene in sediments to maintain low MMHg concentrations and the importance of studying *merB* genes even in the absence of *merA* since the highest *merB* transcriptional activity belonged to MAGs without the *merA* present in its genome. We demonstrated that Gammaproteobacteria have a key role in the demethylation of Hg in marine sediments and we described a new phyla (Krumholzibacteria) with the ability to reduce Hg^{II} and proved they are transcriptionally relevant. Overall, we showed that the bacteria involved in Hg^{II} reduction and MMHg demethylation are metabolically diverse, pointing out that the mechanisms involved in these processes in marine sediments are highly complex and need to be revisited to include new bacterial key players that are not only present but also actively expressing the *merA* and *merB* genes. Our results emphasize the complexity and metabolic versatility of bacteria involved in these processes within marine sediments, influencing the overall mercury bioavailability and ecological impacts, which is key for exploring Hg removal strategies.


Chapter
Three

Chapter 3: Unmasking the physiology of mercury detoxifying bacteria from polluted sediments

Abstract

Marine sediments polluted from anthropogenic activities can be major reservoirs of toxic mercury species. Some microorganisms in these environments have the capacity to detoxify these pollutants, by using the *mer* operon. In this study, we characterized microbial cultures isolated from polluted marine sediments growing under diverse environmental conditions of salinity, oxygen availability and mercury tolerance. Specific growth rates and percentage of mercury removal were measured in batch cultures for a selection of isolates. A culture affiliated with *Pseudomonas putida* (MERCC_1942), which contained a *mer* operon as well as other genes related to metal resistances, was selected as the best candidate for mercury elimination. In order to optimize mercury detoxification conditions for strain MERCC_1942 in continuous culture, three different dilution rates were tested in bioreactors until the cultures achieved steady state, and they were subsequently exposed to a mercury spike; after 24 h, strain MERCC_1942 removed up to 76 % of the total mercury. Moreover, when adapted to high growth rates in bioreactors, this strain exhibited the highest specific mercury detoxification rates. Finally, an immobilization protocol using the sol-gel technology was optimized. These results highlight that some sediment bacteria show capacity to detoxify mercury and could be used for bioremediation applications (Figure 27).

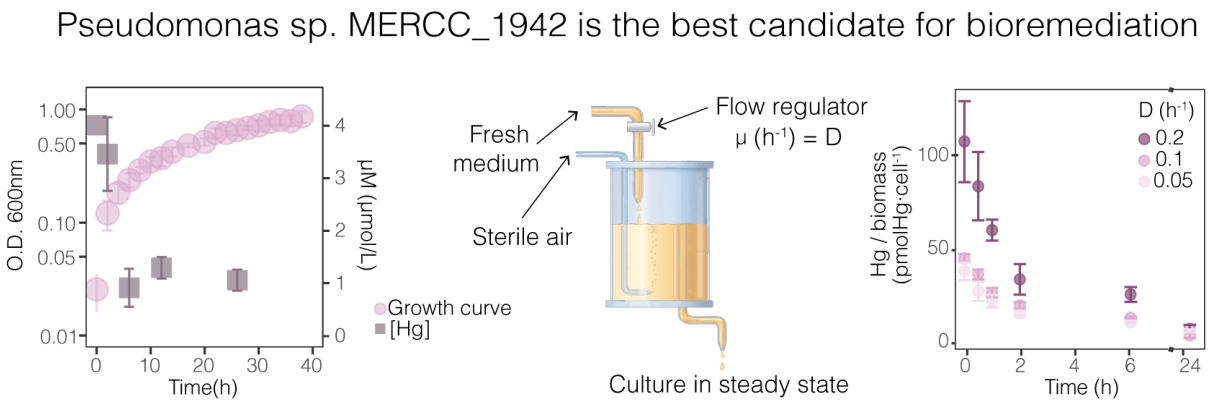


Figure 27: Graphical abstract for Chapter 3. From left to right: growth curve (optical density: OD.) at 4 μM and Hg concentrations over time, schematic of continuous culture set up and specific degradation rate from the three continuous culture conditions.

Introduction

Many natural processes, e.g. volcan eruptions, emit mercury (Hg) – an extremely toxic heavy metal – to the environment (Priyadarshanee et al., 2022) but the majority of current releases originate from historical Hg and anthropogenic activities, such as mining and coal combustion (Kocman et al., 2017). Hg in aquatic environments binds to fine sediment particles through different processes (Scanu et al., 2016), making coastal sediments both a sink (Chakraborty et al., 2014) and a source of Hg to offshore pelagic food webs (Fitzgerald et al., 2007). Once the environment is contaminated, Hg removal is a significant challenge for environmental management. Various conventional approaches have been used for mercury remediation, e.g. adsorption or soil washing, but they have serious drawbacks because they are costly, time-consuming, and produce a large quantity of sludge (Mahbub et al., 2017). In contrast, bioremediation by means of bacteria is a cost-efficient and environmentally supportive technique for the remediation of Hg pollution. Bacteria can withstand many selection pressures, making them efficient for converting and degrading Hg compounds to a safe environmental level (Mosa et al., 2016).

Hg-resistant bacteria exhibit different Hg tolerance mechanisms, such as the direct efflux of Hg (Naik & Dubey, 2017), its extracellular/intracellular sequestration (Kaur et al., 2022), and enzymatic transformation of Hg compounds (Barkay et al., 2003). This enzymatic transformation can be encoded in the *mer* operon, which consists of regulatory genes (*merR* and *merD*), transporters (*merT*, *merP*, *merD*, *merF*, *merC*) and two enzymes, which presence differs between microorganisms (*merA* and *merB*). Gene *merA* codes for a mercuric reductase, which converts Hg^{II} (reactive mercury) to Hg^{0} (volatile elemental mercury) and gives the bacteria a narrow spectrum resistance (only to inorganic compounds) (Boyd & Barkay, 2012). Gene *merB* codes for organomercurial lyase, which breaks the bond between carbon and Hg, and confers a broader spectrum resistance to organomercurials (Boyd & Barkay, 2012). The taxonomic distribution of Hg resistant bacteria is very wide (Matsui et al., 2016; Naik & Dubey, 2017; Nath et al., 2019; Sanz-Sáez et al., 2022; Yang et al., 2017; Yu et al., 2016; Zheng et al., 2018a) as the *mer* operon can be horizontally transferred (Boyd & Barkay, 2012; Matsui et al., 2016).

Many studies have isolated and characterized Hg resistant bacteria, and their Hg removal capabilities have usually been determined using the batch culture technique (Ma et al., 2018; Naik & Dubey, 2017; Nath et al., 2019; Yang et al., 2017; Yu et al., 2016; Zheng et al., 2018a). This technique is simple and does not require any special setup, thus incurring low costs (Sandberg et al., 2019). However, population density, which depends on the residual amount of nutrients, and parameters such as pH or dissolved oxygen may vary along time during the growth cycle of a batch culture (Lee & Kim, 2020). Instead, continuous culture, in which the growth medium is continuously fed with a pump into a culture vessel at a steady flow rate, maintains consistent environmental conditions and a constant nutrient supply, managing to keep cell density and growth rate invariable along time. Thus, continuous culture can reproducibly cultivate microorganisms at submaximal growth rates under different growth limitations, maintaining culture conditions virtually constant (in “steady state”) over extended

periods of time. In this steady state, the growth of organisms can be studied in great detail under precisely controlled physiochemical conditions (Kuenen, 2019). Although continuous culture is the best tool for studying the physiology of microorganisms at different growth rates and under different controlled conditions, very few studies have used it to optimize the growth conditions of Hg resistant bacteria (Chang & Law, 1998).

In this study, our primary objective was the isolation and characterization of a culturable microorganism from Hg-polluted sediments with potential for efficient mercury removal capabilities under diverse growth conditions. For this purpose, we generated a large culture collection in the context of the MERCLUB project (www.mer-club.eu), which included marine bacterial strains isolated from sediment samples collected at different Hg polluted locations. Additionally, using the continuous culture technique, we aimed at investigating the influence of growth rate on this selected microorganism to determine the optimal settings for mercury detoxification. We also tested the best conditions to immobilize the selected candidate on an versatile carrier to enable field deployment and potential use at industrial scale bioremediation actions.

Methods

Study areas and isolation

Coastal sediment samples were collected at different stations from Hg-contaminated sediment locations (Figure S2) in (i) the Bay of Biscay (estuaries Nervión (EN) and Suances (CS)) in the Basque Country and Cantabria, Spain, (ii) the Gulf of Bothnia (KPH), in Köpmanholmen, Sweden, and (iii) the Mediterranean coast (BCN), in Barcelona, Spain. Sediment samples from the Gulf of Bothnia were obtained during November 2019, while Bay of Biscay and Mediterranean locations were sampled during February and March 2020 (Table S8). The concentration of total Hg as well as the redox of the sediment samples have also been included in Table S8. Determination of total Hg concentration in the latter samples was carried out by thermo-desorption atomic absorption spectrometry (AMA-254, Altec).

For the isolation of bacterial strains, we used an advanced cultivation methodology, the Soil Substrate Membrane System (SSMS), based on the growth of microcolony-forming units using the original sediment as the culture medium (Rasmussen et al., 2008), in combination with a more classical isolation on agar plates with different media (i.e. Marine agar; Becton Dickinson, USA) and 10 % Zobell agar , in order to maximize the number of bacterial species recovered from the sediment. Briefly, sediment sub-samples (1 g) were transferred to sterile tubes with 9 mL 1x Phosphate Buffered Saline (PBS), and microorganisms were suspended by vigorous vortex for 3 min. This sediment-PBS mix was serially diluted and 100 µL of each dilution was used to inoculate 0.2 µm pore filters placed onto polycarbonate inserts in contact with the original sediment, as well as to plate Marine agar and 10 % Zobell agar plates. After 7 days, the 0.2 µm pore filters were mixed with 9 mL 1x PBS, serially diluted and 100 µL of each dilution was used to plate new Marine agar and 10 % Zobell agar plates.

On the other hand, to ensure the retrieval of mercury resistant bacterial species, an additional pre-treatment with $HgCl_2$ was also performed prior to isolation for samples from stations BCN_4, EN_17, CS_7 and KPH. Briefly, one mL of the sediment-PBS mix was inoculated into liquid 40 mL Zobell with three different concentrations of Hg (12.5, 25 and 50 µM) and incubated for 48 hours. After 2 days, the incubated samples were serially diluted and 100 µl of each dilution was plated on Zobell agar plates. All samples were incubated at room temperature (RT).

All agar plates, i.e. from the classical isolation approach and from the SSMS cultivation approach, were incubated at RT for 4 days. Plates showing between 10 and 60 colonies were selected and colonies were picked for further purification of the isolates in fresh medium. All selected isolates were cryopreserved in glycerol at -80ºC. From the total number of isolates obtained, a selection was performed according to: i) taxonomic affiliation, ii) results from a PCR screening for detecting *merA* genes (Rincón-Tomás et al., 2023), iii) the isolation method (pre-treatment with $HgCl_2$ before isolation or not) and iv) presence of same species in multiple sites. Those isolated selected were further analyzed by salinity, anaerobiosis and Hg tolerance tests as described below.

Physiological tests

An assay was performed on the selected isolates to analyze their ability to grow in a wide range of salinities. For this purpose, two different media, a marine medium with a typical salinity of 3.5 %, and a brackish medium (0.5 % salinity), modified from the medium of Zech et al. (2009) were tested (Tables S10 and S11). The isolates were inoculated in both media at RT in 24-well plates. Growth was measured as optical density (OD) at 600 nm after 38 h using an automated plate reader (Infinite M200, Tecan), and data were collected using the Magellan Data Analysis Software (Tecan Diagnostics). Moreover, negative controls (medium without microorganisms) were performed to check for potential contamination.

For those isolates able to grow in both media, a second selection was made based on their ability to grow or tolerate anoxic conditions as well as different concentrations of Hg. In brief, 100 µL of a liquid culture of the selected strains grown overnight at RT with Zobell medium were spread onto Zobell agar plates and incubated in an anaerobiosis box with a reagent mixture (Anaerocult A, Merck Millipore) to generate an anoxic environment. On the other hand, Hg tolerance was determined measuring the minimum inhibitory concentration (MIC) in inorganic mercury (mercury (II) chloride, $HgCl_2$) and organic mercury (methyl-mercury chloride, CH_3HgCl or MMHgCl) in 24-well plates, which allowed the detection of candidates able to grow at high Hg concentrations. MIC assays were designed based on previous studies (Sanz-Sáez et al., 2022) including different concentrations of $HgCl_2$ and CH_3HgCl, and thus related to the activity of *merA* and *merB* genes, respectively. Zobell broth with $HgCl_2$ at concentration of 5, 10, 50, 100 and 200 µM were inoculated with a fresh culture of the different candidates. The tolerance to CH_3HgCl was also tested at concentrations of 0.5, 1, 2, 5 and 15 µM. For each candidate, both positive (liquid culture of the strains without amendment of $HgCl_2$ or CH_3HgCl) and a negative control (broth medium without the

inoculation of bacteria to check for possible environmental contamination) were also included in the assays. Liquid cultures were sealed with parafilm and incubated at RT in the dark for 72 h. Visual examination was done at 24, 48 and 72 h. Finally, those candidates able to grow under aerobic and anaerobic conditions and at high Hg concentrations were selected for further analysis. (strains MERCC_1069, MERCC_1942 and MERCC_2833).

Growth curves

For measuring growth rates of strains MERCC_1069, MERCC_1942 and MERCC_2833 at different concentrations of $HgCl_2$, the microorganisms were grown in 500 mL liquid cultures with the marine medium (modified from Zech et al., (2009)) described above, supplemented with $HgCl_2$ at 4 and 12 µM (concentrations equivalent to contaminated locations). No further tests were done in the presence of MMHg due to negligible or very low MMHg concentration found at our selected sites. A positive control without $HgCl_2$ was also included for each strain, as well as an abiotic control with Hg but without cells. The experiments with the different strains started with an initial OD at 600 nm of 0.05. Every 2 hours, samples (1 mL) were taken and OD at a wavelength of 600 nm was measured with a spectrophotometer (Biorad SmartSpec Plus). The OD readings allowed the determination of the specific growth rates using the slope of the regression between the ln of OD versus time, for the time interval during which exponential growth was observed.

Continuous culture experiments

The continuous culture setup was performed with the best candidate selected from previous experiments in 1 L bioreactors at room temperature. The modified marine medium described above from Zech et al., (2009) was used, and the culture was continuously stirred by means of a magnetic stirrer. Aerobic conditions were chosen to perform the experiment as the best candidate (MERCC_1942) showed better growth in the presence of oxygen. Furthermore, anaerobic conditions could lead to the production of MMHg, causing a potential challenge in future bioremediation plants designed to treat polluted sediments. To maintain aerobic conditions, the culture vessel was bubbled with filtered air at a pressure of 0.1 bar. The dilution rate was determined by collecting the overflow of the culture over an extended period of time; three dilution rates were used for the experiments (0.2, 0.1 and 0.05 h^{-1}). The conditions of the culture remained unchanged until it reached steady state, which was periodically checked by the measurement of the OD at 600 nm. Once steady state was achieved, triplicate 300 mL samples were taken directly from the culture vessel and distributed into three different 500 mL bottles supplemented with 4 µM $HgCl_2$ for batch experiments. The three bottles were incubated in the dark at RT at 120 rpm and samples were taken at different time intervals (0, 0.5, 1, 2, 6 and 24 h).

Five mL samples were collected from the effluent of the continuous culture or directly from the 500 mL bottles and centrifuged at 3500 rpm for 20 minutes and 4°C for further DNA and RNA extractions. After discarding the supernatants, the pellets were frozen and kept at -80°C until analysis. Additional aliquots of the effluent and from the bottles were fixed in

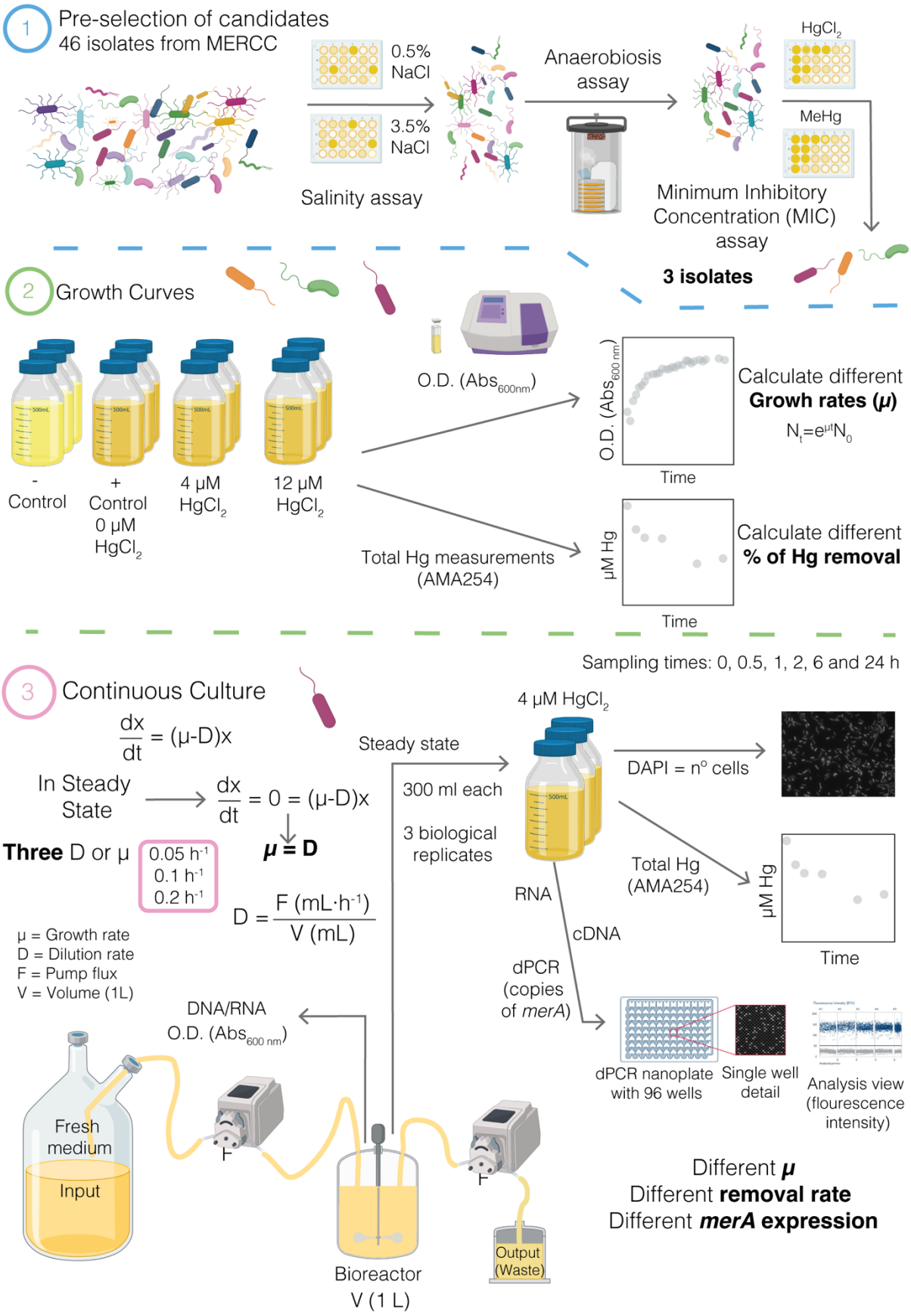


Figure 28: Schematics of the methodology of chapter 3.

formaldehyde (2 % final concentration), stained with DAPI (4´,6´-diamino-2-phenylindole), and counted using a Zeiss AXIO Imager A1 epifluorescence microscope, following previously described statistical recommendations (Kirchman et al., 1982).

Measurement of Hg concentration and Hg detoxification rates

In order to determine Hg concentrations in the different experiments (growth curves and experiments derived from continuous culture), 990 µL samples were taken from the cultures at different time intervals to measure the concentration of total Hg along time. Negative controls were used as abiotic controls for Hg removal. To fix Hg, 10 µL of HCl were added to each sample, which was kept at 4ºC until Hg was measured with an Advanced Mercury Analyzer AMA254. In the experiments from the continuous culture, mercury removal rates were calculated using the time course measurements and derived from the slope of the linear regression between Hg concentration versus time.

DNA and RNA extraction

DNA and RNA were extracted from samples obtained from the effluent in the continuous culture and the subsequent batch incubations spiked with mercury explained above. Cells were pelletized from 5 mL samples by 10 minutes centrifugation at 3000 rpm before nucleic acid extraction. RNA was extracted from approximately 10^8 cells of the culture pellets using the TRIzol Max Bacterial RNA Isolation Kit (Ambion, USA). Coextracted DNA was cleaned up from RNA extracts by using the DNase digestion and RNA Cleanup protocols of RNeasy Mini Kit (QIAGEN, Germany). cDNA was synthesized with the High Capacity cDNA Reverse Transcription kit (Applied Biosystems, USA) according to the manufacturer's instructions. The extracts were distributed in aliquots and stored at -80 ºC. DNA and RNA concentration and purity were checked using a Nanodrop spectrophotometer (NanoDrop Technologies, Inc., Wilmington, DE).

Measurement of *merA* gene transcription

To quantify the expression of *merA* gene in the selected candidate (strain MERCC_1942), digital PCR (dPCR) was performed using the QIAcuity Digital PCR system (Qiagen). Reactions were prepared in a volume of 12 µL using the QIAcuity EG PCR kit (Qiagen), an amount of cDNA template ranging from 2 to 20 ng and the pair of *merA* primers NsfF-NsfR (Wang et al., 2011). The dPCR reactions were carried out with the following thermal cycling parameters: initial denaturation at 95°C for 2 min, followed by 40 cycles of denaturation (95°C, 30 s), annealing (59°C, 30 s) and elongation (72°C, 30 s), and finished with a 5 min final elongation at 72°C. QIAcuity Software Suite was used to analyze the results. Imported files were individually assessed and fluorescence thresholds were set manually to obtain estimates of *merA* copies/uL, which were finally converted to *merA* copies/ng cDNA.

Genome assembly and annotation of the selected candidate

DNA from the selected candidate (strain MERCC_1942) was extracted using the Blood & Tissue DNA ® extraction kit (Qiagen) following the manufacture's protocol for bacterial cells.

DNA was sequenced and raw sequencing reads were checked with fastQC v0.11.7 and trimmed in fastp v0.21.0 (options *--length_required 50 --adapter_sequence=* CTGTCTCTTATACACATCTCCGAGCCCACGAGACATGTGTATAAGAGACA *--adapter_sequence_r2=* CTGTCTCTTATACACATCTCGCAGGGGATAGTCAGATGACGCTGCCGACGAATGTGTATAAGAGACA *--cut_tail --cut_window_size 1 --cut_mean_quality 25 --trim_front1 15 --trim_tail1 1 --correction --overrepresentation_analysis*). Clean reads were then assembled in shovill v1.1.0 (options *--depth 150 --minlen 0 --assembler spades --opts --isolate*) and contigs shorter than 1000bp were discarded from the final assembly. The taxonomy of the isolate was estimated using a phylogenomic approach with GTDB-Tk v1.7 against the Genome Taxonomy Database release 207_v2 (Chaumeil et al., 2020), and genome completeness and contamination was estimated with checkM v1.1.3 (Parks et al., 2015).

We used prokka v1.14.6 (Seemann, 2014) with options *--gcode 11 --kingdom Bacteria* to make the gene prediction as well as a basal annotation, that comprises identification of coding DNA sequences (CDS) annotated as clusters of orthologous groups (COGs) and Enzyme Comission numbers (EC). Prokka also identifies and annotates transfer RNAs (tRNAs and tmRNAs), ribosomal RNAs (rRNAs) and CRISPR arrays. Amino acid sequences from all predicted CDS were further annotated against the KEGG orthology database KO, release 98.0 (Kanehisa & Goto, 2000) with kofamscan v1.3.0 (Aramaki et al., 2019) and against the Pfam database release 34.0 (El-Gebali et al., 2019) with HMMR v3.3 (Eddy, 2011) with options *--domtblout -E 0.1* and then filtered accordingly so that the best hit for each model aligned with no overlaps to the target CDS. Finally, carbohydrate active enzymes (CAZy) were annotated using HMMER v3.3 against dbCAN v10 (Yin et al., 2012). Predicted 16S rRNA genes were aligned to NCBI's rRNA/ITS database in the blastn web server (https://blast.ncbi.nlm.nih.gov/Blast.cgi, September 2022) to confirm taxonomy.

Genes involved in mercury detoxification *merA* and *merB* are often missed or misannotated by the KO and Pfam databases due to their similarity to other paralogs that also bind to divalent metallic ions (like Cu^{2+}). A further annotation step of all amino acid sequences of the predicted CDS was carried out using custom MerA and MerB hidden Markov models (HMM) BioStudies accession number S-BSST1154 (Rincón-Tomás et al., 2023). Sequences annotated with the custom HMMs, plus all sequences previously annotated as either *merA* (K00520) or *merB* (PF03243, K00221) were confirmed by checking the presence of conserved amino acids: a cysteine pair at positions 207 and 212, numbered based on the MerA from *Bacillus* sp. RC607, and a cysteine pair at positions 96 and 159 based on the MerB on plasmid R831b (Gionfriddo et al., 2016). The final assembly was used to calculate the average nucleotide identity (ANI) to public genomes of *Pseudomonas* sp. on the NCBI using online tool JSpeciesWS (Richter et al., 2016).

Results

Preliminary selection of candidates and physiological assays

From a total of 2878 pure isolates obtained from all sampling sites and sequenced based on 16S rRNA, 46 isolates were initially selected for further characterization (Table S12). Among this selection, 31 isolates were obtained by the enrichment protocol with $HgCl_2$ thus showing tolerance to high Hg concentrations, and 22 presented positive results in a PCR screening indicating that they contained *merA* genes (Table S12). However, 9 isolates did not survive cryopreservation and we finally ended with a selection of 37 isolates for next steps.

Salinity assays

We carried out the salinity assay for 37 isolates, in which we aimed to select those candidates able to grow under both brackish and marine conditions (0.5 and 3.5 % NaCl, respectively) (Table S13). We established a minimal OD threshold of 0.1 after an overnight incubation to consider that the candidate was able to grow in the corresponding medium. The maximum ODs in brackish and marine media were 0.484 and 0.553 respectively and they were measured in isolate MERCC_2129 (*Arthobacter humicola*). Other candidates like *Pseudomonas* sp. (MERCC_403 and MERCC_1942), *Bacillus pumilus* (MERCC_2020) and *Shewanella baltica* (MERCC_2023) grew well in both media with ODs between 0.45 and 0.35. Some candidates grew well only under one salinity condition, like MERCC_2702 (*Dietzia* sp.), which showed an OD of 0.41 in brackish conditions but only 0.13 in the marine medium, or MERCC_2833 (*Bacillus* sp.) with an OD of 0.16 in brackish and 0.34 in marine conditions. Based on these findings, we selected 22 isolates which exhibited high OD at 600 nm in both, marine and brackish media after 38 h of incubation, considering also the taxonomy of the candidate.

Anaerobiosis and MIC assays

The results for anaerobiosis and Minimum Inhibitory Concentration (MIC) assays are summarized in Table 1. A total of 22 candidates were tested in the anaerobiosis assay. Most of the candidates were able to tolerate anaerobic conditions, showing growth capacity after being in the anaerobic box for three weeks. Only 3 candidates did not grow under these conditions.

MIC assays were then performed for both organic (CH_3HgCl or MMHg) and inorganic ($HgCl_2$ or IHg) mercury in these 22 isolates. Visual assessments of well plates were done after 24, 48 and 72 hours. As the aim of the study was to select candidates with the highest tolerance to Hg and fastest growth, as they may be better suited for bioremediation, good results after 24 were prioritized. Fourteen isolates showed virtually no tolerance for IHg (MIC values of 5 µM), although we observed a variety of MIC values for MMHg, ranging from 1 µM up to 15 µM, this last value shown by MERCC_498 (*Citrobacter freundii*). Four candidates displayed MIC values of 10 µM for IHg, and three of them presented a MIC value up to 5 µM for MMHg (MERCC_473, MERCC_491 and MERCC_2124) while only one showed a MIC value of 1µM for MMHg (MERCC_2063). The highest MIC recorded for IHg was 50 µM; it was found in

MERCC_1069, MERCC_1942, MERCC_2833 and MERCC_2702. These four isolates had a MIC of 5 µM for MMHg.

Table 1: Results from anaerobiosis tolerance and Minimum Inhibitory Concentration (MIC) assay at 24 h for the studied isolates. In bold, those candidates selected for the characterization of growth rate and Hg removal assay.

Taxonomy	MERCC ID code	Anaerobiosis tolerance	MIC (24h) $HgCl_2$ (µM)	MIC 24 h MMHg (µM)
Acinetobacter equi	MERCC_2063	No	10	1
Acinetobacter johnsonii	MERCC_491	Yes	10	5
Aeromonas hydrophila	MERCC_1069	Yes	50	5
Arthrobacter humicola	MERCC_2129	No	5	5
Bacillus pumilus	MERCC_2020	Yes	5	1
***Bacillus* sp.**	MERCC_2833	Yes	50	5
Bacillus sp.	MERCC_2054	Yes	5	5
Citrobacter freundii	MERCC_498	Yes	5	15
Dietzia sp.	MERCC_2702	Yes	50	5
Klebsiella michiganensis	MERCC_473	Yes	10	5
Marinobacter sp.	MERCC_1908	Yes	5	5
Micrococcaceae sp.	MERCC_2873	Yes	5	1
Micrococcaceae sp.	MERCC_2865	Yes	5	5
Pseudomonas fluorescens	MERCC_2124	No	10	5
Pseudomonas fluorescens	MERCC_403	Yes	-	2
Pseudomonas migulae	MERCC_2147	Yes	5	5
Pseudomonas putida	MERCC_1942	Yes	50	5
Pseudomonas sp.	MERCC_2037	Yes	5	5
Shewanella baltica	MERCC_2023	Yes	-	1
Shewanella baltica	MERCC_2088	Yes	5	5
Shewanella sp.	MERCC_2048	Yes	5	5
Vibrionaceae	MERCC_2796	Yes	5	5

Growth curves and specific growth rates of selected candidates

After all the physiological assays, we finally selected three candidates (MERCC_1069, MERCC_1942 and MERCC_2833) that were all able to grow at a wide range of salinity and oxygen concentrations, and also had high MIC value for $HgCl_2$ (50 µM). They were identified as *Aeromonas hydrophila* (strain MERCC_1069), *Bacillus* sp. (strain MERCC_2833) and *Pseudomonas putida*. (strain MERCC_1942), according to 16S rRNA. We then characterized their growth curves and calculated their specific growth rates at two different concentrations of $HgCl_2$ (4 and 12 µM), together with a control without $HgCl_2$ (not amended culture).

Figure 29 shows the growth curves and the values of the growth rates calculated from the slope of the exponential phase from the three isolates grown at different $HgCl_2$ concentrations. Two of the isolates (*Aeromonas hydrophila* MERCC_1069 and *Bacillus* sp. MERCC_2833) formed aggregates, which compromised the validity of OD measurements. Thus, in Figure 29 we only included the value of growth rates for those experiments not affected by the presence of aggregates. In the case of strain MERCC_1069, we observed that it developed small filamentous aggregates after a first initial exponential growth at 0 and 4 µM $HgCl_2$, subsequently observing a decrease in OD (at t = 8-10 hours), which raised again as the aggregates increased in size and number. This drop in OD was more pronounced at 4 µM $HgCl_2$. We did not observe this trend at 12 µM, although in this case a great variability in the OD measurements of the replicates was found. On the other hand, for strain *Bacillus* sp. MERCC_2833, the formation of aggregates was only noticed when $HgCl_2$ was present, so that the measurements of OD in the control experiment without Hg were not interfered by their presence. Finally, we did not observe the presence of aggregates for strain *Pseudomonas putida* MERCC_1942 at any concentration, and the growth rate of this strain was not impacted by the presence of Hg (ca. 0.11 h^{-1} in all treatments) (Figure 29). Even though the growth rates were similar, a rather long lag phase (22 hours) was observed when growing at 12 µM $HgCl_2$ at the beginning of the curve, coincident with a decrease in Hg concentration (see below), suggesting that this strain was performing the detoxification of Hg before starting exponential growth (Figure 30).

Mercury removal from selected candidates

The variations in Hg concentration along time in the incubations was measured for each candidate for the two concentrations of $HgCl_2$ tested (4 and 12 µM, Figure 30). To assess the detoxification capability of the candidates, we calculated the percentage of removal after 24 hours of incubation, which is also presented in Figure 30. A control without cells was additionally included in this experiment to account for the abiotic losses, which were only 10 % in the 4 µM but they increased significantly in the 12 µM reaching almost 36 %.

The candidates *Aeromonas hydrophila* MERCC_1069 and *Pseudomonas putida* MERCC_1942 presented the highest mean percentages of removal at 4 µM $HgCl_2$ after 24 h incubation, with values of 79.0 and 74.6 % respectively. At 12 µM $HgCl_2$, the mean % of removal was 53.8 % and 24.1 % for both strains respectively after 24 h of growth, although *Pseudomonas putida* MERCC_1942 reached a value of 67.0 % of removal after 66 h.

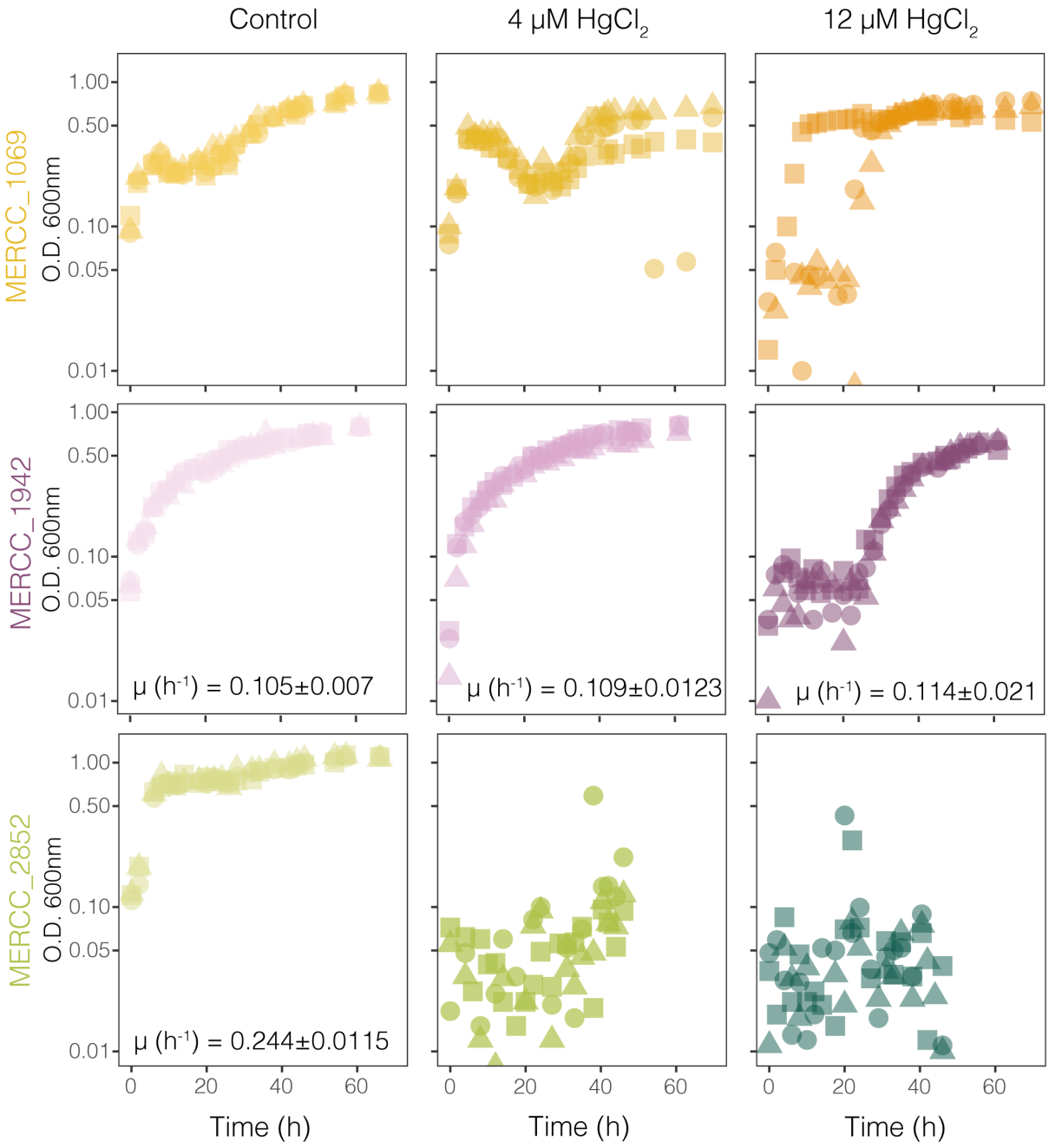


Figure 29: Growth curves of the three isolates studied in this work exposed to different concentrations of $HgCl_2$ (0, 4 and 12 µM). The different symbols correspond to individual replicates within each condition. The mean growth rate ± standard deviation was calculated when possible. MERCC_1069: *Aeromonas hydrophila*, MERCC_1942: *Pseudomonas putida,* and MERCC_2833: *Bacillus* sp.

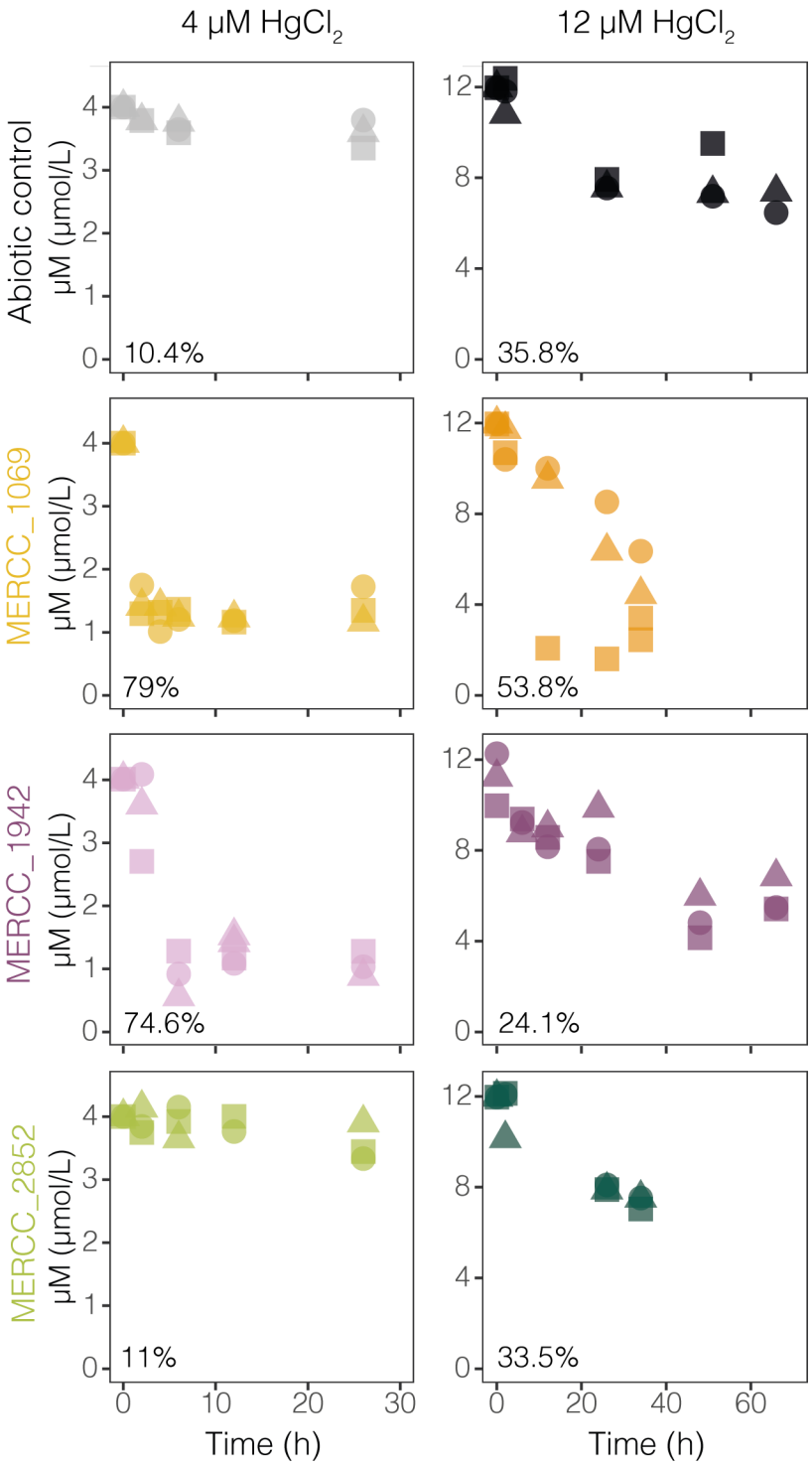


Figure 30: Concentration of total Hg (µM) along time of an abiotic control and the three isolates studied in this work exposed to different concentrations of $HgCl_2$ (4 and 12 µM). The different symbols correspond to individual replicates within each condition. MERCC_1069: *Aeromonas hydrophila*, MERCC_1942: *Pseudomonas putida*, and MERCC_2833: *Bacillus* sp.

This suggests that both strains were able to detoxify $HgCl_2$ at similar levels, although strain MERCC_1942 seemed to need slightly more time. *Bacillus* sp. strain MERCC_2833 showed removal rates similar to the abiotic control, 11 % (4 µM) and 33 % (12 µM) (Figure 30). In summary, the candidates which presented the best capacity for mercury detoxification were strains MERCC_1069 and MERCC_1942; however, as *Aeromonas* sp. MERCC_1069 developed aggregates, this feature made it unsuitable for continuous culture growth, and *Pseudomonas putida* MERCC_1942 was selected to be further characterized.

Growth in continuous culture and measurement of Hg detoxification rates

Pseudomonas putida MERCC_1942 was grown in bioreactors at three different dilution rates (0.2, 0.1 and 0.05 h^{-1}), until reaching steady state, where the culture adjusts their specific growth rate (equal to the dilution rate, D). According to the cell counts performed under the microscope, a decrease in biomass was observed at steady state as the dilution rate increased, from $1.61 \cdot 10^8$ (D=0.05 h^{-1}) to $2.59 \cdot 10^7$ cells·mL^{-1} (D = 0.2 h^{-1}). On the other hand, the visualization of DAPI stained cells (Figure S5) interestingly showed that the isolate was able to develop filaments, particularly when it was growing faster (at 0.2 h^{-1}).

After reaching steady state, 4 µM of $HgCl_2$ was added to strain MERCC_1942, and changes in concentration of Hg over time was measured from cells grown in bioreactors at the three different dilution rates and thus adapted to grow at a high (0.2 h^{-1}), medium (0.1 h^{-1}) and low (0.05 h^{-1}) growth rates. The percentage of removal after 2 and 24 h of incubation as well as the Hg removal rates (Table 2) were determined. Although there was a certain reduction of Hg due to abiotic losses (up to 20 % after 24 h), most of the Hg was removed biotically. *Pseudomonas putida* MERCC_1942 showed high detoxification rates (Table 2), which were virtually identical for the three growth rates (around 1 µM·h^{-1}), and after 2 h, the % of Hg removal was very similar between experiments (55.6 % - 58.4 %). After 24 h *Pseudomonas* sp. was able to detoxify in average 75.8 % of the total Hg.

Mercury detoxification rates correspond to bulk removal rates of the metal from the whole community. However, for the sake of comparison among samples, the concentration of Hg was normalized by the biomass (cell number in cell·mL^{-1}) in order to obtain the specific amount of Hg detoxified per cell (pmolHg·$cell^{-1}$) for each experiment (Figure 31). The specific concentration of Hg along time allowed the calculation of the specific rate of Hg detoxification for each growth rate (Table 2). Interestingly, the highest detoxification rate per cell was achieved at high growth rates (0.2 h^{-1}) and corresponded to 36.8 $\pm$ 14.9 pmol Hg·$cell^{-1}$·h^{-1}. The microorganism increased its specific mercury detoxification rate as the growth rate increased.

Table 2: Mean percentage of Hg removal from abiotic control and *Pseudomonas putida* strain MERCC_1942 grown at different dilution rates (D) in the continuous culture after 2 and 24 h of incubation with $HgCl_2$. In the case of the isolate, results from Hg detoxification rates and specific Hg detoxification rates per cell are shown (sd: standard deviation).

	D (h^{-1})	% Hg removal ± sd (2 h)	% Hg removal ± sd (24 h)	Detoxification rate ± sd ($\mu M \cdot h^{-1}$)	Specific Hg detoxification rate ± sd (pmol $Hg \cdot cell^{-1} \cdot h^{-1}$)
Abiotic control		3.0 ± 2.8	20.6 ± 5.1		
P. putida MERCC_1942	0.05	58.4 ± 3.1	75.6 ± 2.1	1.07 ± 0.06	10.8 ± 1.9
	0.1	55.6 ± 3.8	74.1 ± 1.5	1.04 ± 0.04	12.6 ± 0.6
	0.2	58.0 ± 7.7	77.6 ± 3.3	1.02 ± 0.21	36.8 ± 14.9

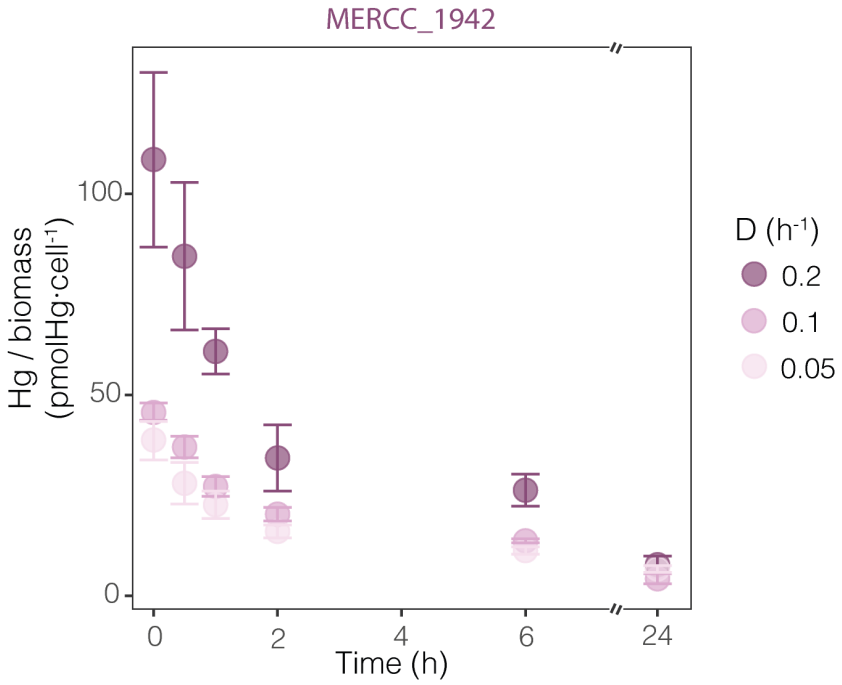


Figure 31: THg detoxified per cell of *Pseudomonas* sp. MERCC_1942 previously grown at different growth rates in bioreactors and spiked with 4 µM HgCl2. D = dilution rate = growth rate (see equation in Figure 28).

merA gene transcription

The expression of the *merA* gene from *Pseudomonas putida* MERCC_1942 under steady state and after adding $HgCl_2$ along time was analyzed to verify that this isolate was inducing the *mer* operon for Hg removal (Figure 32). dPCR results revealed that *merA* expression was low when there was no Hg in the medium, i.e., the *merA* gene was detected at very low levels before the addition of Hg to the medium in any case (≤ 1 copy of *merA* transcript/ng cDNA). After adding the spike of Hg to the culture, a rapid increase in *merA* gene transcription was observed, with the highest values detected during the first hour of incubation and decreasing after that point. The maximum number of *merA* transcripts was found at 0.5 hours (around 150 *merA* copies/ng cDNA) when the growth rate was 0.1 h^{-1}, while for 0.2 h^{-1}, the maximum expression value was in average 16 *merA* copies/ng cDNA (Figure 32). On the other hand, *merA* expression was significantly lower when growth rate was 0.05 h^{-1}. After 24 hours of incubation values were rather low in all treatments (0.49 ± 0.29, 19.15 ± 2.96 and 5.48 ± 1.19 copies/ng cDNA when growth rate was 0.05, 0.1 and 0.2 h^{-1}, respectively).

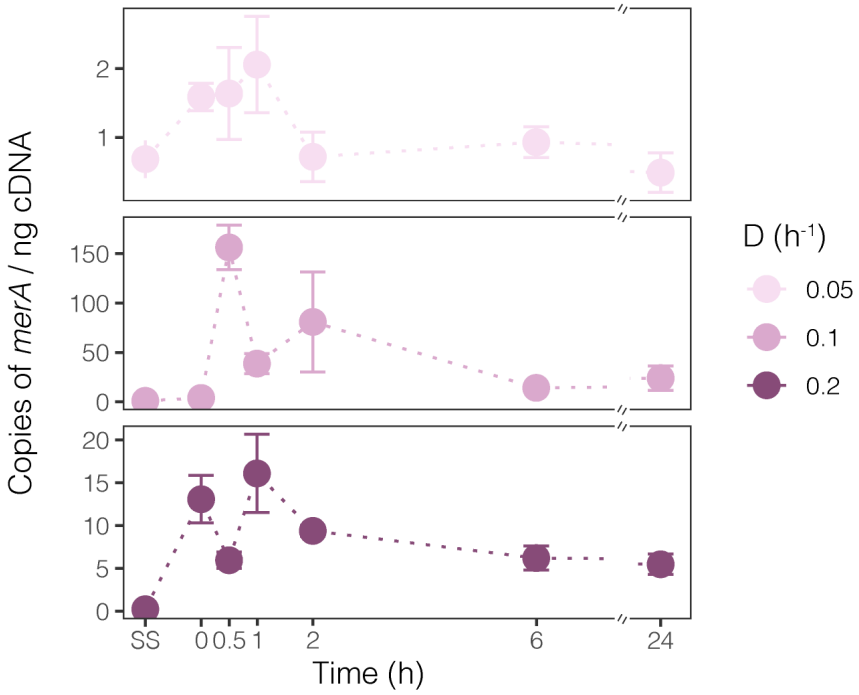
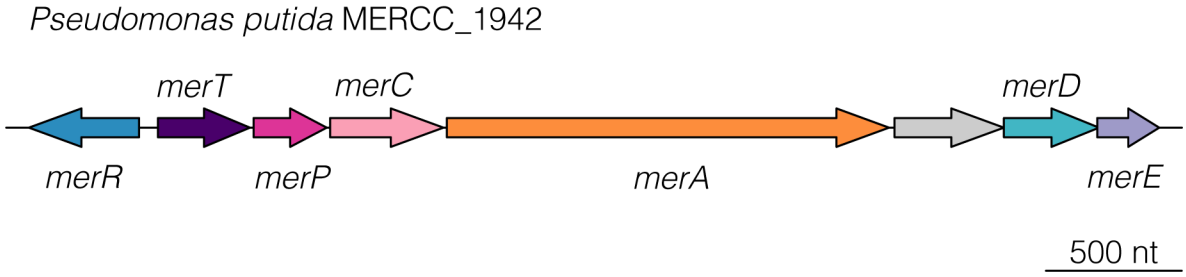


Figure 32: Average number of mRNA copies of the *merA* gene normalized by ng of cDNA (circles) and average Hg concentration along time (squares) from *Pseudomonas putida* MERCC_1942 previously grown at three different dilution rates in bioreactors and spiked with 4 µM HgCl2. SS: steady state in continuous culture. D = dilution rate = growth rate (see equation in Figure 28).

Genomic analysis of *Pseudomonas putida* MERCC_1942

In order to have a broader comprehension of the potential metal tolerance and metabolic traits of our chosen candidate, the genome of *Pseudomonas putida* MERCC_1942 was sequenced and assembled. We observed a 98.18 % average nucleotide identity (ANI) with *Pseudomonas putida* Simmons01 (GCF_001542955.1). We found one unique *mer* operon with *merA*, four transporters (*merT, merP, merC* and *merE*) and the two regulators (*merR* and *merD*) (Figure 33), while no *merB* was detected in the genome. Additionally, we found genes related to other metal and antibiotic resistances, including complete arsenic and gold resistance operons, partial silver and tellurium operons as well as essential genes for cadmium, cobalt and zinc resistance. Additionally, multiple drug resistance genes were found, including *vanAB*, *strAB* and *sul1*. In terms of metabolism, the genomic analysis showed that *Pseudomonas putida* MERCC_1942 has the typical metabolism of a heterotrophic bacterium i.e. glycolysis, citrate cycle, amino acid biosynthesis, as well as other genes related to metabolisms like dissimilatory nitrite reduction, C1 metabolism or thiosulfate



oxidation by the SOX complex.

Figure 33: Synteny of the *mer* operon found in *Pseudomonas putida* strain MERCC_1942 genome.

Discussion

From a screening of 37 sediment isolates provided with mechanisms for Hg tolerance and/or detoxification, our results identified a novel strain (strain MERCC_1942) with high potential for Hg bioremediation affiliated with *Pseudomonas putida*. Previous studies have already shown the tolerance of other members of *Pseudomonas* sp. to Hg and other metals (Cabral et al., 2013; Deng & Wang, 2012; Fortunato et al., 2005; Horn et al., 1994; Joshi et al., 2021; Kiyono et al., 1997; Pepi et al., 2011; von Canstein et al., 1999). For instance, a *Pseudomonas* sp. culture isolated from Chesapeake Bay sediment was reported to exhibit the highest resistance to $HgCl_2$ (up to 185 µM) among all isolated bacteria (Walker & Colwell, 1974). The isolation of *Pseudomonas* sp. with high tolerance to Hg^{II} and MMHg has been also successfully achieved from various contaminated environments, such as a landfarming soil in Brazil (Cabral et al., 2013; Giovanella et al., 2016, 2017), the deep Central Indian Ocean (Joshi et al., 2021; Kiyono et al., 1997) or seawater and sediments of a mangrove in China (Deng & Wang, 2012), showing an interesting potential to detoxify polluted sites by this bacterial genus. In previous studies using *Pseudomonas* sp. isolates, mercury removal typically ranged from 37 % to 80 % when using culture media (Cabral et al., 2013; Giovanella et al., 2016; Joshi et al., 2021; Tanwer et al., 2022), which is similar to the value obtained for

the strain *Pseudomonas putida* MERCC_1942 reported here. Notably, MERCC_1942 was able to tolerate a wide range of salinity and anaerobic conditions, suggesting that it could be potentially used for Hg bioremediation under different environmental conditions.

On the other hand, our work contributes to the limited pool of research that has examined mercury detoxification with environmental isolates grown under continuous culture conditions. This type of culture is typically reserved for the removal of Hg in bioreactors and pilot plants used in wastewater treatment. For instance, von Canstein et al. (1999) isolated *Pseudomonas putida* from contaminated river sediments, loaded on a porous bioreactor containing chloralkali wastewater. After treatment, 90 % to 98 % of the total mercury content was effectively removed from the medium. This method has also been applied in treating industrial wastewater (Wagner-Döbler, 2003) and environmentally polluted water (Okino et al., 2000), with *Pseudomonas* sp. being one of the main organisms used in such bioreactors due to its ability to grow in continuous culture and remove Hg. Continuous reactors enable microorganisms to handle higher mercury loadings compared to batch cultures since the microorganisms are never exposed to high mercury concentrations for extended periods of time due to the continuous outflow of the medium (Leonhäuser et al., 2006). In an experiment using a hydrophobic polyvinylidene fluoride (PVDF) membrane as a support for *Pseudomonas stutzeri* to decontaminate aqueous solutions containing heavy metals, a better efficiency in the removal of the pollutants was found in a continuous culture than in a batch culture (Manirethan et al., 2020). Besides, Chang & Law, (1998) showed that *Pseudomonas aeruginosa*, when grown in continuous culture, was able to remove the same amount of mercury and with similar efficiency once the culture reached steady state regardless of the growth rate. By contrast, strain MERCC_1942 showed a better removal specific rate at a high growth rate.

Another isolate considered in our study, *Aeromonas hydrophila* MERCC_1069, also proved to be a good candidate for bioremediation in experiments performed in batch culture. However, due to the formation of exceptionally large aggregates, it would not be a good candidate for growth on a chemostat, as achieving steady state would be challenging. Nevertheless, this strain could be potentially considered for a different type of bioreactor, such as immobilized cells in a column, as previously performed by von Canstein et al. (1999) with *P. putida*. However, to the best of our knowledge, there are no studies with *Aeromonas* sp. as a candidate for Hg bioremediation, probably due to high number of species within this genus that are human-pathogenic and show antibiotic multi-resistance genes (Ahmad, 2018; Fernández-Bravo & Figueras, 2020).

On the other hand, candidate *Bacillus* sp. MERCC_2833 was not able to detoxify Hg in batch cultures. Thus, this strain was not an option for our present study, although it is important to highlight its exceptional high MIC for Hg, 50 µM in culture medium. Further studies would be needed to elucidate what mechanism this strain is using to tolerate this pollutant, since *merA* gene was not detected in this strain. A possibility is the Hg biosorption capacity due to the secretion of exopolysaccharides (EPS) as previously reported for other *Bacillus* sp. strains

(François et al., 2012; Kalpana et al., 2018). Candidate MERCC_2833 also showed a mucoid phenotype, which is consistent with EPS production (François et al., 2012).

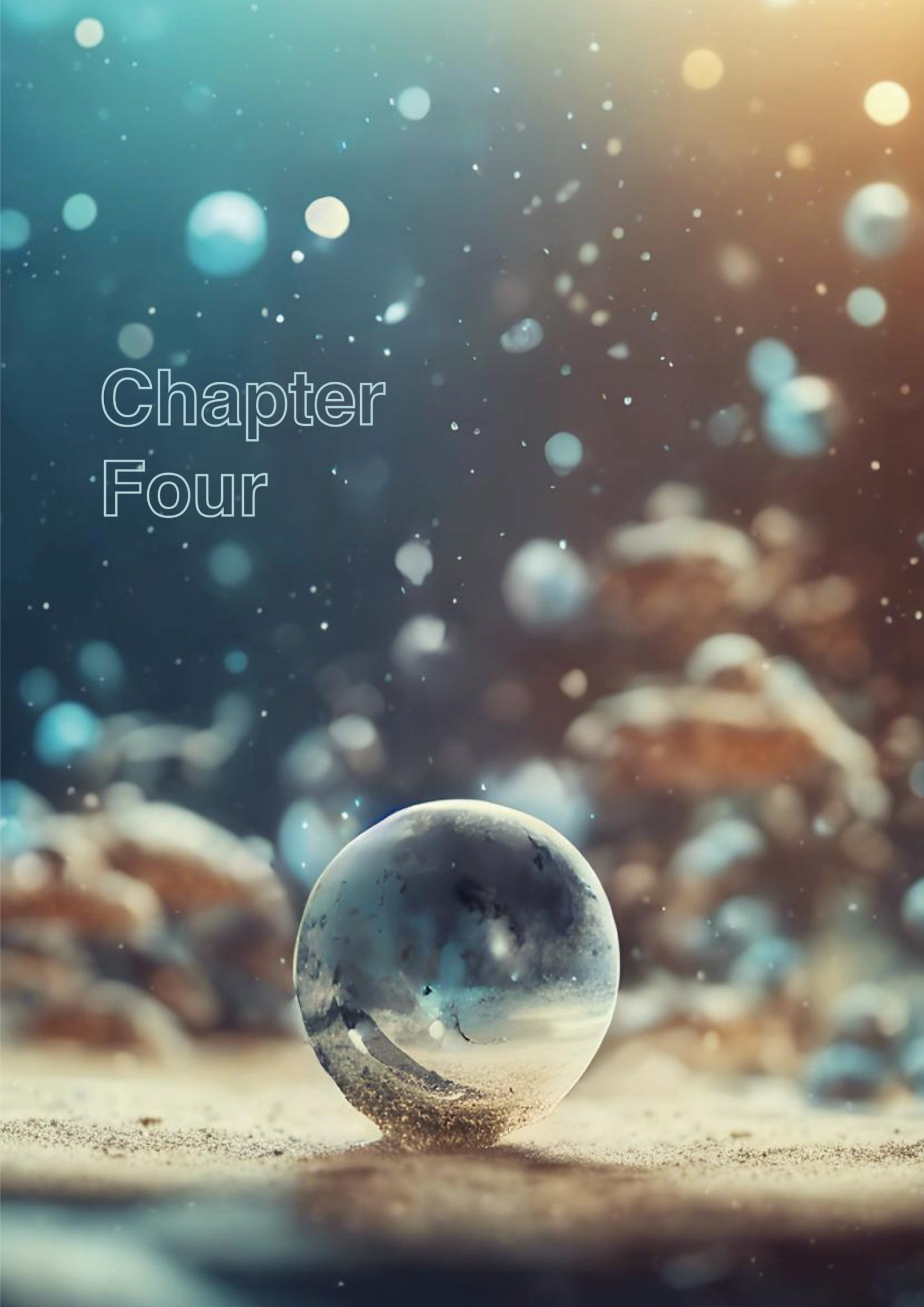
As in the case of *Pseudomonas putida* MERCC_1942 we assumed that Hg tolerance was conferred by the components of the *mer* operon encoded in its genome, we analyzed whether the marker gene *merA* was expressed when exposed to Hg. The rapid increase in *merA* gene transcription after adding a spike of Hg to the culture in *Pseudomonas putida* MERCC_1942 confirmed the mercury resistance mechanism mediated by *mer* genes. Chen & Chang (2000) reported that lower growth rates were correlated with compromised Hg-resistance in *Pseudomonas aeruginosa*, suggesting a potentially more efficient *mer* operon at high growth rates. In our case, a lower number of *merA* transcripts was initially found in the incubation with Hg when *Pseudomonas* sp. was growing at a rate of 0.2 h^{-1} compared with 0.1 h^{-1}. However, it is important to note that *merA* transcripts were generally immediately induced after the spike, and rapid changes in the transcript inventory were measured over time. Thus, at the time resolution of our sampling, we may have missed the maximum number of transcripts in the case of 0.2 h^{-1} samples. In any case, it is clear that the *mer* operon did not show a constitutive expression, but it was induced by the presence of mercury in the culture medium as previously reported in different isolates, *Pseudomonas* sp. among them (Giovanella et al., 2016), and the expression of the *merA* gene may decrease or even be suppressed when there is a deficiency or absence of Hg in the culture medium over the course of incubation. Overall, our analyses showed a similar trend to that observed by other authors in environmental samples (Nazaret et al., 1994) or in pure cultures of *Marinomonas* sp. (Al-Ansari, 2022), with an initial peak of expression of the *merA* gene followed by a significant decrease over time.

Conclusion

In this study, we have successfully isolated mercury-resistant bacteria from polluted sediments and highlighted the importance of understanding their physiological properties for potential bioremediation applications. We have obtained an isolate, *Pseudomonas putida* MERCC_1942, capable of growing in a wide range of mercury concentrations, oxygen levels and salinity conditions. The presence and active expression of the *merA* gene in this strain further supports its suitability for bioremediation, consistent with previous findings involving other *Pseudomonas* strains.

Furthermore, our investigation, focused on the impact of growth rate on the efficiency of mercury removal in this detoxifying strain, revealed interesting insights. We observed that *Pseudomonas putida* MERCC_1942 mercury removal was affected by the growth rate, with higher growth rates leading to an increase of specific Hg detoxification rates.

Thus, the findings from our study hold promise for potential future bioremediation applications, including pilot plant experiments and *in situ* bioremediation assays, to help mitigate problems associated with mercury pollution in marine sediments.


Chapter
Four

Chapter 4: Genomic and transcriptomic characterization of methylmercury detoxification in a deep ocean *Alteromonas mediterranea* ISS312

Abstract

Monomethylmercury (MMHg) is one of the most worrisome pollutants in marine systems. MMHg detoxification is mediated by *merB* and *merA genes*, responsible for the demethylation of MMHg and the reduction of inorganic mercury, respectively. Little is known about the biological capacity to detoxify this compound in marine environments, and even less the bacterial transcriptional changes during MMHg detoxification. This study provides the genomic and transcriptomic characterization of the deep ocean bacteria *Alteromonas mediterranea* ISS312 with capacity for MMHg degradation. Its genome sequence revealed four *mer* operons containing three *merA* gene and two *mer*B gene copies, that could be horizontally transferred among distant related genomes by mobile genetic elements. The transcriptomic profiling in the presence of 5 µM MMHg showed that *merA* and *merB* genes are within the most expressed genes, although not all *mer* genes were equally transcribed. Besides, we aimed to identify functional orthologous genes that displayed expression profiles highly similar or identical to those genes within the *mer* operons, which could indicate they are under the same regulatory controls. We found contrasting expression profiles for each *mer* operon that were positively correlated with a wide array of functions mostly related to amino acid metabolism, but also to flagellar assembly or two component systems. Also, this study highlights that all *merAB* genes of the four operons were globally distributed across oceans layers with higher transcriptional activity in the mesopelagic deeper waters. Our study provides new insights about the transcriptional patterns related to the capacity of marine bacteria to detoxify MMHg, with important implications for the understanding of this process in marine ecosystems (Figure 34).

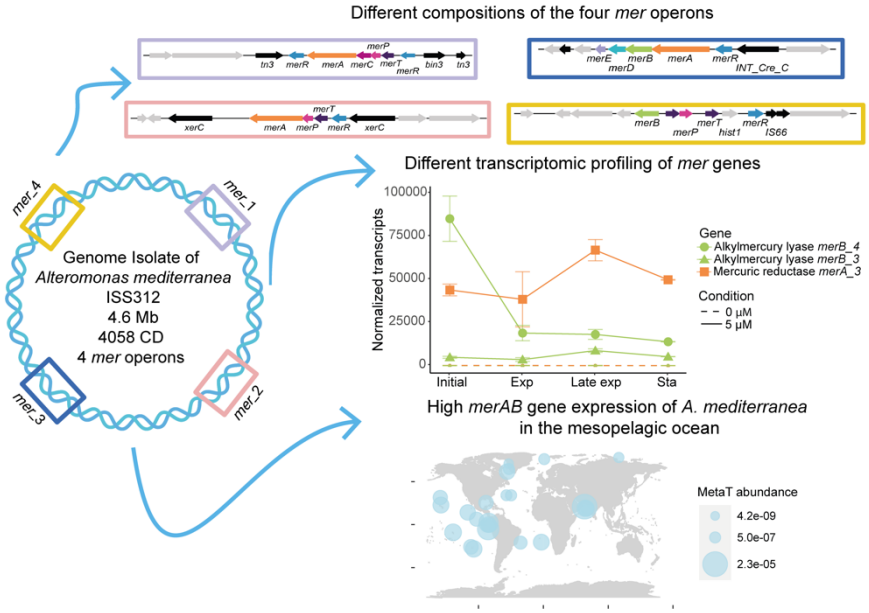


Figure 34: Graphical abstract of chapter 4.

Introduction

Hg is one of the most toxic and widespread trace metals found in the environment and its levels have increased since the 1850's due to anthropogenic activities, such as fossil fuel combustion, metal industries, and sewage treatments, among others (Pirrone et al., 2010; Streets et al., 2017). The concentration of Hg in the oceans has raised accordingly, however a matter of special concern is its organic form monomethylmercury (MMHg), which bioaccumulates and biomagnifies in aquatic food webs. As a consequence, marine fish consumption is one of the major sources of human exposure to MMHg (Chen et al., 2012; Kim & Zoh, 2012; Mason et al., 2012). Therefore, the cellular processes and metabolic pathways of MMHg degradation and mercury reduction in bacteria of the water column need to be studied.

Once released, Hg is transported and recycled through air, soil and water. Elemental mercury (Hg^0) and divalent mercury (Hg^{II}) can travel long distances in the atmosphere until they are deposited onto the surface of different water bodies. Once in the water column, Hg^{II} can: i) be reduced and reemitted to the atmosphere, ii) be biotically or abiotically methylated forming MMHg, or iii) bind to other organic forms and then be deposited onto the sediments. It has been shown that most of the MMHg formation in aquatic systems is mediated by microorganisms carrying the *hgcA* and *hgcB* genes (Parks et al., 2013). These microorganisms are widely spread across different aquatic environments such as anoxic marine water columns, fresh waters, and marine sediments (Bowman et al., 2020; Gionfriddo et al., 2016; Podar et al., 2015). While many studies focused on biological MMHg formation, very few have studied the processes involved in MMHg degradation, particularly in the ocean. Sunlight can demethylate MMHg, but in the oceans sunlight only reaches down to 200 m, i.e. the photic zone. However, in the aphotic zone of the ocean, the biological processes likely govern MMHg degradation (Bowman, et al., 2020; Sanz-Sáez et al., 2022).

The biological degradation of MMHg is mediated by proteins encoded in the *mer* operon, which can be found in both Gram-positive and Gram-negative bacteria. Some of the *mer* components are membrane proteins or transporters (MerC, MerE, MerF, MerP and MerT). The *mer* operon has two regulators: MerR and MerD, being the first a transcriptional activator-repressor while MerD is an antagonist of MerR, (Barkay et al., 2003). The key catalytic enzymes encoded by the operon are MerA and MerB. The *merA* gene codes for a mercuric reductase, a cytosolic flavin disulfide oxidoreductase that converts Hg^{II} in a volatile, uncharged and lipid-soluble Hg^0 form, that diffuses through the cell membranes. The other enzyme of the operon is an organomercurial lyase encoded by *merB*. This enzyme confers organic mercurial resistance to the bacterium by transferring a proton to a C-H bond in alkyl-mercurial, liberating ionic mercury that will then be reduced to Hg^0 by the mercuric reductase (Barkay et al., 2003). The *mer* operon has been studied in different species; its interspecific diversity is very high, and its evolution is unclear – a new theory proposes *merB* evolving as a mechanistic defense to MMHg produced by *hgcAB* (Lin et al., 2023).

Some studies have shown that the *merAB* genes are present in different environments such as Antarctic sea-ice (Gionfriddo et al., 2016), the Arctic(Bowman, et al., 2020; Møller et al., 2014), lagoons (Vigneron et al., 2021), thermal springs (Wang et al., 2011) and across all oceans (Sanz-Sáez et al., 2022; Tada et al., 2023). Metagenomics and metatranscriptomics analyses have allowed the identification of new phyla containing *mer* genes. Christakis et al. invested much effort into the taxonomic classification and phylogenetic analyses of the newly identified genes (Christakis et al., 2021). Also, they revealed that the existence of multiple *merAB* gene copies per genome was mostly associated with the bacterial domain, with 12.4 % and 9.2 % of the genomes displaying multiple copies of *merA* and *merB* genes respectively (Christakis et al., 2021). Some of these genomes reached up to 8 *merA* genes per genome, as in *Cupriavidus metallidurans,* which presented known strains isolated from metal and/or chemically impacted environments (Diels & Mergeay, 1990; Goris et al., 2001), or *Bacillus cereus* strain17 , with 8 copies of the *merB* gene in its genome. However, the majority of MerA encoding archaeal genomes coded for a single copy (Christakis et al., 2021).

However, metagenomic oriented studies miss the possibility of studying the physiology of cells under the effect of MMHg and therefore, we lack knowledge about the metabolic pathways directly or indirectly involved in *merB* mediated MMHg degradation in the environment and especially in marine systems.

Previous studies working with bacterial isolates have allowed their physiological characterization in the presence of mercury (Joshi et al., 2021; Zheng et al., 2018). However, the isolation of microorganisms able to degrade MMHg from the ocean representing ecologically relevant taxa remains challenging. Therefore, the capacity of marine bacteria to degrade this compound from different phylogenetic taxa and the understanding of transcriptional changes taking place during the process remains unknown. To fill this gap of knowledge, this study focuses on the genomic and transcriptomic characterization of *Alteromonas* sp. ISS312, a bacterium isolated from the deep South Atlantic Ocean (4,000 m depth) widely distributed in the ocean. This strain of *Alteromonas* sp. has the highest tolerance among the tested isolates in our previous work (Sanz-Sáez et al., 2022), and it showed a very high MMHg removal capacity, 98.2 % of MMHg in 24 h higher than other previously studied isolates (Cabral et al., 2013; Giovanella et al., 2016, 2017). Our study provides a detailed genomic characterization of the four *mer* operons present in this bacterium, the identification of the genes most upregulated and downregulated in the presence of MMHg and the mechanistic understanding of the expression profiles for the different *mer* operons positively correlated with a broad array of functions.

Materials and methods

Strain selection.

Alteromonas sp. strain ISS312 was isolated from the deep South Atlantic Ocean (4,000 m depth) at station 43 (ST43: 32º 48.8'S 12º 46.2'E) of the Malaspina 2010 Circumnavigation Expedition (Duarte, 2015). This strain was selected after a functional screening of *merAB* genes from a large collection of marine bacterial isolates (Sanz-Sáez, et al., 2020), and

showed a high tolerance to grow on $HgCl_2$ and to grow on and degrade MMHg, with a Minimum Inhibitory Concentration (MIC) of 70 µM and 10 µM for $HgCl_2$ and MMHg, respectively (Sanz-Sáez et al., 2022). Additionally, it was demonstrated that *Alteromonas* sp. ISS312 was present in the bathypelagic ocean worldwide (Sanz-Sáez et al., 2022) thus making this strain the perfect model organism to study the transcriptional changes in the presence of MMHg.

Growth curves.

The microorganism was grown in aerobic conditions by triplicate in 2L-bottles in Zobell broth (5 g/L of bactopeptone, 1 g/L of yeast extract in a ¼ of MiliQ and ¾ of 0,22 µm pre-filtered seawater per liter) supplemented with 0 µM (control or not amended) and 5 µM of MMHg. The starting OD_{600nm} was 0.05 in order to ensure enough biomass for growth. The experiment lasted 73 h. A total of 17 samples for OD. measurements were taken approximately every 2-3 hours at the beginning of the experiment, when changes were more likely to happen, and every 12 hours after t=35 h. OD. was measured at 600 nm with a spectrophotometer (Varian Cary® 100 UV-Vis).

Samples for DNA and RNA extraction were collected at every growth phase in 50 ml Falcons and centrifuged for 15 minutes at 3,000 rpm (1730 g), resuspended in Zobell Broth, aliquoted and centrifuged for 3 minutes at 12,000 rpm (15294 g). The final pellets were stored at -80 ^{o}C until nucleic acid extraction.

DNA and RNA extraction.

The DNeasy Blood&Tissue® kit (Qiagen) was used for DNA extraction. We followed the manufacturer's protocol for Gram-negative bacterial DNA extraction. Once it was extracted, we measured the DNA concentration with a Thermo Scientific NanoDrop™ 1000 UV/VIS Spectrophotometer and then sent to Sequentia Biotech (Barcelona) for whole genome sequencing.

RNA was extracted using TRI reagent and treated with Turbo DNase (Ambion Inc., Austin, TX, USA) following manufacturer instructions. Samples were stored at -80 ^{o}C and then sent to Sequentia Biotech for mRNA sequencing

Genome sequencing and assembly.

The genome of *Alteromonas* sp. ISS312 was sequenced with paired-ended 300 bp long reads by IGA-Tech with a MiSeq Illumina platform. The library was prepared with a Celero™ DNA-seq library system. The sequences were clean, assembled and annotated (further details in Supplementary Methods). To better understand our strains, we searched for plasmids and genomic islands within its genome and compared it to public genomes (further details in Supplementary Methods)

RNA sequencing and transcriptomic analysis.

The RNA was prepared for sequencing, libraries were made with TruSeq® Stranded Total RNA and the rRNA was removed with Ribo-Zero™. The RNA sequencing was carried out in a NextSeq500 with paired-end reads.

A sequence subsampling of the lag and stationary phase samples of the control, and of the stationary phase sample from the culture grown with MMHg was carried out prior to transcriptomic analyses with bbtools v38.08 (https://sourceforge.net/projects/bbmap/) by randomly taking 80 % of the reads three times to obtain three pseudo-replicates. The rest of the samples had biological triplicates. To check the variability in terms of transcripts composition through the samples at different growth states, a principal coordinates analysis (PCoA) was performed using the Trimmed Mean of M-values (TMM, Table S14) with the vegan package (Oksanen et al., 2020).

The analysis of the RNA sequences was performed with A.I.R transcriptomics software of Sequentia (https://transcriptomics.sequentiabiotech.com/) that integrates different statistical packages (DESeq2, edgeR and NOISeq) allowing a comparison among them (Table S15). To identify which genes were up- and downregulated in the presence of MMHg, comparative transcriptomic analyses, using edgeR, were performed at different timings and stages of the growth curve of *Alteromonas* sp. ISS312 with 5 µM and without MMHg. Two sets of analyses were done: i) comparing all the control samples with all samples from the 5 µM experiment, and ii) comparing the different growth phases from both conditions.

Aiming to establish how the transcriptional patterns of *mer* genes compared to the remaining genes of the transcriptome, a correlation-based analysis was performed. The TMM values of all genes in the *Alteromonas* sp. ISS312 transcriptome were compared to the TMM values of the *mer* genes, by calculating pairwise Pearson correlation coefficients among them. The objective was to identify genes that displayed expression profiles that were very similar or identical to those of *mer* genes, which could indicate they are under the same regulatory controls. Thus, only correlations that displayed a positive Pearson coefficients equal or above 0.9 were considered for further analysis. Finally, for each *mer* gene, we calculated the total number of correlations (within the aforementioned threshold) that were detected with other genes in the transcriptome, grouped according to the KEGG modules to which the latter were assigned. Importantly, many genes were assigned to multiple KEGG modules. In those cases, correlations were counted multiple times.

Recruitment of Mer enzymes in metatranscriptomics of *Tara* Oceans.

Each nucleotide sequence of all five *mer* gene found in the assembly were searched in the *Tara* Oceans Microbiome Reference Gene Catalog v2 + metaG Arctic Inside (OM-RGCv2 + G) with a minimum e-value of 10^{-200}. A total of five hits of *merAB* genes with a 99.5 % identity were detected and subsequently, their transcriptional abundances were retrieved from the *Tara* Oceans Microbiome Reference Gene Catalog v2 + metaT Arctic Inside (OM-RGCv2 + T) to investigate the transcriptional activity of those genes in the global ocean. The generation

and annotation of OMRGC.v2, the taxonomic profiling, and the abundance normalization used for the extraction of the abundance of the *merA* and *merB* genes homologous were thoroughly explained in Salazar et al. (2019). Analyses could be performed thanks to the Ocean Gene Atlas Web resource (Vernette et al., 2022) and abundance results from metagenomes and metatranscriptomes were normalized based on the percentage of mapped reads.

To infer potential statistical differences between *merA* and *merB* genes and ocean layers Kruskal-Wallis test followed by post-hoc Wilcox test was performed. A significative alpha value of 0.05 was assign.

Data availability

The genome assembly was submitted to the European Nucleotide Archive (ENA) under the accession number GCA_927797765. The transcriptomic experiment (project: PRJEB61460) was uploaded to the European Nucleotide Archive (ENA), including the raw RNA sequences (accession numbers: ERS14940911 to ERS14940928).

Results and Discussion

Genetic characterization of *mer* operons in *Alteromonas* sp. ISS312.

Genome Assembly.

The genome of *Alteromonas* sp. ISS312 strain was sequenced, and the optimized assembly resulted in a total of 97 contigs, with a N_{50} of 145125 bp, a L_{50} of 8 and a 44.75 GC % content. A total of 99.94 % of the reads (8.538.875) mapped to the assembly with a coverage of 100X. Only 60 of the initial 97 contigs remained after the annotation and 4.616.455 pairs of bases (pb) and 4058 CDs were obtained (Figure 35). The completeness and the contamination of the genome was obtained with CheckM and was 100 % and 0.85 % respectively. *Alteromonas* sp. ISS312 genome was compared with other *Alteromonas* sp. and showed a high ANI (99,96 %) with *Alteromonas mediterranea* DE (CP001103) (Ivars-Martinez et al., 2008) and therefore our strain ISS312 was taxonomically assigned as *Alteromonas mediterranea* ISS312.

The mer *operons of* Alteromonas mediterranea *ISS312.*

The analyses of the genome assemblies of the *Alteromonas mediterranea* ISS312 showed the presence of four *mer* operons (Figure 35). The first operon (*mer*_1), located between gene ID ISS312_00964 and ISS312_00969, has 4 structural genes encoded between two regulators (*merR*). It has only one catalytic enzyme coded in *merA*, accompanied by three transporters: MerC, MerP, and MerT. All six genes of the operon have the same orientation in the genome, which was surrounded by two transposons (Tn3). Transposons present in *mer* operons have been reported in Gram-negative bacteria, including the Tn21-, Tn501- and Tn5053-lineages, (Bogdanova et al., 2001; Wang et al., 1989; Bogdanova et al., 1998) and in Gram-positive *Bacilli* strains (Matsui et al., 2016). This operon had a high identity (96 %) with the nucleotide sequence of the *mer* operon from *Pseudomonas haloplanktis* M1, first

found in Minamata Bay (Iohara et al., 2001) providing further hint on the horizontal gene transfer events of these genes. The second operon (*mer*_2) corresponds to gene IDs ISS312_02735 to ISS312_02738 and has only four genes: a MerA enzyme (*merA*), two transporters (*merP* and *merT*) and one regulator (*merR*), all of them in the same orientation. Operon *mer*_3 is the most metabolically complete of all *mer* operons and it has both enzymes, MerA and MerB, but it lacks most transporters, except *merE* gene. It encodes two regulators as well, MerR and MerD. This operon is encoded by genes ID ISS312_03666 to ISS312_03670. The fourth operon, *mer*_4 (ID ISS312_04105 to ISS312_04108 and ISS312_04110), is the only one of the four that has genes with different orientations, since the only enzyme present, *merB* gene, goes in one direction and the other components in the opposite direction. Besides *merB*, it contains two *merT* and one *merP* genes (transporters), as well as a *merR* regulator. The taxonomic annotation of the genes is highly unreliable due to the high probability of horizontal gene transfer. The enzymes found in our operons have a high identity with a wide array of different species from different environments, including one plasmid (Figure S6).

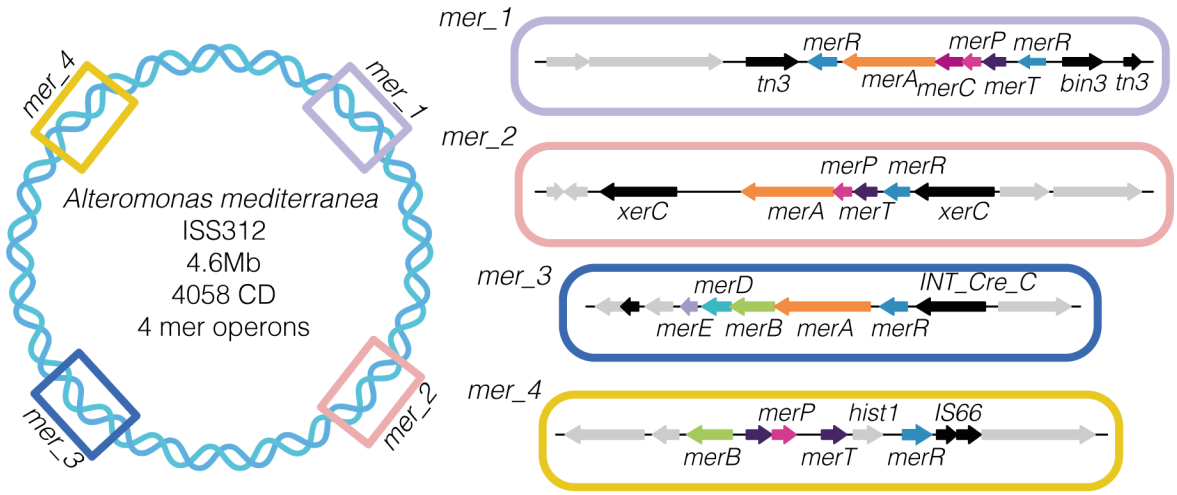


Figure 35: Summary of the assembly's characteristics and synteny of the four *mer* operons found in *Alteromonas mediterranea* strain ISS312 genome. The black arrows are mobile elements (transposases, integrases…). Grey arrows are genes outside the operon.

Previous studies have shown that in Gram-negative bacteria the operon *mer* has two orientations for the genes encoded in it (Naguib et al., 2018). The *merR* is usually encoded in the opposite direction to the rest, which means that the *merR* transcription is divergent from the structural genes, with the exception of *Pseudoalteromonas haloplantkis* (Iohara et al., 2001; Naguib et al., 2018). In strain ISS312, only *mer_4* has genes encoded in different orientations, showing that although variability among *mer* operons of different species has already been reported (Naguib et al., 2018), our results provide evidence of variability in *mer* operons also within the same genome.

Hg detoxification genes are often part of mobile genetic elements (MGE), either transposons or plasmids (Barkay et al., 2003). Supporting this general trend, the four operons of strain ISS312 have either upstream or downstream mobility elements, such as recombinases,

insertion elements, transposases, or integrases (black arrows in Figure 35). As none of ISS312's *mer* operons were found in plasmids (data not shown), we studied the possibility of *mer* genes being part of a genomic island (GI) as previously described for *Alteromonas mediterranea* DE (Ivars-Martinez et al., 2008). We found that the operon *mer*_3 and its surroundings, as well as part of operon *mer_4*, seem to have the same structure as GI9, a genomic island with several *mer* genes encoded on it as previously described (Ivars-Martinez et al., 2008). Indeed, the existence of a GI integrating the mer-3 operon was further predicted with IslandViewr4 (Bertelli et al., 2017).

Physiological responses of *Alteromonas mediterranea* ISS312 to MMHg

Effect of MHg on the growth of Alteromonas mediterranea *ISS312*

We compared the growth curves (in triplicates) of *Alteromonas mediterranea* strain ISS312 in the presence of MMHg 5 µM vs the control (not-amended) (Figure 36). The length of the lag phase, when bacteria adapt themselves to the growth conditions, differed between the exposed isolate and the control (Figure 36). A longer lag phase (20-23 h) was observed at 5 µM MMHg compared to the control, which started to grow immediately after inoculation. Other studies with taxa related to *Pseudomonas* and *Enterobacter* have shown similar patterns, that is, a longer lag phase depending on the concentration of mercury in the culture (Deng & Wang, 2012; Sinha & Khare, 2011). For example, Deng & Wang (2012) experiments showed that *Pseudomonas* sp. S1 has a minimum of 38 hours lag phase at 30 mg/L of Hg^{II} and a maximum of more 160 hours in the highest concentration, 140 mg/L. From our previous study on the same strain, we know that the culture grown with MMHg entered the exponential phase only after all mercury was removed from the medium (Figure 4 in Sanz-Sáez et al., 2022) and that once both cultures started to grow, their growth rates and maximum carrying capacity were very similar, regardless of the initial MMHg concentrations (Sanz-Sáez et al., 2022). The stationary phase was reached after 20 hours in the control but almost 50 hours in the amended cultures differing from what was previously observed in Sanz-Sáez et al. (2022).

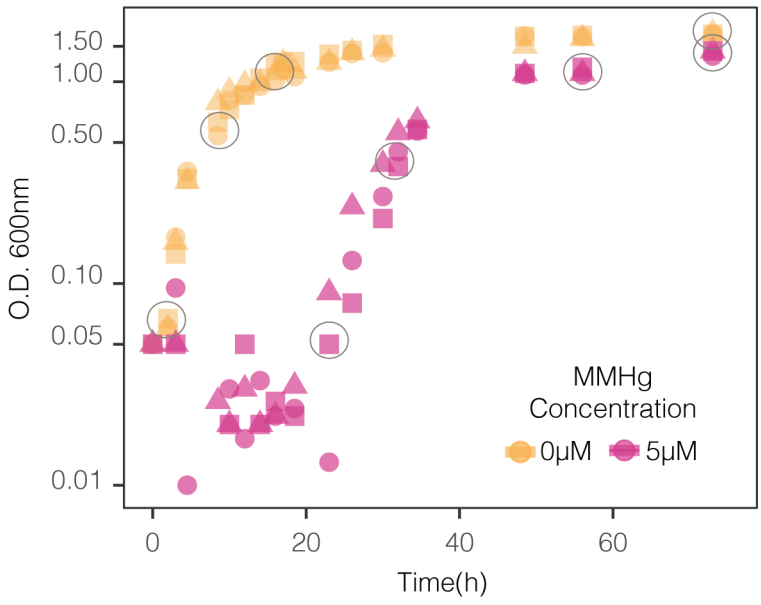


Figure 36: Growth curve of Alteromonas mediterranea ISS312 in the presence of 5 µM of MMHg (pink) and the control without MMHg (yellow). Different symbols (square, triangle, circle) represent the three replicates and gray circles display the samples taken for transcriptomics.

Mono-methylmercury affects whole genome transcriptional patterns.

The expression patterns of the whole genome at different growth phases (lag, exponential, late exponential and stationary phases) were investigated across replicates at both conditions (control vs 5 µM MMHg). We performed a Principal Coordinates Analysis (PCoA) based on the normalized abundances (TMM) to evaluate differences in all gene's transcription (Figure 37). The first axis explained 84.11 % of the variance in gene expression composition corresponding to the variance between growth phases. The main transcriptional differences between the control and the exposed cultures were observed during the exponential and stationary phase. In particular, PCoA analysis indicated that the lag and exponential phases of the MMHg-amended culture were similar in terms of the composition of expressed genes and largely differed from the genomic composition at the exponential phase of the control. At the end of the incubation, the difference in the gene expression composition between the control and the MMHg-amended cultures was less prominent (Figure 37). The gene expression composition of MMHg-amended cultures at the stationary phase clustered together with the samples collected in the late exponential phase in the control due to the effect of a longer lag phase (20-23 h) in the MMHg-amended culture. Therefore, the composition of expressed genes at the stationary phase in the control was completely different than the rest because at time of sampling (72 h), when both MMHg and control cultures reached a similar OD, the control was already in stationary phase for almost 10 hours, while the MMHg-exposed were just reaching the plateau of the growth curve, with transcripts levels closer to late exponential than to stationary phase.

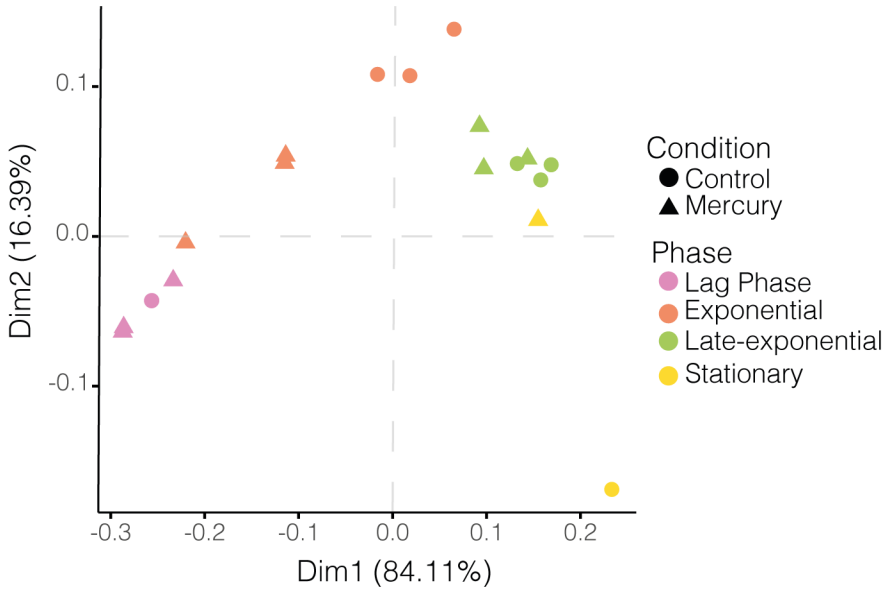


Figure 37: PCoA of the TMM (normalized transcripts), resulting of the transcriptomic analysis with egdeR package. Colors represent phases of the growth and symbols if the culture was amended with MMHg (triangles) or not (circles).

Considering the differences during growth observed between the control and MMHg-amended treatments (Figure 36), and the overall changes in the transcriptome (Figure 37), it is likely that the presence of high concentrations of MMHg affects multiple aspects of bacterial physiology. Thus, we sought to delve deeper into the effects of this contaminant in the *Alteromonas mediterranea* ISS312 transcriptome, and to characterize these transcriptional changes in further detail. A correlation-based analysis between TMM values of *mer* genes and TMM values of the remaining genes in the transcriptome was performed (Figure 38). We aimed to identify

functional orthologous genes that displayed expression profiles highly similar or identical to those genes within the *mer* operons, pointing to probably similar regulatory controls. Notable differences were observed between the correlation profiles of the control (Figure S7) and experimental treatments (Figure 38). Namely, across control treatment samples, a higher proportion of correlations were detected between *mer* genes and those assigned to KEGG modules of energy metabolism, signal molecules and interaction (Figure S7). While across MMHg treatment samples, a higher proportion of correlations were detected between *mer* genes and those assigned to KEGG modules of amino acid metabolism (Figure 38).

We found contrasting expression profiles for each *mer* operon that were positive correlated with a wide array of functions mostly related to amino acid and carbohydrate metabolism, but also to flagellar assembly, quorum sensing or two-component systems. Additionally, we found similar patterns between transporters from different operons, mostly relating them to biofilm formation, quorum sensing and two component systems but very different among the enzymes.

Operon *mer*_3 enzymes within the amended samples displayed different patterns, the *merA* gene was linked to carbohydrate metabolisms such as to pyruvate, propanoate, glyoxylate and dicarboxylate metabolism, glycolysis/gluconeogenesis, citrate cycle and to some amino acids and cofactors and vitamins metabolism while the *merB* was mostly related to multiple amino acids metabolisms and biosynthesis of other secondary metabolites such antibiotics. In the control, we also observed different expression patterns for *merA* and *merB* genes within operon 3 (Figure S7). Although some of the KEGG correlations were found in both (MMHg amended and non-amended samples) such as those related to carbohydrate metabolisms associated with *merA* gene, the *merB* gene in the control was correlated to bacterial secretion systems, protein export, and purine and pyruvate metabolisms. More importantly, the KEGG pathways associated with amino acids were indicated of the amended samples (Figure 38).

In a previous study in *E.coli* four well-defined Conserved Orthologous Groups (COG) were identified within the most differential expressed genes under both inorganic ($HgCl_2$) and organic PMA (phenylmercuric acetate) mercury exposure (LaVoie & Summers, 2018) which were energy production, amino acid metabolism, carbohydrate metabolism, and transcription which also agree with some of our findings. In the same study, *E. coli* had different responses in other four categories (nucleotide metabolism, translation, motility and intracellular trafficking) in the presence of both compounds. Moreover, genetic and physiological analyses have shown that the presence of Hg^{II} in *Pseudomonas stutzeri* 273 downregulates flagellar development, motility and biofilm formation (Zheng et al., 2018). When looking at the transcriptomic analysis by phases, we also found 15 DE genes (9 down-regulated and 6 up-regulated) related to biofilm formation, bacterial mobility, or flagella assembly, finding more down-regulation of these categories in the exponential phase (6 genes) and almost no effect on the stationary phase (1 genes) (Table S16-19). From previous studies, we know that once the culture enters the exponential phase, the Hg concentration is almost zero (Sanz-Sáez et al., 2022). Thus, if mobility/biofilm/flagella are affected in the

presence of Hg, it is reasonable to believe that the effect of Hg in the transcription would dissipate over time. Contrary to what Zheng et al. (2018) found, in the lag phase 3 out of 4 differentially expressed (DE) genes within the mentioned categories were upregulated. These contradictory results could be a consequence of exposure to different compounds as LaVoie & Summers (2018) found in their study. We would need to do physiological studies in ISS312 in the presence of Hg^{II} as well as MMHg to further understand the relationship between biofilm formation and flagella development and *mer* genes.

These results suggest that the high concentrations of MMHg affect not only the detoxification metabolism in *Alteromonas mediterranea* ISS312, but that it also impacts other important aspects of the physiology of these organisms, specially related to amino acid and carbohydrate metabolisms and signal transduction. Considering the extension of mercury contamination across aquatic ecosystems, and the widespread distribution of taxa within *Alteromonadales* across these habitats, it is likely that mercury contamination impacts ecological processes of global relevance that are at least partially driven by these organisms, such as biogeochemical cycles and recycling of organic matter in aquatic ecosystems (Ivars-Martinez et al., 2008; Pedler Sherwood et al., 2015).

Differential expression patterns of the mer *operon of* Alteromonas mediterranea *ISS312*

We evaluated if the amendment of MMHg had a direct impact on the expression of the different *mer* operon copies. For this purpose, we performed a comparative analysis of the genes transcribed between all the amended and all the control samples and detected 52 significantly DE genes (Table S15). Moreover, the comparative transcriptomic analysis by phases revealed a higher number of DE genes. The total number of statistically significant DE genes is 195 for lag-phase, 223 for the exponential, 63 for the late exponential and 142 for the stationary (Table S16-S19 respectively). The comparison of transcriptomic profiles between MMHg amended and the control allowed the recognition of the top up-regulated and down-regulated genes. As expected, the 10 more up-regulated genes were related to Hg resistance (Table 3) including the whole *mer*_3 operon as well as *merB* gene from operon *mer*_4. Interestingly, not all the *mer* operons were equally transcribed (Figure 39). While operon *mer_1* (with the *merA*_00965) was either down-regulated or not differentially expressed, the rest of the *merA* and *merB* genes from the remaining operons were up-regulated. The *merA_1* has the essential amino acids (Boyd & Barkay, 2012) for the enzyme to be functional and it displayed a 96 % identity to the *merA* gene found in *P. haloplanktis* which functionality has been proven (Iohara et al., 2001). Therefore, we speculated that may be a higher concentration of inorganic Hg^{II} or different environmental conditions are required to activate *mer_1*, and further experiments would be needed to completely understand the differences in transcription. Nevertheless, our results showed that not all *mer* genes from the four operons needed to be upregulated at the same time to detoxify the 5 μM MMHg concentration.

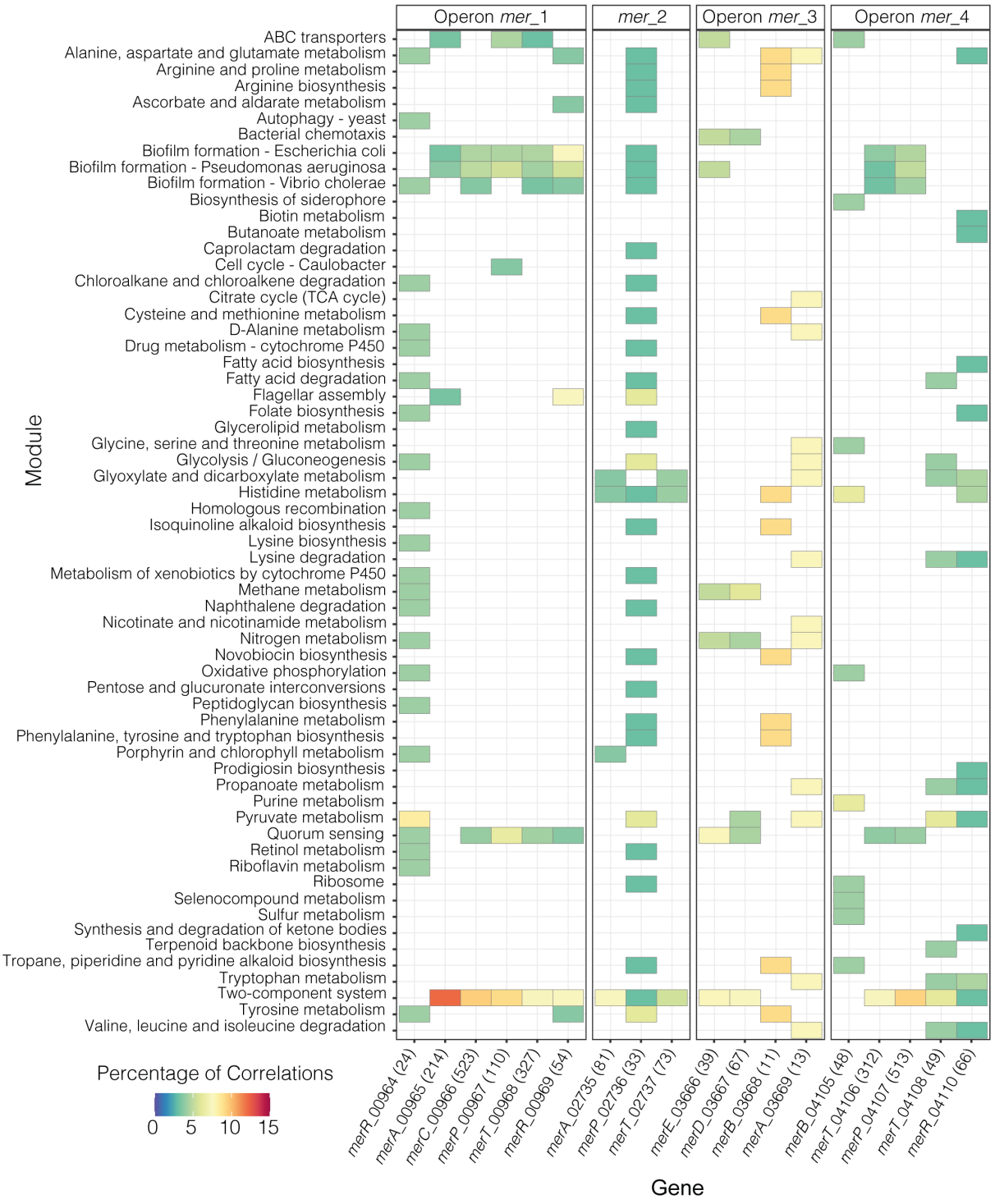


Figure 38: Heatmap of the percentage of correlation classified in the KEGG pathway database; all positive pairwise Pearson correlations ($r > 0.9$) between the expression of mercury related genes and other expressed genes in each amended transcriptome were taken to calculate the percentages (please see the methods section 2.5 for details of the calculation).

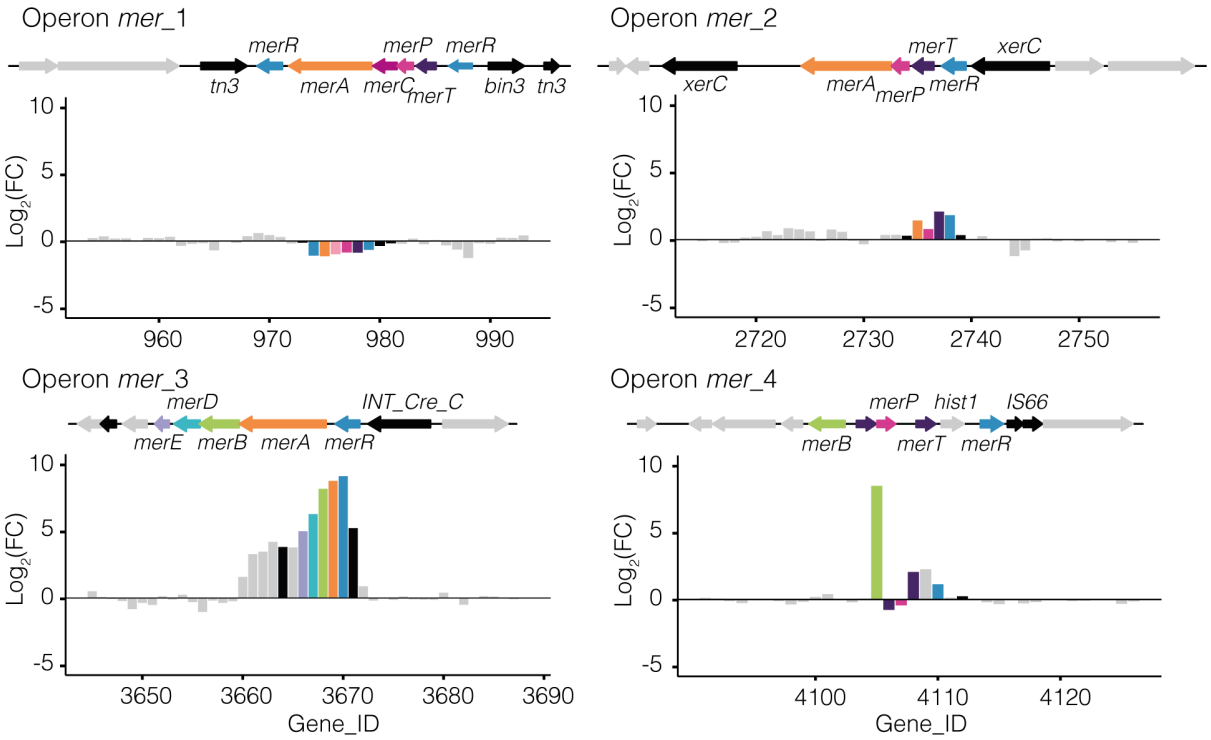


Figure 39: Synteny of the four *mer* operons found in *Alteromonas mediterranea* strain ISS312 genome and their log_2(Fold-Change) considering all samples regardless of the growth phase (Amended vs. control).

Table 3: The ten most upregulated genes comparing all amended transcriptomes with all the control transcriptomes regardless of the growth phase. FC: Fold-Change. FRD: False Discovery Rate.

Gene ID	Log_2(FC)	P-value	FDR	Gene description
iss312_03670	9.107	0	0	MerR transcriptional regulator (*merR*)
iss312_03669	8.760	$1.050 \cdot 10^{-181}$	$2.130 \cdot 10^{-178}$	Mercuric reductase (*merA*)
iss312_04105	8.472	$5.846 \cdot 10^{-72}$	$4.745 \cdot 10^{-69}$	Alkylmercury lyase (*merB*)
iss312_03668	8.163	$1.315 \cdot 10^{-152}$	$1.779 \cdot 10^{-149}$	Alkylmercury lyase (*merB*)
iss312_03667	6.271	$5.080 \cdot 10^{-30}$	$3.436 \cdot 10^{-27}$	MerD transcriptional regulator (*merD*)
iss312_03671	5.229	$3.451 \cdot 10^{-89}$	$3.502 \cdot 10^{-86}$	Phage integrase family
iss312_03666	4.997	$1.436 \cdot 10^{-23}$	$7.282 \cdot 10^{-21}$	Mercuric ion transport protein (*merE)*
iss312_03663	4.208	$7.817 \cdot 10^{-20}$	$3.172 \cdot 10^{-17}$	Group 3 truncated hemoglobin (*ctb*)
iss312_03664	3.813	$1.289 \cdot 10^{-16}$	$4.022 \cdot 10^{-14}$	Transposase, IS5 family
iss312_03665	3.781	$1.237 \cdot 10^{-24}$	$7.170 \cdot 10^{-22}$	DoxX

Furthermore, we investigated how the TMM evolved along time for some of the most differentially expressed genes and how the mercury related proteins have massive expression in the culture grown with MMHg compared to the control. The operon *mer_3* was the only operon in which upregulation was shown for all the operon components including *merA* and *merB* encoding the enzymes, its transporter *merE,* and regulators *merR* and *merD* genes (Figure 40).

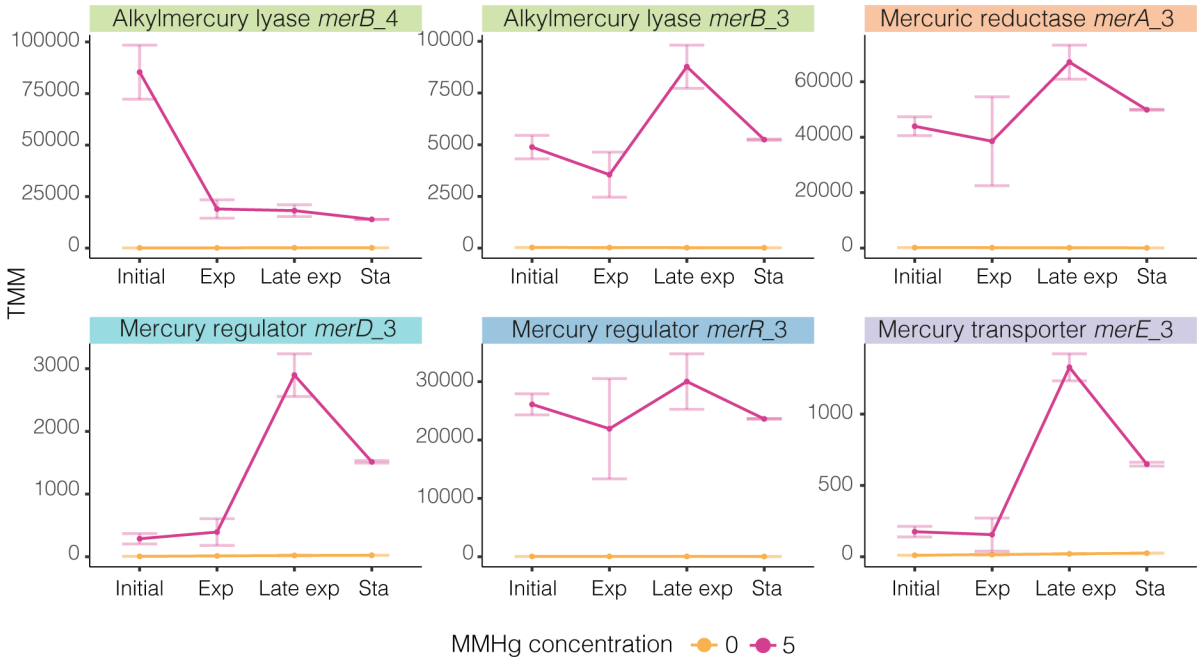


Figure 40: TMM (normalized transcripts) of *mer*_3 genes and *merB*_4 across different phases of the growth curve in the presence of 5 µM of MMHg (pink) vs the control (yellow). Error bars represent the standard deviation between the three replicates.

The *merB*_4 was heavily overexpressed on the lag phase while *merB*_3 expression increased over time only to drop during stationary phase (Figure 40), which suggests that most of the demethylation was being carried out by *merB*_4 because after 24 hours MMHg was undetectable in the medium (Sanz-Sáez et al., 2022). The high overexpression of *merB_4* during the lag phase, points to *merB* having an independent regulation or specific regulation in the presence of MMHg. It has not been reported a different regulator from *merR* or the possibility of *merR* reacting differently to Hg^{II} and MMHg but considering our results more studies should be conducted.

We observed a wide variability of expression between operons but oddly also within the same operon, *merE_3* had its highest expression around 1,500 TMM while *merA_3* displayed more than 60,000 TMM (Figure 40). Despite their differences we can appreciate the same pattern for all *mer* genes from operon *mer_3*, it was lower during the lag and exponential phases, reached its maximum during the late-exponential, and dropped again during the stationary phase. Interestingly, we detected the same trait in the IS5 family transposase (geneID: 03664) found downstream to the mercury genes. *MerR* is the only gene in *mer*_3 that has a slightly different pattern and shares it with the tyrosine-type recombinase (geneID: 03671) found upstream respectively to the mercury genes (Figure 39).

Prevalence of *merAB* genes related to *Alteromonas mediterranea* ISS312 across oceans layers.

In a previous study, we examined the prevalence of the *merAB* genes from the operon *mer*_3 of *Alteromonas mediterranea* ISS312 in marine microbial metagenomes (MetaG) and metatranscriptomes (MetaT) (Sanz-Sáez et al., 2022) using Ocean Microbial Reference Gene Catalog v2 (OM-RGCv2) (Salazar et al., 2019) from the *Tara* Oceans expedition through the Ocean Gene Atlas 2 (OGA2) resource (Vernette et al., 2022). This time, we performed a more detailed analysis including the rest of the *merAB* gene copies from the four *mer* operons of *Alteromonas mediterranea* ISS312, meaning a total of 3 *merA* and 2 *merB* genes. We retrieved one sequence per gene from *Tara* Oceans datasets that matched with more than 99.5 % identity with ISS312's sequences. Therefore, a total of five gene sequences were searched in the metaG and metaT. From those five sequences, only one was assigned to the genus *Alteromonas* (*merA_2*), while the other four could only be assigned to Proteobacteria (*merA_1* and *merB_4*) and to biota (*merAB_3*). The taxonomic assignations were provided by the OGA2.

A throughout search of *mer* genes in the metagenomes of the OM-RGCv2 dataset (Salazar et al., 2019; Vernette et al., 2022) showed that both *merA* and *merB* genes were globally distributed throughout ocean basins and layers (Figure 41), although *merA* was generally more abundant than *merB* (p-value < 0.01). This trait was also observed in genomes of isolates with *merA* genes being roughly ten times more abundant than the *merB* genes (Boyd & Barkay, 2012). The most abundant of the searched genes in the ocean was the *merA_1*, followed by *merB_4* (Figure S8). *merA_1* and *merA_3* were found in a total of 162 and 143 of the 370 analyzed samples respectively while *merA_2* was only found in 88 samples. This would concur with *merA_1* and *merA_3* being present in multiple taxonomic genera instead of just one like *merA_2* (Figure S6A). In general, we found higher abundances of both *merA* and *merB* genes in the mesopelagic than in the rest of the layers, surface (SRF) and deep chlorophyll maximum (DCM) (Figure 41A). An exception to this was the *merA_2* which reached the maximum value in in the DCM of the Mediterranean Sea, by the coast of Algeria.

The *merA* and *merB* abundance of the studied isolate in the analyzed metatranscriptomes of the OM-RGCv2 reveal the potential implication of this bacteria in MMHg demethylation and Hg^{II} reduction in the ocean. In general, we observed a higher transcription potential of *merA* compared to *merB,* but these changes were not statistically significant (Figure 41A). It is important to highlight that *merA* and *merB* transcripts of all variants were detected in all depths, although the maximum was observed in the mesopelagic ocean, as previously observed in Sanz-Sáez et al. (2022), followed by DCM and then SRF (p-value ≤ 0.01). Interestingly, *merA_1* transcripts of our isolate were the most prevalent in the global ocean even though in our experimental conditions the gene expression was down-regulated. Earlier, we discussed the possibility of a higher concentration of iHg or specific environmental conditions being needed to trigger the transcription of *merA_1*, this may be true in vitro conditions but not necessarily in the environment. Many studies have measured total Hg and MMHg concentrations across oceans, and show that the concentrations in the ocean range

in the picomolar. Gionfriddo et al. (2016) measured concentrations in the Antarctic sea water, sea ice, brine and snow (1 - 895 pM) as well as compile the global ocean mean (~ 1.5 pM). Cossa et al. (2011) measurements ranged between 0.63 to 1.76 pM for total Hg and between 0.02 to 0.86 pM for MMHg, in the Southern Ocean. The Mediterranean Sea range between 0.32 and 3.25 pM (Cossa et al., 2009), the eastern tropical South Pacific Ocean reported a maximum of 2 pM total Hg (Bowman et al., 2016) and the Arctic's means is 1.19 pM (Dastoor et al., 2022). This proves that the concentrations needed to induce transcription are very low and that the environmental conditions can be different.

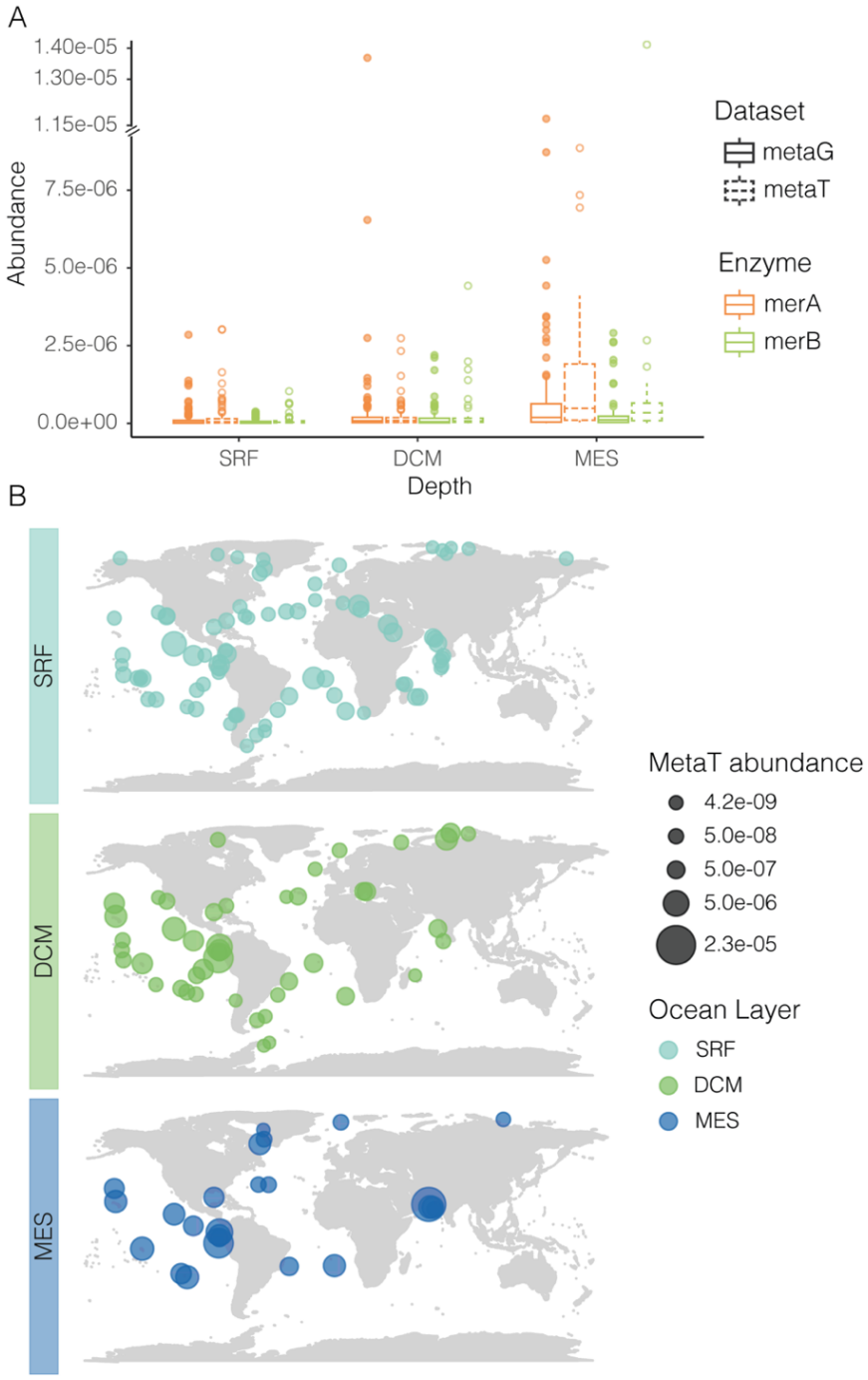


Figure 41. A) Box plot of the metaG (solid line) and metaT (dash line) abundances of *merA* (orange) and *merB* (green) genes in the different layers of the ocean extracted from Tara Oceans datasets. B) Geographical distribution of the *merAB* genes with their metaT abundances coded by size. SRF: surface. DCM: deep chlorophyll maximum. MES: mesopelagic. Size of the dots indicate abundance of transcripts in the database.

The highest transcription of all *merAB* genes was found in station TARA037 at the mesopelagic layer (Figure 41 and Figure S9) and it corresponded to *merB_4*. This station is at the oxygen minimum zone (OMZ) of the north Indian Ocean (Arabian Sea), with an oxygen concentration 2.85 µmol/kg. It is well known that mercury methylation increases under anoxic or hypoxic conditions, so a higher MMHg formation could be expected at this station. A higher transcription of *merB* could be explained by a higher formation of MMHg and result in a steady concentration of MMHg under low oxygen conditions (Malcolm et al., 2010).

Conclusion

Our results provide a better understanding of the MMHg detoxification processes in microorganisms isolated from the deep ocean (*Alteromonas mediterranea* strain ISS312), as well as an overview of the whole cell transcriptional changes in the presence of MMHg. This study demonstrated the capacity of this isolate to detoxify elevated concentrations (5 µM) of MMHg but also a high adaptation capacity to restore the control conditions after 50 hours. In particular, this study shows contrasting transcriptional patterns of the four *mer* operons present in its genome under the conditions tested. We believe that the transcriptional patterns found in this study will prevail in lower concentrations of MMHg. This high adaptative capacity could make *A. mediterranea* ISS312 a great candidate for MMHg bioremediation for contaminated waters. Moreover, the throughout search of *mer* genes of *A. mediterranea* strain ISS312 in metagenomes and metatranscriptomes from the global ocean indicate that this bacterium can be involved in MMHg demethylation and Hg^{II} reduction at the low concentrations found in the ocean.


General
Discussion

General discussion

This thesis aimed to improve the understanding of the ecology of marine bacteria involved in the Hg cycle, as well as to study their physiology and evaluate their role in biological transformations (Hg^{II} methylation, MMHg demethylation, and Hg^{II} reduction) in both environmental samples and in vivo using cultured isolates. In the present thesis, I used a combination of culture-dependent and culture-independent techniques together with chemical analyses to (i) explore the conditions prone to MMHg formation in the Venice lagoon, (ii) unveil the taxonomy, metabolic potential and activity of MMHg demethylating and Hg^{II} reducing bacteria in contaminated sediments, (iii) determine the best candidate to detoxify $HgCl_2$ (Hg^{II}) from the MERCLUB culture collection (with more than 2000 isolates), and determine the best operational conditions in continuous culture and (iv) characterize the genomic structure of the *mer* operon responsible for MMHg demethylation and Hg^{II} reduction, considering the transcriptional effect of MMHg related to other metabolic and functional traits in *Alteromonas* sp. ISS312. In this section, I summarize the main results of my research, highlighting their relevance and discussing different questions that have arisen.

Will global change enhance MMHg formation? The case study of the Venice Lagoon (Chapter 1)

The entire world, including the oceans, is experiencing a global change mainly due to human activity, and many of the changing parameters influence the Hg cycle (Figure 42). We are experiencing, among other factors, higher temperatures (Cheng et al., 2019), higher sea levels which lead to an increased flooding risk (Cazenave & Cozannet, 2014; Taherkhani et al., 2020; Vitousek et al., 2017), lower oxygen concentrations in the ocean (Breitburg et al., 2018; Keeling et al., 2010; Oschlies et al., 2018; Schmidtko et al., 2017), and a shift in the microbiome (Hutchins & Fu, 2017). By incubating sediment cores, we simulated the biogeochemical conditions of oxygen depletion during a MOSE-closing event in the Venice Lagoon (Chapter 1). The experimental results from this study showed that after closing the lagoon in the warmer season, there was a decline of dissolved oxygen (DO), a release of DOC and THg and a higher relative abundance of protein-like peak T of FDOM (associated to a higher bacterial activity). These changes resulted in higher methylation rates in the sediment and a higher MMHg concentration in water.

The Venice Lagoon has been extensively studied due to its social, economic, and cultural importance. Previous studies and monitoring efforts have measured daily DO, temperature, salinity and chlorophyll-*a* (SAMANET dataset), sediment oxygen demand (SOD) (Leoni et al., 2022), metals and other sediment characteristics (Zonta et al., 2018), as well as the impact of global change (Alberti et al., 2023; Amos et al., 2017; Zennaro et al., 2023). Venice has suffered floods throughout history, like the extreme event occurred in 1966 (Trincardi et al., 2016), but in the last decade the number of floods has doubled (Lionello et al., 2021). Actually, extreme sea level events (ESL or flooding) are increasing around the world. Other Mediterranean World Heritage sites are at risk of flooding as well (Reimann et al., 2018).

Taherkhani et al. (2020) concluded that the odds of flooding in 200 United States of America sites will increase 1000-fold in the next century. The Climate Change – 2021 report (IPCC, 2021) stated that ESL will increase 20 to 30 fold by 2050 and 160 to 530 fold by 2100 depending on the Shared Socioeconomic Pathway (SPP) scenario that collectively we choose to follow. Over the years many protection or adaptation strategies have been proposed, but the majority still consist of hard protection systems, like seawalls or dikes (Dedekorkut-Howes et al., 2020), and both structures have reported negative consequences in the coastal environments. In Venice, the MOSE was built to protect the city, but the possible environmental consequences of its operation remain largely unknown.

Extreme flooding has been correlated to the release of organic matter (Figure 42; Majidzadeh et al., 2017; Voynova et al., 2017; Wang et al., 2023), Hg and other metals (Figure 42 ; Bargagli & Rota, 2024; LeMonte et al., 2017; Tsui et al., 2020) and even to higher Hg^{II} methylation rates (Singer et al., 2016). Likewise, tidal flooding, which is a natural cyclic event, is also linked to the mobilization of organic matter and Hg (Bergamaschi et al., 2012; Stoichev et al., 2004); concretely in the Venice Lagoon, tidal flooding has been linked to higher concentrations of dissolved THg and MMHg (Guédron et al., 2012). Even though the MOSE blocks the water exchange with the Adriatic Sea (stops the tide and prevents flooding), in our simulation experiment, we still observed an increase of DOC and THg in the overlaying water. Moreover, Guédron et al. (2012) found higher concentration of total suspended solids (TSS) and higher concentrations of particulate THg and MMHg (ng Hg/L) during the flood tide but a higher MMHg concentration within the TSS (ng Hg/g solids) during the ebb tide, linked to smaller, likely organic, MMHg enriched particles. They suggested that the release of MMHg from the sediment was the main driver of the changes in the concentrations in water. However, more recent studies have proved methylation activity within sinking particles (Capo et al., 2023; Gascón Díez et al., 2016), which opens the possibility of part of the MMHg being formed within the particles. While in the Venice Lagoon I studied the methylating capacity of the sediments, one may ask if the changing conditions might increase the anaerobic micro-environment within the particles of the water column and also enhance *in situ* Hg methylation in the water column.

Other changing factors, like temperature, may also affect the concentration and speciation of Hg in the lagoon. Temporal or seasonal shifts in MMHg concentrations (Cesário et al., 2016; Mitchell et al., 2012) and in Hg methylation rates (Marvin-DiPasquale & Agee, 2003; Monperrus et al., 2007) have been shown in other coastal areas; e.g. higher MMHg concentrations along the Tagus estuary (Lisbon, Portugal) have been found during the summer compared with the winter (Canário et al., 2007; Cesário et al., 2016). Moreover, temperature has been linked to the sediment oxygen demand (SOD; higher SOD at higher temperatures) in the Venice Lagoon (Leoni et al., 2022), but more important factors controlling the SOD are total nitrogen (nutrients) or grain size. All these factors cause a temporal-spatial variation of the SOD along the lagoon, in which the marginal areas (like the Osellino site of our study) have a higher SOD. The areas with higher SOD are more prone to occasional hypoxic conditions, which may lead to higher Hg methylation rates. Our study is

limited to only two samplings (November 2019 and September 2021); thus, it is not possible to determine a temporal shift. Interestingly, we found a higher Hg^{II} methylation rate constant during the warmer sampling (September 2021) but lower concentrations of MMHg in sediments and porewaters compared to November 2019, likely due to a higher demethylation rate associated with higher temperatures (Marvin-DiPasquale & Agee, 2003). With this study we cannot conclude how the increased temperature might affect the speciation of Hg and Hg^{II} methylation/MMHg demethylation processes throughout the year, but our results suggest that in a context of global warming MMHg concentrations might increase in the Venice lagoon and therefore would be very important to assess the variation of MMHg concentrations both environmental and in biota.

Furthermore, it has been observed that higher temperatures and higher concentrations of DOM increase the overall microbial activity (Figure 42). An enhanced microbial activity contributes to the decline of oxygen concentrations (Brewer & Peltzer, 2017) and also to shifts in the composition of the organic matter to a more autochthonous type (lower molecular weight, higher aromaticity and more labile) (Chen et al., 2021), which simultaneously might change the bioavailability of Hg (Gutensohn et al., 2023; Schartup et al., 2015) and the concentration of MMHg (or percentage of the total Hg) (Bravo et al., 2018; Jiang et al., 2018). The composition and concentration of the organic matter may change likewise due to flooding, as I mentioned above, or due to human impact, e.g. waste or agricultural discharge. Having a large input of nutrients may lead to eutrophication, which is already an environmental problem by itself, but additionally has been associated with higher Hg methylation rates (Rodríguez et al., 2022). Higher temperatures are expected to enhance MeHg bioaccumulation as well (Figure 42), resulting in higher MeHg concentrations in biota (Schartup et al., 2019), which will increase human exposure through seafood consumption.

Collectively, the results from the Venice Lagoon plus all the studies mentioned in this section help us to better understand the potential effects of global change in the MMHg formation rates of coastal areas. The net formation of MMHg and therefore the concentrations of MMHg in environments and biota are likely to be affected by: i) rising numbers or duration of flooding events, ii) increasing temperatures and decrease in oxygen, iii) alterations of the concentration and/or composition of organic matter, either as a result of direct human action or as a result of the flooding itself, and lastly iv) the adaptation of the microbial community to the 'new' conditions, which in turn will affect some of the above-mentioned factors (e.g. composition of OM or oxygen concentrations) (Figure 42). Besides the efforts understanding MMHg formation, the lack of knowledge about MMHg demethylation processes impede to predict MMHg concentration in the environment. Providing new insights into MMHg demethylation might help to develop new remediation and management strategies to decrease MMHg in the environment.

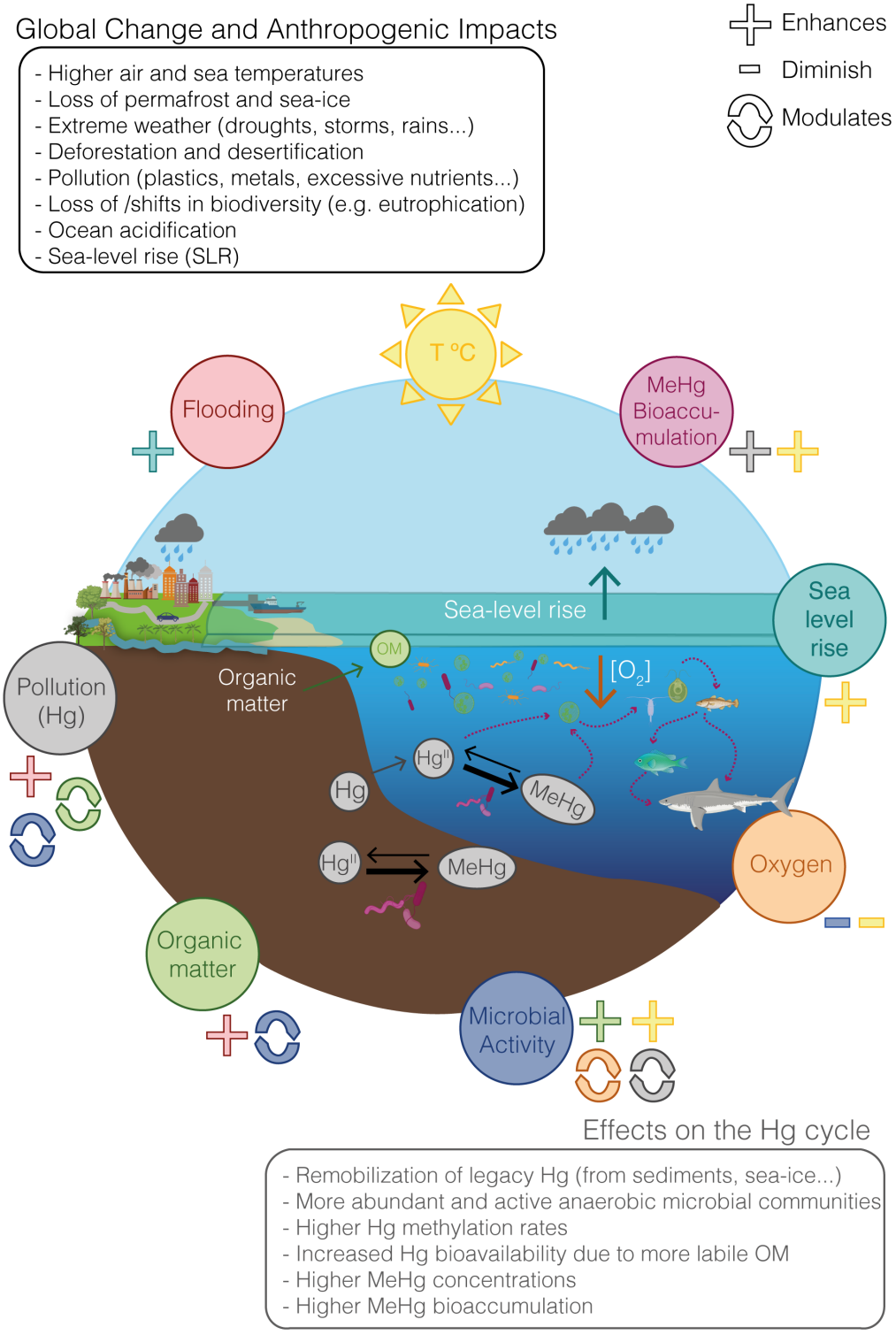


Figure 42: Diagram of the possible effects of global change in coastal environments in relation to Hg concentration, speciation, bioavailability and bioaccumulation. Colored pluses (+) and minuses (-) represent the enhancing or diminishing effect of the increased action/condition of the same color: e.g. the yellow + next to the microbial activity bubble indicates that at higher temperatures, microbial activity will be enhanced; instead, the blue - next to the oxygen bubble, means that at higher microbial activity, oxygen concentrations will be diminished.

Prokaryotes involved in MMHg demethylation and Hg^{II} reduction in sediments (Chapters 2 and 3)

The prokaryotes involved in demethylation and reduction of mercury have been studied in this thesis through culture dependent and independent techniques. Sediment samples were taken from three coastal contaminated sites in Europe (Baltic Sea, Mediterranean Sea and Atlantic Ocean) and used to generate the MERCLUB Culture Collection (MERCC) and the MERCLUB-MAG collection. From the MERCC in which there are more than 2000 isolates, I preselected 37 candidates based on i) positive results of a *merA* PCR, ii) taxonomy and iii) presence in more than one site, to study their Hg and MMHg tolerance as well as removal capacity. After several assays, I selected three strains (*Aeromonas* sp., *Pseudomonas putida* and *Bacillus* sp.) for further physiological and Hg removal capacity characterization. Parallelly, in the MERCLUB-MAG collection, in which there are 803 prokaryotic genomes, I found 43 MAGs that contained either *merA* or *merB*, which theoretically would provide tolerance to Hg^{II} and organomercurials respectively. Also, two additional MAGs displayed the potential to conduct both processes (Hg^{II} reduction and MMHg demethylation – or other organomercurial decomposition) at the same time because they contained both genes (*merA* and *merB*). From this set of MAGs, I studied their abundance, biogeography, activity and metabolic capacities. Having a microbiological study that included both a culturable point of view and an environmental approach through metagenomics allowed to obtain a wider picture of the MMHg demethylating and Hg^{II} reducing community.

The broad approach of this project (mer-club.eu) allowed to compare the culture and the microbial MAGs genome collections. First, I compared both datasets (isolates genomes vs 45 MAGs *merA/merB* containing genomes) to identify potential matches with the following question: are the studied isolates with proven capacities for Hg resistance (Chapter 3) part of the MAG collection (Chapter 2). Our comparative analyses revealed that any of the studied culturable species with capacities for Hg resistance corresponded to the *merAB* containing MAGs. However, it could be possible that due to incompleteness of some of the MAGs, the *mer* genes were missing from the MAG but might be part of the complete genome (medium and high-quality MAGs are considered to be >50 % complete). Thus, I inspected the entire MAG collection with a total of 803 genomes and only one taxa of the tested isolates was found, *Dietzia* sp. There were three MAGs which belonged to genus *Dietzia* (CS3-bin.85, CS4-bin.352 and CS7-bin.66) but none of these MAGs had >95 % ANI with the isolate, which could indicate that they belonged to a different species. Indeed, the three *Dietzia* MAGs displayed an ~83 % ANI against our cultured *Dieztia*, while they displayed between 98 % and 99 % ANI among themselves (further information about methods in Supplementary Material).

As mentioned above, I selected three candidates (*Aeromonas* sp., *Pseudomonas putida* and *Bacillus* sp.) for further characterization, including growth curves and Hg removal, but also genome sequencing. As part of the comparative analysis between both studies, I explored the environmental abundances of the three final candidates, as well as the *merAB* containing

MAGs by performing a fragment recruitment analysis of all MERCLUB-MAGs collection and the three isolates against the metagenomes (following the same methodology as in Chapter 2). Strain *Bacillus* sp. MERCC_2852 was absent in all metagenomic samples. The other two isolates (*Aeromonas* sp. MERCC_1069 and *Pseudomonas putida* MERCC_1942) were present only in two of the studied areas, the Nervión and Suances Estuaries, from which both species were isolated (sites CS14 and CS3, respectively). None of the isolates were present in either the Mediterranean or the Baltic sediments. Concerning the presence of *mer* genes, we have to take into account several premises. First, the *mer* genes have been historically found in aerobic microorganisms and they have been described to be active under oxic conditions and at high concentrations of Hg (Barkay & Gu, 2022; Schaefer et al., 2002). Additionally, the MERCLUB Culture Collection was obtained using aerobic methods of isolation. As the sediments are mostly anaerobic, it would thus be expected that all *merAB* containing bacteria (MAGs and isolates) would belong to the rare biosphere (relative abundance < 0.01 %). Contrary to the expected, most of the *merAB* containing genomes were in the mid-abundant ranking (0.01 % < relative abundance < 1 %) (Figure 43) and one (EN15-bin.81, a Gammaproteobacteria) was even found among the abundant biosphere (relative abundance > 1 %; 1.23 %). Isolate *Aeromonas* sp. MERCC_1069 was found in the mid-abundant biosphere in both Suances and Nervión Estuaries, instead *Pseudomonas putida* MERCC_1942 belonged to the rare biosphere in both areas (Figure 43). The reason for the majority of the *merAB* containing bacteria being mid-abundant remains unknown and it will need further exploration, but I may hypothesize that: i) the sampled sediments were not completely anoxic, there might have been aerobic or microaerophilic microorganisms colonizing the surface of the sediments, ii) our MAGs collection only represents a fraction of the total prokaryotic diversity or iii) the *merAB* containing community is diverse and its abundance is dynamic depending on the environmental parameters and conditions (some *merB* MAGs like EN15-bin.81 were more abundant in Barcelona than the rest of the sites).

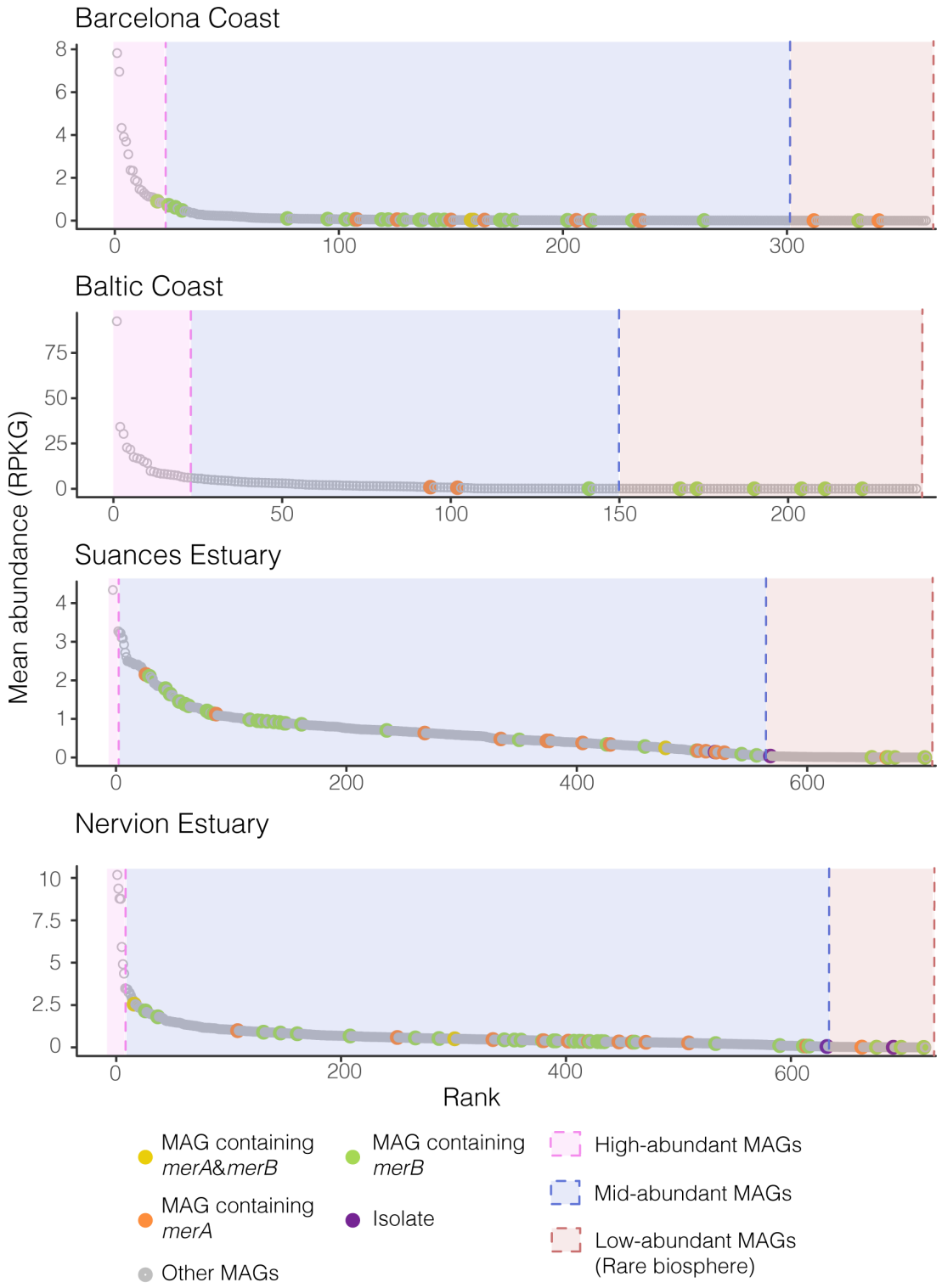


Figure 43: Rank plots showing the *merAB* containing genomes (MAGs or isolates) in the different sampling areas. From top to bottom: Barcelona's coast, Baltic's coast, Suances Estuary and Nervión Estuary. Grey dots belong to the MAGs that did not have neither *merA* nor *merB*. High-abundant MAG correspond to >1 % relative abundance, mid abundant to those <1 % but >0.01 % and low-abundant to <0.01 % relative abundance.

Due to the cost effectiveness and technological advances, metagenomic and metatranscriptomic studies have recently been increasingly used, and mercury cycling genes have been informed in their datasets. For instance, Gionfriddo et al. (2016) reported them in sea-ice, while Bowman et al. (2020), Lin et al. (2021), and Tada et al. (2023) found them in sea water from different places around the world, although any of these studies reconstructed MAGs in their studies. Recent works were able to reconstruct a few MAGs that carried *merA* or *merB*, such as Rincón-Tomás et al. (2023), who described three MAGs with *merA* in marine sediments, or Vigneron et al. (2021), who recovered 11 *merA*- and 2 *merB*-containing MAGs from microbial mats. Nevertheless, my study (**Chapter 2**) is the first to reconstruct MAGs with both *merA* and *merB* genes, and also contributes a larger number (up to 45) of *mer*-containing MAGs which presence and potential transcriptional activity were investigated. The two MAGs that contained both *merAB* genes were associated with *Microbacterium* sp. (EN17.bin27) and Rhodobacteraceae (EN17.bin60), belonging to genus JL08, from which there is only one genome available. *Microbacterium* sp. public genomes have *merAB* genes and this bacterium has been studied as a bioremediation agent for enhanced phytoextraction of Hg from soils (Mariano et al., 2020). On the other hand, among the genes of the representative belonging to genus JL08 (GenBank ID: GCA_003352045.1) neither *merA* nor *merB* could be found, although other Rhodobacteraceae do have *merAB* in their genomes.

Recovering the genomes and using the HMM-models as filters allowed to identify possible reductors or demethylators, which is a great advance, although true Hg reductors or MMHg demethylators validation requires of a culturable candidate of the species with the corresponding genes to perform experimental assays. In some cases, the necessary gene has been found but the function carried out by the corresponding gene has been not proven. The case of *Nitrospira* is the perfect example of this event. The *hcgA*-like genes have been found in *Nitrospira* sp. genomes (Gionfriddo et al., 2016, 2021; Villar et al., 2020), but the methylating activity has not been proven in any culturable *Nitrospira* to date, which proves the importance of working simultaneously with both sequences and cultures.

Is Hg bioremediation possible based on isolated cultured bacteria from Hg contaminant environments? (Chapters 3 and 4)

Having cultures with proven capacity for removal of Hg from the medium (either inorganic Hg or organomercurials) are crucial for a large array of studies and applications. One of my principal aims in **Chapter 3** was to found the best candidate for Hg bioremediation using the continuous culture technique from a selection of strains obtained from a culture collection from Hg contaminated sediments, and *Pseudomonas putida* MERCC_1942 was finally selected as the best option. However, this strain had *merA* gene but lacked *merB*, so in a situation with high MMHg concentrations, *Alteromonas mediterranea* ISS312 (**Chapter 4**) might be a better candidate. In general, both isolates showed a good capacity for Hg^{II} or MMHg removal from the medium, which makes them good candidates for bioremediation. However, to be part of a bioremediation process, several extra steps are required, such as

Hg removal tests in the particular environment to bioremediate (e.g. highly contaminated water from an industrial area), as well as multiple scalation steps and an exhaustive planning and collaboration among ecologists, industrial microbiologists, and engineers.

Using microbes for environmental bioremediation is extremely challenging, but with time and research this goal can be achieved (Dixit et al., 2015; González-Reguero et al., 2023). Multiple microbiological strategies can be used to remove Hg, such as the above mentioned detoxification (which uses MerA and MerB enzymes), as well as biosorption or bioaccumulation (Dixit et al., 2015). The different bacterial strains that I have used during this thesis could be used for detoxification, except *Bacillus* sp. MERCC_2833, which did not remove Hg from the medium. However, *Bacillus* sp. MERCC_2833 would be a nice candidate to study bioremediation via biosorption as it showed a mucoid phenotype, consistent with the production of exopolysaccharides, previously linked to biosorption capacities (François et al., 2012; Kalpana et al., 2018). This strain would need to be further characterized and determine the link between exopolysaccharides production and Hg biosorption. However, most of the current studies focus on finding the right candidate and characterizing the process and the parameters controlling it (Cabral et al., 2013; Dash et al., 2014; Gasong et al., 2017; Joshi et al., 2021; Pepi et al., 2011; Saranya et al., 2017), instead of investigating a cost effective, environmentally respectful and industrially viable approach.

Alteromonas mediterranea ISS312: a case study

In **Chapter 4**, I showed that *A. mediterranea* ISS312 had multiple *mer* operons. Multiple copies of *mer* genes or multiple operons have been previously described (Christakis et al., 2021; Ivars-Martinez et al., 2008; Monsieurs et al., 2013) and some researchers attributed this trend to the high concentrations of Hg in the environment in which the bacterium was found. However, *A. mediterranea* ISS312 was isolated from seawater where the concentration of Hg is normally along the picomolar (pM) range. Moreover, the MERCLUB-MAG collection was obtained from sediments with much higher concentration of Hg and only two MAGs contained two *merB* and only one contained two *merA* genes.

Furthermore, growth curves in presence and absence of MMHg were performed to investigate the effect of MMHg on the transcriptional patterns of the culture along the growth curve. Interestingly, I found that not all the *mer* operons were used for detoxification (some of them were either not differentially transcribed between the control and the MMHg or were downregulated). Besides the *mer* genes expression, I searched for correlations between the expression patterns of *mer* genes and the rest of the transcriptome, so I could elucidate what other genes might share the same expression pattern. The different *mer* operons were correlated to different KEGG categories hinting that they might be under different regulation processes. Other studies, (e.g. LaVoie & Summers, 2018) also aimed to characterize the transcriptional changes in the presence of organic Hg (PMA: phenylmercuric acetate) and inorganic Hg ($HgCl_2$). They reported different expression profiles for PMA and for $HgCl_2$, and they found that some Cluster of Orthologous Groups (COGs) like carbohydrates metabolism or biofilm formation, were differently expressed under both Hg compounds and along

exposure time. Contrasting transcriptomic responses were found as well in multicellular organisms such as *Caenorhabditis elegans* (McElwee et al., 2013). Similarly, it would be expected to see different transcriptomic profiles of *A. mediterranea* ISS312 in the presence of organic or inorganic compounds of Hg. Future research might include using knock-outs of the different operons to study the tolerances to different concentrations and compounds of Hg, to maybe elucidate what ecological advantage lays behind having multiple *mer* operons.

Lastly, *A. mediterranea* ISS312's *mer*_4 operon had the largest expression of *merB* although the regulator (*merR*) of the operon was not differentially expressed. Similarly, many of the MAGs that contained the *merB* genes did not have a complete operon, some of them exhibited one or two transporters (usually *merT* and *merP*) but none of them had *merR* close to the *merB* gene. These findings may hint at the possibility that *merB* has a different regulation method than the known *merR*. The search of this 'unknown' regulation method could also be a possible line of future research from this thesis.

Future research

As I have mentioned in the discussion new research questions have arisen from this thesis. Personally, the most interesting future projects or initiatives include:

1. Temporal and spatial study of the net methylation in the Venice Lagoon associated to the increasing temperatures and the MOSE. Monitoring the concentrations of Hg, and specially MMHg, in the lagoon is of great importance. The ISMAR (Istituto delle Scienze Marine, Venice) has an intense monitoring of many parameters; however, measuring Hg methylation rates is complicated, time-consuming, and costly. This type of study would be helpful for understanding the effects of the evolving conditions in the Hg cycle not only in the Venice Lagoon, but also in other coastal lagoons.
2. The industrialization and implementation of the Hg bioremediation processes. Candidates for bioremediation have been found in this thesis, as well as in other studies, but extra efforts are required before being able to implement a functioning bioremediation system in marine environments.
3. *Alteromonas mediterranea* ISS312 can represent a model organism to understand the ecological advantage of i) having *mer* genes in the ocean where Hg concentrations are low and ii) having multiple and different *mer* operons. As well, *A. mediterranea* ISS312 could be used to test whether *merB* has its own transcriptional regulation.

Conclusions



Conclusions

1. The incubation experiments used to simulate the closing of the MOSE (isolating the Venice Lagoon) triggered an anoxic event in the warm sampling (September) but not in the cold-one (November).
2. The MOSE-closing simulation experiment showed a release of dissolved organic carbon and an enrichment of protein-like substances as well as enhanced in situ Hg^{II} methylation in the sediments.
3. The overlying water and the porewater of the sediment cores showed higher MMHg concentrations in the anaerobic incubated samples (MOSE-closing simulation) than in the non-incubated samples ('normal' conditions of the lagoon).
4. Enhanced Hg methylation, higher MMHg concentrations and higher temperatures might result in larger bioaccumulation in biota.
5. Future implementations of flooding adaptations should take into consideration: the Hg concentration of the area, the possibility of enhanced fluxes of organic matter, THg and MMHg release from sediments into the water column and the possibility of enhanced microbial activity, which might lead to higher Hg methylation rates.
6. The MERCLUB Hg-detoxification reference gene catalog contains a larger number of *merB* (188) genes than *merA* (74). Similarly, the MERCLUB Microbial MAG collection showed a larger number of *merB*-containing MAGs (32) than *merA*-containing (15) ones. These numbers demonstrate the importance of *merB* in maintaining a low concentration of MMHg in the sediments.
7. Many of the *merB* genes found in the MAGs were not part of an operon, highlighting the importance of studying them even in the absence of *merA*. Higher diversity of *merB* genes was found among the metatranscriptomes, which also showed higher abundances than *merA* transcripts, suggesting that *merB* can be transcribed individually.
8. The majority of the *merAB*-containing MAGs (26 out of 45) were assigned to Gammaproteobacteria, proving their key role in the demethylation in coastal sediments.
9. Phylum Krumholzibacteriota was described to have 2 *merA* sequences within its genome for the first time. Both sequences were found among the 5 *merA* transcribed genes found in the metatranscriptomes.
10. The MMHg demethylating and Hg^{II} reducing communities are phylogenetically and metabolically very diverse. Among the most prevalent metabolisms are the Calvin cycle, H_2 oxidation, denitrification and dissimilatory sulfate reduction. The metabolic diversity shows that the *merAB*-containing MAGs can use a variety of electron donors and acceptors.

11. *Pseudomonas putida* MERCC_1942, *Aeromonas* sp. MERCC1069 and *Bacillus* sp. MERCC_2852, as well as other tested isolates, are capable of growing in a wide range of Hg concentrations as well as salinities and oxygen levels.
12. *Pseudomonas putida* MERCC_1942 is the best candidate for bioremediation in continuous culture conditions, showing the highest removal efficiency when grown under high dilution rates (i.e. growth rates).
13. *Aeromonas* sp. MERCC_1069 has a high Hg^{II} removal capacity (up to 79 % in 4 μM $HgCl_2$ and 53 % in 12 μM $HgCl_2$) but is not apt for continuous culture conditions due to the large aggregates that forms during its growth.
14. *Bacillus* sp. MERCC_2852 showed high Hg tolerance (MIC = 50 μM) and adaptative growth (very large, cloud-like aggregates) in both tested $HgCl_2$ concentrations in batch (4 μM and 12 μM) with no *merA* present in its genome.
15. *Aeromonas* sp. MERCC_1069 is among the mid abundant taxa within the metagenomic samples while *Pseudomonas putida* MERCC_1942 belongs to the rare biosphere. Both species were found only in two of the four areas studied, in the Cantabrian coast (Suances and Nervión estuaries).
16. *Alteromonas mediterranea* ISS312 from the MARINET culture collection contains 4 *mer* operons in its genome. All four *mer* operons are phylogenetically different and have different genetic compositions, hinting that they were integrated by horizontal gene transfer by different microorganisms and at different times.
17. Five micromolar (5 μM) of MMHg alters the growth of *A. mediterranea* ISS312 by extending its lag phase up to 23 hours and changing the transcriptional pattern, although it was able to restore control condition after 50 hours.
18. ISS312's *mer* operons showed different transcriptional patterns, downregulating *mer_1* operon, not differentially expressing *mer_2* and upregulating *mer_3* and one *merB* gene of *mer_4*.
19. The different *mer* operons show correlations to different KEGG categories, implying that the physiological effect might change in the presence of diverse Hg compounds or concentrations, as they might use a different operon for detoxification.
20. A total of five sequences of *merA* and *merB* from the different *mer* operons of *A. mediterranea* ISS312 were found in public metagenomic and metatranscriptomic data, worldwide and in all ocean's layers, showing that they might be important in the demethylating capacity of the global ocean.



Bibliography

Bibliography

Acinas, S. G., Sánchez, P., Salazar, G., Cornejo-Castillo, F. M., Sebastián, M., Logares, R., Royo-Llonch, M., Paoli, L., Sunagawa, S., Hingamp, P., Ogata, H., Lima-Mendez, G., Roux, S., González, J. M., Arrieta, J. M., Alam, I. S., Kamau, A., Bowler, C., Raes, J., … Gasol, J. M. (2021). Deep ocean metagenomes provide insight into the metabolic architecture of bathypelagic microbial communities. *Communications Biology*, *4*(1), 604. https://doi.org/10.1038/s42003-021-02112-2

Ahmad, M. (2018). Mercuric resistant bacteria *Aeromonas* exhibits neurologic toxic effects on the developmental motor reflexes, and brain oxidative stress in mice offspring. *Microbial Pathogenesis*, *114*, 169–175. https://doi.org/10.1016/j.micpath.2017.11.063

Akito, M., Shinichiro, Y., Akihiro, H., Michiaki, K., Ikuko, S., Akihide, T., & Hirokatsu, A. (2014). Reevaluation of Minamata Bay, 25 years after the dredging of mercury-polluted sediments. *Marine Pollution Bulletin*, *89*(1–2), 112–120. https://doi.org/10.1016/j.marpolbul.2014.10.019

Al-Ansari, M. M. (2022). Biodetoxification mercury by using a marine bacterium *Marinomonas* sp. RS3 and its *merA* gene expression under mercury stress. *Environmental Research*, *205*, 112452. https://doi.org/10.1016/j.envres.2021.112452

Alberti, T., Anzidei, M., Faranda, D., Vecchio, A., Favaro, M., & Papa, A. (2023). Dynamical diagnostic of extreme events in Venice lagoon and their mitigation with the MoSE. *Scientific Reports*, *13*(1), 10475. https://doi.org/10.1038/s41598-023-36816-8

Altschul, S. (1997). Gapped BLAST and PSI-BLAST: A new generation of protein database search programs. *Nucleic Acids Research*, *25*(17), 3389–3402. https://doi.org/10.1093/nar/25.17.3389

Amos, C. L., Umgiesser, G., Ghezzo, M., Kassem, H., & Ferrarin, C. (2017). Sea surface temperature trends in Venice Lagoon and the adjacent waters. *Journal of Coastal Research*, *332*, 385–395. https://doi.org/10.2112/JCOASTRES-D-16-00017.1

Amos, H. M., Jacob, D. J., Streets, D. G., & Sunderland, E. M. (2013). Legacy impacts of all-time anthropogenic emissions on the global mercury cycle. *Global Biogeochemical Cycles*, *27*(2), 410–421. https://doi.org/10.1002/gbc.20040

An, J., Zhang, L., Lu, X., Pelletier, D. A., Pierce, E. M., Johs, A., Parks, J. M., & Gu, B. (2019). Mercury uptake by *Desulfovibrio desulfuricans* ND132: Passive or active? *Environmental Science & Technology*, *53*(11), 6264–6272. https://doi.org/10.1021/acs.est.9b00047

Aramaki, T., Blanc-Mathieu, R., Endo, H., Ohkubo, K., Kanehisa, M., Goto, S., & Ogata, H. (2019). *KofamKOALA: KEGG ortholog assignment based on profile HMM and adaptive score threshold*.

Auguie, B. (2015). *gridExtra: Miscellaneous functions for "Grid" graphics. R package version 2.0.0.* [Computer software]. http://CRAN.R-project.org/package=gridExtra

Bakir, F., Damluji, S. F., Amin-Zaki, L., Murtadha, M., Khalidi, A., Al-Rawi, N. Y., Tikriti, S., Dhahir, H. I., Clarkson, T. W., Smith, J. C., & Doherty, R. A. (1973). Methylmercury poisoning in Iraq: An interuniversity report. *Science*, *181*(4096), 230–241. https://doi.org/10.1126/science.181.4096.230

Baldi, F., Pepi, M., & Filippelli, M. (1993). Methylmercury resistance in *Desulfovibrio desulfuricans* strains in relation to methylmercury degradation. *Applied and Environmental Microbiology*, *59*(8), 2479–2485. https://doi.org/10.1128/aem.59.8.2479-2485.1993

Bargagli, R., & Rota, E. (2024). Mercury biogeochemistry and biomagnification in the Mediterranean Sea: Current knowledge and future prospects in the context of climate change. *Coasts*, *4*(1), 89–107. https://doi.org/10.3390/coasts4010006

Barkay, T., Fouts, D. L., & Olson, B. H. (1985). Preparation of a DNA gene probe for detection of mercury resistance genes in gram-negative bacterial communities. *Applied and Environmental Microbiology*, *49*(3), 686–692. https://doi.org/10.1128/aem.49.3.686-692.1985

Barkay, T., & Gu, B. (2022). Demethylation—The other side of the mercury methylation coin: A critical review. *ACS Environmental Au*, *2*(2), 77–97. https://doi.org/10.1021/acsenvironau.1c00022

Barkay, T., Liebert, C., & Gillman, M. (1989). Hybridization of DNA probes with whole-community genome for detection of genes that encode microbial responses to pollutants: *Mer* genes and Hg^{2+} resistance. *Applied and Environmental Microbiology*, *55*(6), 1574–1577.

Barkay, T., Miller, S. M., & Summers, A. O. (2003). Bacterial mercury resistance from atoms to ecosystems. *FEMS Microbiology Reviews*, *27*(2–3), 355–384. https://doi.org/10.1016/S0168-6445(03)00046-9

Behar, F., Beaumont, V., & De B. Penteado, H. L. (2001). Rock-Eval 6 Technology: Performances and developments. *Oil & Gas Science and Technology*, *56*(2), 111–134. https://doi.org/10.2516/ogst:2001013

Bergamaschi, B. A., Krabbenhoft, D. P., Aiken, G. R., Patino, E., Rumbold, D. G., & Orem, W. H. (2012). Tidally driven export of dissolved organic carbon, total mercury, and methylmercury from a mangrove-dominated estuary. *Environmental Science & Technology*, *46*(3), 1371–1378. https://doi.org/10.1021/es2029137

Bertelli, C., Laird, M. R., Williams, K. P., Simon Fraser University Research Computing Group, Lau, B. Y., Hoad, G., Winsor, G. L., & Brinkman, F. S. (2017). IslandViewer 4: Expanded prediction of genomic islands for larger-scale datasets. *Nucleic Acids Research*, *45*(W1), W30–W35. https://doi.org/10.1093/nar/gkx343

Binish, M. B., Shini, S., Sinha, R. K., Krishnan, K. P., & Mohan, M. (2021). Mercuric reductase gene (*merA*) activity in a mercury tolerant sulphate reducing bacterium isolated from the Kongsfjorden, Arctic. *Polar Science*, *30*, 100745. https://doi.org/10.1016/j.polar.2021.100745

Black, F. J., Poulin, B. A., & Flegal, A. R. (2012). Factors controlling the abiotic photo-degradation of monomethylmercury in surface waters. *Geochimica et Cosmochimica Acta*, *84*, 492–507. https://doi.org/10.1016/j.gca.2012.01.019

Bloom, N. S., Moretto, L. M., & Ugo, P. (2004). A comparison of the speciation and fate of mercury in two contaminated coastal marine ecosystems: The Venice Lagoon (Italy) and Lavaca Bay (Texas). *Limnology and Oceanography*, *49*(2), 367–375. https://doi.org/10.4319/lo.2004.49.2.0367

Bogdanova, E., Minakhin, L., Bass, I., Volodin, A., Hobman, J. L., & Nikiforov, V. (2001). Class II broad-spectrum mercury resistance transposons in Gram-positive bacteria from natural

environments. *Research in Microbiology*, *152*(5), 503–514. https://doi.org/10.1016/S0923-2508(01)01224-4

Bogdanova, E. S., Bass, A., Minakhin, L. S., Petrova, M. A., Mindlin, Z., Volodin, A. A., Tiedjet, J. M., HbrnanN, J. L., Brown, L., & Nikiforov', V. G. (1998). Horizontal spread of rner operons among Gram-positivebacteria in natural environments. *Microbioloy*, *144*(3), 609–620.

Boschker, H. T. S., Vasquez-Cardenas, D., Bolhuis, H., Moerdijk-Poortvliet, T. W. C., & Moodley, L. (2014). Chemoautotrophic carbon fixation rates and active bacterial communities in intertidal marine sediments. *PLoS ONE*, *9*(7), e101443. https://doi.org/10.1371/journal.pone.0101443

Bouchet, S., Amouroux, D., Rodriguez-Gonzalez, P., Tessier, E., Monperrus, M., Thouzeau, G., Clavier, J., Amice, E., Deborde, J., Bujan, S., Grall, J., & Anschutz, P. (2013). MMHg production and export from intertidal sediments to the water column of a tidal lagoon (Arcachon Bay, France). *Biogeochemistry*, *114*(1–3), 341–358. https://doi.org/10.1007/s10533-012-9815-z

Bouchet, S., Goñi-Urriza, M., Monperrus, M., Guyoneaud, R., Fernandez, P., Heredia, C., Tessier, E., Gassie, C., Point, D., Guédron, S., Achá, D., & Amouroux, D. (2018). Linking microbial activities and low-molecular-weight thiols to Hg methylation in biofilms and periphyton from high-altitude tropical lakes in the Bolivian Altiplano. *Environmental Science & Technology*, *52*(17), 9758–9767. https://doi.org/10.1021/acs.est.8b01885

Bowers, R. M., Kyrpides, N. C., Stepanauskas, R., Harmon-Smith, M., Doud, D., Reddy, T. B. K., Schulz, F., Jarett, J., Rivers, A. R., Eloe-Fadrosh, E. A., Tringe, S. G., Ivanova, N. N., Copeland, A., Clum, A., Becraft, E. D., Malmstrom, R. R., Birren, B., Podar, M., Bork, P., … Woyke, T. (2017). Minimum information about a single amplified genome (MISAG) and a metagenome-assembled genome (MIMAG) of bacteria and archaea. *Nature Biotechnology*, *35*(8), 725–731. https://doi.org/10.1038/nbt.3893

Bowman, K. L., Collins, R. E., Agather, A. M., Lamborg, C. H., Hammerschmidt, C. R., Kaul, D., Dupont, C. L., Christensen, G. A., & Elias, D. A. (2020). Distribution of mercury-cycling genes in the Arctic and equatorial Pacific Oceans and their relationship to mercury speciation. *Limnology and Oceanography*, *65*(S1), S310–S320. https://doi.org/10.1002/lno.11310

Bowman, K. L., & Hammerschmidt, C. R. (2011). Extraction of monomethylmercury from seawater for low-femtomolar determination. *Limnology and Oceanography: Methods*, *9*(4), 121–128. https://doi.org/10.4319/lom.2011.9.121

Bowman, K. L., Hammerschmidt, C. R., Lamborg, C. H., & Swarr, G. (2015). Mercury in the North Atlantic Ocean: The U.S. GEOTRACES zonal and meridional sections. *Deep Sea Research Part II: Topical Studies in Oceanography*, *116*, 251–261. https://doi.org/10.1016/j.dsr2.2014.07.004

Bowman, K. L., Hammerschmidt, C. R., Lamborg, C. H., Swarr, G. J., & Agather, A. M. (2016). Distribution of mercury species across a zonal section of the eastern tropical South Pacific Ocean (U.S. GEOTRACES GP16). *Marine Chemistry*, *186*, 156–166. https://doi.org/10.1016/j.marchem.2016.09.005

Bowman, K. L., Lamborg, C. H., & Agather, A. M. (2020). A global perspective on mercury cycling in the ocean. *Science of The Total Environment*, *710*, 136166. https://doi.org/10.1016/j.scitotenv.2019.136166

Boyd, E. S., & Barkay, T. (2012). The mercury resistance operon: From an origin in a geothermal environment to an efficient detoxification machine. *Frontiers in Microbiology*, *3*. https://doi.org/10.3389/fmicb.2012.00349

Bratkič, A., Koron, N., Ribeiro Guevara, S., Faganeli, J., & Horvat, M. (2017). Seasonal variation of mercury methylation potential in pristine coastal marine sediment from the Gulf of Trieste (Northern Adriatic Sea). *Geomicrobiology Journal*, *34*(7), 587–595. https://doi.org/10.1080/01490451.2016.1247482

Bravo, A. G., Bouchet, S., Guédron, S., Amouroux, D., Dominik, J., & Zopfi, J. (2015). High methylmercury production under ferruginous conditions in sediments impacted by sewage treatment plant discharges. *Water Research*, *80*, 245–255. https://doi.org/10.1016/j.watres.2015.04.039

Bravo, A. G., Bouchet, S., Tolu, J., Björn, E., Mateos-Rivera, A., & Bertilsson, S. (2017). Molecular composition of organic matter controls methylmercury formation in boreal lakes. *Nature Communications*, *8*(1), 14255. https://doi.org/10.1038/ncomms14255

Bravo, A. G., Kothawala, D. N., Attermeyer, K., Tessier, E., Bodmer, P., Ledesma, J. L. J., Audet, J., Casas-Ruiz, J. P., Catalán, N., Cauvy-Fraunié, S., Colls, M., Deininger, A., Evtimova, V. V., Fonvielle, J. A., Fuß, T., Gilbert, P., Herrero Ortega, S., Liu, L., Mendoza-Lera, C., … Amouroux, D. (2018). The interplay between total mercury, methylmercury and dissolved organic matter in fluvial systems: A latitudinal study across Europe. *Water Research*, *144*, 172–182. https://doi.org/10.1016/j.watres.2018.06.064

Bravo, A. G., Loizeau, J.-L., Dranguet, P., Makri, S., Björn, E., Ungureanu, V. Gh., Slaveykova, V. I., & Cosio, C. (2016). Persistent Hg contamination and occurrence of Hg-methylating transcript (*hgcA*) downstream of a chlor-alkali plant in the Olt River (Romania). *Environmental Science and Pollution Research*, *23*(11), 10529–10541. https://doi.org/10.1007/s11356-015-5906-4

Breitburg, D., Levin, L. A., Oschlies, A., Grégoire, M., Chavez, F. P., Conley, D. J., Garçon, V., Gilbert, D., Gutiérrez, D., Isensee, K., Jacinto, G. S., Limburg, K. E., Montes, I., Naqvi, S. W. A., Pitcher, G. C., Rabalais, N. N., Roman, M. R., Rose, K. A., Seibel, B. A., … Zhang, J. (2018). Declining oxygen in the global ocean and coastal waters. *Science*, *359*(6371), eaam7240. https://doi.org/10.1126/science.aam7240

Brewer, P. G., & Peltzer, E. T. (2017). Depth perception: The need to report ocean biogeochemical rates as functions of temperature, not depth. *Philosophical Transactions of the Royal Society A: Mathematical, Physical and Engineering Sciences*, *375*(2102), 20160319. https://doi.org/10.1098/rsta.2016.0319

Brown, N. L., Stoyanov, J. V., Kidd, S. P., & Hobman, J. L. (2003). The MerR family of transcriptional regulators. *FEMS Microbiology Reviews*, *27*(2–3), 145–163. https://doi.org/10.1016/S0168-6445(03)00051-2

Bruce, K. D., Hiorns, W. D., Hobman, J. L., Osborn, A. M., Strike, P., & Ritchie, D. A. (1992). Amplification of DNA from native populations of soil bacteria by using the polymerase chain reaction. *Applied and Environmental Microbiology*, *58*(10), 3413–3416. https://doi.org/10.1128/aem.58.10.3413-3416.1992

Bruce, K. D., Osborn, A. M., Pearson, A. J., Strike, P., & Ritchie, D. A. (1995). Genetic diversity within *mer* genes directly amplified from communities of noncultivated soil and sediment bacteria. *Molecular Ecology*, *4*(5), 605–612. https://doi.org/10.1111/j.1365-294X.1995.tb00260.x

Cabral, L., Giovanella, P., Gianello, C., Bento, F. M., Andreazza, R., & Camargo, F. A. O. (2013). Isolation and characterization of bacteria from mercury contaminated sites in Rio Grande do Sul, Brazil, and assessment of methylmercury removal capability of a *Pseudomonas putida* V1 strain. *Biodegradation*, *24*(3), 319–331. https://doi.org/10.1007/s10532-012-9588-z

Camuffo, D. (1993). Analysis of the sea surges at Venice from A.D. 782 to 1990. *Theoretical and Applied Climatology*, *47*(1), 1–14. https://doi.org/10.1007/BF00868891

Canário, J., Branco, V., & Vale, C. (2007). Seasonal variation of monomethylmercury concentrations in surface sediments of the Tagus Estuary (Portugal). *Environmental Pollution*, *148*(1), 380–383. https://doi.org/10.1016/j.envpol.2006.11.023

Capo, E., Cosio, C., Gascón Díez, E., Loizeau, J.-L., Mendes, E., Adatte, T., Franzenburg, S., & Bravo, A. G. (2023). Anaerobic mercury methylators inhabit sinking particles of oxic water columns. *Water Research*, *229*, 119368. https://doi.org/10.1016/j.watres.2022.119368

Capo, E., Feng, C., Bravo, A. G., Bertilsson, S., Soerensen, A. L., Pinhassi, J., Buck, M., Karlsson, C., Hawkes, J., & Björn, E. (2022). Expression levels of *hgcAB* genes and mercury availability jointly explain methylmercury formation in stratified brackish waters. *Environmental Science & Technology*, *56*(18), 13119–13130. https://doi.org/10.1021/acs.est.2c03784

Capo, E., Peterson, B. D., Kim, M., Jones, D. S., Acinas, S. G., Amyot, M., Bertilsson, S., Björn, E., Buck, M., Cosio, C., Elias, D. A., Gilmour, C., Goñi-Urriza, M., Gu, B., Lin, H., Liu, Y., McMahon, K., Moreau, J. W., Pinhassi, J., … Gionfriddo, C. M. (2023). A consensus protocol for the recovery of mercury methylation genes from metagenomes. *Molecular Ecology Resources*, *23*(1), 190–204. https://doi.org/10.1111/1755-0998.13687

Castelle, C. J., Hug, L. A., Wrighton, K. C., Thomas, B. C., Williams, K. H., Wu, D., Tringe, S. G., Singer, S. W., Eisen, J. A., & Banfield, J. F. (2013). Extraordinary phylogenetic diversity and metabolic versatility in aquifer sediment. *Nature Communications*, *4*(1), 2120. https://doi.org/10.1038/ncomms3120

Cazenave, A., & Cozannet, G. L. (2014). Sea level rise and its coastal impacts. *Earth's Future*, *2*(2), 15–34. https://doi.org/10.1002/2013EF000188

Cesário, R., Hintelmann, H., Mendes, R., Eckey, K., Dimock, B., Araújo, B., Mota, A. M., & Canário, J. (2017). Evaluation of mercury methylation and methylmercury demethylation rates in vegetated and non-vegetated saltmarsh sediments from two Portuguese estuaries. *Environmental Pollution*, *226*, 297–307. https://doi.org/10.1016/j.envpol.2017.03.075

Cesário, R., Monteiro, C. E., Nogueira, M., O'Driscoll, N. J., Caetano, M., Hintelmann, H., Mota, A. M., & Canário, J. (2016). Mercury and methylmercury dynamics in sediments on a protected area of Tagus Estuary (Portugal). *Water, Air, & Soil Pollution*, *227*(12), 475. https://doi.org/10.1007/s11270-016-3179-2

Chakraborty, P., Raghunadh Babu, P. V., Vudamala, K., Ramteke, D., & Chennuri, K. (2014). Mercury speciation in coastal sediments from the central east coast of India by modified BCR method. *Marine Pollution Bulletin*, *81*(1), 282–288. https://doi.org/10.1016/j.marpolbul.2013.12.054

Champier, L., Duarte, V., Michaud-Soret, I., & Covès, J. (2004). Characterization of the MerD protein from *Ralstonia metallidurans* CH34: A possible role in bacterial mercury resistance by switching off the induction of the *mer* operon. *Molecular Microbiology*, *52*(5), 1475–1485. https://doi.org/10.1111/j.1365-2958.2004.04071.x

Chang, J.-S., & Law, W.-S. (1998). Development of microbial mercury detoxification processes using mercury-hyperresistant strain of *Pseudomonas aeruginosa* PU21. *Biotechnology and Bioengineering*, *57*(4), 462–470. https://doi.org/10.1002/(SICI)1097-0290(19980220)57:4<462::AID-BIT10>3.0.CO;2-E

Chaumeil, P.-A., Mussig, A. J., Hugenholtz, P., & Parks, D. H. (2020). GTDB-Tk: A toolkit to classify genomes with the Genome Taxonomy Database. *Bioinformatics*, *36*(6), 1925–1927. https://doi.org/10.1093/bioinformatics/btz848

Chen, B.-Y., & Chang, J.-S. (2000). Characterization and theoretical analysis on toxicological threshold of mercuric ions to *Pseudomonas aeruginosa* PU21 (Rip64). *Bioprocess Engineering*, *23*(6), 675–680. https://doi.org/10.1007/s004490000219

Chen, C. Y., Driscoll, C. T., Lambert, K. F., Mason, R. P., Rardin, L. R., Serrell, N., & Sunderland, E. M. (2012). Marine mercury fate: From sources to seafood consumers. *Environmental Research*, *119*, 1–2. https://doi.org/10.1016/j.envres.2012.10.001

Chen, Q., Chen, F., Gonsior, M., Li, Y., Wang, Y., He, C., Cai, R., Xu, J., Wang, Y., Xu, D., Sun, J., Zhang, T., Shi, Q., Jiao, N., & Zheng, Q. (2021). Correspondence between DOM molecules and microbial community in a subtropical coastal estuary on a spatiotemporal scale. *Environment International*, *154*, 106558. https://doi.org/10.1016/j.envint.2021.106558

Chen, S., Zhou, Y., Chen, Y., & Gu, J. (2018). fastp: An ultra-fast all-in-one FASTQ preprocessor. *Bioinformatics*, *34*(17), i884–i890. https://doi.org/10.1093/bioinformatics/bty560

Cheng, L., Abraham, J., Hausfather, Z., & Trenberth, K. E. (2019). How fast are the oceans warming? *Science*, *363*(6423), 128–129. https://doi.org/10.1126/science.aav7619

Chiasson-Gould, S. A., Blais, J. M., & Poulain, A. J. (2014). Dissolved organic matter kinetically controls mercury bioavailability to bacteria. *Environmental Science & Technology*, *48*(6), 3153–3161. https://doi.org/10.1021/es4038484

Choi, B. H., Lapham, L. W., Amin-Zaki, L., & Saleem, T. (1978). Abnormal neuronal migration, deranged cerebral cortical organization, and diffuse white matter astrocytosis of human fetal brain: A major effect of methylmercury poisoning *in utero*. *Journal of Neuropathology & Experimental Neurology*, *37*(6), 719–733.

Christakis, C. A., Barkay, T., & Boyd, E. S. (2021). Expanded diversity and phylogeny of *mer* genes broadens mercury resistance paradigms and reveals an origin for MerA among thermophilic archaea. *Frontiers in Microbiology*, *12*, 682605. https://doi.org/10.3389/fmicb.2021.682605

Christensen, G. A., Wymore, A. M., King, A. J., Podar, M., Hurt, R. A., Santillan, E. U., Soren, A., Brandt, C. C., Brown, S. D., Palumbo, A. V., Wall, J. D., Gilmour, C. C., & Elias, D. A. (2016). Development and validation of broad-range qualitative and clade-specific quantitative molecular probes for assessing mercury methylation in the environment. *Applied and Environmental Microbiology*, *82*(19), 6068–6078. https://doi.org/10.1128/AEM.01271-16

Clark, D. L., Weiss, A. A., & Silver, S. (1977). Mercury and organomercurial resistances determined by plasmids in *Pseudomonas*. *Journal of Bacteriology*, *132*(1), 186–196. https://doi.org/10.1128/jb.132.1.186-196.1977

Clarkson, T. W., & Magos, L. (2006). The toxicology of mercury and its chemical compounds. *Critical Reviews in Toxicology*, *36*(8), 609–662. https://doi.org/10.1080/10408440600845619

Coble, P. G. (1996). Characterization of marine and terrestrial DOM in seawater using excitation-emission matrix spectroscopy. *Marine Chemistry*, *51*(4), 325–346. https://doi.org/10.1016/0304-4203(95)00062-3

Compeau, G., & Bartha, R. (1984). Methylation and demethylation of mercury under controlled redox, pH and salinity conditions. *Applied and Environmental Microbiology*, *48*(6), 1203–1207. https://doi.org/10.1128/aem.48.6.1203-1207.1984

Compeau, G. C., & Bartha, R. (1985). Sulfate-reducing bacteria: Principal methylators of mercury in anoxic estuarine sedimentt. *Applied and Environmental Microbiology*, *50*(2), 498–502.

Cossa, D., Averty, B., & Pirrone, N. (2009). The origin of methylmercury in open Mediterranean waters. *Limnology and Oceanography*, *54*(3), 837–844. https://doi.org/10.4319/lo.2009.54.3.0837

Cossa, D., Heimbürger, L.-E., Lannuzel, D., Rintoul, S. R., Butler, E. C. V., Bowie, A. R., Averty, B., Watson, R. J., & Remenyi, T. (2011). Mercury in the Southern Ocean. *Geochimica et Cosmochimica Acta*, *75*(14), 4037–4052. https://doi.org/10.1016/j.gca.2011.05.001

Dash, H. R., Mangwani, N., & Das, S. (2014). Characterization and potential application in mercury bioremediation of highly mercury-resistant marine bacterium *Bacillus thuringiensis* PW-05. *Environmental Science and Pollution Research*, *21*(4), 2642–2653. https://doi.org/10.1007/s11356-013-2206-8

Dastoor, A., Angot, H., Bieser, J., Christensen, J. H., Douglas, T. A., Heimbürger-Boavida, L.-E., Jiskra, M., Mason, R. P., McLagan, D. S., Obrist, D., Outridge, P. M., Petrova, M. V., Ryjkov, A., St. Pierre, K. A., Schartup, A. T., Soerensen, A. L., Toyota, K., Travnikov, O., Wilson, S. J., & Zdanowicz, C. (2022). Arctic mercury cycling. *Nature Reviews Earth & Environment*, *3*(4), Article 4. https://doi.org/10.1038/s43017-022-00269-w

Dedekorkut-Howes, A., Torabi, E., & Howes, M. (2020). When the tide gets high: A review of adaptive responses to sea level rise and coastal flooding. *Journal of Environmental Planning and Management*, *63*(12), 2102–2143. https://doi.org/10.1080/09640568.2019.1708709

Deng, X., & Wang, P. (2012). Isolation of marine bacteria highly resistant to mercury and their bioaccumulation process. *Bioresource Technology*, *121*, 342–347. https://doi.org/10.1016/j.biortech.2012.07.017

Despins, M. C., Mason, R. P., Aguilar-Islas, A. M., Lamborg, C. H., Hammerschmidt, C. R., & Newell, S. E. (2023). Linked mercury methylation and nitrification across oxic subpolar regions. *Frontiers in Environmental Chemistry*, *4*. https://www.frontiersin.org/articles/10.3389/fenvc.2023.1109537

Diels, L., & Mergeay, M. (1990). DNA probe-mediated detection of resistant bacteria from soils highly polluted by heavy metals. *Applied and Environmental Microbiology*, *56*(5), 1485–1491. https://doi.org/10.1128/aem.56.5.1485-1491.1990

DiMento, B. P., Mason, R. P., Brooks, S., & Moore, C. (2019). The impact of sea ice on the air-sea exchange of mercury in the Arctic Ocean. *Deep Sea Research Part I: Oceanographic Research Papers*, *144*, 28–38. https://doi.org/10.1016/j.dsr.2018.12.001

Dixit, R., Wasiullah, Malaviya, D., Pandiyan, K., Singh, U., Sahu, A., Shukla, R., Singh, B., Rai, J., Sharma, P., Lade, H., & Paul, D. (2015). Bioremediation of heavy metals from soil and aquatic environment: An overview of principles and criteria of fundamental processes. *Sustainability*, *7*(2), 2189–2212. https://doi.org/10.3390/su7022189

Dolbec, J., Mergler, D., Sousa Passos, C.-J., Sousa de Morais, S., & Lebel, J. (2000). Methylmercury exposure affects motor performance of a riverine population of the Tapajós river, Brazilian Amazon. *International Archives of Occupational and Environmental Health*, *73*(3), 195–203. https://doi.org/10.1007/s004200050027

Dominik, J., Tagliapietra, D., Bravo, A. G., Sigovini, M., Spangenberg, J. E., Amouroux, D., & Zonta, R. (2014). Mercury in the food chain of the Lagoon of Venice, Italy. *Marine Pollution Bulletin*, *88*(1–2), 194–206. https://doi.org/10.1016/j.marpolbul.2014.09.005

Drott, A., Lambertsson, L., Björn, E., & Skyllberg, U. (2008). Do potential methylation rates reflect accumulated methyl mercury in contaminated sediments? *Environmental Science & Technology*, *42*(1), 153–158. https://doi.org/10.1021/es0715851

Duarte, C. M. (2015). Seafaring in the 21st century: The Malaspina 2010 circumnavigation expedition. *Limnology and Oceanography Bulletin*, *24*(1), 11–14. https://doi.org/10.1002/lob.10008

Eckley, C. S., & Hintelmann, H. (2006). Determination of mercury methylation potentials in the water column of lakes across Canada. *Science of The Total Environment*, *368*(1), 111–125. https://doi.org/10.1016/j.scitotenv.2005.09.042

Eddy, S. R. (2011). Accelerated profile HMM searches. *PLoS Computational Biology*, *7*(10), e1002195. https://doi.org/10.1371/journal.pcbi.1002195

El-Gebali, S., Mistry, J., Bateman, A., Eddy, S. R., Luciani, A., Potter, S. C., Qureshi, M., Richardson, L. J., Salazar, G. A., Smart, A., Sonnhammer, E. L. L., Hirsh, L., Paladin, L., Piovesan, D., Tosatto, S. C. E., & Finn, R. D. (2019). The Pfam protein families database in 2019. *Nucleic Acids Research*, *47*(D1), D427–D432. https://doi.org/10.1093/nar/gky995

Elhassani, S. B. (1982). The many faces of methylmercury poisoning. *Journal of Toxicology: Clinical Toxicology*, *19*(8), 875–906. https://doi.org/10.3109/15563658208992523

Eriksen, H. H., & Perrez, F. X. (2014). The Minamata convention: A comprehensive response to a global problem. *Review of European, Comparative & International Environmental Law*, *23*(2), 195–210. https://doi.org/10.1111/reel.12079

Espitalié, J., Deroo, G., & Marquis, F. (1985). La pyrolyse Rock-Eval et ses applications – Deuxième partie. *Revue de l'Institut Français Du Pétrole*, *40*(6), 755–784.

Espitalié, J., Deroo, G., & Marquis, F. (1986). La pyrolyse Rock-Eval et ses applications – Troisième partie. *Revue de l'Institut Français Du Pétrole*, *41*(1), 73–89.

Fernández-Bravo, A., & Figueras, M. J. (2020). An update on the genus *Aeromonas*: Taxonomy, epidemiology, and pathogenicity. *Microorganisms*, *8*(1), 129. https://doi.org/10.3390/microorganisms8010129

Ferrarin, C., Ghezzo, M., Umgiesser, G., Tagliapietra, D., Camatti, E., Zaggia, L., & Sarretta, A. (2013). Assessing hydrological effects of human interventions on coastal systems: Numerical applications to the Venice Lagoon. *Hydrology and Earth System Sciences*, *17*(5), 1733–1748. https://doi.org/10.5194/hess-17-1733-2013

Fiedler, N., Udasin, I., Gochfeld, M., Buckler, G., Kelly-McNeil, K., & Kipen, H. (1999). Neuropsychological and stress evaluation of a residential mercury exposure. *Environmental Health Perspectives*, *107*(5).

Fitzgerald, W. F., Lamborg, C. H., & Hammerschmidt, C. R. (2007). Marine biogeochemical cycling of mercury. *Chemical Reviews*, *107*(2), 641–662. Scopus. https://doi.org/10.1021/cr050353m

Fleming, E. J., Mack, E. E., Green, P. G., & Nelson, D. C. (2006). Mercury methylation from unexpected sources: Molybdate-inhibited freshwater sediments and an iron-reducing bacterium. *Applied and Environmental Microbiology*, *72*(1), 457–464. https://doi.org/10.1128/AEM.72.1.457-464.2006

Fortunato, R., Crespo, J. G., & Reis, M. a. M. (2005). Biodegradation of thiomersal containing effluents by a mercury resistant Pseudomonas putida strain. *Water Research*, *39*(15), 3511–3522. https://doi.org/10.1016/j.watres.2005.06.012

Foster, T. J. (1987). The genetics and biochemistry of mercury resistance. *Critical Reviews in Microbiology*, *15*(2), 117–140. https://doi.org/10.3109/10408418709104455

François, F., Lombard, C., Guigner, J.-M., Soreau, P., Brian-Jaisson, F., Martino, G., Vandervennet, M., Garcia, D., Molinier, A.-L., Pignol, D., Peduzzi, J., Zirah, S., & Rebuffat, S. (2012). Isolation and characterization of environmental bacteria capable of extracellular biosorption of mercury. *Applied and Environmental Microbiology*, *78*(4), 1097–1106. https://doi.org/10.1128/AEM.06522-11

French, T. D., Houben, A. J., Desforges, J.-P. W., Kimpe, L. E., Kokelj, S. V., Poulain, A. J., Smol, J. P., Wang, X., & Blais, J. M. (2014). Dissolved organic carbon thresholds affect mercury bioaccumulation in Arctic lakes. *Environmental Science & Technology*, *48*(6), 3162–3168. https://doi.org/10.1021/es403849d

Furukawa, K., & Tonomura, K. (1971). Enzyme system involved in the decomposition of phenyl mercuric acetate by mercury-resistant *Pseudomonas*. *Agricultural and Biological Chemistry*, *35*(4), 604–610. https://doi.org/10.1080/00021369.1971.10859956

Furukawa, K., & Tonomura, K. (1972). Metallic mercury-releasing enzyme in mercury-resistant *Pseudomonas*. *Agricultural and Biological Chemistry*, *36*(2), 217–226. https://doi.org/10.1080/00021369.1972.10860232

Gan, S., Schmidt, F., Heuer, V. B., Goldhammer, T., Witt, M., & Hinrichs, K.-U. (2020). Impacts of redox conditions on dissolved organic matter (DOM) quality in marine sediments off the River Rhône, Western Mediterranean Sea. *Geochimica et Cosmochimica Acta*, *276*, 151–169. https://doi.org/10.1016/j.gca.2020.02.001

Garcia-Soto, C., Cheng, L., Caesar, L., Schmidtko, S., Jewett, E. B., Cheripka, A., Rigor, I., Caballero, A., Chiba, S., Báez, J. C., Zielinski, T., & Abraham, J. P. (2021). An overview of ocean climate change indicators: Sea surface temperature, ocean heat content, ocean pH, dissolved oxygen concentration, Arctic Sea ice extent, thickness and volume, sea level and strength of the

AMOC (Atlantic Meridional Overturning Circulation). *Frontiers in Marine Science*, *8*. https://doi.org/10.3389/fmars.2021.642372

Gascón Díez, E., Loizeau, J.-L., Cosio, C., Bouchet, S., Adatte, T., Amouroux, D., & Bravo, A. G. (2016). Role of settling particles on mercury methylation in the oxic water column of freshwater systems. *Environmental Science & Technology*, *50*(21), 11672–11679. https://doi.org/10.1021/acs.est.6b03260

Gasong, B. T., Abrian, S., & Sigit Setyabudi, F. M. C. (2017). Methylmercury biosorption activity by methylmercury-resistant lactic acid bacteria isolated from West Sekotong, Indonesia. *HAYATI Journal of Biosciences*, *24*(4), 182–186. https://doi.org/10.1016/j.hjb.2017.10.001

Giani, M., Rampazzo, F., Berto, D., Maggi, C., Mao, A., Horvat, M., Emili, A., & Covelli, S. (2012). Bioaccumulation of mercury in reared and wild *Ruditapes philippinarum* of a Mediterranean lagoon. *Estuarine, Coastal and Shelf Science*, *113*, 116–125. https://doi.org/10.1016/j.ecss.2012.05.031

Gilmour, C. C., Bullock, A. L., McBurney, A., Podar, M., & Elias, D. A. (2018). Robust mercury methylation across diverse methanogenic archaea. *mBio*, *9*(2), e02403-17. https://doi.org/10.1128/mBio.02403-17

Gilmour, C. C., Henry, E. A., & Mitchell, R. (1992). Sulfate stimulation of mercury methylation in freshwater sediments. *Environmental Science & Technology*, *26*(11), 2281–2287. https://doi.org/10.1021/es00035a029

Gilmour, C. C., Podar, M., Bullock, A. L., Graham, A. M., Brown, S. D., Somenahally, A. C., Johs, A., Hurt, R. A., Bailey, K. L., & Elias, D. A. (2013). Mercury methylation by novel microorganisms from new environments. *Environmental Science & Technology*, *47*(20), 11810–11820. https://doi.org/10.1021/es403075t

Gionfriddo, C. M., Capo, E., Peterson, B. D., Lin, H., Jonas, D., Bravo, A. G., Bertilsson, S., Moreau, J. W., McMahon, K., Elias, D., & Gilmour, C. (2021). *Hg-MATE-Db: Hg-cycling microorganisms in aquatic and terrestrial ecosystems database*. https://doi.org/doi:10.25573/serc.13105370

Gionfriddo, C. M., Soren, A. B., Wymore, A. M., Hartnett, D. S., Podar, M., Parks, J. M., Elias, D. A., & Gilmour, C. C. (2023). Transcriptional control of *hgcAB* by an ArsR-like regulator in *Pseudodesulfovibrio mercurii* ND132. *Applied and Environmental Microbiology*, *89*(4), e01768-22. https://doi.org/10.1128/aem.01768-22

Gionfriddo, C. M., Tate, M. T., Wick, R. R., Schultz, M. B., Zemla, A., Thelen, M. P., Schofield, R., Krabbenhoft, D. P., Holt, K. E., & Moreau, J. W. (2016). Microbial mercury methylation in Antarctic sea ice. *Nature Microbiology*, *1*(10), 16127. https://doi.org/10.1038/nmicrobiol.2016.127

Gionfriddo, C. M., Wymore, A. M., Jones, D. S., Wilpiszeski, R. L., Lynes, M. M., Christensen, G. A., Soren, A., Gilmour, C. C., Podar, M., & Elias, D. A. (2020). An improved *hgcAB* primer set and direct high-throughput sequencing expand Hg-methylator diversity in nature. *Frontiers in Microbiology*, *11*, 541554. https://doi.org/10.3389/fmicb.2020.541554

Giovanella, P., Cabral, L., Bento, F. M., Gianello, C., & Camargo, F. A. O. (2016). Mercury (II) removal by resistant bacterial isolates and mercuric (II) reductase activity in a new strain of *Pseudomonas* sp. B50A. *New Biotechnology*, *33*(1), 216–223. https://doi.org/10.1016/j.nbt.2015.05.006

Giovanella, P., Cabral, L., Costa, A. P., De Oliveira Camargo, F. A., Gianello, C., & Bento, F. M. (2017). Metal resistance mechanisms in Gram-negative bacteria and their potential to remove Hg in the presence of other metals. *Ecotoxicology and Environmental Safety*, *140*, 162–169. https://doi.org/10.1016/j.ecoenv.2017.02.010

Gochfeld, M. (2003). Cases of mercury exposure, bioavailability, and absorption. *Ecotoxicology and Environmental Safety*, *56*(1), 174–179. https://doi.org/10.1016/S0147-6513(03)00060-5

González-Reguero, D., Robas-Mora, M., Probanza Lobo, A., & Jiménez Gómez, P. A. (2023). Bioremediation of environments contaminated with mercury. Present and perspectives. *World Journal of Microbiology and Biotechnology*, *39*(9), 249. https://doi.org/10.1007/s11274-023-03686-1

Goris, J., De Vos, P., Coenye, T., Hoste, B., Janssens, D., Brim, H., Diels, L., Mergeay, M., Kersters, K., & Vandamme, P. (2001). Classification of metal-resistant bacteria from industrial biotopes as *Ralstonia campinensis* sp. Nov., *Ralstonia metallidurans* sp. Nov. And *Ralstonia basilensis* Steinle et al. 1998 emend. *International Journal of Systematic and Evolutionary Microbiology*, *51*(5), 1773–1782. https://doi.org/10.1099/00207713-51-5-1773

Graham, A. M., Aiken, G. R., & Gilmour, C. C. (2013). Effect of dissolved organic matter source and character on microbial Hg methylation in Hg–S–DOM solutions. *Environmental Science & Technology*, *47*(11), 5746–5754. https://doi.org/10.1021/es400414a

Graham, E. D., Heidelberg, J. F., & Tully, B. J. (2018). Potential for primary productivity in a globally-distributed bacterial phototroph. *The ISME Journal*, *12*(7), Article 7. https://doi.org/10.1038/s41396-018-0091-3

Green, S. M. (1962). Mercury sensitivity of *staphylococci*. *Journal of Clinical Pathology*, *15*(3), 249–251. https://doi.org/10.1136/jcp.15.3.249

Grégoire, D. S., & Poulain, A. J. (2018). Shining light on recent advances in microbial mercury cycling. *FACETS*, *3*(1), 858–879. https://doi.org/10.1139/facets-2018-0015

Guédron, S., Duwig, C., Prado, B. L., Point, D., Flores, M. G., & Siebe, C. (2014). (Methyl)mercury, arsenic, and lead contamination of the world's largest wastewater irrigation system: The Mezquital Valley (Hidalgo State—Mexico). *Water, Air, & Soil Pollution*, *225*(8), 2045. https://doi.org/10.1007/s11270-014-2045-3

Guédron, S., Huguet, L., Vignati, D. A. L., Liu, B., Gimbert, F., Ferrari, B. J. D., Zonta, R., & Dominik, J. (2012). Tidal cycling of mercury and methylmercury between sediments and water column in the Venice Lagoon (Italy). *Marine Chemistry*, *130–131*, 1–11. https://doi.org/10.1016/j.marchem.2011.12.003

Guimarães, J. R. D., Mauro, J. B. N., Meili, M., Sundbom, M., Haglund, A. L., Coelho-Souza, S. A., & Hylander, L. D. (2006). Simultaneous radioassays of bacterial production and mercury methylation in the periphyton of a tropical and a temperate wetland. *Journal of Environmental Management*, *81*(2), 95–100. https://doi.org/10.1016/j.jenvman.2005.09.023

Gutensohn, M., Schaefer, J. K., Yunda, E., Skyllberg, U., & Björn, E. (2023). The combined effect of Hg(II) speciation, thiol metabolism, and cell physiology on methylmercury formation by *Geobacter sulfurreducens*. *Environmental Science & Technology*, *57*(18), 7185–7195. https://doi.org/10.1021/acs.est.3c00226

Gworek, B., Bemowska-Kałabun, O., Kijeńska, M., & Wrzosek-Jakubowska, J. (2016). Mercury in marine and oceanic waters—A review. *Water, Air, & Soil Pollution*, *227*(10), 371. https://doi.org/10.1007/s11270-016-3060-3

Hamelin, S., Amyot, M., Barkay, T., Wang, Y., & Planas, D. (2011). Methanogens: Principal methylators of mercury in lake periphyton. *Environmental Science & Technology*, *45*(18), 7693–7700. https://doi.org/10.1021/es2010072

Hamlett, N. V., Landele, E. C., David, B. H., & Summer, A. O. (1992). Roles of the Tn*21 merT, merP*, and *merC* gene products in mercury resistance and mercury binding. *Journal of Bacteriology*, *174*(20), 6377–6385.

Han, S., Obraztsova, A., Pretto, P., Choe, K.-Y., Gieskes, J., Deheyn, D. D., & Tebo, B. M. (2007). Biogeochemical factors affecting mercury methylation in sediments of the Venice Lagoon, Italy. *Environmental Toxicology and Chemistry*, *26*(4), 655. https://doi.org/10.1897/06-392R.1

Harada, M. (1978). Minamata disease as a social and medical problem. *Japan Quarterly*, *25*(1).

Harada, M. (1995). Minamata disease: Methylmercury poisoning in Japan caused by environmental pollution. *Critical Reviews in Toxicology*, *25*(1), 1–24. https://doi.org/10.3109/10408449509089885

He, C., Keren, R., Whittaker, M. L., Farag, I. F., Doudna, J. A., Cate, J. H. D., & Banfield, J. F. (2021). Genome-resolved metagenomics reveals site-specific diversity of episymbiotic CPR bacteria and DPANN archaea in groundwater ecosystems. *Nature Microbiology*, *6*(3), 354–365. https://doi.org/10.1038/s41564-020-00840-5

Helms, J. R., Stubbins, A., Ritchie, J. D., Minor, E. C., Kieber, D. J., & Mopper, K. (2008). Absorption spectral slopes and slope ratios as indicators of molecular weight, source, and photobleaching of chromophoric dissolved organic matter. *Limnology and Oceanography*, *53*(3), 955–969. https://doi.org/10.4319/lo.2008.53.3.0955

Herrero Ortega, S., Catalán, N., Björn, E., Gröntoft, H., Hilmarsson, T. G., Bertilsson, S., Wu, P., Bishop, K., Levanoni, O., & Bravo, A. G. (2018). High methylmercury formation in ponds fueled by fresh humic and algal derived organic matter: High methylmercury formation in ponds. *Limnology and Oceanography*, *63*(S1), S44–S53. https://doi.org/10.1002/lno.10722

Hintelmann, H., & Evans, R. D. (1997). Application of stable isotopes in environmental tracer studies—Measurement of monomethylmercury (CH_3Hg^+) by isotope dilution ICP-MS and detection of species transformation. *Fresenius' Journal of Analytical Chemistry*, *358*(3), 378–385. https://doi.org/10.1007/s002160050433

Horn, J. M., Brunke, M., Deckwer, W. D., & Timmis, K. N. (1994). *Pseudomonas putida* strains which constitutively overexpress mercury resistance for biodetoxification of organomercurial pollutants. *Applied and Environmental Microbiology*, *60*(1), 357–362. https://doi.org/10.1128/aem.60.1.357-362.1994

Horowitz, H. M., Jacob, D. J., Amos, H. M., Streets, D. G., & Sunderland, E. M. (2014). Historical mercury releases from commercial products: Global environmental implications. *Environmental Science & Technology*, *48*(17), 10242–10250. https://doi.org/10.1021/es501337j

Horowitz, H. M., Jacob, D. J., Zhang, Y., Dibble, T. S., Slemr, F., Amos, H. M., Schmidt, J. A., Corbitt, E. S., Marais, E. A., & Sunderland, E. M. (2017). A new mechanism for atmospheric mercury

redox chemistry: Implications for the global mercury budget. *Atmospheric Chemistry and Physics*, *17*(10), 6353–6371. https://doi.org/10.5194/acp-17-6353-2017

Howarth, R. W. (1984). The ecological significance of sulfur in the energy dynamics of salt marsh and coastal marine sediments. *Biogeochemistry*, *1*(1), 5–27. https://doi.org/10.1007/BF02181118

Huang, C.-C., Narita, M., Yamagata, T., & Endo, G. (1999). Identification of three *merB* genes and characterization of a broad-spectrum mercury resistance module encoded by a class II transposon of *Bacillus megaterium* strain MB1. *Gene*, *239*(2), 361–366. https://doi.org/10.1016/S0378-1119(99)00388-1

Huang, H. (2024). *Mercury methylation and methylmercury demethylation in boreal soils and sediment – anthropogenic impacts*.

Huguet, A., Vacher, L., Relexans, S., Saubusse, S., Froidefond, J. M., & Parlanti, E. (2009). Properties of fluorescent dissolved organic matter in the Gironde Estuary. *Organic Geochemistry*, *40*(6), 706–719. https://doi.org/10.1016/j.orggeochem.2009.03.002

Hutchins, D. A., & Fu, F. (2017). Microorganisms and ocean global change. *Nature Microbiology*, *2*(6), 17058. https://doi.org/10.1038/nmicrobiol.2017.58

Iohara, K., Iiyama, R., Nakamura, K., Silver, S., Sakai, M., Takeshita, M., & Furukawa, K. (2001). The *mer* operon of a mercury-resistant *Pseudoalteromonas haloplanktis* strain isolated from Minamata Bay, Japan. *Applied Microbiology and Biotechnology*, *56*(5–6), 736–741. https://doi.org/10.1007/s002530100734

IPCC. (2021). *Climate change 2021 – The physical science basis. Contribution working group I to the sixth assessment report of the intergovernmental panel on climate change*. Cambridge University Press. https://doi.org/10.1017/9781009157896

Ivars-Martinez, E., Martin-Cuadrado, A.-B., D'Auria, G., Mira, A., Ferriera, S., Johnson, J., Friedman, R., & Rodriguez-Valera, F. (2008). Comparative genomics of two ecotypes of the marine planktonic copiotroph *Alteromonas macleodii* suggests alternative lifestyles associated with different kinds of particulate organic matter. *The ISME Journal*, *2*(12), 1194–1212. https://doi.org/10.1038/ismej.2008.74

Izaki, K., Tashiro, Y., & Funaba, T. (1974). Mechanism of mercuric chloride resistance in microorganisms: III. Purification and properties of a mercuric ion reducing enzyme from *Escherichia coli* bearing R factor. *The Journal of Biochemistry*, *75*(3), 591–599. https://doi.org/DOI: 10.1093/oxfordjournals.jbchem.a130427

Jeffrey, W. H., Nazaret, S., & Barkay, T. (1996). Detection of the *merA* gene and its expression in the environment. *Microbial Ecology*, *32*(3). https://doi.org/10.1007/BF00183064

Jeffrey, W. H., Nazaret, S., & Von Haven, R. (1994). Improved method for recovery of mRNA from aquatic samples and its application to detection of *mer* expression. *Applied and Environmental Microbiology*, *60*(6), 1814–1821. https://doi.org/10.1128/aem.60.6.1814-1821.1994

Jensen, S., & Jernelöv, A. (1969). Biological methylation of mercury in aquatic organisms. *Nature*, *223*, 753–754.

Jiang, T., Bravo, A. G., Skyllberg, U., Björn, E., Wang, D., Yan, H., & Green, N. W. (2018). Influence of dissolved organic matter (DOM) characteristics on dissolved mercury (Hg) species

composition in sediment porewater of lakes from southwest China. *Water Research*, *146*, 146–158. https://doi.org/10.1016/j.watres.2018.08.054

Jiskra, M., Heimbürger-Boavida, L.-E., Desgranges, M.-M., Petrova, M. V., Dufour, A., Ferreira-Araujo, B., Masbou, J., Chmeleff, J., Thyssen, M., Point, D., & Sonke, J. E. (2021). Mercury stable isotopes constrain atmospheric sources to the ocean. *Nature*, *597*(7878), 678–682. https://doi.org/10.1038/s41586-021-03859-8

Joshi, G., Meena, B., Verma, P., Nayak, J., Vinithkumar, N. V., & Dharani, G. (2021). Deep-sea mercury resistant bacteria from the Central Indian Ocean: A potential candidate for mercury bioremediation. *Marine Pollution Bulletin*, *169*, 112549. https://doi.org/10.1016/j.marpolbul.2021.112549

Kalpana, R., Angelaalincy, M. J., Kamatchirajan, B. V., Vasantha, V. S., Ashokkumar, B., Ganesh, V., & Varalakshmi, P. (2018). Exopolysaccharide from *Bacillus cereus* VK1: Enhancement, characterization and its potential application in heavy metal removal. *Colloids and Surfaces B: Biointerfaces*, *171*, 327–334. https://doi.org/10.1016/j.colsurfb.2018.07.043

Kanehisa, M., & Goto, S. (2000). *KEGG: Kyoto Encyclopedia of Genes and Genomes*.

Kang, D. D., Li, F., Kirton, E., Thomas, A., Egan, R., An, H., & Wang, Z. (2019). MetaBAT 2: An adaptive binning algorithm for robust and efficient genome reconstruction from metagenome assemblies. *PeerJ*, *7*, e7359. https://doi.org/10.7717/peerj.7359

Kaur, A., Nirwan, J., Tiwana, A. S., Singh, A., Singh, R. P., Verma, A., & Gupta, S. (2022). Sequestration of mercury and cadmium by a heavy metals' tolerant *Bacillus cereus* strain JS-3: A microbial preparedness for terrestrial and anthropogenic hazards. *Bioremediation Journal*, *26*(3), 198–207. https://doi.org/10.1080/10889868.2021.1965083

Keeling, R. F., Körtzinger, A., & Gruber, N. (2010). Ocean deoxygenation in a warming world. *Annual Review of Marine Science*, *2*(1), 199–229. https://doi.org/10.1146/annurev.marine.010908.163855

Kim, M.-K., & Zoh, K.-D. (2012). Fate and Transport of Mercury in Environmental Media and Human Exposure. *Journal of Preventive Medicine & Public Health*, *45*(6), 335–343. https://doi.org/10.3961/jpmph.2012.45.6.335

King, J. K., Kostka, J. E., Frischer, M. E., Saunders, F. M., & Jahnke, R. A. (2001). A quantitative relationship that demonstrates mercury methylation rates in marine sediments are sased on the community composition and activity of sulfate-reducing bacteria. *Environmental Science & Technology*, *35*(12), 2491–2496. https://doi.org/10.1021/es001813q

Kirchman, D., Sigda, J., Kapuscinski, R., & Mitchell, R. (1982). Statistical analysis of the direct count method for enumerating bacteria. *Applied and Environmental Microbiology*, *44*(2), 376–382. https://doi.org/10.1128/aem.44.2.376-382.1982

Kiyono, M., Omura, T., Inuzuka, M., Fujimori, H., & Pan-Hou, H. (1997). Nucleotide sequence and expression of the organomercurial-resistance determinants from a Pseudomonas K-62 plasmid pMR26. *Gene*, *189*(2), 151–157. https://doi.org/10.1016/s0378-1119(96)00741-x

Kleindienst, A., Živković, I., Tessier, E., Koenig, A., Heimbürger-Boavida, L.-E., Horvat, M., & Amouroux, D. (2023). Assessing comparability and uncertainty of analytical methods for methylated mercury species in seawater. *Analytica Chimica Acta*, *1278*, 341735. https://doi.org/10.1016/j.aca.2023.341735

Kocman, D., Wilson, S., Amos, H., Telmer, K., Steenhuisen, F., Sunderland, E., Mason, R., Outridge, P., & Horvat, M. (2017). Toward an assessment of the global inventory of present-day mercury releases to freshwater environments. *International Journal of Environmental Research and Public Health*, *14*(2), 138. https://doi.org/10.3390/ijerph14020138

Komura, I., Funaba, T., & Izaki, K. (1971). Mechanism of mercuric chloride resistance in microorganisms: II. NADPH-dependent reduction of mercuric chloride and vaporization of mercury from mercuric chloride by a multiple drug resistant strain of *Escherichia coli*. *The Journal of Biochemistry*, *70*(6), 895–901. https://doi.org/DOI: 10.1093/oxfordjournals.jbchem.a129719

Komura, I., & Izaki, K. (1971). Mechanism of mercuric chloride resistance in microorganisms: I. vaporization of a mercury compound from mercuric chloride by multiple drug resistant strains of *Escherichia coli*. *The Journal of Biochemistry*, *70*(6), 885–893. https://doi.org/DOI: 10.1093/oxfordjournals.jbchem.a129718

Kothawala, D. N., Murphy, K. R., Stedmon, C. A., Weyhenmeyer, G. A., & Tranvik, L. J. (2013). Inner filter correction of dissolved organic matter fluorescence: Correction of inner filter effects. *Limnology and Oceanography: Methods*, *11*(12), 616–630. https://doi.org/10.4319/lom.2013.11.616

Kotnik, J., Horvat, M., Tessier, E., Ogrinc, N., Monperrus, M., Amouroux, D., Fajon, V., Gibičar, D., Žižek, S., Sprovieri, F., & Pirrone, N. (2007). Mercury speciation in surface and deep waters of the Mediterranean Sea. *Marine Chemistry*, *107*(1), 13–30. https://doi.org/10.1016/j.marchem.2007.02.012

Krabbenhoft, D. P., & Sunderland, E. M. (2013). Global change and mercury. *Science*, *341*(6153), 1457–1458. https://doi.org/10.1126/science.1242838

Krout, I. N., Scrimale, T., Vorojeikina, D., Boyd, E. S., & Rand, M. D. (2022). Organomercurial lyase (MerB)-mediated demethylation decreases bacterial methylmercury resistance in the absence of mercuric reductase (MerA). *Applied and Environmental Microbiology*, *88*(6), e00010-22. https://doi.org/10.1128/aem.00010-22

Kuenen, J. G. (2019). Continuous Cultures (Chemostats). In T. M. Schmidt (Ed.), *Encyclopedia of Microbiology (Fourth Edition)* (pp. 743–761). Academic Press. https://doi.org/10.1016/B978-0-12-801238-3.02490-9

Kumar, A., Wu, S., Huang, Y., Liao, H., & Kaplan, J. O. (2018). Mercury from wildfires: Global emission inventories and sensitivity to 2000–2050 global change. *Atmospheric Environment*, *173*, 6–15. https://doi.org/10.1016/j.atmosenv.2017.10.061

Kumar, S., Stecher, G., Li, M., Knyaz, C., & Tamura, K. (2018). MEGA X: molecular evolutionary genetics analysis across computing platforms. *Mol Biol Evol*, *35*(6), 1547–1549. https://doi.org/10.1093/molbev/msy096

Langmead, B., & Salzberg, S. L. (2012). Fast gapped-read alignment with Bowtie 2. *Nature Methods*, *9*(4), 357–359. https://doi.org/10.1038/nmeth.1923

LaVoie, S. P., & Summers, A. O. (2018). Transcriptional responses of *Escherichia coli* during recovery from inorganic or organic mercury exposure. *BMC Genomics*, *19*(1), 52. https://doi.org/10.1186/s12864-017-4413-z

Lawaetz, A. J., & Stedmon, C. A. (2009). Fluorescence intensity calibration using the Raman scatter peak of water. *Applied Spectroscopy*, *63*(8), 936–940. https://doi.org/10.1366/000370209788964548

Lee, I. W., Livrelli, V., Park, S. J., Totis, P. A., & Summers, A. O. (1993). In vivo DNA-protein interactions at the divergent mercury resistance (*mer*) promoters. II. Repressor/activator (MerR)-RNA polymerase interaction with *merOP* mutants. *Journal of Biological Chemistry*, *268*(4), 2632–2639. https://doi.org/10.1016/S0021-9258(18)53821-7

Lee, S., & Kim, P. (2020). *Current Status and Applications of Adaptive Laboratory Evolution in Industrial Microorganisms*. *30*(6), 793–803. https://doi.org/10.4014/jmb.2003.03072

Leermakers, M., Baeyens, W., Quevauviller, P., & Horvat, M. (2005). Mercury in environmental samples: Speciation, artifacts and validation. *TrAC Trends in Analytical Chemistry*, *24*(5), 383–393. https://doi.org/10.1016/j.trac.2004.01.001

Lehnherr, I., St. Louis, V. L., Hintelmann, H., & Kirk, J. L. (2011). Methylation of inorganic mercury in polar marine waters. *Nature Geoscience*, *4*(5), Article 5. https://doi.org/10.1038/ngeo1134

LeMonte, J. J., Stuckey, J. W., Sanchez, J. Z., Tappero, R. V., Rinklebe, J., & Sparks, D. L. (2017). Sea level rise induced arsenic release from historically contaminated coastal soils. *Environmental Science & Technology*, *51*(11), 5913–5922.

Leonhäuser, J., Röhricht, M., Wagner-Döbler, I., & Deckwer, W.-D. (2006). Reaction engineering aspects of microbial mercury removal. *Engineering in Life Sciences*, *6*(2), 139–148. https://doi.org/10.1002/elsc.200620904

Leoni, S., Dominik, J., Cassin, D., Manfè, G., Tagliapietra, D., Acri, F., & Zonta, R. (2022). Sediment oxygen demand rate in a flow regulated lagoon (Venice, Italy). *Frontiers in Environmental Science*, *10*, 1000665. https://doi.org/10.3389/fenvs.2022.1000665

Li, D., Luo, R., Liu, C.-M., Leung, C.-M., Ting, H.-F., Sadakane, K., Yamashita, H., & Lam, T.-W. (2016). MEGAHIT v1.0: A fast and scalable metagenome assembler driven by advanced methodologies and community practices. *Methods*, *102*, 3–11. https://doi.org/10.1016/j.ymeth.2016.02.020

Li, P., & Hur, J. (2017). Utilization of UV-Vis spectroscopy and related data analyses for dissolved organic matter (DOM) studies: A review. *Critical Reviews in Environmental Science and Technology*, *47*(3), 131–154. https://doi.org/10.1080/10643389.2017.1309186

Lim, A. G., Jiskra, M., Sonke, J. E., Loiko, S. V., Kosykh, N., & Pokrovsky, O. S. (2020). A revised pan-Arctic permafrost soil Hg pool based on Western Siberian peat Hg and carbon observations. *Biogeosciences*, *17*(12), 3083–3097. https://doi.org/10.5194/bg-17-3083-2020

Lin, C.-C., Yee, N., & Barkay, T. (2011). Microbial transformations in the mercury cycle. In G. Liu, Y. Cai, & N. O'Driscoll (Eds.), *Environmental Chemistry and Toxicology of Mercury*. https://doi.org/10.1002/9781118146644.ch5

Lin, H., Ascher, D. B., Myung, Y., Lamborg, C. H., Hallam, S. J., Gionfriddo, C. M., Holt, K. E., & Moreau, J. W. (2021). Mercury methylation by metabolically versatile and cosmopolitan marine bacteria. *The ISME Journal*, *15*(6), Article 6. https://doi.org/10.1038/s41396-020-00889-4

Lin, H., Moody, E. R. R., Williams, T. A., & Moreau, J. W. (2023). On the origin and evolution of microbial mercury methylation. *Genome Biology and Evolution*, *15*(4). https://doi.org/10.1093/gbe/evad051

Lionello, P. (2012). The climate of the Venetian and North Adriatic region: Variability, trends and future change. *Physics and Chemistry of the Earth, Parts A/B/C*, *40–41*, 1–8. https://doi.org/10.1016/j.pce.2012.02.002

Lionello, P., Nicholls, R. J., Umgiesser, G., & Zanchettin, D. (2021). Venice flooding and sea level: Past evolution, present issues, and future projections (introduction to the special issue). *Natural Hazards and Earth System Sciences*, *21*(8), 2633–2641. https://doi.org/10.5194/nhess-21-2633-2021

Lipsewers, Y. A., Vasquez-Cardenas, D., Seitaj, D., Schauer, R., Hidalgo-Martinez, S., Sinninghe Damsté, J. S., Meysman, F. J. R., Villanueva, L., & Boschker, H. T. S. (2017). Impact of seasonal hypoxia on activity and community structure of chemolithoautotrophic bacteria in a coastal sediment. *Applied and Environmental Microbiology*, *83*(10), e03517-16. https://doi.org/10.1128/AEM.03517-16

Liu, M., Zhang, Q., Maavara, T., Liu, S., Wang, X., & Raymond, P. A. (2021). Rivers as the largest source of mercury to coastal oceans worldwide. *Nature Geoscience*, *14*(9), 672–677. https://doi.org/10.1038/s41561-021-00793-2

Loizeau, J.-L., Arbouille, D., Santiago, S., & Vernet, J.-P. (1994). Evaluation of a wide range laser diffraction grain size analyser for use with sediments. *Sedimentology*, *41*(2), 353–361. https://doi.org/10.1111/j.1365-3091.1994.tb01410.x

Lønborg, C., Álvarez-Salgado, X. A., Davidson, K., Martínez-García, S., & Teira, E. (2010). Assessing the microbial bioavailability and degradation rate constants of dissolved organic matter by fluorescence spectroscopy in the coastal upwelling system of the Ría de Vigo. *Marine Chemistry*, *119*(1), 121–129. https://doi.org/10.1016/j.marchem.2010.02.001

Lund, P. A., & Brown, N. L. (1987). Role of the *merT* and *merP* gene products of transposon Tn*501* in the induction and expression of resistance to mercuric ions. *Gene*, *52*(2–3), 207–214. https://doi.org/10.1016/0378-1119(87)90047-3

Ma, B., Lu, C., Wang, Y., Yu, J., Zhao, K., Xue, R., Ren, H., Lv, X., Pan, R., Zhang, J., Zhu, Y., & Xu, J. (2023). A genomic catalogue of soil microbiomes boosts mining of biodiversity and genetic resources. *Nature Communications*, *14*(1), 7318. https://doi.org/10.1038/s41467-023-43000-z

Ma, M., Gong, Y., & Hu, Q. (2018). Identification and feeding characteristics of the mixotrophic flagellate Poterioochromonas malhamensis, a microalgal predator isolated from outdoor massive Chlorella culture. *Algal Research*, *29*, 142–153. https://doi.org/10.1016/j.algal.2017.11.024

Magos, L., Tuffery, A. A., & Clarkson, T. W. (1964). Volatilization of mercury by bacteria. *Occupational and Environmental Medicine*, *21*(4), 294–298. https://doi.org/10.1136/oem.21.4.294

Mahbub, K. R., Bahar, M. M., Labbate, M., Krishnan, K., Andrews, S., Naidu, R., & Megharaj, M. (2017). Bioremediation of mercury: Not properly exploited in contaminated soils! *Applied Microbiology and Biotechnology*, *101*(3), 963–976. https://doi.org/10.1007/s00253-016-8079-2

Maia, R., Eliason, C. M., Bitton, P.-P., Doucet, S. M., & Shawkey, M. D. (2013). pavo: An R package for the analysis, visualization and organization of spectral data. *Methods in Ecology and Evolution*, *4*, 906–913. https://doi.org/10.1111/2041-210X.12069

Majidzadeh, H., Uzun, H., Ruecker, A., Miller, D., Vernon, J., Zhang, H., Bao, S., Tsui, M. T. K., Karanfil, T., & Chow, A. T. (2017). Extreme flooding mobilized dissolved organic matter from coastal forested wetlands. *Biogeochemistry*, *136*(3), 293–309. https://doi.org/10.1007/s10533-017-0394-x

Malcolm, E. G., Schaefer, J. K., Ekstrom, E. B., Tuit, C. B., Jayakumar, A., Park, H., Ward, B. B., & Morel, F. M. M. (2010). Mercury methylation in oxygen deficient zones of the oceans: No evidence for the predominance of anaerobes. *Marine Chemistry*, *122*(1–4), 11–19. https://doi.org/10.1016/j.marchem.2010.08.004

Manirethan, V., Gupta, N., Balakrishnan, R. M., & Raval, K. (2020). Batch and continuous studies on the removal of heavy metals from aqueous solution using biosynthesised melanin-coated PVDF membranes. *Environmental Science and Pollution Research*, *27*(20), 24723–24737. https://doi.org/10.1007/s11356-019-06310-8

Mariano, C., Mello, I. S., Barros, B. M., Da Silva, G. F., Terezo, A. J., & Soares, M. A. (2020). Mercury alters the rhizobacterial community in Brazilian wetlands and it can be bioremediated by the plant-bacteria association. *Environmental Science and Pollution Research*, *27*(12), 13550–13564. https://doi.org/10.1007/s11356-020-07913-2

Marvin-DiPasquale, M., & Agee, J. L. (2003). Microbial mercury cycling in sediments of the San Francisco Bay-Delta. *Estuaries*, *26*(6), 1517–1528. https://doi.org/10.1007/BF02803660

Mason, R. P., Choi, A. L., Fitzgerald, W. F., Hammerschmidt, C. R., Lamborg, C. H., Soerensen, A. L., & Sunderland, E. M. (2012). Mercury biogeochemical cycling in the ocean and policy implications. *Environmental Research*, *119*, 101–117. https://doi.org/10.1016/j.envres.2012.03.013

Mason, R. P., Hammerschmidt, C. R., Lamborg, C. H., Bowman, K. L., Swarr, G. J., & Shelley, R. U. (2017). The air-sea exchange of mercury in the low latitude Pacific and Atlantic Oceans. *Deep Sea Research Part I: Oceanographic Research Papers*, *122*, 17–28. https://doi.org/10.1016/j.dsr.2017.01.015

Mason, R. P., Reinfelder, J. R., & Morel, F. M. M. (1995). Bioaccumulation of mercury and methylmercury. *Water, Air, and Soil Pollution*, *80*(1), 915–921. https://doi.org/10.1007/BF01189744

Matsui, K., Yoshinami, S., Narita, M., Chien, M.-F., Phung, L. T., Silver, S., & Endo, G. (2016). Mercury resistance transposons in Bacilli strains from different geographical regions. *FEMS Microbiology Letters*, *363*(5), fnw013. https://doi.org/10.1093/femsle/fnw013

McElwee, M. K., Ho, L. A., Chou, J. W., Smith, M. V., & Freedman, J. H. (2013). Comparative toxicogenomic responses of mercuric and methyl-mercury. *BMC Genomics*, *14*(1), 698. https://doi.org/10.1186/1471-2164-14-698

McKnight, D. M., Boyer, E. W., Westerhoff, P. K., Doran, P. T., Kulbe, T., & Andersen, D. T. (2001). Spectrofluorometric characterization of dissolved organic matter for indication of precursor organic material and aromaticity. *Limnology and Oceanography*, *46*(1), 38–48. https://doi.org/10.4319/lo.2001.46.1.0038

Mel, R. A., Viero, D. P., Carniello, L., Defina, A., & D'Alpaos, L. (2021). The first operations of Mo.S.E. system to prevent the flooding of Venice: Insights on the hydrodynamics of a regulated lagoon. *Estuarine, Coastal and Shelf Science*, *261*, 107547. https://doi.org/10.1016/j.ecss.2021.107547

Mergler, D., Philibert, A., Fillion, M., & Da Silva, J. (2023). The contribution across three generations of mercury exposure to attempted suicide among children and youth in Grassy Narrows First Nation, Canada: An intergenerational analysis. *Environmental Health Perspectives*, *131*(7), 077001. https://doi.org/10.1289/EHP11301

Miki, T., Easton, A. M., & Rownd, R. H. (1978). Mapping of the resistance genes of the R plasmid *NR1*. *Molecular and General Genetics*, *158*(3), 217–224. https://doi.org/10.1007/BF00267192

Mitchell, C. P. J., Jordan, T. E., Heyes, A., & Gilmour, C. C. (2012). Tidal exchange of total mercury and methylmercury between a salt marsh and a Chesapeake Bay sub-estuary. *Biogeochemistry*, *111*(1–3), 583–600. https://doi.org/10.1007/s10533-011-9691-y

Møller, A. K., Barkay, T., Hansen, M. A., Norman, A., Hansen, L. H., Sørensen, S. J., Boyd, E. S., & Kroer, N. (2014). Mercuric reductase genes (*merA*) and mercury resistance plasmids in High Arctic snow, freshwater and sea-ice brine. *FEMS Microbiology Ecology*, *87*(1), 52–63. https://doi.org/10.1111/1574-6941.12189

Momper, L., Aronson, H. S., & Amend, J. P. (2018). Genomic Description of '*Candidatus* Abyssubacteria,' a Novel Subsurface Lineage Within the Candidate Phylum Hydrogenedentes. *Frontiers in Microbiology*, *9*, 1993. https://doi.org/10.3389/fmicb.2018.01993

Monperrus, M., Rodriguez Gonzalez, P., Amouroux, D., Garcia Alonso, J. I., & Donard, O. F. X. (2008). Evaluating the potential and limitations of double-spiking species-specific isotope dilution analysis for the accurate quantification of mercury species in different environmental matrices. *Analytical and Bioanalytical Chemistry*, *390*(2), 655–666. https://doi.org/10.1007/s00216-007-1598-z

Monperrus, M., Tessier, E., Amouroux, D., Leynaert, A., Huonnic, P., & Donard, O. F. X. (2007). Mercury methylation, demethylation and reduction rates in coastal and marine surface waters of the Mediterranean Sea. *Marine Chemistry*, *107*(1), 49–63. https://doi.org/10.1016/j.marchem.2007.01.018

Monsieurs, P., Provoost, A., Mijnendonckx, K., Leys, N., Gaudreau, C., & Van Houdt, R. (2013). Genome sequence of *Cupriavidus metallidurans* strain H1130, isolated from an invasive human infection. *Genome Announcements*, *1*(6), e01051-13. https://doi.org/10.1128/genomeA.01051-13

Moore, B. (1960). A new screen test and selective medium for the rapid detection of epidemic strains of *Staph. Aureus*. *The Lancet*, *2*(7148), 453–458. https://doi.org/doi: 10.1016/s0140-6736(60)91591-9.

Moreau, J. W., Gionfriddo, C. M., Krabbenhoft, D. P., Ogorek, J. M., DeWild, J. F., Aiken, G. R., & Roden, E. E. (2015). The effect of natural organic matter on mercury methylation by *Desulfobulbus propionicus* 1pr3. *Frontiers in Microbiology*, *6*. https://doi.org/10.3389/fmicb.2015.01389

Mosa, K. A., Saadoun, I., Kumar, K., Helmy, M., & Dhankher, O. P. (2016). Potential biotechnological strategies for the cleanup of heavy metals and metalloids. *Frontiers in Plant Science*, *7*(MAR2016). Scopus. https://doi.org/10.3389/fpls.2016.00303

Mukhopadhyay, D., Yu, H. R., Nucifora, G., & Misra, T. K. (1991). Purification and functional characterization of MerD. A coregulator of the mercury resistance operon in gram-negative bacteria. *Journal of Biological Chemistry*, *266*(28), 18538–18542. https://doi.org/10.1016/S0021-9258(18)55095-X

Munson, K. M., Lamborg, C. H., Boiteau, R. M., & Saito, M. A. (2018). Dynamic mercury methylation and demethylation in oligotrophic marine water. *Biogeosciences*, *15*(21), 6451–6460. https://doi.org/10.5194/bg-15-6451-2018

Munson, K. M., Lamborg, C. H., Swarr, G. J., & Saito, M. A. (2015). Mercury species concentrations and fluxes in the Central Tropical Pacific Ocean. *Global Biogeochemical Cycles*, *29*(5), 656–676. https://doi.org/10.1002/2015GB005120

Naguib, M. M., El-Gendy, A. O., & Khairalla, A. S. (2018). Microbial diversity of *mer* operon genes and their potential rules in mercury bioremediation and resistance. *The Open Biotechnology Journal*, *12*(1), 56–77. https://doi.org/10.2174/1874070701812010056

Naik, M. M., & Dubey, S. K. (2017). Lead- and Mercury-Resistant Marine Bacteria and Their Application in Lead and Mercury Bioremediation. In M. M. Naik & S. K. Dubey (Eds.), *Marine Pollution and Microbial Remediation* (pp. 29–40). Springer. https://doi.org/10.1007/978-981-10-1044-6_3

Nakamura, K., Iwahara, M., & Furukawa, K. (2001). Screening of organomercurial-volatilizing bacteria in the mercury-polluted sediments and seawater of Minamata Bay in Japan. *Clean Products and Processes*, *3*(2), 104–107. https://doi.org/10.1007/s100980100107

Narita, M., Chiba, K., Nishizawa, H., Ishii, H., Huang, C.-C., Kawabata, Z., Silver, S., & Endo, G. (2003). Diversity of mercury resistance determinants among *Bacillus* strains isolated from sediment of Minamata Bay. *FEMS Microbiology Letters*, *223*(1), 73–82. https://doi.org/10.1016/S0378-1097(03)00325-2

Narita, M., Huang, C.-C., Koizumi, T., & Endo, G. (1999). Molecular analysis of *merA* gene possessed by anaerobic mercury-resistant bacteria isolated from sediment of Minamata Bay. *Microbes and Environments*, *14*(2), 77–84.

Nascimento, A. M. A., & Chartone-Souza, E. (2003). Operon mer: Bacterial resistance to mercury and potential for bioremediation of contaminated environments. *Genetics and Molecular Research*, 10.

Nath, S., Paul, P., Roy, R., Bhattacharjee, S., & Deb, B. (2019). Isolation and identification of metal-tolerant and antibiotic-resistant bacteria from soil samples of Cachar district of Assam, India. *SN Applied Sciences*, *1*(7). Scopus. https://doi.org/10.1007/s42452-019-0762-3

National Research Council. (2000). What determines susceptibility to nutrient over-enrichment? In *Clean Coastal Waters: Understanding and Reducing the Effects of Nutrient Pollution* (Washington, DC: The National Academies Press.). https://doi.org/10.17226/9812

Nazaret, S., Jeffrey, W. H., Saouter, E., Von Haven, R., & Barkay, T. (1994). *merA* gene expression in aquatic environments measured by mRNA production and Hg(II) volatilization. *Applied and Environmental Microbiology*, *60*(11), 4059–4065. https://doi.org/10.1128/aem.60.11.4059-4065.1994

Nelson, J. D., & Colwell, R. R. (1975). The ecology of mercury-resistant bacteria in Chesapeake Bay. *Microbial Ecology*, *1*(1), 191–218. https://doi.org/10.1007/BF02512389

Ní Chadhain, S. M., Schaefer, J. K., Crane, S., Zylstra, G. J., & Barkay, T. (2006). Analysis of mercuric reductase (*merA*) gene diversity in an anaerobic mercury-contaminated sediment enrichment. *Environmental Microbiology*, *8*(10), 1746–1752. https://doi.org/10.1111/j.1462-2920.2006.01114.x

Norambuena, J., Miller, M., Boyd, J. M., & Barkay, T. (2020). Expression and regulation of the *mer* operon in *Thermus thermophilus*. *Environmental Microbiology*, *22*(4), 1619–1634. https://doi.org/10.1111/1462-2920.14953

Novick, R. P., & Roth, C. (1968). Plasmid-linked resistance to inorganic salts in *Staphylococcus aureus*. *Journal of Bacteriology*, *95*(4), 1335–1342. https://doi.org/10.1128/jb.95.4.1335-1342.1968

Nucifora, G., Silver, S., & Misra, T. K. (1989). Down regulation of the mercury resistance operon by the most promoter-distal gene *merD*. *Molecular and General Genetics MGG*, *220*(1), 69–72. https://doi.org/10.1007/BF00260858

Nydahl, A., Panigrahi, S., & Wikner, J. (2013). Increased microbial activity in a warmer and wetter climate enhances the risk of coastal hypoxia. *FEMS Microbiology Ecology*, *85*(2), 338–347. https://doi.org/10.1111/1574-6941.12123

Obrist, D., Kirk, J. L., Zhang, L., Sunderland, E. M., Jiskra, M., & Selin, N. E. (2018). A review of global environmental mercury processes in response to human and natural perturbations: Changes of emissions, climate, and land use. *Ambio*, *47*(2), 116–140. https://doi.org/10.1007/s13280-017-1004-9

O'Halloran, T. V., Frantz, B., Shin, M. K., Ralston, D. M., & Wright, J. G. (1989). The MerR heavy metal receptor mediates positive activation in a topologically novel transcription complex. *Cell*, *56*(1), 119–129. https://doi.org/10.1016/0092-8674(89)90990-2

O'Halloran, T. V., & Walsh, C. T. (1987). Metalloregulatory DNA-binding protein encoded by *merR* gene: Isolation and characterization. *Science*, *253*, 211–214.

Ohno, T. (2002). Fluorescence inner-filtering correction for determining the humification index of dissolved organic matter. *Environmental Science and Technology*, *36*(4), 742–746. https://doi.org/10.1021/es0155276

Okino, S., Iwasaki, K., Yagi, O., & Tanaka, H. (2000). Development of a biological mercury removal-recovery system. *Biotechnology Letters*, *22*, 783–788.

Oksanen, J., Blanchet, F. G., Friendly, M., Kindt, R., Legendre, P., McGlinn, D., Minchin, P. R., O'Hara, R. B., Simpson, G. L., Solymos, P., Stevens, M. H. H., Szoecs, E., & Wagner, H. (2020). *Vegan: Community ecology package. R package version 2.5-7.* https://CRAN.R-project.org/package=vegan

Olson, B. H., Barkay, T., & Colwell, R. R. (1979). Role of plasmids in mercury transformation by bacteria isolated from the aquatic environment. *Applied and Environmental Microbiology*, *38*(3), 478–485. https://doi.org/10.1128/aem.38.3.478-485.1979

Oremland, R. S., Culbertson, C. W., & Winfrey, M. R. (1991). Methylmercury decomposition in sediments and bacterial cultures: Involvement of methanogens and sulfate reducers in

oxidative demethylation. *Applied and Environmental Microbiology*, *57*(1), 130–137. https://doi.org/10.1128/aem.57.1.130-137.1991

Oschlies, A., Brandt, P., Stramma, L., & Schmidtko, S. (2018). Drivers and mechanisms of ocean deoxygenation. *Nature Geoscience*, *11*(7), 467–473. https://doi.org/10.1038/s41561-018-0152-2

Overmann, J., Abt, B., & Sikorski, J. (2017). Present and future of culturing bacteria. *Annual Review of Microbiology*, *71*(1), 711–730. https://doi.org/10.1146/annurev-micro-090816-093449

Pak, K.-R., & Bartha, R. (1998). Mercury methylation and demethylation in anoxic lake sediments and by strictly anaerobic bacteria. *Applied and Environmental Microbiology*, *64*(3), 1013–1017. https://doi.org/10.1128/AEM.64.3.1013-1017.1998

Parks, D. H., Imelfort, M., Skennerton, C. T., Hugenholtz, P., & Tyson, G. W. (2015). CheckM: Assessing the quality of microbial genomes recovered from isolates, single cells, and metagenomes. *Genome Research*, *25*(7), 1043–1055. https://doi.org/10.1101/gr.186072.114

Parks, J. M., Johs, A., Podar, M., Bridou, R., Hurt, R. A., Smith, S. D., Tomanicek, S. J., Qian, Y., Brown, S. D., Brandt, C. C., Palumbo, A. V., Smith, J. C., Wall, J. D., Elias, D. A., & Liang, L. (2013). The genetic basis for bacterial mercury methylation. *Science*, *339*(6125), 1332–1335. https://doi.org/10.1126/science.1230667

Pathak, A., Jaswal, R., & Chauhan, A. (2020). Genomic characterization of a mercury resistant *Arthrobacter* sp. H-02-3 reveals the presence of heavy metal and antibiotic resistance determinants. *Frontiers in Microbiology*, *10*, 3039. https://doi.org/10.3389/fmicb.2019.03039

Pavoni, B., Marcomini, A., Sfriso, A., Donazzolo, R., & Orio, A. A. (1992). Changes in an estuarine ecosystem. In *The Science of Global Change* (Vol. 483, pp. 287–305). American Chemical Society. https://doi.org/10.1021/bk-1992-0483.ch014

Pedler Sherwood, B., Shaffer, E. A., Reyes, K., Longnecker, K., Aluwihare, L. I., & Azam, F. (2015). Metabolic characterization of a model heterotrophic bacterium capable of significant chemical alteration of marine dissolved organic matter. *Marine Chemistry*, *177*, 357–365. https://doi.org/10.1016/j.marchem.2015.06.027

Pepi, M., Focardi, S., Tarabelli, A., Volterrani, M., & Focardi, S. E. (2013). Bacterial strains resistant to inorganic and organic forms of mercury isolated from polluted sediments of the Orbetello Lagoon, Italy, and their possible use in bioremediation processes. *E3S Web of Conferences*, *1*, 31002. https://doi.org/10.1051/e3sconf/20130131002

Pepi, M., Gaggi, C., Bernardini, E., Focardi, S., Lobianco, A., Ruta, M., Nicolardi, V., Volterrani, M., Gasperini, S., Trinchera, G., Renzi, P., Gabellini, M., & Focardi, S. E. (2011). Mercury-resistant bacterial strains *Pseudomonas* and *Psychrobacter* spp. Isolated from sediments of Orbetello Lagoon (Italy) and their possible use in bioremediation processes. *International Biodeterioration & Biodegradation*, *65*(1), 85–91. https://doi.org/10.1016/j.ibiod.2010.09.006

Pereira-García, C., Del Amo, E. H., Vigués, N., Rey-Velasco, X., Rincón-Tomás, B., Pérez-Cruz, C., Sanz-Sáez, I., Hu, H., Bertilsson, S., Pannier, A., Soltmann, U., Sánchez, P., Acinas, S. G., Bravo, A. G., Alonso-Sáez, L., & Sánchez, O. (2024). Unmasking the physiology of mercury detoxifying bacteria from polluted sediments. *Journal of Hazardous Materials*, 133685. https://doi.org/10.1016/j.jhazmat.2024.133685

Pereira-Garcia, C., Sanz-Sáez, I., Sánchez, P., Coutinho, F. H., Bravo, A. G., Sánchez, O., & Acinas, S. G. (2024). Genomic and transcriptomic characterization of methylmercury detoxification in a deep ocean *Alteromonas mediterranea* ISS312. *Environmental Pollution*, *347*, 123725. https://doi.org/10.1016/j.envpol.2024.123725

Pirrone, N., Cinnirella, S., Feng, X., Finkelman, R. B., Friedli, H. R., Leaner, J., Mason, R., Mukherjee, A. B., Stracher, G. B., Streets, D. G., & Telmer, K. (2010). Global mercury emissions to the atmosphere from anthropogenic and natural sources. *Atmospheric Chemistry and Physics*, *10*(13), 5951–5964. https://doi.org/10.5194/acp-10-5951-2010

Pitcher, G. C., Aguirre-Velarde, A., Breitburg, D., Cardich, J., Carstensen, J., Conley, D. J., Dewitte, B., Engel, A., Espinoza-Morriberón, D., Flores, G., Garçon, V., Graco, M., Grégoire, M., Gutiérrez, D., Hernandez-Ayon, J. M., Huang, H.-H. M., Isensee, K., Jacinto, M. E., Levin, L., … Zhu, Z. (2021). System controls of coastal and open ocean oxygen depletion. *Progress in Oceanography*, *197*, 102613. https://doi.org/10.1016/j.pocean.2021.102613

Podar, M., Gilmour, C. C., Brandt, C. C., Soren, A., Brown, S. D., Crable, B. R., Palumbo, A. V., Somenahally, A. C., & Elias, D. A. (2015). Global prevalence and distribution of genes and microorganisms involved in mercury methylation. *Science Advances*, *1*(9), e1500675. https://doi.org/10.1126/sciadv.1500675

Priyadarshanee, M., Chatterjee, S., Rath, S., Dash, H. R., & Das, S. (2022). Cellular and genetic mechanism of bacterial mercury resistance and their role in biogeochemistry and bioremediation. *Journal of Hazardous Materials*, *423*, 126985. https://doi.org/10.1016/j.jhazmat.2021.126985

Pucher, M., Wünsch, U., Weigelhofer, G., Murphy, K., Hein, T., & Graeber, D. (2019). staRdom: Versatile software for analyzing spectroscopic data of dissolved organic matter in R. *Water*, *11*(11), 2366. https://doi.org/10.3390/w11112366

Qian, C., Johs, A., Chen, H., Mann, B. F., Lu, X., Abraham, P. E., Hettich, R. L., & Gu, B. (2016). Global proteome response to deletion of genes related to mercury methylation and dissimilatory metal reduction reveals changes in respiratory metabolism in *Geobacter sulfurreducens* PCA. *Journal of Proteome Research*, *15*(10), 3540–3549. https://doi.org/10.1021/acs.jproteome.6b00263

R Core Team. (2013). *R: A language and environment for statistical computing*. [R]. R Foundation for Statistical Computing, Vienna, Austria. http://www.R-project.org/

Rasmussen, L. D., Zawadsky, C., Binnerup, S. J., Øregaard, G., Sørensen, S. J., & Kroer, N. (2008). Cultivation of hard-to-culture subsurface mercury-resistant bacteria and discovery of new *merA* gene sequences. *Applied and Environmental Microbiology*, *74*(12), 3795–3803. https://doi.org/10.1128/AEM.00049-08

Reimann, L., Vafeidis, A. T., Brown, S., Hinkel, J., & Tol, R. S. J. (2018). Mediterranean UNESCO World Heritage at risk from coastal flooding and erosion due to sea-level rise. *Nature Communications*, *9*(1), 4161. https://doi.org/10.1038/s41467-018-06645-9

Richter, M., Rosselló-Móra, R., Oliver Glöckner, F., & Peplies, J. (2016). JSpeciesWS: A web server for prokaryotic species circumscription based on pairwise genome comparison. *Bioinformatics*, *32*(6), 929–931. https://doi.org/10.1093/bioinformatics/btv681

Rincón-Tomás, B., Lanzén, A., Sánchez, P., Estupiñán, M., Sanz-Sáez, I., Bilbao, M. E., Rojo, D., Mendibil, I., Pérez-Cruz, C., Ferri, M., Capo, E., Abad-Recio, I. L., Amouroux, D., Bertilsson, S., Sánchez, O., Acinas, S. G., & Alonso-Sáez, L. (2023). Revisiting the mercury cycle in marine sediments: A potential multifaceted role for Desulfobacterota. *Journal of Hazardous Materials*, *465*, 133120. https://doi.org/10.1016/j.jhazmat.2023.133120

Rodríguez, J., Andersson, A., Björn, E., Timonen, S., Brugel, S., Skrobonja, A., & Rowe, O. (2022). Inputs of terrestrial dissolved organic matter enhance bacterial production and methylmercury formation in oxic coastal water. *Frontiers in Microbiology*, *13*, 809166. https://doi.org/10.3389/fmicb.2022.809166

Rodríguez-Castrillón, J. Á., Moldovan, M., Ruiz Encinar, J., & García Alonso, J. I. (2008). Isotope pattern deconvolution for internal mass bias correction in the characterisation of isotopically enriched spikes. *J. Anal. At. Spectrom.*, *23*(3), 318–324. https://doi.org/10.1039/B710595A

Rodriguez-Gonzalez, P., Bouchet, S., Monperrus, M., Tessier, E., & Amouroux, D. (2013). In situ experiments for element species-specific environmental reactivity of tin and mercury compounds using isotopic tracers and multiple linear regression. *Environmental Science and Pollution Research*, *20*(3), 1269–1280. https://doi.org/10.1007/s11356-012-1019-5

Romera-Castillo, C., Sarmento, H., Álvarez-Salgado, X. A., Gasol, J. M., & Marrasé, C. (2011). Net production and consumption of fluorescent colored dissolved organic matter by natural bacterial assemblages growing on marine phytoplankton exudates. *Applied and Environmental Microbiology*, *77*(21), 7490–7498. https://doi.org/10.1128/AEM.00200-11

Rosati, G., Solidoro, C., & Canu, D. (2020). Mercury dynamics in a changing coastal area over industrial and postindustrial phases: Lessons from the Venice Lagoon. *Science of The Total Environment*, *743*, 140586. https://doi.org/10.1016/j.scitotenv.2020.140586

Royo-Llonch, M., Sánchez, P., Ruiz-González, C., Salazar, G., Pedrós-Alió, C., Sebastián, M., Labadie, K., Paoli, L., M. Ibarbalz, F., Zinger, L., Churcheward, B., Tara Oceans Coordinators, Babin, M., Bork, P., Boss, E., Cochrane, G., De Vargas, C., Gorsky, G., Grimsley, N., … Acinas, S. G. (2021). Compendium of 530 metagenome-assembled bacterial and archaeal genomes from the polar Arctic Ocean. *Nature Microbiology*, *6*(12), 1561–1574. https://doi.org/10.1038/s41564-021-00979-9

Ruelas-Inzunza, J., Delgado-Alvarez, C., Frías-Espericueta, M., & Páez-Osuna, F. (2013). Mercury in the atmospheric and coastal environments of Mexico. In D. M. Whitacre (Ed.), *Reviews of Environmental Contamination and Toxicology Volume 226* (Vol. 226). Springer New York. https://doi.org/10.1007/978-1-4614-6898-1

Sadhukhan, P. C., Ghosh, S., Chaudhuri, J., Ghosh, D. K., & Mandal, A. (1997). Mercury and organomercurial resistance in bacteria isolated from freshwater fish of wetland fisheries around Calcutta. *Environmental Pollution*, *97*(1–2), 71–78. https://doi.org/10.1016/S0269-7491(97)00068-7

Salazar, G., Paoli, L., Alberti, A., Huerta-Cepas, J., Ruscheweyh, H.-J., Cuenca, M., Field, C. M., Coelho, L. P., Cruaud, C., Engelen, S., Gregory, A. C., Labadie, K., Marec, C., Pelletier, E., Royo-Llonch, M., Roux, S., Sánchez, P., Uehara, H., Zayed, A. A., … Wincker, P. (2019). Gene expression changes and community turnover differentially shape the global ocean metatranscriptome. *Cell*, *179*(5), 1068-1083.e21. https://doi.org/10.1016/j.cell.2019.10.014

Sandberg, T. E., Salazar, M. J., Weng, L. L., Palsson, B. O., & Feist, A. M. (2019). The emergence of adaptive laboratory evolution as an efficient tool for biological discovery and industrial biotechnology. *Metabolic Engineering*, *56*, 1–16. https://doi.org/10.1016/j.ymben.2019.08.004

Sangal, V., Goodfellow, M., Jones, A. L., Schwalbe, E. C., Blom, J., Hoskisson, P. A., & Sutcliffe, I. C. (2016). Next-generation systematics: An innovative approach to resolve the structure of complex prokaryotic taxa. *Scientific Reports*, *6*(1), 38392. https://doi.org/10.1038/srep38392

Sanz-Saez, I. (2020). *Contribution of marine heterotrophic cultured bacteria to microbial diversity and mercury detoxification*. Universitat Autònoma de Barcelona.

Sanz-Sáez, I., Pereira-García, C., Bravo, A. G., Trujillo, L., Pla i Ferriol, M., Capilla, M., Sánchez, P., Rodríguez Martín-Doimeadios, R. C., Acinas, S. G., & Sánchez, O. (2022). Prevalence of heterotrophic methylmercury detoxifying bacteria across oceanic regions. *Environmental Science & Technology*, *56*(6), 3452–3461. https://doi.org/10.1021/acs.est.1c05635

Sanz-Sáez, I., Pereira-Garcia, C., Bravo, A. G., Trujillo, L., Pla i Ferriol, M., Capilla, M., Sanchez, P., Rodriguez Martín-Doimeadios, R. del C., Acinas, S. G., & Sanchéz, O. (2021). *Prevalence of heterotrophic methylmercury detoxifying bacteria across oceanic regions*. 32. https://doi.org/10.1101/2021.08.09.455674

Sanz-Sáez, I., Salazar, G., Sanchez, P., Acinas, S. G., & Sanchéz, O. (2020). *Diversity and distribution of marine heterotrophic bacteria from a large culture collection*. 16.

Saranya, K., Sundaramanickam, A., Shekhar, S., Swaminathan, S., & Balasubramanian, T. (2017). Bioremediation of mercury by *Vibrio fluvialis* screened from industrial effluents. *BioMed Research International*, *2017*, 1–6. https://doi.org/10.1155/2017/6509648

Scanu, S., Piazzolla, D., Frattarelli, F. M., Mancini, E., Tiralongo, F., Brundo, M. V., Tibullo, D., Pecoraro, R., Copat, C., Ferrante, M., & Marcelli, M. (2016). Mercury enrichment in sediments of the coastal area of northern Latium, Italy. *Bulletin of Environmental Contamination and Toxicology*, *96*(5), 630–637. Scopus. https://doi.org/10.1007/s00128-016-1776-9

Scarascia, L., & Lionello, P. (2013). Global and regional factors contributing to the past and future sea level rise in the Northern Adriatic Sea. *Global and Planetary Change*, *106*, 51–63. https://doi.org/10.1016/j.gloplacha.2013.03.004

Schaefer, J. K., Kronberg, R. -M., Morel, F. M. M., & Skyllberg, U. (2014). Detection of a key Hg methylation gene, *hgcA* , in wetland soils. *Environmental Microbiology Reports*, *6*(5), 441–447. https://doi.org/10.1111/1758-2229.12136

Schaefer, J. K., Letowski, J., & Barkay, T. (2002). *Mer* -mediated resistance and volatilization of Hg(II) under anaerobic conditions. *Geomicrobiology Journal*, *19*(1), 87–102. https://doi.org/10.1080/01490450231724619 2

Schaefer, J. K., Szczuka, A., & Morel, F. M. M. (2014). Effect of divalent metals on Hg(II) uptake and methylation by bacteria. *Environmental Science & Technology*, *48*(5), 3007–3013. https://doi.org/10.1021/es405215v

Schaefer, J. K., Yagi, J., Reinfelder, J. R., Cardona, T., Ellickson, K. M., Tel-Or, S., & Barkay, T. (2004). Role of the bacterial organomercury lyase (MerB) in controlling methylmercury accumulation in mercury-contaminated natural waters. *Environmental Science & Technology*, *38*(16), 4304–4311. https://doi.org/10.1021/es049895w

Schartup, A. T., Ndu, U., Balcom, P. H., Mason, R. P., & Sunderland, E. M. (2015). Contrasting effects of marine and terrestrially derived dissolved organic matter on mercury speciation and bioavailability in seawater. *Environmental Science & Technology*, *49*(10), 5965–5972. https://doi.org/10.1021/es506274x

Schartup, A. T., Thackray, C. P., Qureshi, A., Dassuncao, C., Gillespie, K., Hanke, A., & Sunderland, E. M. (2019). Climate change and overfishing increase neurotoxicant in marine predators. *Nature*, *572*(7771), 648–650. https://doi.org/10.1038/s41586-019-1468-9

Schelert, J., Rudrappa, D., Johnson, T., & Blum, P. (2013). Role of MerH in mercury resistance in the archaeon *Sulfolobus solfataricus*. *Microbiology*, *159*(Pt_6), 1198–1208. https://doi.org/10.1099/mic.0.065854-0

Schmidtko, S., Stramma, L., & Visbeck, M. (2017). Decline in global oceanic oxygen content during the past five decades. *Nature*, *542*(7641), 335–339. https://doi.org/10.1038/nature21399

Schottel, J. L. (1978). The mercuric and organomercurial detoxifying enzymes from a plasmid-bearing strain of *Escherichia coli*. *Journal of Biological Chemistry*, *253*(12), 4341–4349. https://doi.org/10.1016/S0021-9258(17)34725-7

Schuster, P. F., Schaefer, K. M., Aiken, G. R., Antweiler, R. C., Dewild, J. F., Gryziec, J. D., Gusmeroli, A., Hugelius, G., Jafarov, E., Krabbenhoft, D. P., Liu, L., Herman-Mercer, N., Mu, C., Roth, D. A., Schaefer, T., Striegl, R. G., Wickland, K. P., & Zhang, T. (2018). Permafrost stores a globally significant amount of mercury. *Geophysical Research Letters*, *45*(3), 1463–1471. https://doi.org/10.1002/2017GL075571

Seemann, T. (2014). Prokka: Rapid prokaryotic genome annotation. *Bioinformatics*, *30*(14), 2068–2069. https://doi.org/10.1093/bioinformatics/btu153

Seller, P., Kelly, C. A., Rudd, J. W. M., & MacHutchon, A. R. (1996). Photodegradation of methylmercury in lakes. *Nature*, *380*(6576), 694–697. https://doi.org/10.1038/380694a0

Sharif, A., Monperrus, M., Tessier, E., Bouchet, S., Pinaly, H., Rodriguez-Gonzalez, P., Maron, P., & Amouroux, D. (2014). Fate of mercury species in the coastal plume of the Adour River estuary (Bay of Biscay, SW France). *Science of The Total Environment*, *496*, 701–713. https://doi.org/10.1016/j.scitotenv.2014.06.116

Singer, M. B., Harrison, L. R., Donovan, P. M., Blum, J. D., & Marvin-DiPasquale, M. (2016). Hydrologic indicators of hot spots and hot moments of mercury methylation potential along river corridors. *Science of The Total Environment*, *568*, 697–711. https://doi.org/10.1016/j.scitotenv.2016.03.005

Sinha, A., & Khare, S. K. (2011). Mercury bioaccumulation and simultaneous nanoparticle synthesis by *Enterobacter* sp. Cells. *Bioresource Technology*, *102*(5), 4281–4284. https://doi.org/10.1016/j.biortech.2010.12.040

Skyllberg, U., Bloom, P. R., Qian, J., Lin, C.-M., & Bleam, W. F. (2006). Complexation of Mercury(II) in Soil Organic Matter: EXAFS Evidence for Linear Two-Coordination with Reduced Sulfur Groups. *Environmental Science & Technology*, *40*(13), 4174–4180. https://doi.org/10.1021/es0600577

Smith, D. H. (1967). R factors mediate resistance to mercury, nickel, and cobalt. *Science*, *156*, 1114–1115.

Smith, P. B. (1962). Growth of *staphylococci* on mercuric chloride agar. *Journal of Bacteriology*, *84*(5), 1016–1019. https://doi.org/10.1128/jb.84.5.1016-1019.1962

Smith, S. D., Bridou, R., Johs, A., Parks, J. M., Elias, D. A., Hurt, R. A., Brown, S. D., Podar, M., & Wall, J. D. (2015). Site-directed mutagenesis of HgcA and HgcB reveals amino acid residues important for mercury methylation. *Applied and Environmental Microbiology*, *81*(9), 3205–3217. https://doi.org/10.1128/AEM.00217-15

Soerensen, A. L., Mason, R. P., Balcom, P. H., Jacob, D. J., Zhang, Y., Kuss, J., & Sunderland, E. M. (2014). Elemental mercury concentrations and fluxes in the tropical atmosphere and ocean. *Environmental Science & Technology*, *48*(19), 11312–11319. https://doi.org/10.1021/es503109p

Soerensen, A. L., Schartup, A. T., Skrobonja, A., & Björn, E. (2017). Organic matter drives high interannual variability in methylmercury concentrations in a subarctic coastal sea. *Environmental Pollution*, *229*, 531–538. https://doi.org/10.1016/j.envpol.2017.06.008

Sone, Y., Nakamura, R., Pan-Hou, H., Itoh, T., & Kiyono, M. (2013). Role of MerC, MerE, MerF, MerT, and/or MerP in resistance to mercurials and the transport of mercurials in *Escherichia coli*. *Biological and Pharmaceutical Bulletin*, *36*(11), 1835–1841. https://doi.org/10.1248/bpb.b13-00554

Sonke, J. E., Angot, H., Zhang, Y., Poulain, A., Björn, E., & Schartup, A. (2023). Global change effects on biogeochemical mercury cycling. *Ambio*, *52*(5), 853–876. https://doi.org/10.1007/s13280-023-01855-y

Spangler, W. J., Spigarelli, J. L., Rose, J. M., Flippin, R. S., & Miller, H. H. (1973). Degradation of methylmercury by bacteria isolated from environmental samples. *Applied Microbiology*, *25*(4), 488–493.

Spangler, W. J., Spigarelli, J. L., Rose, J. M., & Miller, H. M. (1973). Methylmercury: Bacterial degradation in lake sediments. *Science*, *180*, 192–193. https://doi.org/DOI: 10.1126/science.180.4082.192

Steinegger, M., & Söding, J. (2017). MMseqs2 enables sensitive protein sequence searching for the analysis of massive data sets. *Nature Biotechnology*, *35*(11), 1026–1028. https://doi.org/10.1038/nbt.3988

Stoichev, T., Amouroux, D., Wasserman, J. C., Point, D., De Diego, A., Bareille, G., & Donard, O. F. X. (2004). Dynamics of mercury species in surface sediments of a macrotidal estuarine–coastal system (Adour River, Bay of Biscay). *Estuarine, Coastal and Shelf Science*, *59*(3), 511–521. https://doi.org/10.1016/j.ecss.2003.10.007

Streets, D. G., Horowitz, H. M., Jacob, D. J., Lu, Z., Levin, L., ter Schure, A. F. H., & Sunderland, E. M. (2017). Total mercury released to the environment by human activities. *Environmental Science & Technology*, *51*(11), 5969–5977. https://doi.org/10.1021/acs.est.7b00451

Summers, A. O., & Lewis, E. (1973). Volatilization of mercuric chloride by mercury-resistant plasmid-bearing strains of *Escherichia coli, Staphylococcus aureus* , and *Pseudomonas aeruginosa*. *Journal of Bacteriology*, *113*(2), 1070–1072. https://doi.org/10.1128/jb.113.2.1070-1072.1973

Summers, A. O., & Silver, S. (1972). Mercury resistance in a plasmid-bearing strain of *Escherichia coli*. *Journal of Bacteriology*, *112*(3), 1228–1236. https://doi.org/10.1128/jb.112.3.1228-1236.1972

Tada, Y., Marumoto, K., Iwamoto, Y., Takeda, K., & Sakugawa, H. (2023). Distribution and phylogeny of mercury methylation, demethylation, and reduction genes in the Seto Inland Sea of Japan. *Marine Pollution Bulletin*, *186*, 114381. https://doi.org/10.1016/j.marpolbul.2022.114381

Taherkhani, M., Vitousek, S., Barnard, P. L., Frazer, N., Anderson, T. R., & Fletcher, C. H. (2020). Sea-level rise exponentially increases coastal flood frequency. *Scientific Reports*, *10*(1), 6466. https://doi.org/10.1038/s41598-020-62188-4

Tanwer, N., Bumbra, P., Khosla, B., & Laura, J. S. (2022). Chapter 35—Mercury pollution and its bioremediation by microbes. In J. A. Malik (Ed.), *Microbes and Microbial Biotechnology for Green Remediation* (pp. 651–664). Elsevier. https://doi.org/10.1016/B978-0-323-90452-0.00005-0

Taylor, V. F., Buckman, K. L., Seelen, E. A., Mazrui, N. M., Balcom, P. H., Mason, R. P., & Chen, C. Y. (2019). Organic carbon content drives methylmercury levels in the water column and in estuarine food webs across latitudes in the Northeast United States. *Environmental Pollution*, *246*, 639–649. https://doi.org/10.1016/j.envpol.2018.12.064

Tezuka, T., & Tonomura, K. (1976). Purification and properties of an enzyme catalyzing the splitting of carbon-mercury linkages from mercury-resistant *Pseudomonas* K-62 strain I. Splitting Enzyme 1. *The Journal of Biochemistry*, *80*(1).

Tezuka, T., & Tonomura, K. (1978). Purification and properties of a second enzyme catalyzing the splitting of carbon-mercury linkages from mercury-resistant Pseudomonas K-62. *Journal of Bacteriology*, *135*(1), 138–143. https://doi.org/10.1128/jb.135.1.138-143.1978

The Met Museum. (2009). *Cinnabar: The Chinese Art of Carved Lacquer*. https://www.metmuseum.org/es/exhibitions/listings/2009/cinnabar

Tjerngren, I., Meili, M., Björn, E., & Skyllberg, U. (2012). Eight boreal wetlands as sources and sinks for methyl mercury in relation to soil acidity, C/N ratio, and small-scale flooding. *Environmental Science & Technology*, *46*(15), 8052–8060. https://doi.org/10.1021/es300845x

Trincardi, F., Barbanti, A., Bastianini, M., Benetazzo, A., Cavaleri, L., Chiggiato, J., Papa, A., Pomaro, A., Sclavo, M., Tosi, L., & Umgiesser, G. (2016). The 1966 flooding of Venice: What time taught us for the future. *Oceanography*, *29*(4). https://doi.org/10.5670/oceanog.2016.87

Tsui, M. T., Uzun, H., Ruecker, A., Majidzadeh, H., Ulus, Y., Zhang, H., Bao, S., Blum, J. D., Karanfil, T., & Chow, A. T. (2020). Concentration and isotopic composition of mercury in a blackwater river affected by extreme flooding events. *Limnology and Oceanography*, *65*(9), 2158–2169. https://doi.org/10.1002/lno.11445

UN. (2013). *Minamata Convention on Mercury*. https://wedocs.unep.org/20.500.11822/8458

UNEP. (2013). *Global Mercury Assessment 2013: Sources, emissions, releases, and environmental transport*. https://wedocs.unep.org/20.500.11822/7984

UNEP. (2018). *Global Mercury Assessment 2018*. https://www.unep.org/resources/publication/global-mercury-assessment-2018

UNEP, & IOMC. (2002). *Global Mercury Assessment*. https://wedocs.unep.org/20.500.11822/31253.

Vaituzis, Z., Nelson, J. D., Wan, L. W., & Colwell, R. R. (1975). Effects of mercuric chloride on growth and morphology of selected strains of mercury-resistant bacteria. *Applied Microbiology*, *29*(2), 275–286.

Vernette, C., Lecubin, J., Sánchez, P., Tara Oceans Coordinators, Acinas, S. G., Babin, M., Bork, P., Boss, E., Bowler, C., Cochrane, G., de Vargas, C., Gorsky, G., Guidi, L., Grimsley, N., Hingamp1, P., Iudicone, D., Jaillon, O., Kandels-Lewis, S., Karp-Boss, L., … Lescot, M. (2022). The Ocean Gene Atlas v2.0: Online exploration of the biogeography and phylogeny of plankton genes. *Nucleic Acids Research*, *50*(W1), W516–W526. https://doi.org/10.1093/nar/gkac420

Vigneron, A., Cruaud, P., Aubé, J., Guyoneaud, R., & Goñi-Urriza, M. (2021). Transcriptomic evidence for versatile metabolic activities of mercury cycling microorganisms in brackish microbial mats. *Npj Biofilms and Microbiomes*, *7*(1), 83. https://doi.org/10.1038/s41522-021-00255-y

Villar, E., Cabrol, L., & Heimbürger-Boavida, L. (2020). Widespread microbial mercury methylation genes in the global ocean. *Environmental Microbiology Reports*, *12*(3), 277–287. https://doi.org/10.1111/1758-2229.12829

Vitousek, S., Barnard, P. L., Fletcher, C. H., Frazer, N., Erikson, L., & Storlazzi, C. D. (2017). Doubling of coastal flooding frequency within decades due to sea-level rise. *Scientific Reports*, *7*(1), 1399. https://doi.org/10.1038/s41598-017-01362-7

von Canstein, H., Li, Y., Timmis, K. N., Deckwer, W.-D., & Wagner-Döbler, I. (1999). Removal of mercury from chloralkali electrolysis wastewater by a mercury-resistant *Pseudomonas putida* strain. *Applied and Environmental Microbiology*, *65*(12), 5279–5284.

Vousdoukas, M. I., Mentaschi, L., Voukouvalas, E., Bianchi, A., Dottori, F., & Feyen, L. (2018). Climatic and socioeconomic controls of future coastal flood risk in Europe. *Nature Climate Change*, *8*(9), 776–780. https://doi.org/10.1038/s41558-018-0260-4

Vousdoukas, M. I., Mentaschi, L., Voukouvalas, E., Verlaan, M., Jevrejeva, S., Jackson, L. P., & Feyen, L. (2018). Global probabilistic projections of extreme sea levels show intensification of coastal flood hazard. *Nature Communications*, *9*(1), 2360. https://doi.org/10.1038/s41467-018-04692-w

Voynova, Y. G., Brix, H., Petersen, W., Weigelt-Krenz, S., & Scharfe, M. (2017). Extreme flood impact on estuarine and coastal biogeochemistry: The 2013 Elbe flood. *Biogeosciences*, *14*(3), 541–557. https://doi.org/10.5194/bg-14-541-2017

Wagner-Döbler, I. (2003). Pilot plant for bioremediation of mercury-containing industrial wastewater. *Applied Microbiology and Biotechnology*, *62*(2), 124–133. https://doi.org/10.1007/s00253-003-1322-7

Walker, J. D., & Colwell, R. R. (1974). Mercury-resistant bacteria and petroleum degradation. *Applied Microbiology*, *27*(1), 285–287. https://doi.org/10.1128/am.27.1.285-287.1974

Wang, J., Liu, Q., Chen, J., Chen, H., Lin, H., & Sun, X. (2018). Total mercury flux and offshore transport via submarine groundwater discharge and coal-fired power plant in the Jiulong River estuary, China. *Marine Pollution Bulletin*, *127*, 794–803. https://doi.org/10.1016/j.marpolbul.2017.09.064

Wang, K., Pang, Y., Yi, Y., Yang, S., Wang, Y., He, C., Shi, Q., & He, D. (2023). Response of dissolved organic matter chemistry to flood control of a large river reservoir during an extreme storm event. *Water Research*, *230*, 119565. https://doi.org/10.1016/j.watres.2023.119565

Wang, Y., Boyd, E., Crane, S., Lu-Irving, P., Krabbenhoft, D., King, S., Dighton, J., Geesey, G., & Barkay, T. (2011). Environmental conditions constrain the distribution and diversity of archaeal

merA in Yellowstone National Park, Wyoming, U.S.A. *Microbial Ecology*, *62*(4), 739–752. https://doi.org/10.1007/s00248-011-9890-z

Wang, Y., Moore, M., Levinson, H. S., Silver, S., Walsh, C., & Mahler, I. (1989). Nucleotide sequence of a chromosomal mercury resistance determinant from a *Bacillus* sp. With broad-spectrum mercury resistance. *Journal of Bacteriology*, *171*(1), 83–92. https://doi.org/10.1128/jb.171.1.83-92.1989

Weiss, A. A., Murphy, S. D., & Silver, S. (1977). Mercury and organomercurial resistances determined by plasmids in *Staphylococcus aureus*. *Journal of Bacteriology*, *132*(1), 197–208. https://doi.org/10.1128/jb.132.1.197-208.1977

Wheeler, T. J., Clements, J., Eddy, S. R., Hubley, R., Jones, T. A., Jurka, J., Smit, A. F. A., & Finn, R. D. (2012). Dfam: A database of repetitive DNA based on profile hidden Markov models. *Nucleic Acids Research*, *41*(D1), D70–D82. https://doi.org/10.1093/nar/gks1265

Wickham, H. (2016). *ggplot2: Elegant Graphics for Data Analysis.* Springer-Verlag New York. https://ggplot2.tidyverse.org

Wood, J. M., Kennedy, F. S., & Rosen, C. G. (1968). Synthesis of methyl-mercury compounds by extracts of a methanogenic bacterium. *Nature*, *220*(5163), 173–174. https://doi.org/10.1038/220173a0

World Health Organization. (2020). *The 10 chemicals of major public health concerns*. https://www.who.int/teams/environment-climate-change-and-health/chemical-safety-and-health/health-impacts/chemicals

Xu, S., Dai, Z., Guo, P., Fu, X., Liu, S., Zhou, L., Tang, W., Feng, T., Chen, M., Zhan, L., Wu, T., Hu, E., Jiang, Y., Bo, X., & Yu, G. (2021). ggtreeExtra: Compact visualization of richly annotated phylogenetic data. *Molecular Biology and Evolution*, *38*(9), 4039–4042. https://doi.org/10.1093/molbev/msab166

Yang, W., Chen, X., Zhu, B., & Zhu, Y. (2017). Isolation of mercury-resistant strains and its characteristic for mercury-removed. *Chinese Journal of Environmental Engineering*, *11*(1), 602–607. Scopus. https://doi.org/10.12030/j.cjee.201509006

Yin, Y., Mao, X., Yang, J., Chen, X., Mao, F., & Xu, Y. (2012). dbCAN: A web resource for automated carbohydrate-active enzyme annotation. *Nucleic Acids Research*, *40*(W1), W445–W451. https://doi.org/10.1093/nar/gks479

Yorifuji, T., & Tsuda, T. (2014). Minamata. In *Encyclopedia of Toxicology* (pp. 340–344). Elsevier. https://doi.org/10.1016/B978-0-12-386454-3.00038-5

Youssef, N. H., Farag, I. F., Hahn, C. R., Premathilake, H., Fry, E., Hart, M., Huffaker, K., Bird, E., Hambright, J., Hoff, W. D., & Elshahed, M. S. (2019). *Candidatus* Krumholzibacterium zodletonense gen. Nov., sp nov, the first representative of the candidate phylum Krumholzibacteriota phyl. Nov. Recovered from an anoxic sulfidic spring using genome resolved metagenomics. *Systematic and Applied Microbiology*, *42*(1), 85–93. https://doi.org/10.1016/j.syapm.2018.11.002

Yu, G., Smith, D. K., Zhu, H., Guan, Y., & Lam, T. T.-Y. (2017). ggtree: An r package for visualization and annotation of phylogenetic trees with their covariates and other associated data. *Methods in Ecology and Evolution*, *8*(1), 28–36. https://doi.org/10.1111/2041-210X.12628

Yu, J.-G., Yue, B.-Y., Wu, X.-W., Liu, Q., Jiao, F.-P., Jiang, X.-Y., & Chen, X.-Q. (2016). Removal of mercury by adsorption: A review. *Environmental Science and Pollution Research*, *23*(6), 5056–5076. https://doi.org/10.1007/s11356-015-5880-x

Yu, R.-Q., Reinfelder, J. R., Hines, M. E., & Barkay, T. (2013). Mercury methylation by the methanogen *Methanospirillum hungatei*. *Applied and Environmental Microbiology*, *79*(20), 6325–6330. https://doi.org/10.1128/AEM.01556-13

Zech, H., Thole, S., Schreiber, K., Kalhöfer, D., Voget, S., Brinkhoff, T., Simon, M., Schomburg, D., & Rabus, R. (2009). Growth phase-dependent global protein and metabolite profiles of *Phaeobacter gallaeciensis* strain DSM 17395, a member of the marine *Roseobacter*-clade. *Proteomics*, *9*(14), 3677–3697. https://doi.org/10.1002/pmic.200900120

Zennaro, F., Furlan, E., Canu, D., Aveytua Alcazar, L., Rosati, G., Solidoro, C., Aslan, S., & Critto, A. (2023). Venice lagoon chlorophyll-a evaluation under climate change conditions: A hybrid water quality machine learning and biogeochemical-based framework. *Ecological Indicators*, *157*, 111245. https://doi.org/10.1016/j.ecolind.2023.111245

Zhang, H., Feng, X., Larssen, T., Shang, L., & Li, P. (2010). Bioaccumulation of methylmercury versus inorganic mercury in rice (*Oryza sativa* L.) grain. *Environmental Science & Technology*, *44*(12), 4499–4504. https://doi.org/10.1021/es903565t

Zheng, R., Wu, S., Ma, N., & Sun, C. (2018). Genetic and physiological adaptations of marine bacterium *Pseudomonas stutzeri* 273 to mercury stress. *Frontiers in Microbiology*, *9*, 682. https://doi.org/10.3389/fmicb.2018.00682

Zonta, R., Botter, M., Cassin, D., Bellucci, L. G., Pini, R., & Dominik, J. (2018). Sediment texture and metal contamination in the Venice Lagoon (Italy): A snapshot before the installation of the MOSE system. *Estuarine, Coastal and Shelf Science*, *205*, 131–151. https://doi.org/10.1016/j.ecss.2018.03.007

Zonta, R., Botter, M., Cassin, D., Pini, R., Scattolin, M., & Zaggia, L. (2007). Sediment chemical contamination of a shallow water area close to the industrial zone of Porto Marghera (Venice Lagoon, Italy). *Marine Pollution Bulletin*, *55*(10–12), 529–542. https://doi.org/10.1016/j.marpolbul.2007.09.024

List of figures and tables



List of figures

Figure 1: Timeline of Hg uses, poisonings and legislation throughout history. 14

Figure 2: The marine Hg cycle. The shown transformations focus on the processes, occurring either in sediments or in the seawater column. Hg^0: elemental mercury. Hg^{II}: divalent mercury. MMHg: Monomethylmercury. DMHg: Dimethylmercury. Figure modified from Sanz-Saez, 2020. 18

Figure 3: Simplified unrooted phylogenetic tree of *hgcA* sequences from the Hg-MATE database (Gionfriddo et al., 2021). Taxonomy is based on the GTDB classification. Microbial groups with the highest diversity of *hgc*+ microorganisms are denoted by colours. Illustration from Capo et al. (2023). 19

Figure 4: A. Generic *mer* operon with all possible genes. Note that not all genes need to be present in the operon to be functional and confer Hg resistance. B. Cellular *mer* -encoded Hg resistance mechanisms. The outer membrane is dashed, illustrating that is not present in all prokaryotes. The colors of various Mer proteins correspond with the colors of the genes that encode for these proteins in panel A. PMA: phenylmercuric acetate. MMHg: Monomethylmercury. PM: phenylmercury. Modified from Lin et al., (2011). 20

Figure 5: Phylogenetic tree of MerA protein homologs (plasmid MerA not included). Archaeal clade are colored in blue and bacterial clades in red, while purple-colored clades denote mixed lineages. The colors covering the labels denote the three main groups of MerA: group A in light blue, group B in orange and group C in green. The outgroup consists of 6 bacterial and archaeal dihydrolipoamide dehydrogenase sequences. Tree scale is in amino acid substitutions per site. Yellow stars mark lineages in which MerA activity has been confirmed. Illustration from Christakis et al. (2021). 22

Figure 6: Graphic representation of the main research question or objective of each chapter of this thesis. 33

Figure 7: Graphical abstract of Chapter 1; left half represents the normal conditions of the lagoon with the MOSE open, and right half represents the changes in conditions when the MOSE is closed. k_m: Hg^{II} methylation rate constant. DOC: Dissolved organic carbon. 37

Figure 8: Location of the two studied sites Osellino (OS, 45.4750°, 12.2859°) and San Giuliano (SG, 45.4638°, 12.2949°) in the Venice Lagoon (in the insert). 40

Figure 9: Scheme of the methodology pipeline for incubations and core processing. 41

Figure 10: Drawing (left) and photo (right) of the benthic chamber. 42

Figure 11: Principal Component Analysis (PCA) of fresh sediments (n = 24) showing the explained variability arising from principal components 1 (PC1) and 2 (PC2) based on general sediment attributes, mercury concentrations (THg and MMHg) and organic matter traits, as presented in (A) the scores plot displaying the 24 samples and (B) the loadings plot displaying the characteristics used. 46

Figure 12: Vertical profiles of THg (A and B) and MMHg (C and D) concentrations in overlying water and porewater of six sediment cores from OS site (A and C, purple) and SG site (B and D, orange) collected in Sep 2021. Open symbols represent the measurements performed in fresh cores (cores number 13, 14 and 15) and closed symbols refer to the incubated cores (cores number 16, 17 and 18). Error bars correspond to the standard deviation of analytical triplicates. 47

Figure 13: Potential Hg methylation rate constants (k_m, d-1) determined in both sites (OS in purple and SG in orange) during the 2019 (A and C) and 2021 (B and D) incubations. Open and close symbols refer to fresh and incubated cores respectively. Error bars correspond to the standard deviation of the three replicates per core. 49

Figure 14: DOC and fluorescent dissolved organic matter (FDOM) characterization of the overlying water collected in the Sep 2021 sampling campaign. Values of fresh (open symbols) and incubated cores (close symbols) from both sites (OS in purple and SG in orange). Peaks A, C and T are normalized by total fluorescence. 50

Figure 15: Conceptual figure coupling the consumption of dissolved oxygen (DO, lines) in benthic chambers in Sep 2021 with the simultaneous increase in methylmercury concentration (MMHg, squares) in the overlying waters of fresh (t0) and incubated cores (48h). 52

Figure 16: Pearson correlation matrix between k_m, Hg and MMHg concentrations and organic matter composition. Data from both fresh and incubated cores from Sep 2021 sampling were used to construct the Pearson correlation matrix. Only significant ($p<0.05$) correlations are shown. 53

Figure 17: Diagram of the methodology used in Chapter 2, from sample collection to assembling and post analyses. 67

Figure 19: Phylogenetic analysis integrating 90 MerA amino acid sequences retrieved from both Hg-RGC and MERCLUB MAGs datasets. The analysis includes 3 extra sequences from isolates of the MERCLUB Culture Collection. The histogram (in grey) represents the number of sites in which the sequence was found. The colors of the lines in the phylogenetic tree correspond to the phylum. 70

Figure 20: Phylogenetic analyses integrating 223 MerB amino acid sequences retrieved from both Hg-RGC and MERCLUB MAGs datasets. The histogram (in grey) represents the number of sites in which the sequence was found. The colors of the lines in the phylogenetic tree correspond to the phylum. 71

Figure 21: Taxonomic annotation and novelty of the MERCLUB MAGs containing *merA* and/or *B* genes. A) Phylogenomic-based taxonomy of the 45 MERCLUB MAGs dataset at the phylum level (except for Proteobacteria that were split at the class level). Gammaproteobacteria were further visualized at the order level as well. The figures indicate the number of MAGs for each taxonomic level. B) Stacked bar plot for novelty quantification of the *merAB* containing MERCLUB MAGs (x-axis) at different taxonomic ranks (y-axis). The

taxonomically unclassified portion is depicted in white; the taxonomically classified portion is shown in dark magenta. 74

Figure 22: Metabolic pathways of the 45 MAGs harboring *merA* and/or *merB* genes involved in inorganic carbon fixation (yellow), nitrogen (green), sulfur (blue), hydrogen (purple) and methane (red), shown with the names of the genes. A complete list of the KO involved in all represented pathways is indicated in Table S9 as well as in github.com/bjtully/BioData/tree/master/KEGGDecoder (Graham et al., 2018) 76

Figure 23: Metabolic potential of the 45 MAGs containing *merA* and/or *merB* genes. Each MAG is colored based on its taxonomic affiliation at the highest possible resolution. Different pathways associated with Sulfur, Nitrogen, Methene, Hydrogen, and Carbon metabolism are shown in different colors. 77

Figure 24: Functional traits associated to metal metabolism, motility, and biofilm formation of the 45 *merAB* MAGs. Each MAG is colored based on its taxonomic affiliation at the highest possible resolution. 78

Figure 25: Abundance and transcriptional activity measured by RPKG for each MAG and across the different Hg-impacted sediments. The metatranscriptomes of stations CS14 and EN17 were absent due to their low quality. 81

Figure 26: Transcriptional level of *merA* (A) and *merB* (B) genes expressed by Transcript Per Million (TPM). 82

Chapter 3: Unmasking the physiology of mercury detoxifying bacteria from polluted sediments 87

Figure 27: Graphical abstract for Chapter 3. From left to right: growth curve (optical density: OD.) at 4 μM and Hg concentrations over time, schematic of continuous culture set up and specific degradation rate from the three continuous culture conditions. 87

Figure 28: Schematics of the methodology of chapter 3. 92

Figure 29: Growth curves of the three isolates studied in this work exposed to different concentrations of $HgCl_2$ (0, 4 and 12 μM). The different symbols correspond to individual replicates within each condition. The mean growth rate ± standard deviation was calculated when possible. MERCC_1069: *Aeromonas hydrophila*, MERCC_1942: *Pseudomonas putida,* and MERCC_2833: *Bacillus* sp. 98

Figure 30: Concentration of total Hg (μM) along time of an abiotic control and the three isolates studied in this work exposed to different concentrations of $HgCl_2$ (4 and 12 μM). The different symbols correspond to individual replicates within each condition. MERCC_1069: *Aeromonas hydrophila*, MERCC_1942: *Pseudomonas putida*, and MERCC_2833: *Bacillus* sp. 99

Figure 31: THg detoxified per cell of *Pseudomonas* sp. MERCC_1942 previously grown at different growth rates in bioreactors and spiked with 4 μM HgCl2. D = dilution rate = growth rate (see equation in Figure 28). 101

Figure 32: Average number of mRNA copies of the *merA* gene normalized by ng of cDNA (circles) and average Hg concentration along time (squares) from *Pseudomonas putida* MERCC_1942 previously grown at three different dilution rates in bioreactors and spiked with 4 μM HgCl2. SS: steady state in continuous culture. D = dilution rate = growth rate (see equation in Figure 28). 102

Figure 33: Synteny of the *mer* operon found in *Pseudomonas putida* strain MERCC_1942 genome. 103

Figure 34: Graphical abstract of chapter 4. 109

Figure 35: Summary of the assembly's characteristics and synteny of the four *mer* operons found in *Alteromonas mediterranea* strain ISS312 genome. The black arrows are mobile elements (transposases, integrases…). Grey arrows are genes outside the operon. 115

Figure 36: Growth curve of Alteromonas mediterranea ISS312 in the presence of 5 μM of MMHg (pink) and the control without MMHg (yellow). Different symbols (square, triangle, circle) represent the three replicates and gray circles display the samples taken for transcriptomics. 116

Figure 37: PCoA of the TMM (normalized transcripts), resulting of the transcriptomic analysis with egdeR package. Colors represent phases of the growth and symbols if the culture was amended with MMHg (triangles) or not (circles). 117

Figure 38: Heatmap of the percentage of correlation classified in the KEGG pathway database; all positive pairwise Pearson correlations ($r > 0.9$) between the expression of mercury related genes and other expressed genes in each amended transcriptome were taken to calculate the percentages (please see the methods section 2.5 for details of the calculation). 120

Figure 39: Synteny of the four *mer* operons found in *Alteromonas mediterranea* strain ISS312 genome and their $\log_2$(Fold-Change) considering all samples regardless of the growth phase (Amended vs. control). 121

Figure 40: TMM (normalized transcripts) of *mer*_3 genes and *merB*_4 across different phases of the growth curve in the presence of 5 μM of MMHg (pink) vs the control (yellow). Error bars represent the standard deviation between the three replicates. 122

Figure 42: Diagram of the possible effects of global change in coastal environments in relation to Hg concentration, speciation, bioavailability and bioaccumulation. Colored pluses (+) and minuses (-) represent the enhancing or diminishing effect of the increased action/condition of the same color: e.g. the yellow + next to the microbial activity bubble indicates that at higher temperatures, microbial activity will be enhanced; instead, the blue - next to the oxygen bubble, means that at higher microbial activity, oxygen concentrations will be diminished. 134

Figure 43: Rank plots showing the *merAB* containing genomes (MAGs or isolates) in the different sampling areas. From top to bottom: Barcelona's coast, Baltic's coast, Suances

Estuary and Nervión Estuary. Grey dots belong to the MAGs that did not have neither *merA* nor *merB*. High-abundant MAG correspond to >1 % relative abundance, mid abundant to those <1 % but >0.01 % and low-abundant to <0.01 % relative abundance. 137

Figure S1: Vertical profiles of dissolved oxygen concentration (µM), redox potential OR E_H (mV) and hydrogen sulfide (H_2S) concentration (µM) (left to right) in the sediment cores from OS (purple) and SG (orange) sites, measured in Nov 2021 at the collecting time (t0h-circles), after 24 (t24h-triangles) and 48 (t48h-squares) hours of incubation. 195

Figure S2: Location of the sediment samples used for this study. 196

Figure S3: Reconstructed operons found in the MAGs. Name of the MAG and taxonomic assignation (to the lowest level possible) are above the corresponding sinteny. 196

Figure S4: Phylogenetic analysis integrating A) 15 MerA amino acid sequences and B) 32 MerB amino acid sequences retrieved from MERCLUB MAGs datasets. The names are colored following the same legend as the Class assignation. 197

Figure S5: Epifluorescence microscope images of DAPI stained *Pseudomonas* strain MERCC_1942 cells grown at three different growth rates in the continuous culture experiments. A: 0.05 h^{-1}, B: 0.1 h^{-1} and C: 0.2 h^{-1}. 198

Figure S6: Phylogenetic trees of A) *merA* and B) *merB* genes of *Alteromonas mediterranea* ISS312 with closely related *merA* and *merB* sequences from different taxa classifications. 199

Figure S7: Heatmap of the percentage of positive Pearson correlations between the mercury related genes and other expressed genes in the control condition, classified in the KEGG pathway database. 200

Figure S8: MetaG abundances of each enzyme in the different ocean layers analyzed. SRF: surface. DCM: deep chlorophyll maximum. MES: mesopelagic. Size of the dots indicate abundance of transcripts in the database. 201

Figure S9: MetaT abundances of each enzyme in the different ocean layers analyzed. SRF: surface. DCM: deep chlorophyll maximum. MES: mesopelagic. Size of the dots indicate abundance of transcripts in the database. 202

List of tables

Table 1: Results from anaerobiosis tolerance and Minimum Inhibitory Concentration (MIC) assay at 24 h for the studied isolates. In bold, those candidates selected for the characterization of growth rate and Hg removal assay. 96

Table 2: Mean percentage of Hg removal from abiotic control and *Pseudomonas putida* strain MERCC_1942 grown at different dilution rates (D) in the continuous culture after 2 and 24 h of incubation with $HgCl_2$. In the case of the isolate, results from Hg detoxification rates and specific Hg detoxification rates per cell are shown (sd: standard deviation). 101

Table 3: The ten most upregulated genes comparing all amended transcriptomes with all the control transcriptomes regardless of the growth phase. FC: Fold-Change. FRD: False Discovery Rate. 121

Table S1: Fluorescent dissolved organic matter parameters examined. Given that peaks A, M and C are not defined at fix emission wavelengths (Coble, 1996), the maximum fluorescence value in the region is extracted. 203

Table S2: Means and standard deviations of descriptive variables characterizing sediments collected at Osellino (OS) and San Giuliano (SG) sites in Nov. 2019 and Sep. 2021. Ratios OS/SG significantly different from 1 highlight notable differences of sediments between two sites in 2019 and 2021 203

Table S3: Dissolved organic matter content and characteristics in overlaying water from two sites Osellino (OS) and San Giuliano (SB) sampled at two different periods. Means and standard deviations from 3 different cores. 204

Table S4: Concentrations of total mercury (THg, mg/kg) and methylmercury (MMHg, µg/kg) in sediment cores. 205

Table S5: THg and MMHg concentrations in filtered porewater and overlaying water from two sites Osellino (OS) and San Giuliano (SG) sampled at two different periods. Means and standard deviations from 3 different cores. *One of the cores couldn't be measured, so n=2. 205

Table S6: Metal sensible to the redox state (Mn) in the overlaying water of the cores. 206

Table S7: Hg, Mn, and DOC content and OM characteristics of the overlaying water inside the benthic chambers 48 hours after deployment in Sep. 2021. 206

Table S8: Location and environmental parameters of the sediment samples used for this study (dw: dry weight, NA: not available). 207

Table S9: Complete list of KOs involved in the metabolisms represented in Figure 22 207

Table S10: Composition of Marine and Brackish media used to perform the salinity test. The growth curves and the experiments with the continuous culture were performed with the Marine medium. 207

Table S11. Composition of the trace element solution used to supplement Marine and Brackish media. 208

Table S12: Taxonomic affiliation, source and isolation method (Soil Substrate Membrane System (SSMS) or classical method using serial dilution and plating) for the 46 selected isolates from the MERCLUB collection. Detection of the *merA* gene with primer pairs NsfF-NsfR (Wang et al., 2011) and application of pretreatment with Hg are also indicated. 208

Table S13: Isolates analyzed in the salinity assay, grown at 0.5 % (brackish medium) and 3.5 % NaCl (marine medium). In bold, those candidates selected to perform the anaerobiosis and MIC tests. 208

Table S14: TMM (normalized abundances of the RNA-seq) for all samples and subsamples used in the comparative transcriptomic analysis. 208

Table S15: Comparison of statistical packages for RNA-seq analysis, all samples were used regardless the phase (DE: differentially expressed). The statistical significance was stablished at p-value 0.05. 208

Table S16: Statistically significant DE, upregulated and downregulated, genes in the lag phase. 209

Table S17: Statistically significant DE, upregulated and downregulated, genes in the exponential phase 209

Table S18: Statistically significant DE, upregulated and downregulated, genes in the late exponential phase. 209

Table S19: Statistically significant DE, upregulated and downregulated, genes in the stationary phase. 209

Table S20: Statistically significant DE, upregulated and downregulated, genes in the overall analysis (regardless the growth phase) 209


Supplementary
material

Supplementary material

Supplementary figures

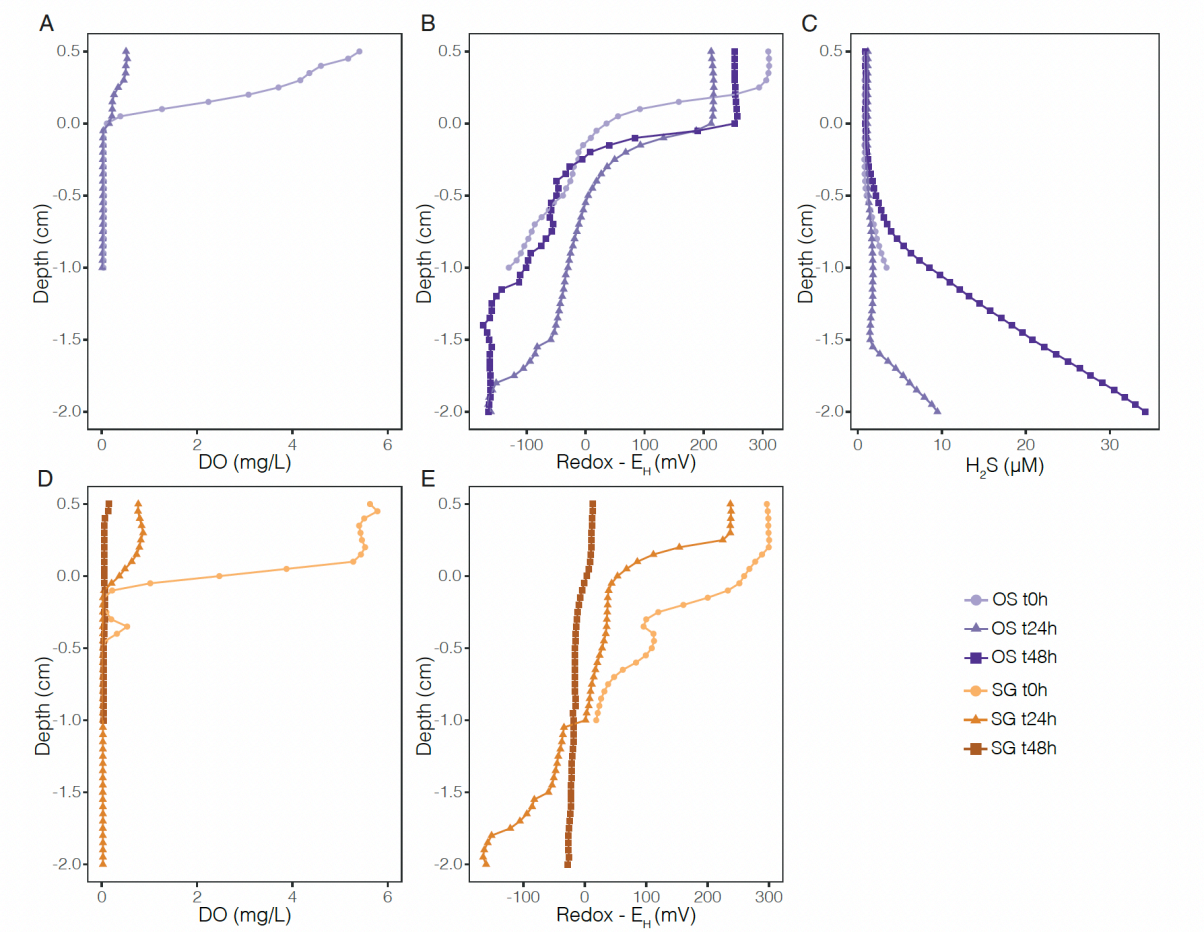


Figure S1: Vertical profiles of dissolved oxygen concentration (µM), redox potential OR E_H (mV) and hydrogen sulfide (H_2S) concentration (µM) (left to right) in the sediment cores from OS (purple) and SG (orange) sites, measured in Nov 2021 at the collecting time (t0h-circles), after 24 (t24h-triangles) and 48 (t48h-squares) hours of incubation.

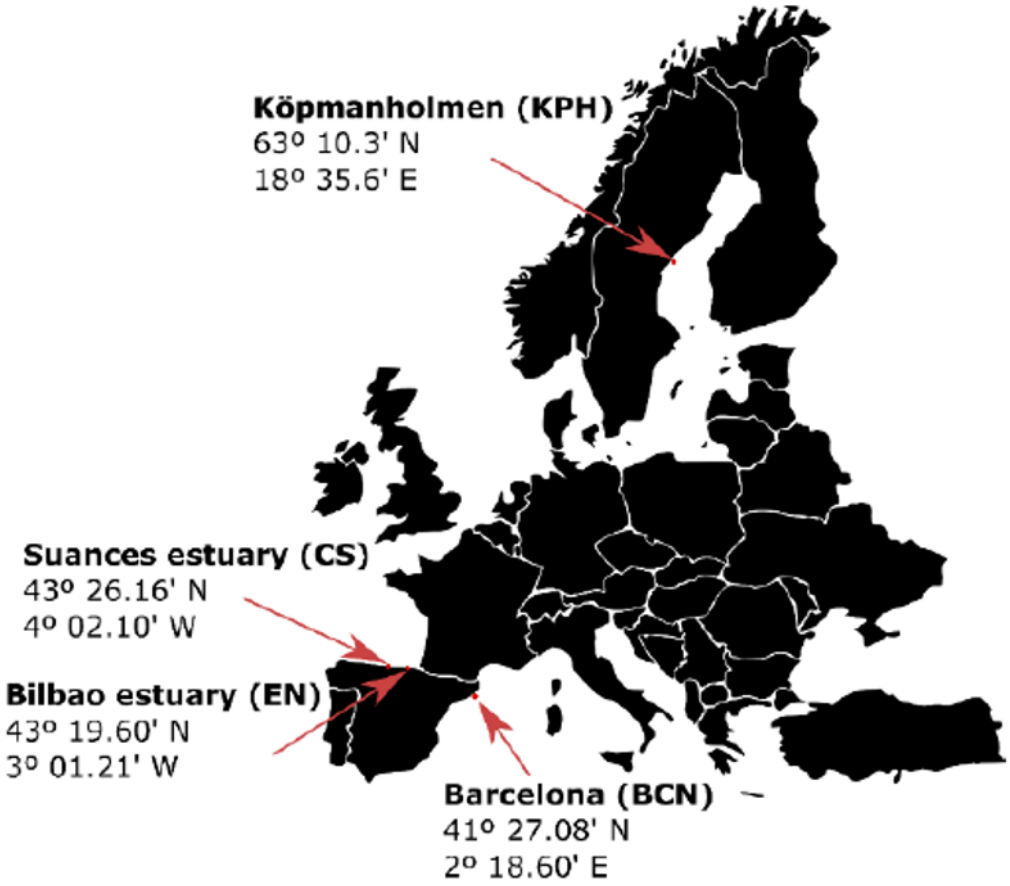


Figure S2: Location of the sediment samples used for this study.

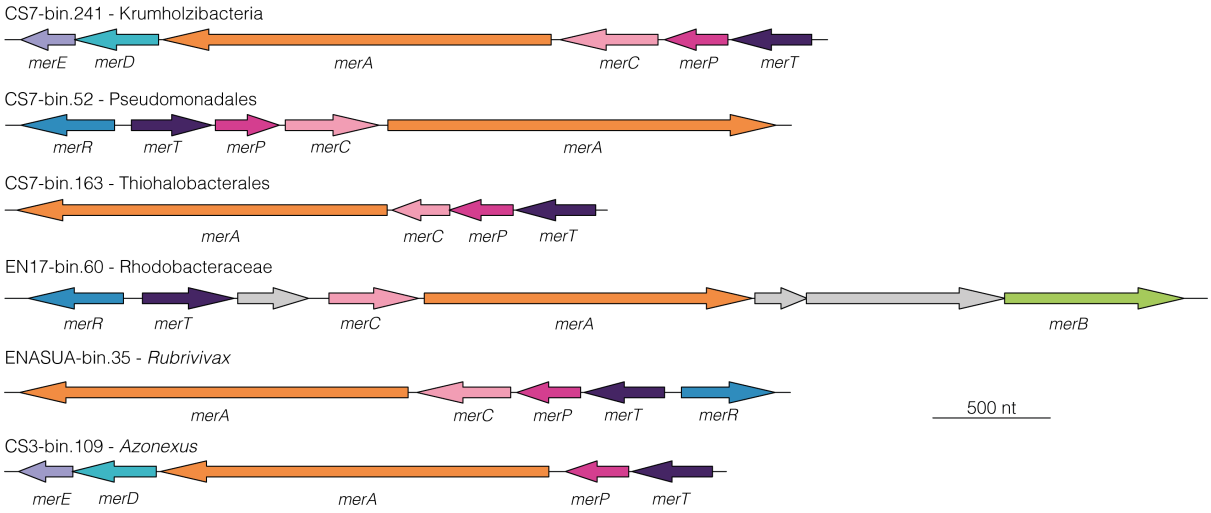


Figure S3: Reconstructed operons found in the MAGs. Name of the MAG and taxonomic assignation (to the lowest level possible) are above the corresponding sinteny.

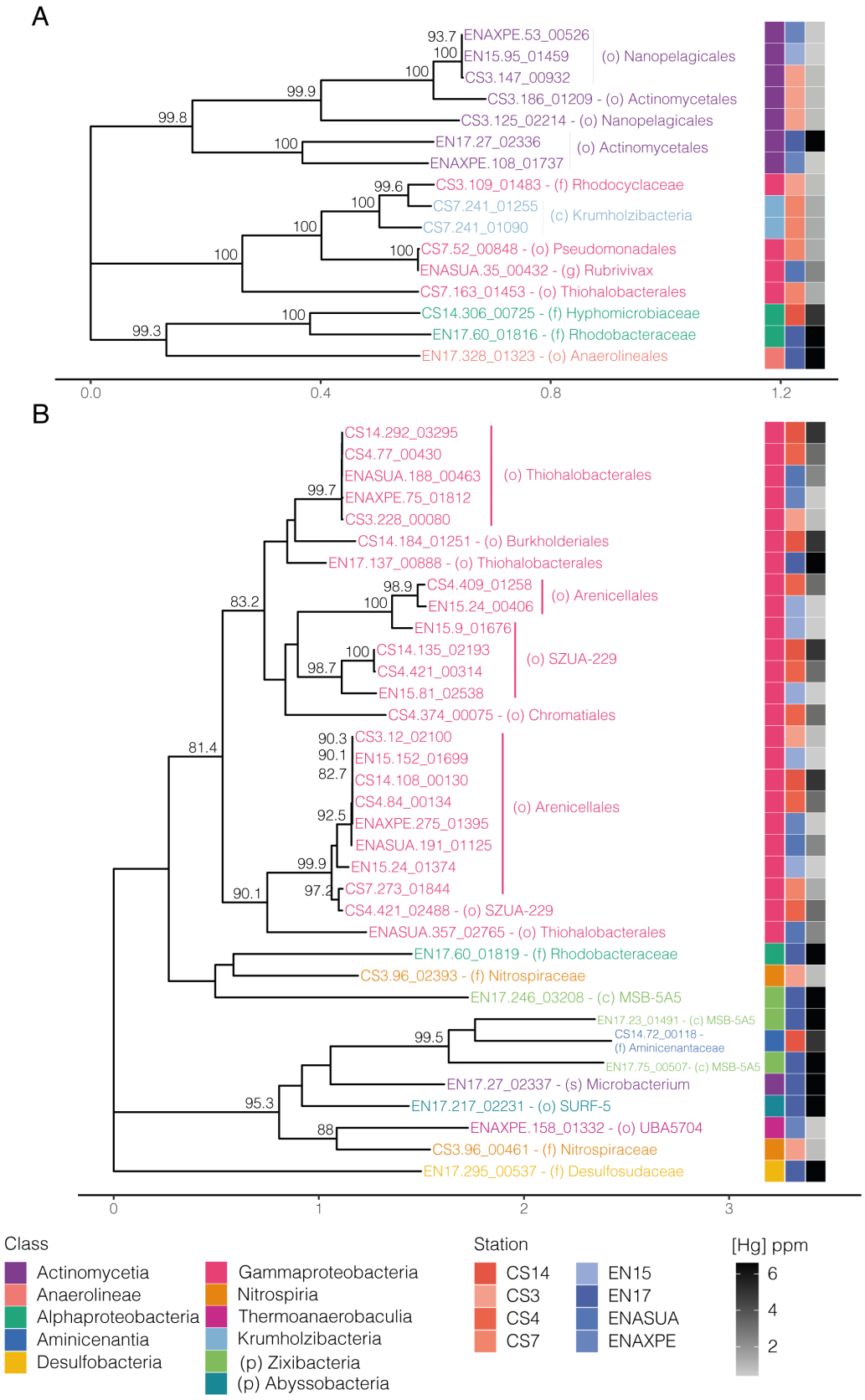


Figure S4: Phylogenetic analysis integrating A) 15 MerA amino acid sequences and B) 32 MerB amino acid sequences retrieved from MERCLUB MAGs datasets. The names are colored following the same legend as the Class assignation.

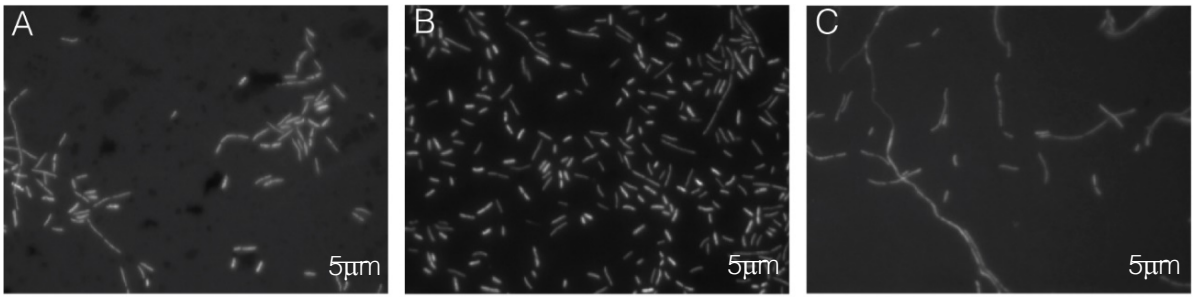


Figure S5: Epifluorescence microscope images of DAPI stained *Pseudomonas* strain MERCC_1942 cells grown at three different growth rates in the continuous culture experiments. A: 0.05 h^{-1}, B: 0.1 h^{-1} and C: 0.2 h^{-1}.

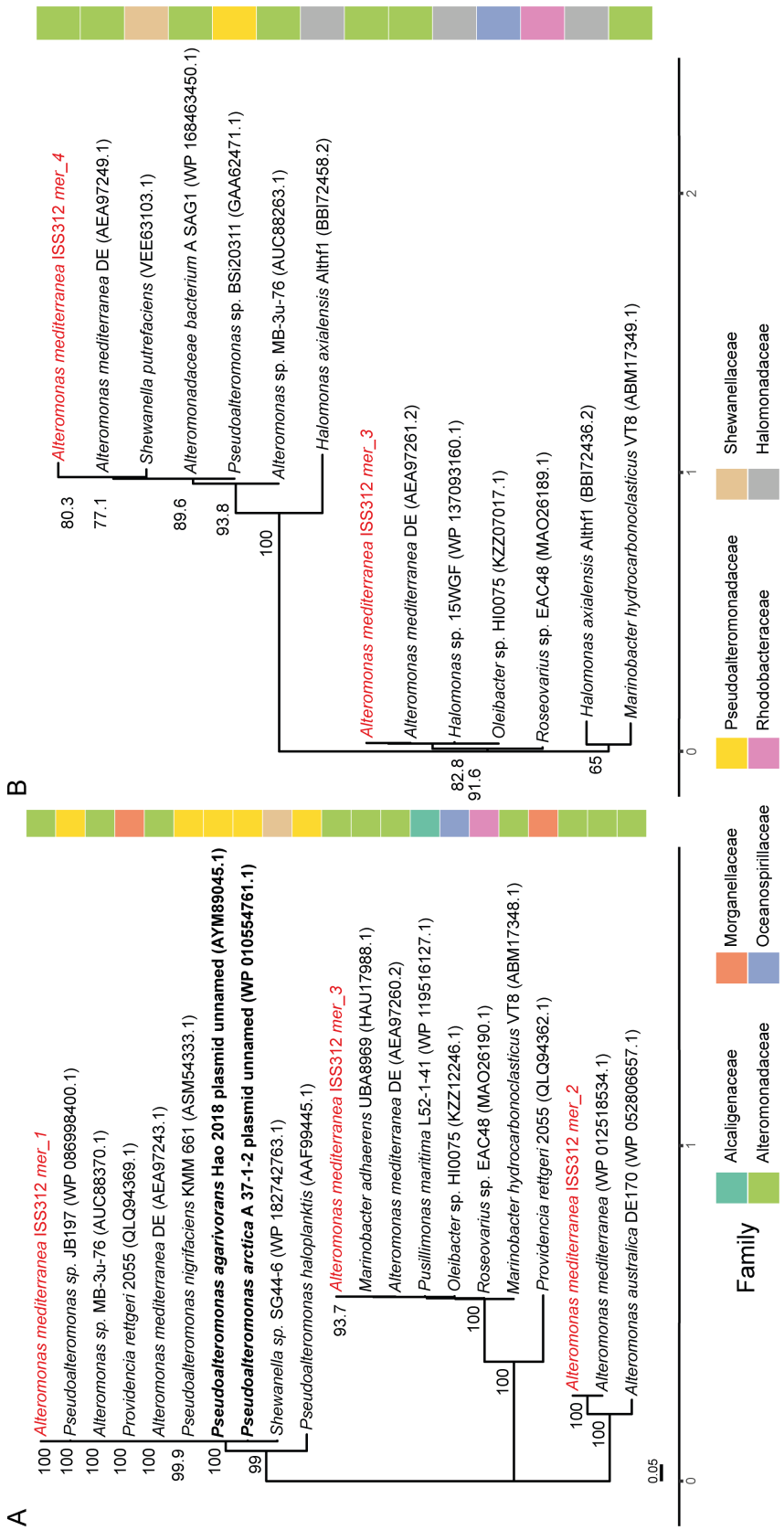


Figure S6: Phylogenetic trees of A) *merA* and B) *merB* genes of *Alteromonas mediterranea* ISS312 with closely related *merA* and *merB* sequences from different taxa classifications.

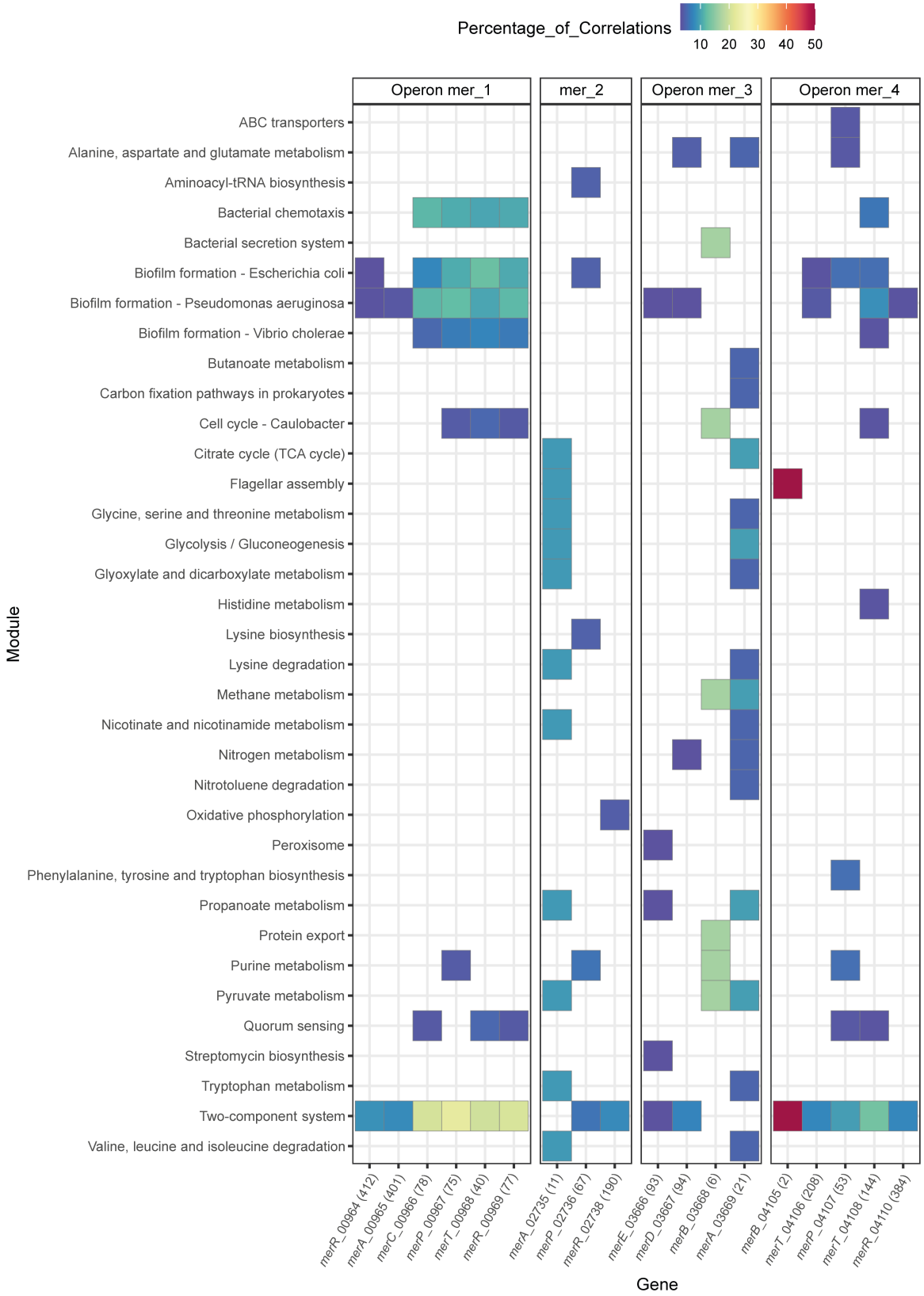


Figure S7: Heatmap of the percentage of positive Pearson correlations between the mercury related genes and other expressed genes in the control condition, classified in the KEGG pathway database.

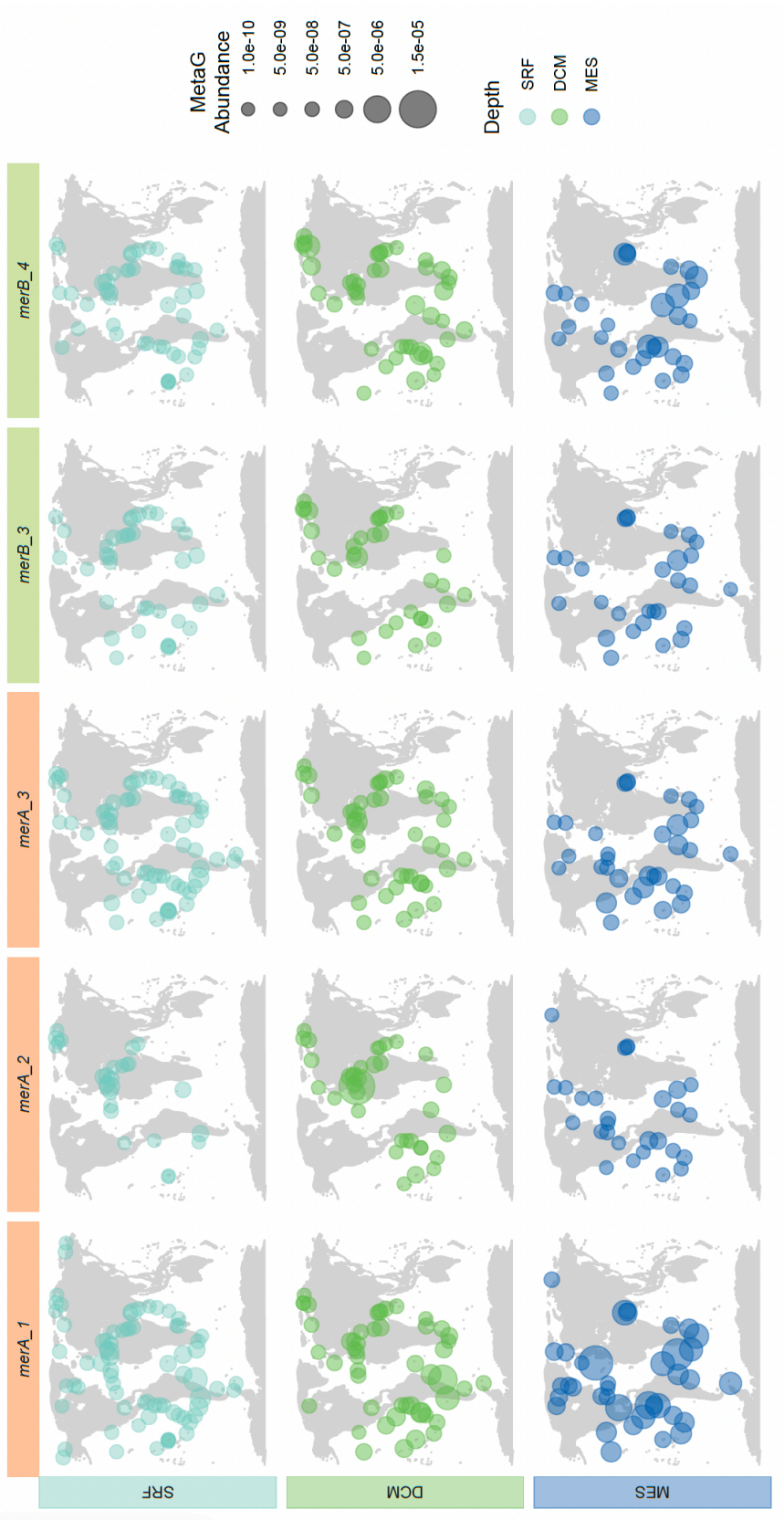


Figure S8: MetaG abundances of each enzyme in the different ocean layers analyzed. SRF: surface. DCM: deep chlorophyll maximum. MES: mesopelagic. Size of the dots indicate abundance of transcripts in the database.

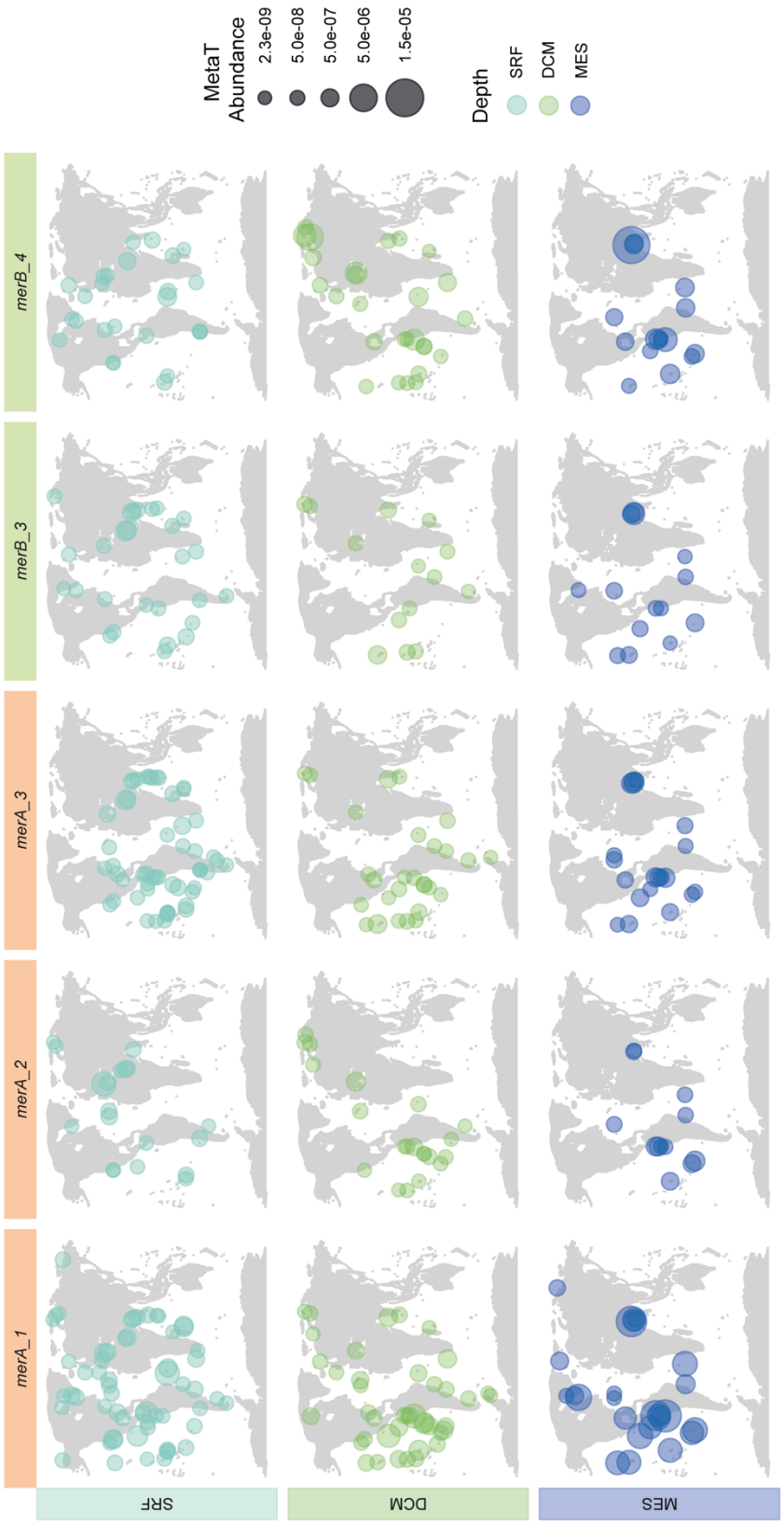


Figure S9: MetaT abundances of each enzyme in the different ocean layers analyzed. SRF: surface. DCM: deep chlorophyll maximum. MES: mesopelagic. Size of the dots indicate abundance of transcripts in the database

Supplementary Tables

Table S1: Fluorescent dissolved organic matter parameters examined. Given that peaks A, M and C are not defined at fix emission wavelengths (Coble, 1996), the maximum fluorescence value in the region is extracted.

FDOM parameter	Abbreviation	Definition (ex/em nm)	Reference
Biological Index	BIX	F(310/380) /F(310/430)	(Huguet et al., 2009)
Humification Index	HIX	F(254/∑(435:480))/F(254/∑(300:345))	(Ohno, 2002)
Fluorescence Index	FI	F(370/450)/F(370/500)	(McKnight et al., 2001)
General humic substances	Peak A	F(260/380:460)	(Coble, 1996)
Terrestrial humic substances	Peak C	F(350/420:480)	(Coble, 1996)
Marine humic substances	Peak M	F(312/ 380:420)	(Coble, 1996)
Tryptophan-like fluorescence	Peak T	F(275/340)	(Coble, 1996)
Tyrosine-like fluorescence	Peak B	F(275/310)	(Coble, 1996)

Table S2: Means and standard deviations of descriptive variables characterizing sediments collected at Osellino (OS) and San Giuliano (SG) sites in Nov. 2019 and Sep. 2021. Ratios OS/SG significantly different from 1 highlight notable differences of sediments between two sites in 2019 and 2021.

	Nov 2019			Sep 2021		
	OS	SG	OS/SG	OS	SG	OS/SG
Water content (%)	65 ± 3	65 ± 3	1 ± 0.06	65 ± 2	48 ± 2	1.37 ± 0.06
Mean diameter (μm)	9.2 ± 1.2	9 ± 1.9	1.02 ± 0.25	9 ± 2.1	8.7 ± 3.2	1.03 ± 0.43
TOC (%)	2.65 ± 0.18	1.98 ± 0.38	1.34 ± 0.2	2.64 ± 0.07	1.44 ± 0.17	1.83 ± 0.12
N (%)	0.33 ± 0.02	0.29 ± 0.04	1.13 ± 0.14	0.32 ± 0.02	0.14 ± 0.01	2.32 ± 0.07
TOC/N	8.1 ± 0.5	6.9 ± 1.2	1.18 ± 0.18	8.2 ± 0.3	10.3 ± 1.3	0.79 ± 0.13
MINC (%)	3.8 ± 0.2	4.9 ± 0.3	0.79 ± 0.08	3.3 ± 0.1	5.4 ± 0.2	0.6 ± 0.05
HI (mg CH/g TOC)	235 ± 14	263 ± 40	0.89 ± 0.16	209 ± 6	141 ± 16	1.49 ± 0.12
OI (mg CO_2/g TOC)	157 ± 11	174 ± 31	0.9 ± 0.19	150 ± 8	136 ± 18	1.1 ± 0.14

Table S3: Dissolved organic matter content and characteristics in overlaying water from two sites Osellino (OS) and San Giuliano (SB) sampled at two different periods. Means and standard deviations from 3 different cores.

	Nov. 2019				Sep. 2021			
	OS		SG		OS		SG	
	Fresh	Incubated	Fresh	Incubated	Fresh	Incubated	Fresh	Incubated
DOC	2.31 ± 0.130	2.38 ± 0.076	2.37 ± 0.215	2.32 ± 0.245	4.17 ± 0.021	10.55 ± 2.205	4.07 ± 0.153	6.00 ± 0.693
Peak A	0.39 ± 0.002	0.38 ± 0.011	0.39 ± 0.007	0.36 ± 0.016	0.31 ± 0.008	0.24 ± 0.034	0.31 ± 0.009	0.28 ± 0.039
Peak C	0.19 ± 0.002	0.19 ± 0.006	0.19 ± 0.004	0.18 ± 0.008	0.15 ± 0.004	0.14 ± 0.005	0.14 ± 0.004	0.14 ± 0.018
Peak M	0.23 ± 0.002	0.23 ± 0.005	0.23 ± 0.006	0.22 ± 0.004	0.18 ± 0.005	0.15 ± 0.011	0.18 ± 0.006	0.17 ± 0.025
Peak T	0.12 ± 0.005	0.13 ± 0.008	0.12 ± 0.009	0.15 ± 0.027	0.21 ± 0.007	0.28 ± 0.032	0.22 ± 0.010	0.24 ± 0.046
Peak B	0.07 ± 0.001	0.08 ± 0.013	0.07 ± 0.009	0.09 ± 0.005	0.15 ± 0.010	0.19 ± 0.018	0.16 ± 0.009	0.18 ± 0.036
FI	1.39 ± 0.010	1.40 ± 0.010	1.40 ± 0.011	1.41 ± 0.015	1.40 ± 0.012	1.49 ± 0.064	1.40 ± 0.001	1.47 ± 0.009
BIX	0.85 ± 0.002	0.85 ± 0.003	0.83 ± 0.009	0.88 ± 0.085	0.92 ± 0.007	0.97 ± 0.034	0.96 ± 0.011	0.97 ± 0.012
HIX	0.85 ± 0.005	0.84 ± 0.010	0.86 ± 0.010	0.84 ± 0.016	0.74 ± 0.010	0.67 ± 0.046	0.73 ± 0.014	0.71 ± 0.054
SR	0.83 ± 0.024	0.84 ± 0.006	0.88 ± 0.032	0.90 ± 0.058	1.19 ± 0.014	1.32 ± 0.074	1.28 ± 0.032	1.23 ± 0.036
SUVA254	2.00 ± 0.110	2.01 ± 0.236	1.90 ± 0.084	1.78 ± 0.115	4.01 ± 0.221	5.99 ± 2.488	1.93 ± 1.180	3.39 ± 0.640
A:C	2.03 ± 0.008	2.02 ± 0.010	2.04 ± 0.011	2.03 ± 0.018	2.14 ± 0.004	1.76 ± 0.203	2.19 ± 0.009	2.04 ± 0.022
T:C	0.65 ± 0.027	0.70 ± 0.071	0.63 ± 0.061	0.85 ± 0.189	1.42 ± 0.089	2.05 ± 0.288	1.58 ± 0.124	1.80 ± 0.538
C:M	0.82 ± 0.001	0.82 ± 0.009	0.82 ± 0.001	0.80 ± 0.026	0.81 ± 0.004	0.90 ± 0.040	0.78 ± 0.003	0.83 ± 0.016

Table S4: Concentrations of total mercury (THg, mg/kg) and methylmercury (MMHg, µg/kg) in sediment cores.

Sampling	Site	Depth	THg (mg/kg)		MMHg (µg/kg)	
			Fresh	Incubated	Fresh	Incubated
Nov. 2019	OS	0-2cm	0.84 ± 0.02	0.81 ±0.08	0.55 ± 0.05	0.49 ± 0.06
		2-4cm	0.90 ± 0.01	0.97 ±0.1	0.45 ± 0.16	0.44 ± 0.16
	SG	0-2cm	0.81 ± 0.06	0.80 ± 0.08	0.49 ± 0.02	0.45 ± 0.05
		2-4cm	0.95 ± 0.06	0.98 ± 0.04	0.52 ± 0.19	0.47 ± 0.21
Sep. 2021	OS	0-2cm	0.89 ± 0.01	0.93 ± 0.003	0.26 ± 0.14	0.18 ± 0.02
		2-4cm	0.87 ± 0.06	0.90 ± 0.03	0.10 ± 0.03	0.15 ± 0.05
	SG	0-2cm	0.89 ± 0.03	0.92 ± 0.03	0.18 ± 0.10	0.21 ± 0.19
		2-4cm	0.95 ± 0.04	0.89 ± 0.002	0.10 ± 0.002	0.09 ± 0.01

Table S5: THg and MMHg concentrations in filtered porewater and overlaying water from two sites Osellino (OS) and San Giuliano (SG) sampled at two different periods. Means and standard deviations from 3 different cores. *One of the cores couldn't be measured, so n=2.

Sampling	Site	Depth	THg (ng/L)		MMHg (ng/L)	
			Fresh	Incubated	Fresh	Incubated
Nov. 2019		Overlaying	<LOD	<LOD	<LOD	0.06
	OS	0-2cm	4.33 ± 1.44	4.23 ± 2.22	0.16 ± 0.04	0.14 ± 0.05
		2-4cm	7.63 ± 8.22	2.32 ± 0.60	0.20 ± 0.12	0.14 ± 0.07
		Overlaying	0.05 ± 0.004	0.05 ± 0.009	0.05 ± 0.015	0.1 ± 0.084
	SG	0-2cm	4.69 ± 1.86	4.51 ± 1.88	0.69 ± 0.93	0.16 ± 0.01
		2-4cm	4.94 ± 1.61	4.89 ± 2.54	0.47 ± 0.27	1.02 ± 1.17
Sep. 2021		Overlaying	3.23 ± 0.117	10.75 ± 1.961	0.04 ± 0.031*	0.11 ± 0.014*
	OS	0-2cm	9.62 ± 2.16	10.61 ± 2.84	0.05 ± 0.04	0.14 ± 0.11
		2-4cm	14.00 ± 5.66	19.43 ± 15.66	0.07 ± 0.02	0.20 ± 0.09
		Overlaying	4.44 ± 0.440	5.34 ± 1.509	0.05 ± 0.031	0.13 ± 0.008
	SG	0-2cm	14.85 ± 7.59	20.26 ± 6.60	0.12 ± 0.05	0.12 ± 0.07
		2-4cm	11.98 ± 1.56	10.46 ± 0.87	0.26 ± 0.17	0.17 ± 0.05

Table S6: Metal sensible to the redox state (Mn) in the overlaying water of the cores.

	2019				2021			
	OS		SG		OS		SG	
	Fresh	Incubated	Fresh	Incubated	Fresh	Incubated	Fresh	Incubated
Mn	1.84 ± 0.75	1.55 ± 1.15	1.77 ± 1.08	1.6 ± 1	28.5 ± 9.9	840 ± 164	7.35 ± 3.62	751 ± 134

Table S7: Hg, Mn, and DOC content and OM characteristics of the overlaying water inside the benthic chambers 48 hours after deployment in Sep. 2021.

	OS	SG
THg (ng/L)	13.51 ± 0.71	10.42 ± 0.49
MMHg (ng/L)	0.066	0.129
DOC (mg/L)	3.728	3.725
Peak A (FTU)	0.314	0.307
Peak C (FTU)	0.151	0.142
Peak M (FTU)	0.201	0.188
Peak T (FTU)	0.202	0.216
Peak B (FTU)	0.132	0.146
FI	1.414	1.407
BIX	0.916	0.952
HIX	0.751	0.728
SR	1.182	1.176
SUVA254	3.892	3.231
A:C	2.084	2.153
T:C	1.338	1.519
C:M	0.75124378	0.755319
Mn (µg/L)	310.54 ± 10.96	226.75 ± 31.68

Table S8: Location and environmental parameters of the sediment samples used for this study (dw: dry weight, NA: not available).

Area	Station Code	Location	Sampling date	Redox (mV)	Hg total ± sd (ng/g dw)
Barcelona (Mediterranean)	BCN_1	41°27.08'N, 2°18.60'E	February 2020	NA	118 ± 8
	BCN_4			NA	1785 ± 189
Bilbao (Bay of Biscay)	EN-15	43°19.60'N, 3°01.21'W	March 2020	-223	412 ± 174
	EN-17			-244	6601 ± 179
	EN-ASUA			-157	2398 ± 20
	EN-AXPE			-185	496 ± 3
Suances (Bay of Biscay)	CS3	43°26.16'N, 4°02.10'W	March 2020	-210	827 ± 89
	CS4			-245	3173 ± 203
	CS7			-273	1315 ± 214
	CS14			-208	5049 ± 124
Köpmalhomen (Baltic)	KPH	63°10.3'N, 18°35.6'E	November 2019	NA	19800 ± 1100

Table S9: Complete list of KOs involved in the metabolisms represented in Figure 22.[1]

Table S10: Composition of Marine and Brackish media used to perform the salinity test. The growth curves and the experiments with the continuous culture were performed with the Marine medium.

Final composition	Marine medium (g/L)	Brackish medium (g/L)
$NaSO_4$	4	4
KH_2PO_4	0.21	0.21
NH_4Cl	0.25	0.25
NaCl	30.04	5.04
$MgCl*6H_20$	3.01	3.02
KCl	0.53	0.51
$CaCl2*2\ H_20$	0.17	0.15
$NaHCO_3$	0.19	0.19
Peptone	0.5	0.5
Yeast extract	0.11	0.1
Trace element solution (Table S11)	100µL	100µL
$FeSO_4$	0.28 g	0.28 g

[1]This tables can not be printed due to their size. They can be access at https://github.com/CPG-Hg/PhD_Thesis_ST_Carla_Pereira-Garcia.git

Table S11. Composition of the trace element solution used to supplement Marine and Brackish media.

Trace element solution	(units/L)
25 % HCl	13 mL
Na_2-EDTA	5.2 g
H_3BO_3	30 mg
$MnCl_2$*4 H_2O	100 mg
$CoCl_2$*6H_2O	190 mg
$NiCl_2$*6 H_2O	24 mg
$CuCl_2$*2H_2O	2 mg
$ZnSO_4$*7H_2O	144 mg
Na_2MoO_4*2H_2O	36 mg

Table S12: Taxonomic affiliation, source and isolation method (Soil Substrate Membrane System (SSMS) or classical method using serial dilution and plating) for the 46 selected isolates from the MERCLUB collection. Detection of the *merA* gene with primer pairs NsfF-NsfR (Wang et al., 2011) and application of pretreatment with Hg are also indicated.[1]

Table S13: Isolates analyzed in the salinity assay, grown at 0.5 % (brackish medium) and 3.5 % NaCl (marine medium). In bold, those candidates selected to perform the anaerobiosis and MIC tests.[1]

Table S14: TMM (normalized abundances of the RNA-seq) for all samples and subsamples used in the comparative transcriptomic analysis. [1]

Table S15: Comparison of statistical packages for RNA-seq analysis, all samples were used regardless the phase (DE: differentially expressed). The statistical significance was stablished at p-value 0.05.

		DESeq2	edgeR	NOISeq
Up-regulated	(	34	29	33
Down-regulated	(	21	23	4
Shared up genes (	DESeq2	34	29	29
	edgeR		29	26
	NOISeq			33
All	26			
Shared down genes (	DESeq2	21	21	4
	edgeR		23	4
	NOISeq			4
All	4			
Total DE genes		55	52	37

[1]This tables can not be printed due to their size. They can be access at https://github.com/CPG-Hg/PhD_Thesis_ST_Carla_Pereira-Garcia.git

Table S16: Statistically significant DE, upregulated and downregulated, genes in the lag phase.[1]

Table S17: Statistically significant DE, upregulated and downregulated, genes in the exponential phase.[1]

Table S18: Statistically significant DE, upregulated and downregulated, genes in the late exponential phase. [1]

Table S19: Statistically significant DE, upregulated and downregulated, genes in the stationary phase.[1]

Table S20: Statistically significant DE, upregulated and downregulated, genes in the overall analysis (regardless the growth phase) [1]

[1]This tables can not be printed due to their size. They can be access at https://github.com/CPG-Hg/PhD_Thesis_ST_Carla_Pereira-Garcia.git

